# Investigation of fibulin-2 in pulmonary fibrosis

David R Pearce

A thesis submitted to University College London for the degree of Doctor of Philosophy

Centre for Inflammation and Tissue Repair

UCL Respiratory

Division of Medicine

University College London

# Declaration

I, David Pearce, confirm that the work presented in this thesis is my own. Where information has been derived from other sources, I confirm that this has been indicated in this thesis.

# Abstract

Pulmonary fibrosis is a chronic and progressive scarring of the lungs for which there is no adequate therapy. Epigenetic mechanisms have been identified in the persistence of phenotype seen in explanted fibrotic fibroblast cells. Gene methylation and expression in fibrotic fibroblasts was compared to that of non-diseased controls and, through progressive filtering, fibulin-2 was identified as a potential gene of interest in pulmonary fibrosis.

Fibulin-2 is an extracellular matrix (ECM) glycoprotein which binds numerous other ECM components and competes with the sequestering of latent transforming growth factor (TGF)-β into the matrix. Fibulin-2 expression may be up- or down-regulated in tumours, and in breast cancer and nasopharyngeal carcinoma downregulation is associated with CpG hypermethylation. Its expression is upregulated during wound healing and fibrosis in several organs. In addition, deletion of fibulin-2 is protective in animal models of cardiac fibrosis. However, there is little information on the role and regulation of fibulin-2 in pulmonary fibrosis.

Expression of *FBLN2* was increased in fibrotic lung fibroblasts compared to controls and methylation analysis identified both hypo- and hyper-methylation of *FBLN2* which correlated with its expression. Immunohistochemical staining showed fibulin-2 localised predominantly to the alveolar interstitium, airway and vessel walls. Additionally, fibrotic lung tissue showed widespread diffuse staining associated with areas of ECM deposition.

In 2D and 3D *in vitro* models, fibulin-2 was strongly expressed and deposited by fibrotic lung fibroblasts and upregulated by treatment with $TGF\beta_1$. Control cells, however, produced comparatively little fibulin-2. Knockdown of FBLN2 expression by siRNA reduced the fibrotic markers collagen I and α smooth muscle actin in fibrotic lung fibroblasts in these models.

The results in this thesis demonstrate a potential role for fibulin-2 in the continued pathogenesis of pulmonary fibrosis and may represent a novel therapeutic target in the disease.

# Impact Statement

The work presented in this thesis describes the investigation of fibulin-2 in pulmonary fibrosis derived lung fibroblasts following its identification from genome wide expression and methylation data. Fibulin-2 is highly expressed within the lung of patients with pulmonary fibrosis and by explanted fibrotic lung fibroblasts but is limited in healthy controls. Depletion of fibulin-2 expression by siRNA treatment reduced expression of fibrotic markers in lung fibroblasts. Targeting fibulin-2 may therefore present novel therapeutic potential in the pathogenesis of pulmonary fibrosis.

The methods described in this thesis may have wider implications in the study of extracellular matrix (ECM) components. Rapid ECM deposition was seen in 2D culture conditions with and without molecular crowding and in 3D spheroid models. Modulation of a single ECM component yielded a quantifiable effect in these assay systems and they may therefore be of great value in the research of fibrotic disease.

# Acknowledgements

I would like to thank my primary supervisor, Professor Robin McAnulty, for all of his support throughout the many years I have spent in his lab. His guidance has been invaluable through my career as a technician and pursuing this PhD. Support and direction from past members of 'Team Robin' - Iona Evans, Josephine Barnes, Lizzie Peix, Cecilia Prêle and Ian Garner - has been vital to this and many other projects.

I would further like to thank the wider UCL Respiratory group, including my secondary supervisor Paul Mercer, Rachel Chambers, Manuela Platè, Ellen Forty, Delphine Guillotin and Jessica Ely.

This project and so much other work in our lab would not have been possible without the assistance, feedback and moral support of the lab 'Tea Club'. The friendship, laughter and informal discussion of every possible topic has been crucial to all of our sanity, in no particular order: Deborah Chong, Gabriella Szylar, Matthew Redding, Giuseppe Ercoli, Theresia Mikolasch, Elisa Ramos-Sevillano, Jagdeep Sahota, Emma Denneny and Gathoni Kamuyu.

Finally, I would like to thank my wife, Sian, my parents and family for their motivation and support throughout my studies.

# Table of Contents

# List of Figures

# List of Tables

# List of abbreviations

5Aza – 5-aza-2'-deoxycytidine
αSMA – alpha smooth muscle actin
ADAM – a disintegrin and metalloproteinase
ADAMTS – ADAM with a thrombospondin motif
ANOVA – analysis of variance
ATI – alveolar epithelium type I cell
ATII – alveolar epithelium type II cell
BSA – bovine serum albumin
CGI – CpG island
COPD – chronic obstructive pulmonary disease
COX–2 – cyclooxygenase-2
CpG – cytosine-guanine dinucleotides
DMEM – Dulbecco's Modified Eagle Medium
DMSO – dimethyl sulfoxide
DNMT – DNA methyl transferase
DNMT – DNA methyltransferase
ECM – extracellular matrix
EDTA – ethylenediaminetetraacetic acid
EMT – epithelial-mesenchymal transition
EndoMT – endothelial-mesenchymal transition
FCS – fetal calf serum
FDR – false discovery rate
GO – gene ontology
HBSS – Hanks' balanced salt solution
HC – high density CpG island
HLA – human leukocyte antigen
HPLC – high performance liquid chromatography
IC – intermediate-density CpG island
ILD – interstitial lung disease
IPF – idiopathic pulmonary fibrosis
LAP – latency–associate peptide
LC – low-density CpG island
LLC – large latent [TGFβ] complex
LOX – lysyl oxidase enzyme
LTBP – latent TGFβ binding protein
MBP – methyl-binding protein
MMP – matrix metalloproteinase
NS – non-significant
NT – non-targeting siRNA
PBS – phosphate buffered saline
PCR – polymerase chain reaction
PF – pulmonary fibrosis
PGE2 – prostaglandin E2

RIPA – Radioimmunoprecipitation assay buffer
RT–qPCR – Reverse transcription quantitative polymerase chain reaction
SDS – sodium dodecyl sulfate
siRNA – small interfering RNA
SSc – systemic sclerosis
TGFβ – transforming growth factor beta
TIMP – tissue-inhibitors of MMPs
TNoM – threshold number of misclassifications
UCSC – University of California, Santa Cruz, genome browser
UIP – usual interstitial pneumonia
UnT – untreated

# 1 Introduction

## 1.1 The Lung

The primary function of the lung is to exchange $O_2$ from inhaled air into the bloodstream and exhale $CO_2$. Gas exchange is achieved by passive diffusion across 480 million specialist alveolar capillary units (Ochs et al. 2004) consisting of epithelium and endothelium separated by an underlying interstitium. Often, the alveolar epithelium and capillary endothelium share a fused basement membrane, giving a diffusion distance ranging from approximately 2.2µm down to less than 0.5µm, and a total area for gas exchange in the lungs of around $70m^2$ (Gehr, Bachofen, and Weibel 1978). In order to adequately ventilate the entire lung including distal airspaces, the lungs must be compliant with the volume change of breathing while resisting strain through an interplay between surface tension forces and the elastic fibre system.

Alongside the mechanical challenges of breathing, the lungs are directly exposed to environmental insults such as pathogens, particulate matter and noxious gasses, including cigarette smoke, throughout life. Failure to maintain a tight regulation of repair mechanisms can lead to disruption of the fine architecture of the lung and to pulmonary diseases including COPD, emphysema and pulmonary fibrosis. The pathogenesis of organ fibrosis has been hypothesised to follow repeated epithelial cell injury which, either directly or indirectly through the recruitment of inflammatory cells, leads to the activation of effector cells, predominantly fibroblasts. Activated fibroblasts develop a highly synthetic and contractile phenotype and act to remodel the extra cellular matrix (ECM). Failure to resolve epithelial injury and inflammation together with autocrine-loop activation of effector cells continues to drive the fibrogenic process (Rockey, Darwin Bell, and Hill 2015).

## 1.2 Pulmonary fibrosis

Pulmonary fibrosis (PF) is a chronic and progressive scarring of the lungs that can occur either in isolation, as in idiopathic pulmonary fibrosis (IPF); as a result of environmental and drug toxicity; or as the pulmonary component of diffuse diseases such as systemic sclerosis (SSc). Although the endpoint of pulmonary dysfunction ultimately leading to respiratory failure and death remains common between these diseases, the pathogenesis of pulmonary fibrosis is heterogenous and poorly characterised.

### 1.2.1 Idiopathic pulmonary fibrosis

Idiopathic pulmonary fibrosis (IPF) is the most common diagnosis of the interstitial pneumonias. IPF prevalence is increasing over time with incidence highest in males and the disease risk increasing with age. Prognosis is poor with a median survival of 3 years and a mortality rate worse than that of many cancers, the disease is however very heterogenous with some patients remaining stable for some time (Navaratnam et al. 2011; Fernández Pérez et al. 2010; Raghu et al. 2011).

The diagnostic criteria for IPF primarily require the exclusion of other know causes of interstitial lung disease (ILD), such as those resulting from specific environmental exposures, drug toxicity or the presence of autoantibodies, followed by a usual interstitial pneumonia (UIP) pattern on high resolution computed tomography (HRCT) with or without confirmatory histological biopsy (Raghu et al. 2018). Radiographic patterns in UIP include subpleural honeycombing (cystic airspaces) and traction bronchiectasis/bronchiolectasis. Histologically UIP shows low magnification dense fibrotic remodelling of lung architecture (**Figure 1.2.1.1**) alternating with areas of less affected parenchyma and only mild inflammation (Raghu et al. 2018). The histological hallmark of IPF is the fibrotic focus, areas of dense ECM and activated fibroblasts underlying a convex abnormal hyperplastic epithelium (Scotton and Chambers 2007; Raghu et al. 2018).

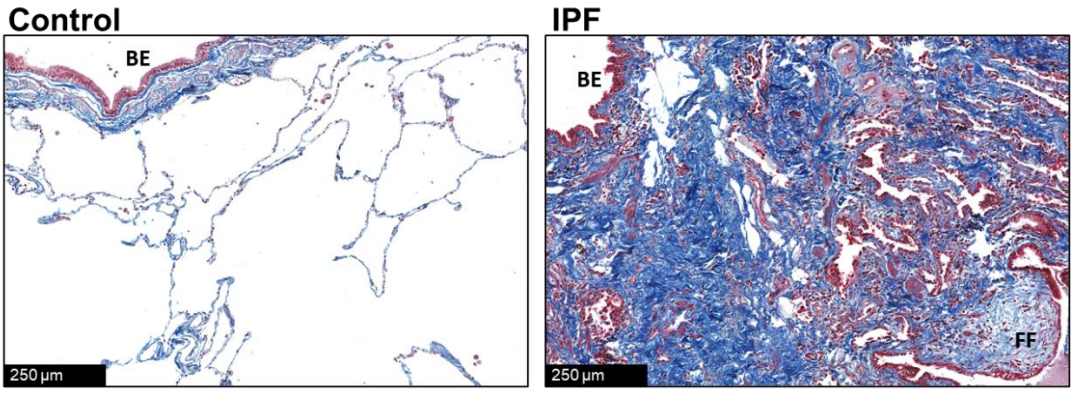


**Figure 1.2.1.1 Histology of the normal and fibrotic lung**

Trichrome staining of normal (control) and fibrotic (IPF) lung which stains collagen / ECM in blue and cellular components, including the bronchial epithelium (BE), red. The distorted architecture in IPF, including the hallmark fibrotic focus (FF), contrasts the open airspaces of the normal lung.

Therapeutic options in IPF are limited with only lung transplantation showing an increase in survival in eligible patients while anti-inflammatory and immunosuppressive medications are

ineffective and potentially deleterious (Raghu et al. 2015; Idiopathic Pulmonary Fibrosis Clinical Research Network et al. 2012). There are currently two drugs available for the treatment of IPF, Pirfenidone which has anti-oxidant and anti-fibrotic actions through unknown mechanisms (Noble et al. 2011; Taniguchi et al. 2010) and Nintedanib which is a tyrosine kinase inhibitor that targets profibrotic signalling receptors such as fibroblast growth factor receptors, platelet-derived growth factor receptors and vascular endothelial growth factor receptors (Wollin et al. 2014; Richeldi et al. 2014). These drugs however do not offer long term therapeutic benefit, therefore greater understanding the mechanism of disease may enable the discovery of therapies to address this unmet need.

The pathogenesis of IPF remains poorly understood with studies of the disease aetiology hampered by patients potentially presenting after the causative insult has passed and difficulty in assessing if, for example, a viral infection might be causative or the result of increased vulnerability to infection. Risk factors associated with IPF include cigarette smoking, exposure to environmental contaminants such as industrial dusts (Baumgartner et al. 2000; N. Zhang et al. 2019) as well as gastro-oesophageal reflux and viral infection.

Patients with IPF have a high prevalence of gastro-oesophageal reflux and it has been hypothesised that chronic micro-aspiration of gastric secretions may be a subclinical source of repetitive epithelial injury in the disease (Tobin et al. 1998; J. S. Lee et al. 2011).

Viral infections such as those caused by herpesviruses, Epstein-Barr virus (EBV), hepatitis C virus or adenoviruses have been implicated in IPF and exacerbations of IPF symptoms (Lawson et al. 2008; B. B. Moore and Moore 2015). However, research into the role of viruses in the pathogenesis of IPF is complicated not only by the lag between viral infection and the presentation of an IPF exacerbation, but also by the potential for viruses to be of significance during their latent state. The increased risk seen in immunosuppressive treatment in IPF patients could be attributed to the need for immune surveillance to control viral infection in the pathogenesis of IPF and IPF exacerbations (Idiopathic Pulmonary Fibrosis Clinical Research Network et al. 2012).

### 1.2.2 Genetic factors in IPF

Development of IPF likely requires a genetic predisposition resulting in sensitivity to repetitive epithelial injury and a failure in repair mechanisms. The strongest and most validated genetic variant associated with familial and sporadic IPF affects hyperexpression of mucin 5B (MUC5B) (Seibold et al. 2011; Noth et al. 2013; Allen et al. 2017). Interestingly, the

MUC5B risk allele (rs35705950; G>T) disrupts a CpG dinucleotide within a region which is differentially methylated in IPF (Helling et al. 2017). The mechanism by which MUC5B hyperexpression results in PF is the topic of continued study by a number of research groups.

Mutations in genes involved in alveolar stability have been associated with familial IPF or identified through genome wide association studies. These include surfactant proteins SFTPC and SFTPA2 and the lipid transport protein ABCA3. In accordance with the increasing incidence of IPF with age, genes involved in telomere maintenance (TERT and TERC) are also associated with increased risk in IPF. Other polymorphisms associated with IPF have been identified in the genes Toll-Like receptor interacting protein (TOLLIP); the cell-cell adhesion proteins desmoplakin (DSP) and DPP9; and the signalling protein AKAP13 (Noth et al. 2013; Fingerlin et al. 2013; Allen et al. 2017; Mathai et al. 2016).

Stratification of IPF patients by genotype will likely be vital for untangling the aetiology and potential therapies in such a heterogenous disease. This has recently been highlighted in a retrospective analysis of clinical trial data showing a therapeutic benefit of N-acetylcysteine in IPF for individuals with a TOLLIP rs3750920TT genotype but harm in those of the CC genotype (Oldham et al. 2015).

### 1.2.3 Systemic sclerosis

PF can also occur as the pulmonary component of a systemic disease such as systemic sclerosis (SSc). SSc is a disease of unknown aetiology with involvement of autoimmunity and vasculopathy resulting in the progressive fibrosis of multiple organs including the skin and lungs (Varga and Abraham 2007). SSc is more common in females, however males, who tend to present later in life, develop more severe disease (Chifflot et al. 2008). SSc exhibits a heterogenous disease course with evidence that vascular injury is an early event in development of the disease (Varga and Abraham 2007) however SSc associated pulmonary fibrosis and pulmonary hypertension are the leading causes of death in people with SSc (Steen and Medsger 2007).

There is a large geographical variation in prevalence of SSc both across the globe and within individual countries suggesting a strong role of environmental factors (Chifflot et al. 2008). Although the pathogenesis of SSc is not fully understood, the consensus is that environmental factors including silica, organic solvents and viral infection trigger the development of highly specific autoantibodies and disease in genetically susceptible individuals (Martinis et al. 2016; Gabrielli, Avvedimento, and Krieg 2009; Farina et al. 2014).

### 1.2.4 Genetic factors in SSc

Although a familial history of SSc or other autoimmune diseases is associated with an increased risk of developing SSc the low concordance rate for SSc disease onset in monozygotic twins indicates genetic predisposition is insufficient to entirely explain the disease development (Feghali-Bostwick, Medsger, and Wright 2003; Angiolilli et al. 2018). Instead, numerous genetic factors have been identified in susceptibility to SSc. The variants with highest associations in SSc are in class II HLA genes (HLA-DR, HLA-DQ, HLA-DP) although in different populations other mutations in HLA genes (HLA-DR and HLA-DQ) have been shown to be protective (Angiolilli et al. 2018; Furukawa et al. 2016). Non-HLA genes associated with SSc are often related to the immune system including interferon regulatory factor genes (IRF4, IRF5), those involved in interleukin-12 signalling (IL12RB1, IL12RB2 and STAT4) and B cell-specific scaffold protein (BANK1) (Angiolilli et al. 2018). A recent genome wide study in SSc confirmed associations with BANK1 and the ILD-related gene TERT, and identified a number of deleterious variants in genes associated with collagen biosynthesis pathways (COL4A3, COL4A4, COL5A2, COL13A1, COL22A1) (Mak et al. 2016).

## 1.3 Cellular functions in pulmonary fibrosis

Normal tissue repair during a wound healing response follows an overlapping sequence of events beginning with the clotting cascade and platelet aggregation which forms a fibrin clot rich in fibronectin, cytokines and growth factors. Along with an immune response to clear dead cells, matrix debris and pathogens, epithelial cells proliferate and migrate to re-establish their barrier function. Activated fibroblasts are then responsible for the deposition and remodelling of a mature matrix, after which they are cleared by apoptosis or de-differentiation (Horowitz and Thannickal 2019). Dysfunctions of multiple cell types involved in wound repair mechanisms have been proposed in the aetiology of PF including death and failed regeneration in the epithelium and persistent activation of fibroblasts.

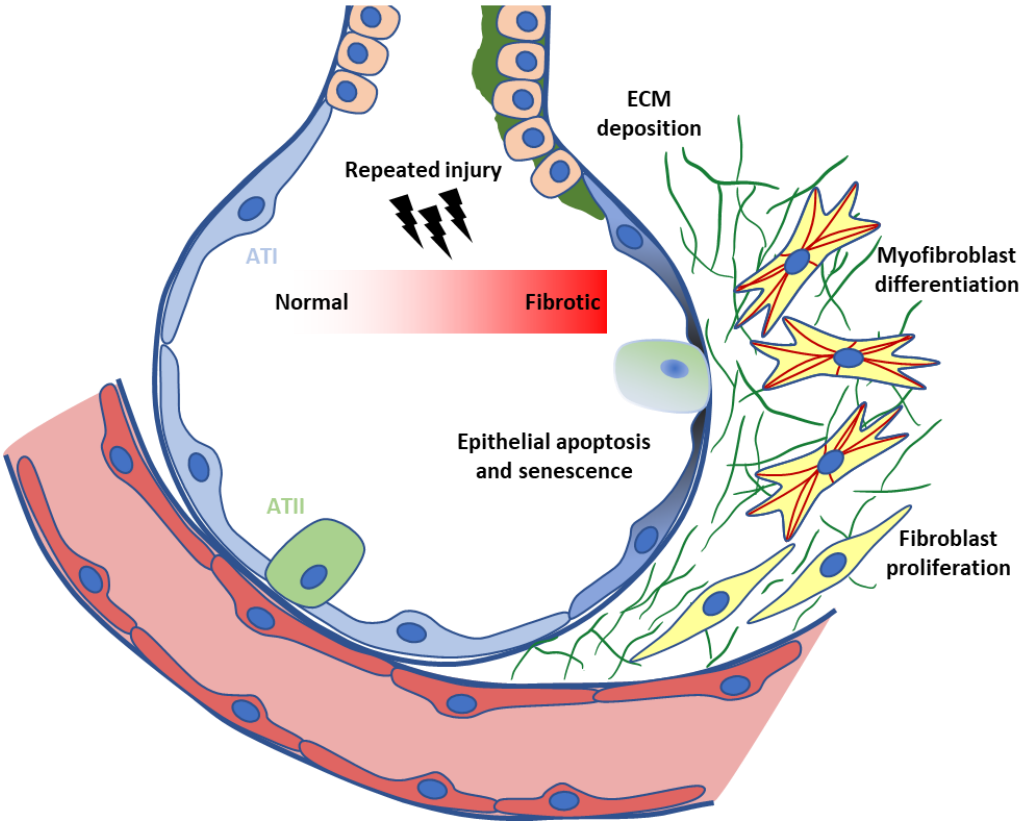


**Figure 1.2.4.1 Representation of the normal and fibrotic alveolus**

Adapted from (Meiners, Eickelberg, and Königshoff 2015)

### 1.3.1 Epithelial cell dysfunction in PF

The lumen of conducting airways are lined by a pseudostratified bronchial epithelium which are the first points of contact with environmental insults within the lung. The bronchial epithelium is composed of multiple cell types which fall into three categories based on their structure and function: basal, secretory and ciliated (Knight and Holgate 2003). Basal cells bind directly to the basement membrane and act both as a structural component and as progenitor cells for more superficial epithelial cells. Mucous cells produce a critical defence barrier by secreting viscoelastic mucus to trap foreign objects. Ciliated cells are the most numerous cells of the bronchial epithelium with the primary function of directional transport of mucus up the airways (Knight and Holgate 2003).

The alveolar surface is made up of a mosaic of alveolar epithelium type I (ATI) cells which have a flattened morphology, interspersed with single alveolar type II (ATII) cells. ATII cells cover ~5% of the alveolar surface area, behaving as limited progenitor cells during repair and regeneration of ATI cells. ATII cells also synthesise components of the basement membrane and secrete surfactant, a specialist fluid consisting predominantly of lipids and surfactant

proteins which act to lower the surface tension within the alveolus, preventing its collapse at low lung volumes.

In IPF there is dysfunction of alveolar epithelial cells and bronchiolisation of the alveoli, a process whereby bronchial epithelial cells proliferate and migrate into the alveolus (Meiners, Eickelberg, and Königshoff 2015). ATII cells show endoplasmic reticulum stress markers, senescence and enhanced apoptosis following environmental insults, viral infection, ageing and due to genetic factors (Lawson et al. 2008; Winters et al. 2019). ATII cells have been reported to produce and activate a number of profibrotic mediators including transforming growth factor beta (TGFβ) (Tatler and Jenkins 2012; Lehmann et al. 2018) and extracellular vesicles produced by epithelial cells have recently been implicated in promoting fibroproliferation (Parimon et al. 2019).

Epithelial cells may also be a direct source of fibroblast like cells through epithelial-mesenchymal transition (EMT) which is essential during embryonic development but has proven controversial in fibrosis research. EMT is the process whereby epithelial cells undergo phenotypic changes in cell adhesion and motility, downregulate epithelial markers and gain a mesenchymal phenotype including production of ECM components. However, there is no consensus on markers for EMT in patient lung samples and lineage tracing experiments in mouse models of fibrosis have shown a varying contribution of EMT to fibroblast numbers (K. K. Kim et al. 2006; Rock et al. 2011; Bartis et al. 2014; Skrypek et al. 2017).

Pirfenidone and Nintedanib demonstrate reductions in profibrotic markers in *ex vivo* lung tissue culture and isolated primary ATII cells. The mechanisms by which Pirfenidone act remain unknown but the tyrosine kinase inhibitor Nintedanib stabilises distal epithelial markers in ATII cells which might contribute to its antifibrotic actions (Lehmann et al. 2018).

### 1.3.2 Fibroblasts in PF

Lung fibroblasts are the key effector cells in fibrotic disease and the focus of this thesis. Fibroblasts are the main cell type responsible for the complex homeostatic balance of the ECM in normal tissues with continuous synthesis and deposition of ECM components and the production of ECM degrading enzymes and their inhibitors. Under wound conditions or in disease, fibroblasts migrate, proliferate and differentiate into highly synthetic myofibroblasts which have a contractile phenotype through expression of alpha smooth muscle actin (αSMA) (R. J. McAnulty 2007; Hinz et al. 2001). Activation of fibroblasts proceeds along a spectrum with quiescent fibroblasts initially becoming protomyofibroblasts

which gain expression of the ED-A fibronectin variant, contain stress fibres with focal adhesions, but which do not contain αSMA (Serini et al. 1998; Falke et al. 2015). During the resolution of normal wound healing, myofibroblasts are cleared by apoptosis, however resistance to apoptosis has been shown in fibroblasts derived from IPF lungs. The mechanisms of apoptosis resistance in fibroblasts include; deficiency in the pro-apoptotic and antifibrotic mediator prostaglandin E2 ($PGE_2$) (Maher et al. 2010; S. K. Huang et al. 2013); deficiency in clusterin expression (Peix et al. 2018); suppression of Fas expression (Matsushima and Ishiyama 2016; Dodi et al. 2018) together with upregulation of a FasL decoy receptor (Im et al. 2016); and activation of pro-survival pathways involving focal adhesion kinase (FAK) (Horowitz et al. 2007; Lagares et al. 2012; Kinoshita et al. 2013).

Multiple sources of activated proto/myofibroblasts, beyond activation and proliferation of resident lung fibroblasts, have been proposed and their contributions to the fibrotic phenotype assessed experimentally (R. J. McAnulty 2007). EMT of the alveolar epithelium is discussed above, however, a study in the bleomycin-induced lung fibrosis mouse model failed to show a contribution from ATII cell EMT, instead demonstrating that proliferation of lung pericyte-like cells in the alveolar interstitium was a significant contributor to the origin of myofibroblasts (Rock et al. 2011; Hung et al. 2013). Transgenic lineage tracing in the bleomycin model has also identified lung fibroblasts expressing endothelial markers, suggesting that endothelial-mesenchymal transition (EndoMT) also contributes to myofibroblast populations (Hashimoto et al. 2010). The contribution of circulating fibrocytes is also suggested in the literature with elevated fibrocyte numbers in the blood being an indicator of poor prognosis in IPF (Moeller et al. 2009). Data from the bleomycin model questions their contribution to lung collagen accumulation (Kleaveland et al. 2014), although this may be a species specific response or a limitation of the model mechanisms.

Fibroblast activation is driven by the imbalance of pro- and anti-fibrotic mediators from a number of sources including the epithelium, immune cells, the ECM, and from fibroblasts through paracrine and autocrine signalling. Numerous cytokines, chemokines and growth factors have been demonstrated to induce a profibrotic phenotype in fibroblasts including IL-6 (O'Donoghue et al. 2012), platelet derived growth factor (PDGF) (Scotton and Chambers 2007), connective tissue growth factor (CTGF; CCN2) (S. Liu et al. 2011), the Wnt/β-Catenin Pathway (T. H. Kim et al. 2011), and the prototypic profibrotic cytokine transforming growth factor-β (TGFβ, discussed in section 1.4).

Fibroblast transdifferentiation is also negatively regulated by a number of factors including prostaglandin E2 ($PGE_2$), prostacyclin ($PGI_2$) (Stratton et al. 2001; Y. Zhu et al. 2010), peroxisome proliferator-activated receptor γ (PPARγ) agonists (Milam et al. 2008) and hepatocyte growth factor (HGF) (Crestani et al. 2012). We and others have shown that there is defective antifibrotic $PGE_2$ production in fibroblasts derived from the lungs of IPF patients compared with controls (Keerthisingam et al. 2001). This is due to reduced expression of the rate limiting enzyme cyclooxygenase-2 (COX-2) (Coward et al. 2009; Evans et al. 2016) and this deficiency leads to fibroproliferation, collagen production and apoptosis resistance in fibrotic lung fibroblasts (Keerthisingam et al. 2001; Maher et al. 2010).

Mechanosensing is also a significant source of fibroblast activation and driver of the myofibroblast phenotype. Myofibroblasts form mature focal adhesions, with *de novo* expression of protein tyrosine kinase 2 (PTK2; also known as focal adhesion kinase, FAK). These focal adhesions contribute to myofibroblast contractile phenotype and enable transduction of matrix stiffness sensing (Dugina et al. 2001). FAK is essential for TGFβ-mediated induction of the myofibroblast phenotype and inhibition of FAK is antifibrotic in the bleomycin mouse model of lung fibrosis (Lagares et al. 2012; Kinoshita et al. 2013). Experiments performed on gel culture substrates containing a stiffness gradient by Liu et al. (2010) demonstrated differences in normal human lung fibroblast cell line morphology from attenuated, rounded cells at stiffnesses below that of normal lung through to spindle-like fibroblasts growing in parallel at high stiffness. Intermediate stiffness, comparable to that of the normal lung, yielded fibroblasts with multiple dendritic processes. These morphological changes accompanied contrasting apoptosis at lower stiffness and proliferation at higher stiffnesses. Collagen expression also increased with increasing stiffness. The authors attributed these findings to autocrine feedback through attenuated COX-2 expression and lower $PGE_2$ production at higher stiffnesses (F. Liu et al. 2010).

A number of other signalling pathways have been implicated in mechanosensing in fibroblasts. Loss of Thy-1 (CD90), which apart from interacting with Fas and promoting apoptosis, also interacts with and enhances αvβ3 integrin activity, results in enhanced fibroblast activation on soft substrates (Fiore et al. 2018). These various roles result in Thy-1 null mice displaying a failure to resolve fibrosis in the bleomycin mouse model (X. Liu et al. 2017). F. Liu et al. (2015) have further shown a role for the Hippo pathway transcriptional coactivators YAP and TAZ in mechanosensing in cultured fibroblasts. STAT3 signalling, which had previously been implicated in PF (O'Donoghue et al. 2012; Pechkovsky et al. 2012; Papaioannou et al. 2018), has also been shown to be activated in a cytokine ligand

independent manner through ROCK and JAK2 on stiff matrix (Oh et al. 2018). Matrix stiffness is also a key player in the activation of latent TGFβ.

## 1.4 TGFβ

Transforming growth factor-β (TGFβ) is a well-established mediator of the fibrotic phenotype in fibroblasts and has been studied extensively. TGFβ stimulation alone is sufficient to induce collagen production and metabolic reprogramming, *de novo* αSMA expression and apoptosis resistance in cultured lung fibroblasts (R J McAnulty et al. 1991; Kulasekaran et al. 2009; Selvarajah et al. 2019). TGFβ is the prototypic member of a growth factor superfamily consisting of TGFβ-like and bone morphogenic protein (BMP)-like members. TGFβ regulates fundamental cellular processes including proliferation, differentiation and cytoskeletal organisation throughout the lifetime of an organism. This makes the cytokine vital during development and for tissue homeostasis, inflammation and immunoregulation (Wahl 1992; Crowe, Doetschman, and Greenhalgh 2000). Three isoforms of TGFβ exist: TGFβ1, TGFβ2 and TGFβ3. Although these isoforms share 71-80% sequence identity they have overlapping and non-overlapping functions (T. Huang, Schor, and Hinck 2014). Despite behaving similarly in cell-based assays, isoform-specific null mice are each unviable with differing phenotypes. Mice deficient in TGFβ1 have a proinflammatory phenotype, especially prominent in the heart and lungs, and die at 3-4 weeks of age (Shull et al. 1992; Kulkarni et al. 1993). TGFβ2 null mice exhibit perinatal mortality with multiple organ defects (Sanford et al. 1997) whereas TGFβ3 null mice die within 20 hours of birth with delayed pulmonary development and cleft palate (Kaartinen et al. 1995; Proetzel et al. 1995).

### 1.4.1 TGFβ synthesis

TGFβ is a small (25kDa) homodimeric protein secreted by multiple cell types including macrophages (Grotendorst, Smale, and Pencev 1989), endothelial cells (Ohno et al. 1995), alveolar type II cells (Xu et al. 2003), bronchial epithelium (Sacco et al. 1992), fibroblasts (Kelley et al. 1991), and from platelet stores (Assoian and Sporn 1986). TGFβ1 is synthesised from a large protein precursor, pre-pro-TGFβ, containing the TGFβ signalling peptide and latency-associate peptide (LAP). Dimerised TGFβ peptides and LAPs are cleaved by furin before secretion but remain non-covalently associated forming the small latent complex (SLC) (Blanchette et al. 1997). After secretion, LAP shields the signalling peptide from receptor recognition (Shi et al. 2011). In order to be efficiently secreted, the SLC must be covalently bound to a latent TGFβ binding protein (LTBP-1, -3 or -4) to form the large latent complex (LLC) (Nüchel et al. 2018). LTBP-2 does not bind TGFβ but is proposed to have a

regulatory role (Robertson et al. 2015). After secretion, this LLC is sequestered into the ECM from which the bioactive signalling peptide must be activated.

### 1.4.2 TGFβ activation from the matrix

Secreted TGFβ is sequestered into the ECM which acts as a 'reservoir' for cytokine signalling without the need for de-novo synthesis. Initial LLC-matrix interactions occur at the cell surface involving fibronectin fibrils and heparan sulfate proteoglycans. Active cell remodelling of the matrix then localises LLCs to fibrillin-rich microfibrils and fibrillin polymers. Although additional binding partners have been identified for different isoforms of LTBPs, their binding into the matrix is predominantly to fibrillin-1 and fibronectin (Ono et al. 2009; Robertson et al. 2015). As such fibrillin-1 deficiency leads to elevated release of active TGFβ and Marfan syndrome, characterised by connective tissue abnormalities (Doyle, Gerber, and Dietz 2012; Costanza et al. 2017). The small leucine-rich proteoglycan (SLRP) family, including decorin, biglycan, asporin and fibromodulin are also negative regulators of TGFβ bioavailability through their ability to bind TGFβ. Biglycan and decorin inhibit TGFβ in a dose dependant manner *in vitro* and decorin overexpression significantly reduced lung fibrosis in a murine TGFβ overexpression model (Kolb et al. 2001).

For TGFβ to be bioactive it must be liberated from its latent complex. Activation can occur through a number of mechanisms such as changes in pH, reaction with radical oxygen species, proteolytic digestion and mechanical stretch mediated by the binding of cell surface integrins (Lyons, Keski-Oja, and Moses 1988; Ono et al. 2009; Shi et al. 2011) (**Figure 1.4.2.1**).

Conformational change of the latent complex induced by cell pulling is a significant mechanism by which TGFβ can be liberated. This is dependent on integrin binding to the RGD tripeptide domain on latent TGFβ1 or -3 and latent protein binding to the matrix and is therefore enhanced in a stiffer matrix (Wipff et al. 2007). Conditional depletion of the $\alpha_V$ integrin subunit in myofibroblasts or its blockade is protective in the bleomycin model of PF (Henderson et al. 2013) and mice with mutated RGD integrin binding sites in the LAP of TGFβ1 display a similar phenotype to TGFβ1-null animals (Z. Yang et al. 2007; Aluwihare et al. 2009). Mechanical activation of TGFβ has been demonstrated via integrins αvβ1, αvβ3, αvβ5 and αvβ6 (Wipff et al. 2007; Costanza et al. 2017). Interestingly αvβ8 integrin does not activate TGFβ by mechanical pulling but through the enzymatic action of membrane type 1 matrix metalloproteinase (MT1-MMP; MMP14) (Mu et al. 2002).

MT1-MMP, along with matrix metalloproteinase (MMP)-2, MMP9, thrombin, plasmin and BMP-1 can also proteolytically cleave LTBP1 resulting in the release of latent TGFβ from the ECM. Active TGFβ can then be liberated by proteolytic cleavage of LAP by MMPs-2, -3, -9 and -13. (Blakytny et al. 2004; Krstic and Santibanez 2014; Costanza et al. 2017). Activation of pericellular TGFβ may be enhanced through the actions of CD44-associated MMP-2 and MMP-9 (Yu and Stamenkovic 2000), and MMP-9 recruited to the cell surface by lysyl hydroxylase 3 (LH3) (Dayer and Stamenkovic 2015). The adhesive glycoprotein Thrombospondin-1 (TSP1; THBS1) is also able to liberate active TGFβ by inducing a conformational change in LAP through direct binding. TSP1 null mice show a phenotype similar to those lacking TGFβ1 (Crawford et al. 1998).

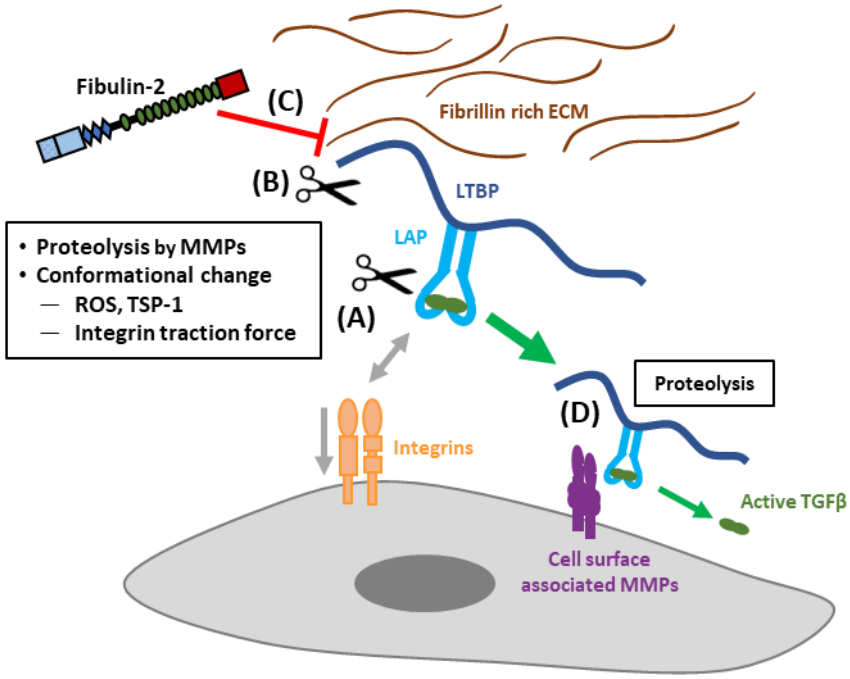


**Figure 1.4.2.1 Latent TGFβ activation from the ECM**

(**A**) TGFβ may be activated directly from the matrix by proteolytic cleavage or conformational change of latency associated peptide (LAP). (**B**) Proteolytic cleavage of latent TGFβ binding protein (LTBP) or (**C**) competition for its binding to the matrix by fibulin-2 allows (**D**) proteolytic activation at the cell surface. Adapted from Costanza et al. (2017).

### 1.4.3 TGFβ signalling

TGFβ signals through the cell surface TGF-β type I and type II receptors (TβRI or ALK5, and TβRII, respectively) by sequential assembly of a $T\beta RI_2$-$T\beta RII_2$ heterotetramer. TGFβ is first bound to the high affinity TβRII which creates a cleft that accommodates recruitment of TβRI

(Groppe et al. 2008). Heterotetramerisation enables the transphosphorylation of the TβRI negative regulatory domain by TβRII, activation of the TβRI serine-threonine kinase and subsequent phosphorylation of the receptor regulated SMADs. TβRI and TβRII have a significantly lower affinity for TGFβ2 than TGFβ1 and 3. For TGFβ2 signalling, TβRIII (betaglycan) is required to present the TGFβ2 ligand which is otherwise unable to bind to TβRII (López-Casillas, Wrana, and Massagué 1993).

Canonical TGFβ signalling entails the phosphorylation of receptor-regulated SMADs, such as SMAD2/3, enabling their binding to SMAD4. This results in the accumulation of SMAD complexes in the nucleus which target specific promoters and utilise high affinity binding partners to regulate gene expression (Weiss and Attisano 2013). Non-canonical TGFβ signalling which occurs in a more cell-specific manner may proceed through various pathways including PI3K-mTOR, Rho family GTPases and MAPKs (Ponticos et al. 2015; Costanza et al. 2017; Selvarajah et al. 2019)

## 1.5 The ECM

The ECM in the lung, composed of the basement membranes and interstitial matrices, provides not only a physical scaffold for the cells but is bioactive, being sensed directly by cells and sequestering growth factors. The interstitial ECM, which creates the 3D cohesiveness and biomechanical characteristics of the tissue, is dominated by collagens which have high tensile strength and low elasticity, and elastic fibres which are of low strength and highly elastic. The basement membranes, which are thin sheets covering the basal side of the epithelium and endothelium, are composed predominantly of collagen IV and the proteoglycan perlecan, alongside nidogen, laminins and fibulin-2.

Recent work has defined ECM components and proteins that may interact or remodel the ECM as the matrisome (Naba et al. 2016). Mass spectroscopy (MS) of decellularized human lung has identified 61 core ECM proteins (collagens, glycoproteins and proteoglycans) and 33 ECM associated proteins in the matrisome of the lung (Booth et al. 2012), though this was likely an underestimate because of the difficulty in fully digesting the ECM to its constituent parts.

### 1.5.1 ECM components of the lung

**Collagen**

Collagens are the most abundant ECM components in the lung with collagens type I and III predominant in the alveolar interstitial ECM (Bateman, Turner-Warwick, and Adelmann-Grill

1981). To date 29 types of collagen have been identified falling into two classes; fibrillar collagens (types I, II, III, V and XI), which form the major structural components of connective tissue, and non-fibrillar collagens, which have a network forming role in the ECM, including collagen IV, a core component of the basement membrane (Domene, Jorgensen, and Abbasi 2016).

The defining structure of collagen molecules is a triple helix formed of three parallel polypeptide strands. Fibrillar collagens are usually heterotrimeric with the most abundant form of collagen in the lung, collagen I, often consisting of two alpha-I and one alpha-II chains. Collagen III however is a homotrimer containing three α1(III) chains. The tight helical structure of collagen requires a repeating amino acid triplet sequence Glycine-X-Y, where X and Y can be any amino acid. Disruption of this Glycine-X-Y triplet at certain locations confers the non-helical domains of non-fibrillar collagens (Brazel et al. 1987). The most frequent trimer is Glycine-Proline-Hydroxyproline with these residues conferring maximal strength by increasing the thermal stability of the triple helix (Ramshaw, Shah, and Brodsky 1998).

Hydroxyproline constitutes approximately 12.2% of collagen by weight while not being present in significant amounts in other proteins making hydroxyproline quantification a valuable experimental technique in fibrosis research (Laurent et al. 1981). Enzymatic hydroxylation of proline and lysine residues is an important initial step in collagen biosynthesis to enable helical folding and requires ascorbic acid as a cofactor (Canty and Kadler 2005). Helix formation is then initiated at the c-terminal propeptide of the procollagen strands to yield a soluble procollagen triple helix. Once secreted, the large non-helical N- and C- terminal peptides are cleaved resulting in insoluble tropocollagen terminated with N- and C- terminal non-helical telopeptides. Collagen fibrillogenesis from tropocollagen is intertwined with fibronectin assembly both of which require cell surface integrins (Canty and Kadler 2005). Once assembled, the extracellular collagen matrix is strengthened by intra- and inter-molecular crosslinking between lysine and hydroxylysine residues by lysyl oxidase (LOX) enzymes (Barry-Hamilton et al. 2010).

**Elastin**

Elastic fibres are responsible for the intrinsic recoil of the lung. The elastic fibre system is established during development and the postnatal period, with mature parenchymal elastic fibres metabolically stable over the human lifespan due to extensive crosslinking with little new synthesis seen in the undiseased lung (Shapiro et al. 1991). Elastogenesis is a multistep process beginning with the secretion and aggregation at the cell surface of soluble

tropoelastin bound to 67kDa elastin-binding protein (EBP67). These aggregates are then recruited to the fibrillin based microfiber scaffold where they fuse and are crosslinked by LOX and LOX-like I enzymes (Mecham 2018). Many proteins are associated with elastic fibres and are required for correct elastogenesis including, LTBPs, proteoglycans and fibulins (Dabovic et al. 2015; Q. Chen et al. 2009; Kielty 2006; Yanagisawa and Davis 2010; Yamauchi et al. 2010). Data from our lab has also shown a potential role for clusterin in the processing and protection of elastic fibres (Peix et al. 2018).

**Glycoproteins**

Fibronectin is a dimeric glycoprotein which contains cell surface integrin binding sites that is widely distributed in the ECM and plasma, and is upregulated in wound healing. Alternative splicing results in numerous isoforms of the protein one of which, containing alternatively spliced domain A (ED-A), is implicated in fibroblast activation (Serini et al. 1998; Kohan et al. 2010). Laminins are heterotrimeric glycoproteins with multiple isoforms having a cross-shaped structure which contain cell binding sites along one long arm and establish non-covalent interactions with other ECM components via the three short arms. Laminin interactions are a pre-requisite for basement membrane assembly (Horejs 2016). Glycoproteins Nidogen-1 and -2 are ubiquitously expressed in basement membranes throughout the body where they bind multiple ECM components (LeBleu, Macdonald, and Kalluri 2007).

**Proteoglycans**

Proteoglycans contain a protein core covalently linked to glycosaminoglycan chains, this makes them highly hydrophilic forming hydrogels which fill the majority of the extracellular space and resist compressive forces in the lung matrix (Frantz, Stewart, and Weaver 2010). Proteoglycans are found in both the basement membranes, such as perlecan and agrin, and in the interstitial ECM, including aggrecan and versican. The proteoglycans decorin and biglycan which are able to bind and inhibit TGFβ were the most abundant proteoglycans in a proteomic analysis of the mouse lung (Kolb et al. 2001; Burgstaller et al. 2017).

### 1.5.2 ECM degradation

The degradation of the ECM is controlled by a balance between the actions of matrix degrading enzymes, predominantly matrix metalloproteinases (MMPs) and adamalysins, along with serine proteases, and their inhibitors, tissue-inhibitors of MMPs (TIMPs).

MMPs are a large group of zinc-dependent endopeptidases with overlapping specificities and redundancy allowing them to collectively degrade all ECM and basement membrane components (P. Lu et al. 2011). Most MMPs are secreted while membrane-type MMPs (MT-MMPs) possess a transmembrane domain. All MMPs are synthesised in inactive pro-MMP forms and may be secreted following intracellular activation or in this pro-MMP form. Activation can then occur by proteolytic cleavage of their pro-domain or by chemical modification such as by reactive oxygen species (Löffek, Schilling, and Franzke 2011). As well as degrading the ECM, MMPs cleave a range of bioactive mediators releasing them from the matrix, including latent TGFβ, and cleave and activate pro-MMP precursors.

The adamalysin family includes a disintegrin and metalloproteinases (ADAMs) and ADAMs with a thrombospondin motif (ADAMTSs) which contain a disintegrin domain that bind integrins and mediates cell-cell and cell-ECM interactions (P. Lu et al. 2011; Bonnans, Chou, and Werb 2014).

TIMPs are a group of 4 secreted proteins which bind and reversibly inhibit MMPs. They are generally broad-spectrum inhibitors of MMPs but with differing abilities to inhibit various MMPs across the family (Selman et al. 2000). TIMP3 which is the main inhibitor of ADAMs and ADAMTSs is, unlike other TIMPs, sequestered into the matrix. TIMP3 has also been shown to inhibit signalling of vascular endothelial growth factor (VEGF) by binding to VEGF receptor-2 indicating a potential role for TIMPs beyond their MMP inhibitory function (Qi et al. 2003).

### 1.5.3 The ECM in PF

The histological hallmark of IPF is the fibrotic focus, a collagen I rich ECM aggregate populated by myofibroblasts and overlaid by a hyperplastic epithelium. The fibrotic focus core is also enriched with collagen III, collagen VI, fibronectin, versican and tenascin C; along with hyaluronan which is not found in the normal lung. Collagen IV expression is variable (Herrera, Henke, and Bitterman 2018; Herrera et al. 2019). Ultrastructurally, transmission electron microscopy of decellularized lung tissue shows organised collagen fibres and elastin bundles traversing the interstitium and intact, homogenous basement membranes in normal lung but disorganised ECM and disrupted basement membranes in IPF (Booth et al. 2012).

Proteomic analysis of IPF lung demonstrates differences in the content of many matrisome and associated proteins including increases in collagens, LTBP1 and fibulin-2 and decreases in components of the alveolar basement membrane (Booth et al. 2012). Proteomic analysis

of lung tissue is however limited by the dissociation techniques used, for example elastin was not identified by Booth et al. (2012) in normal or IPF lung due to its resistance to the trypsin digestion used. Using more robust protein extraction steps, elastin, along with numerous collagens, laminins, fibulin-5 and fibrillin-1 were shown to have upregulated synthesis following bleomycin injury in the mouse. Another study utilising proteome profiling of mouse lung following bleomycin injury during the subsequent phases of inflammation, fibrosis and resolution found 3,032 proteins which were changed significantly in at least one timepoint including 154 matrisome components (Schiller et al. 2015). The authors correlated proteomic data with the compliance ratio of the bleomycin treated lung versus PBS treated controls and found that numerous proteins correlated with lung compliance including negative correlations with tenacin C and fibulin-2 (i.e. higher expression in stiffer lungs); and positive correlations with Col4a5 and desmoplakin (Schiller et al. 2015).

Altered expression of many MMPs and TIMPs has been shown in PF with higher expression of TIMPs than of matrix degrading MMPs shown in IPF lungs contributing to a non-degrading microenvironment (Selman et al. 2000; Pardo et al. 2016). The relationship between MMPs, TIMPs and fibrosis is however not simple with MMPs and TIMPs influencing many cell processes. For example, mice lacking MMP-3, -7 or -8 are protected from bleomycin induced fibrosis whereas MMP-7, -13 and -19 null mice show increased fibrosis (Zuo et al. 2002; Pardo et al. 2016). TIMP3 null mice show persistent inflammation following bleomycin lung injury (Gill et al. 2010) and increased renal fibrosis (Kassiri et al. 2009).

As well as increased expression of collagen in the fibrotic lung, increased collagen cross-linking associated with upregulated expression of LOX and LOXL2 enzymes has been observed in the fibrotic foci of IPF lungs. Enzymatically active LOX-like enzymes are crucial for myofibroblast activation (Aumiller et al. 2017). Inhibition of LOXL2 in the bleomycin mouse model prevented fibrosis and promoted lung repair with a significant reduction in fibroblast activation and recruitment and fibrosis markers (Barry-Hamilton et al. 2010). Increased crosslinking results in a stiffer matrix, and assessment of native tissue stiffness demonstrated a significant increase in mean tissue stiffness in IPF compared to healthy controls (16.52 ±2.25 kPa and 1.96 ±0.13 kPa, respectively) (Booth et al. 2012). The tissue microenvironment is sufficient to drive a fibrotic phenotype. Fibroblasts from either control or IPF donors demonstrate a more profibrotic phenotype when cultured on decellularized ECM derived from IPF patients than on that from control lungs. This is partially through TGFβ independent mechanisms demonstrating the ability of the ECM composition and stiffness to dictate the cellular phenotype (Booth et al. 2012; Parker et al. 2014).

## 1.6 The Fibulins

Fibulin-2, a 180kDa extracellular matrix glycoprotein, was identified in this thesis as upregulated in pulmonary fibrosis through analysis of expression and methylation data from explant fibroblasts, and subsequently in lung tissue from donors with pulmonary fibrosis. The fibulin family comprises eight ECM glycoproteins characterised by a unique C-terminal fibulin-type module domain (fibulin-type carboxyl-terminus, FC) and tandem repeat calcium binding epidermal growth factor (EGF)-like domains. The fibulins serve as scaffold proteins forming intermolecular bridges with a variety of ECM components. Although structurally related, their functions and binding partners vary. The fibulin family is subdivided into three groups: long fibulins, short fibulins and hemicentins.

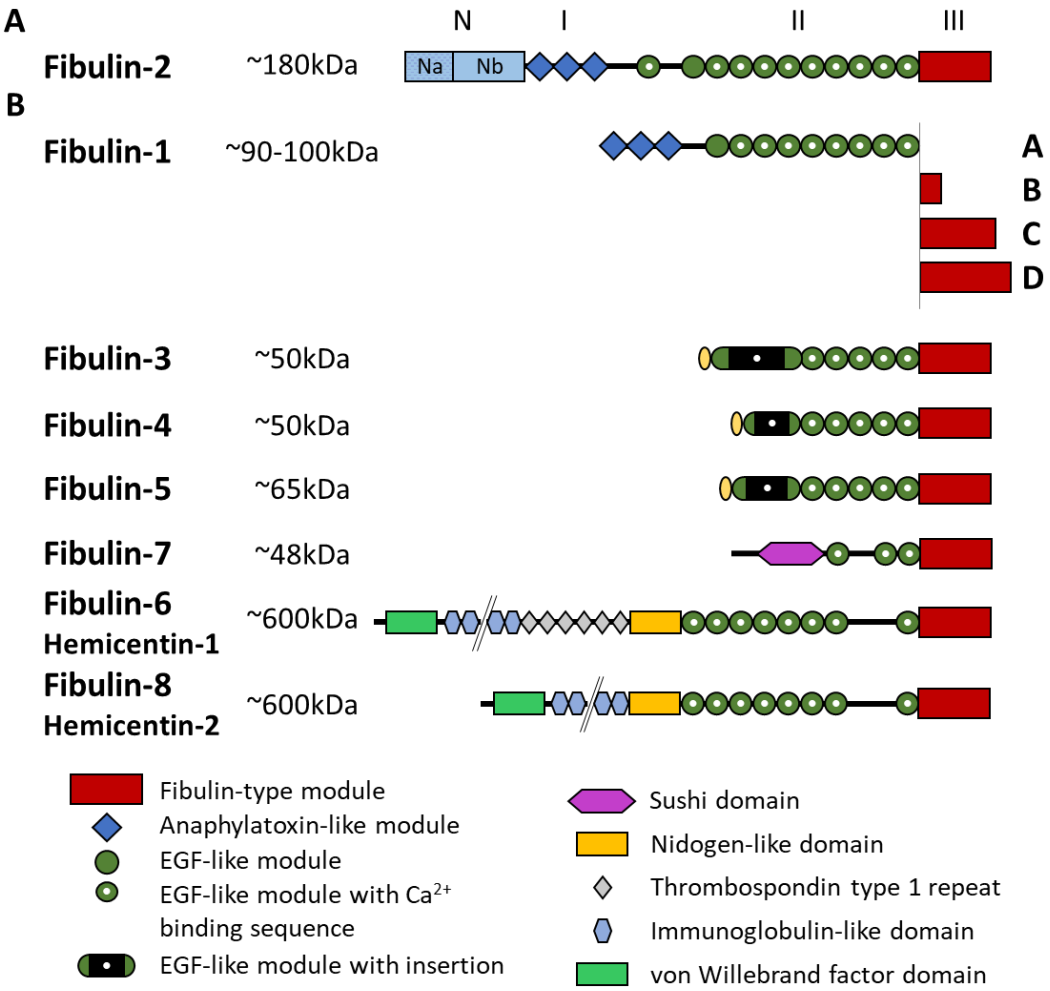


**Figure 1.5.3.1 Fibulin family structures**

(**A**) The structure of Fibulin-2 showing the conserved fibulin-type carboxy-terminus (III) and anaphylatoxin- and EGF-like domains (I and II respectively). Fibulin-2 also contains a unique N-terminal domain consisting of cystine-rich (Na) and cystine free (Nb) regions. (**B**) The structure of the other fibulin family proteins. (Figure adapted from Cangemi et al. 2014 and Nakamura 2018)

### 1.6.1 Long Fibulins

The long fibulins consist of Fibulin-1 and -2. The first fibulin discovered, fibulin-1 (FBLN1, previously also known as BM-90) is present as 4 variants in humans (Fibulin-1a-d) with differing c-terminal domains, however only variants -c and -d are present in mice (Timpl et al. 2003). In the developing mouse fibulin-1 expression is prominent in areas of epithelial-mesenchymal transition (H.-Y. Zhang et al. 1996). Fibulin-1 expression in the adult human is predominantly in tissue rich in elastic fibres such as blood vessels and the lung (Roark et al. 1995). Fibulin-1 binds to multiple ECM components including fibronectin, versican, nidogen,

tropoelastin, LTBP1 and ADAMTS-1 (S. De Vega, Iwamoto, and Yamada 2009; G. Liu et al. 2019; N. V. Lee et al. 2005).

Total Fbln1 deficiency in mice is perinatally lethal due to defects in the basement membranes of various organs resulting in haemorrhage (Kostka et al. 2001), however mice deficient in only Fbln1c are viable and are protected from bleomycin induced pulmonary fibrosis through attenuated TGFβ activation (G. Liu et al. 2019). *In vitro*, fibulin-1c induces airway smooth muscle cell and fibroblast attachment and proliferation (Ge et al. 2015).

Fibulin-1 is also present in plasma where it has been identified as a potential biomarker of IPF. Serum levels of fibulin-1 were increased in IPF patients compared to control subjects, with serum levels predictive of IPF disease progression. Increased levels of fibulin-1 in lung tissue of patients with IPF and increased expression in isolated lung fibroblasts from IPF subjects were also shown (Jaffar et al. 2014).

Fibulin-2 is discussed in detail below in **section 1.7**.

### 1.6.2 Short Fibulins

The short fibulins contain at most 6 EGF-like domains and lack the anaphylatoxin-like domain found in fibulin-1 and -2. The group consists of fibulins-3, -4, -5 and -7.

Fibulin-3 (EFEMP1; EGF-containing fibrillin-like extracellular matrix protein 1) was identified as overexpressed in senescent fibroblasts from a Werner syndrome patient (Lecka-Czernik, Lumpkin, and Goldstein 1995). It is expressed by epithelial and endothelial cells throughout the body in association with elastic tissues and basement membranes. Fibulin-3 deficient mice show early aging and herniation (McLaughlin et al. 2007). Fibulin-3 inhibits TGF-β signalling via interaction with TβRI to decrease TβRI/TβRII complex formation. In the breast cancer microenvironment, reduced fibulin-3 expression promotes TGFβ-mediated EMT, migration and invasion (Tian et al. 2015).

Fibulin-4 (EFEMP2) is highly expressed in the large blood vessels where it is essential for elastic fibre assembly including by tethering lysyl oxidases to tropoelastin (Giltay, Timpl, and Kostka 1999; Q. Chen et al. 2009; Kumra et al. 2019). In mice, fibulin-$4^{-/-}$ is perinatally lethal with severe lung and vascular defects leading to haemorrhage (McLaughlin et al. 2006).

Fibulin-5 (FBLN5, also known as DANCE) expression is high in elastic fibre rich tissues, such as the lung, where it facilitates multiple steps of elastic fibre assembly (Nakamura 2018; Yamauchi et al. 2010). Fibulin-5 interacts with LTBP-4, LOX-like enzymes and directly with

cell surface integrins (Nakamura et al. 2002). Although fibulin-5 deficiency is not lethal, fibulin-$5^{-/-}$ mice have disrupted and disorganised elastic fibres leading to loose skin, vascular abnormalities and emphysema (Nakamura et al. 2002).

Fibulin-7 (FBLN7, also known as TM14) was identified in mouse tooth germ where it has a role in odontoblast adhesion and dentin formation (Susana De Vega et al. 2007).

### 1.6.3 Hemicentins

Fibulins-6 and -8 are also called hemicentin-1 (HMCN1) and -2 (HMCN2) respectively. They are by far the largest of the fibulin family at over 600 kDa and were discovered in *C. elegans* where they have a role in basement membrane integrity, cell-matrix interaction and fibulin-1 deposition (Vogél and Hedgecock 2001; Muriel et al. 2005; Feitosa et al. 2012). Fibulin-6 knockout is lethal at the blastocyst stage, however its deficiency in isolated cardiac fibroblasts inhibits stress fibre formation upon TGFβ stimulation (Chowdhury et al. 2017).

## 1.7 Fibulin-2

Fibulin-2, a 180kDa glycoprotein, was first described following sequence analysis of cDNA from mouse fibroblasts (Pan et al. 1993), and subsequently identified in human cDNA (R. Z. Zhang et al. 1994). Fibulin-2 is encoded by the gene *FBLN2* on chromosome 3 p25.1. FBLN2 contains 19 exons with alternative splicing producing three isoforms in humans (**Figure 3.2.1.1**). In the dominantly expressed isoform 'fibulin-2 short' alternative splicing of exon 9 results in the absence of the third EGF-like domain (Law et al. 2012).

### 1.7.1 Fibulin-2 – Structure

Fibulin-2, like all fibulins, contains a fibulin-type carboxy-terminus (FC, region III in fibulin-2) and a number of epidermal growth factor (EGF)-like modules with calcium binding sequences (region II). Fibulins -1 and -2 also contain anaphylatoxin (AT)-like modules (region I). Fibulin-2 is unique in containing a 408-amino acid N-terminus domain consisting of a cysteine rich 150aa region (Na) and a cysteine free, glutamic acid rich, region (Nb) (Takako Sasaki et al. 1997) see **Figure 1.5.3.1**. Using electron microscopy Sasaki et al. have identified a dimer model for fibulin-2 formed by disulphide bonding between region I of two anti-parallel molecules and variable interactions between N and region II domains. This results in a dimer which can have 2, 3 or 4 arms (**Figure 1.7.1.1**) (Takako Sasaki et al. 1997). There is 81% cDNA sequence homology between human and mouse FBLN2 with regions Na, I, II and III having ~90% sequence homology, and Nb 62% (R. Z. Zhang et al. 1994).

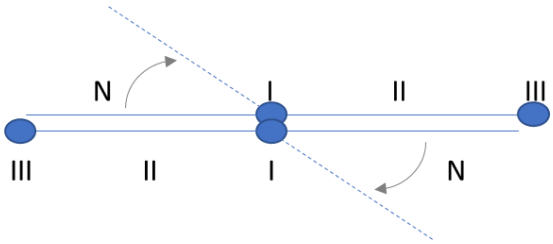


**Figure 1.7.1.1 Fibulin-2 dimer model**

Electron microscopy has identified dimers with 2, 3 and 4 arms formed through disulphide bonding in domain I and varying interactions between domains N and II. Adapted and re-drawn from Sasaki et al. 1997.

### 1.7.2 Fibulin-2 function

Fibulin-2 primarily functions as an ECM scaffold protein through interactions with numerous binding partners. This role is highlighted by the absence of fibulin-2 resulting in disruption to the mammary epithelium basement membrane of mice (Ibrahim et al. 2018). Fibulin-2 is predominantly expressed in the developing cardiovasculature where its expression "serves as an excellent marker of EMT" (Tsuda et al. 2001) and is then downregulated in adult tissues. In the developing mouse, fibulin-2 is further expressed by developing cartilage chondroblasts including nasal cartilage where immunohistochemical staining remains high despite a drop in mRNA, demonstrating a low turnover of the protein (H.-Y. Zhang et al. 1996). In the developing lung, liver and kidney, fibulin-2 is expressed by some endothelial cells in blood vessels and by mesenchymal cells in the visceral pleura (H.-Y. Zhang et al. 1996). Fibulin-2 has also been demonstrated to play an indirect role in the regulation of spinal nerve organisation in spinal development and repair via interaction with semaphorin 3A (Schaeffer et al. 2018). In the adult heart, expression is strongest in coronary artery walls and heart valves suggesting a role in maintaining tensile integrity (H.-Y. Zhang et al. 1995). Little is known about the role of fibulin-2 in adult tissues, including the lung, however fibulin-2 is upregulated during wound healing in both the skin (Fässler et al. 1996) and retina (Kanan et al. 2014), in lesions of atherosclerotic aortas (Ström et al. 2006) and during mammary epithelial outgrowth (Olijnyk et al. 2014).

In a screen of likely binding candidates, Sasaki et al. (1995) demonstrated strong, calcium dependant, binding of fibulin-2 to fibronectin, and to nidogens, which was only partially EDTA sensitive. Weaker binding was described to collagen IV, perlecan and to the collagen VI α3 chain. Tertiary complexes were formed with fibulin-2 binding nidogen which in turn bound collagen IV, perlecan or fibulin-1. No binding was demonstrated with collagens I, III or V. Fibulin-2 has also been shown to bind tropoelastin of elastin fibres (Takako Sasaki et al.

1999; El-Hallous et al. 2007; Kobayashi et al. 2007), laminins (Utani, Nomizu, and Yamada 1997), and to crosslink the glycoproteins aggrecan and versican in its X-shaped dimer form (Olin et al. 2001). Mouse fibulin-2 has been shown to bind to cell surface integrins, predominantly integrin αIIbβ3 through RGD-dependant binding however this sequence is RSS in human fibulin-2 and subsequently shows no cell adhesion (Pfaff et al. 1995; Kobayashi et al. 2007). From a functional perspective in fibrosis, one of the most interesting roles of fibulin-2 is competing with TGFβ latent binding proteins (LTBP) 1 and 4 for binding sites on the third EGF-like domain of fibrillin 1 (Ono et al. 2009). This competition reduces the sequestering of latent TGFβ likely increasing its bioavailability (H. Zhang et al. 2014).

Degradation of transiently upregulated components such as fibulin-2 is required for resolution of wound healing. Fibulin-2 is highly susceptible to degradation by matrix metalloproteinase (MMP)-2 and also MMPs -9, -7 and -3 along with plasmin and thrombin whereas fibulin-1 is much less susceptible (Takako Sasaki et al. 1996; Hergeth et al. 2008; Kleifeld et al. 2010). Fibulin-2 is also degraded by the secreted metalloproteases ADAMTS-5 (a disintegrin and metalloproteinase with thrombospondin motifs-5), to a lesser extent by ADAMTS-4 and resistant to ADAMTS-1 mediated degradation. Degradation by ADAMTS-5 is blocked by the interaction between fibulin-2 and ADAMTS-12, which has a low aggrecanase activity (Fontanil et al. 2017).

### 1.7.3 Fibulin-2 in pulmonary fibrosis

Research presented in the literature to date shows a role in the development of fibrosis for fibulin-1, as both a biomarker and a functional molecule, (Jaffar et al. 2014; Ge et al. 2015; G. Liu et al. 2016) and for fibulin-5 (Nakasaki et al. 2015). However, the role of fibulin-2 in fibrosis is limited to the angiotensin II induced cardiac fibrosis model as detailed in **section 1.7.5** below. Although proteomic analysis of lung fibrosis has shown upregulation of fibulin-2, no functional data for the role it may play in the disease has been presented. In decellularized lung tissue, fibulin-2 was 2.60-fold upregulated in IPF lungs compared to normal controls as identified by mass spectroscopy (Booth et al. 2012). In isolated lung fibroblasts fibulin-2 expression has recently been demonstrated to be 5.38-fold higher in IPF derived cells than controls (Hadjicharalambous et al. 2019). In proteomic profiling of the bleomycin mouse model of fibrosis by Schiller et al. (2015) fibulin-2 was upregulated approximately 2-fold during the fibrotic phase at days 14 and 28, returning to baseline during resolution at day 56. The authors further showed that expression of fibulin-2 negatively correlated to the compliance ratio of the lung across the time course of disease.

### 1.7.4 Fibulin-2 in cancer

In cancer literature, fibulin-2 is both up- and down-regulated in various cancers where it has both oncogenic and tumour suppressive roles. Fibulin-2 can act as a component of the physical barrier to the dissemination of cancer cells; therefore, its loss or disruption can lead to the progression and metastasis of a tumour. Fibulin-2 was one of 64 genes identified as overexpressed in metastatic tumours of various cancer origins (Ramaswamy et al. 2003). In pancreatic cancer, the membrane tethered mucin MUC4, is upregulated and by binding to fibulin-2 disrupts the normal interaction between fibulin-2 and nidogen, thereby decreasing basement membrane integrity and promoting metastasis (Senapati et al. 2012). Although fibulin-2 protein is abundantly expressed in lung adenocarcinoma tumour tissue its expression during metastasis is unclear. It has been shown that tumour cell derived fibulin-2 is necessary for tumour progression and subsequent metastasis (Baird et al. 2013), however, fibulin-2 mRNA expression has been found to be decreased in circulating epithelial cells in metastatic patients compared to healthy controls (Avsar et al. 2019). Danan-Gotthold et al. (2015) demonstrated no significant change in expression of FBLN2 in lung adenocarcinoma but a correlation between cancer survival and the exclusion of alternatively spliced exon 9. Loss of fibulin-2 in breast cancer has been linked to enhanced migration and invasiveness (Yi et al. 2007). Fibulin-2 has also been shown to have a tumour suppressive role with its loss important in the development of nasopharyngeal carcinoma (Law et al. 2012). Fibulin-2 is also downregulated by Kaposi's sarcoma–associated herpesvirus (KSHV) infection in Kaposi's sarcoma, where is may play a role in progression of the disease (Alcendor et al. 2011). Fibulin-2 is also lost in invasive gastric cancer which results in enhanced pro-tumorigenic β-catenin signalling (Ma, Lian, and Song 2019). Digestion of fibulin-2 by ADAMTS-5 increases the tumorigenic potential of breast cancer cell lines which can be blocked by ADAMTS-12 interaction with fibulin-2 (Fontanil et al. 2014; 2017).

### 1.7.5 Fibulin-2 knock out mice

Knockout mice deficient in fibulin-2 are phenotypically normal and develop normal elastic fibres. This is attributed to functional compensation by the much more highly expressed fibulin-1 (Sicot et al. 2008). Fibulin-2 deficient mice are however protected from experimental myocardial infarction (Tsuda et al. 2012) and cardiac fibrosis (H. Zhang et al. 2014; Khan et al. 2016). This protection is attributed to the absence of TGFβ signalling upregulation observed in wildtype animals. Indeed, isolated cardiac fibroblasts from animals lacking fibulin-2 did not demonstrate increased TGFβ expression or SMAD2 phosphorylation

in response to profibrotic angiotensin II as seen in wildtype cells (Tsuda et al. 2012). This phenotype could be partially recreated in wildtype cells with a TGFβ neutralising antibody suggesting an interplay between fibulin-2 and both direct and TGFβ mediated actions of angiotensin II (H. Zhang et al. 2014). Zhang *et al.* suggested that fibulin-2 acts to increase the activity of TGFβ by competing with matrix binding sites of latent TGFβ binding protein. Fibulin-2, particularly through its interaction with TGFβ, may therefore have a role in the pathogenesis of pulmonary fibrosis.

### 1.7.6 Fibulin-2 regulation

The mechanisms regulating fibulin-2 expression are yet to be elucidated. One potential mechanism has been identified in neonatal mice lacking integrin α3β1. These animals experience skin blistering as a result of a loss of basement membrane integrity due to reduced fibulin-2 expression suggesting integrin α3β1 signalling induces fibulin-2 production (Longmate et al. 2014). This could however only be recreated *in vitro* in mouse keratinocytes which had undergone immortalisation and not in primary, non-immortalised mouse cells (Missan, Chittur, and DiPersio 2014). Fibulin-2 expression in coronary smooth muscle cells was upregulated by treatment with the statin simvastatin through a RhoA and Rho-Kinase mediated pathway. Treatment with the ROCK inhibitor Y-27632 was sufficient to upregulate fibulin-2 (Serra et al. 2015). Fibulin-2 has also been identified as a potential NOTCH effector gene in the secretome of mouse embryonic endocardium which was upregulated following NOTCH activation *in vitro* (Torregrosa-Carrión et al. 2019).

In nasopharyngeal carcinoma and breast cancer, where fibulin-2 expression was down regulated, it was shown that this was due to promoter hypermethylation and treatment with the demethylating agent 5-aza-2'-deoxycytidine was sufficient to re-express fibulin-2 (Law et al. 2012; Hill et al. 2010). Fibulin-2 promoter hypermethylation has also been shown in B cell acute lymphoblastic leukaemia (Dunwell et al. 2009). It has further been shown that fibulin-2 expression is negatively regulated by the micro RNA miR-1 (Karakikes et al. 2013) and miR-192-5p (Tang et al. 2019) in mice. The interplay between angiotensin II, TGFβ and fibulin-2 identified in fibulin-2 knockout mice is complex, both angiotensin II and TGFβ alone stimulate an upregulation in fibulin-2 expression in isolated cardiac fibroblasts with angiotensin II effects being partly sensitive to a TGFβ neutralising antibody (H. Zhang et al. 2014). The literature outlined above therefore suggests that, although the precise mechanisms regulating fibulin-2 expression remain unknown, there may be roles for both gene methylation and cytokine signalling.

## 1.8 Epigenetics in PF

We and others have shown that fibroblasts explanted from IPF and SSc donor lungs retain a persistent fibrotic phenotype when compared to those from healthy control donors and that this is due at least in part to epigenetic mechanisms. Epigenetics are modifications to the transcription of DNA without altering the underlying sequence and include DNA methylation, histone modifications and expression of non-coding RNAs such as microRNAs (miRNA) and long non-coding RNAs (lncRNA). Epigenetic modifications are dynamic and heritable, being influenced by age (Hahn et al. 2017) and by environmental factors such as asbestos (Kettunen et al. 2017), cigarette smoke (Guida et al. 2015), pollution (Callahan et al. 2018) and diet (Yoon et al. 2017).

### 1.8.1 Non-coding RNAs

The majority of the transcribed genome gives rise to RNAs which do not encode proteins (Kapranov and St. Laurent 2012). It is now recognised that these transcripts play a regulatory role in gene expression. Non-coding RNAs include short, 21-25 nucleotide, microRNAs (miRNA) and long, >200 nucleotide, long non-coding RNAs (lncRNAs). Primarily, miRNA binds to complementary seed regions in 3' UTRs of mRNA and targets the mRNA for degradation or suppresses translation. In humans miRNA binding to mRNAs does not require sequence specificity across the entire sequence, as a result a single miRNA may bind to hundreds of target mRNAs (Flynt and Lai 2008). Numerous miRNAs have been implicated in PF (Miao et al. 2018), including miR-29 which targets a number of ECM components and is downregulated in fibroblasts grown on decellularized IPF lung ECM. Over expression of miR-29 restores the ECM driven phenotype to baseline levels (Parker et al. 2014). While the role of lncRNAs is currently not well understood, it is hypothesised that they act as an 'addressing' system for ribonucleoprotein complexes in the nucleus and are involved in chromatin modifications (Nishikawa and Kinjo 2017; I. Singh et al. 2018), and that they competitively bind miRNAs acting as "miRNA sponges" (Cesana et al. 2011; Q. Lu et al. 2018). Functional roles for lncRNAs in PF have been demonstrated in regulation of collagen expression (Q. Lu et al. 2018) and fibroblast proliferation and inflammatory response (Hadjicharalambous et al. 2018; 2019).

A study by Dakhlallah et al. (2013) has demonstrated the complex relationship between epigenetic mechanisms regulating the miR-17~92 cluster which contains 6 miRNAs. The cluster is down regulated in lung tissue and fibroblasts from patients with IPF as well as in bleomycin treated mice. The downregulated miR cluster is hypermethylated at its promoter

in IPF. However, miR-19b from this cluster in particular was shown to target expression of the methylation regulating enzyme DNMT1, thereby forming a positive feedback loop.

A microarray study of miRNA expression in IPF lung by Pandit et al. (2010) identified 46 miRNAs which were significantly differentially expressed in IPF lung compared to controls. miR let-7d expression was significantly reduced in IPF lung, in bleomycin treated mouse lung and directly by TGFβ through SMAD3 binding to the let-7d promoter (Pandit et al. 2010). A subsequent study published recently Rubio et al. (2019) detailed the role downregulated let-7d plays in 'compromised epigenetic silencing' in IPF fibroblasts by binding non-coding RNAs. Let-7d – lnc-RNA duplexes provide a framework for assembly of a ribonucleoprotein complex, MiCEE (Mirlet7d-C1D-EXOSC10-EZH2), at specific gene loci which methylates histones and recruits active histone deacetylases (I. Singh et al. 2018). Rubio et al. confirmed that let-7d was downregulated in IPF and showed that let-7d inhibition in control fibroblasts upregulated fibrotic markers αSMA and fibronectin 1, as well as cell migration and proliferation. The authors further demonstrated hyperactive EP300 in IPF fibroblast nuclei which disrupts the MiCEE function and propose this as a target for pharmacological therapy in IPF.

Multiple miRNAs have been mapped as components of the PGE synthesis and signalling pathway and their expression investigated in different cancers (A. E. Moore, Young, and Dixon 2011), however expression of only one miRNA has been investigated in IPF. Recently, Savary et al. (2019) have shown that DNM3OS is strongly and rapidly induced in the nucleus of fibroblasts by TGFβ and is increased in myofibroblast like cells in bleomycin treated mice. DNM3OS is the precursor to miR-199a-5p, miR 199a-3p and miR-214-3p. miR-214-3p maps to the 3'UTR of COX-2 and its overexpression in MRC5 fibroblasts reduced COX2 expression and $PGE_2$ production leading to FASL-mediated apoptosis resistance. Inhibition of DNM3OS with an antimir blocked differentiation of fibroblasts into myofibroblasts, as measured by collagen production and αSMA expression, through impairing both SMAD and non-SMAD signalling.

### 1.8.2 Histone modifications

Modifications to histones, which include phosphorylation, acetylation, methylation and ubiquitination, result in alterations in the chromatin structure of DNA and therefore the accessibility by transcription factors. Altered histone modification have been identified in IPF fibroblasts resulting in decreased FAS expression (S. K. Huang et al. 2013), and decreased expression of COX-2 required for the synthesis of antifibrotic $PGE_2$. Coward et al (2009, 2014)

have demonstrated limited COX-2 upregulation in response to IL-1b in IPF derived fibroblasts compared to controls. This is associated with alterations in transcription factor binding to the COX-2 promoter involving reductions in H3- and H4- acetylation, which generally increase chromatin accessibility, and increases in H3K9- and H3K27- trimethylation, which suppress transcription. This histone methylation and hypoacetylation pattern was dependant on recruitment of the histone methyltransferases G9a and EZH2. Inhibition of G9a and EZH2 was able to restore the COX-2 response to IL-1b. Recently, gene silencing by H3K9 methylation has been shown to be essential for TGFβ or stiff matrix induced fibroblast activation (Ligresti et al. 2019)

### 1.8.3 DNA methylation

The addition of a methyl group to cytosine was first described in 1948 (Hotchkiss 1948) and typically occurs at cytosine-guanine dinucleotides (CpG). Methylation based control of gene expression is required for X chromosome inactivation (Sharp et al. 2011), genomic imprinting (Vangeel et al. 2015) and silencing of viral genes (Shalginskikh et al. 2013). The relationship between gene methylation and expression is complex. The conventional model is that CpG methylation represses the transcription of a gene by hindrance of transcription factor binding, either directly or through recruiting methyl-binding proteins (MBPs). MBPs can also subsequently modify histones, for example by deacetylation, leading to a condensed, suppressive, chromatin structure. However, literature is emerging that some transcription factors preferentially bind to methylated regions or can act to modify methylation directly (H. Zhu, Wang, and Qian 2016). CpG rich regions, termed CpG islands (CGI), occur in the promoter regions of approximately 60% of genes. Increasingly, the methylation status of CGI flanking shore regions (up to 2 kb from CGIs) is being demonstrated to be relevant to gene expression. A genome-wide analysis of tissue specific methylation found that 76% of differentially methylated regions were located in CGI shores, and that the methylation status of CGI shores correlated with the expression of the gene (Irizarry et al. 2009). Intragenic CpG methylation has also been linked to regulation of gene expression. Varley et al. (2013), analysing genome wide data, identified a correlation between gene methylation and expression, the direction of which being dependent on CpG location. CpGs in the transcription start site, whether within a CGI or not, typically demonstrated negative correlation with expression; intragenic CpGs not within CGIs a positive correlation with expression; and intragenic CpGs which are within a CGI had a bimodal positive and negative correlation with expression. The intragenic methylation status has also been shown to play

a role in regulating mRNA splicing, with binding of methyl-CpG-binding protein 2 (MeCP2) to methylated alternatively spliced exons positively regulating their inclusion (Maunakea et al. 2013).

Cytosine residues are methylated by DNA methyl transferase (DNMT) enzymes that transfer a methyl group from S-adenyl methionine (SAM) to carbon position 5. DNMT1, which acts to copy the methylation status of the parental DNA to the daughter strands during replication, has a high affinity for hemi-methylated DNA (**Figure 1.8.3.1**). DNMT2 does not have DNA methyltransferase activity but methylates RNA. DNMT3a and DNMT3b, termed *de novo* DNMTs, are able to add methyl groups to previously unmethylated CpGs through interactions with histones (Ooi et al. 2007) and transcription factors (Sato, Kondo, and Arai 2006). DNMT3L, while lacking DNMT activity is an important co-factor for DNMT3a/3b activity (Pacaud et al. 2014; Ooi et al. 2007).

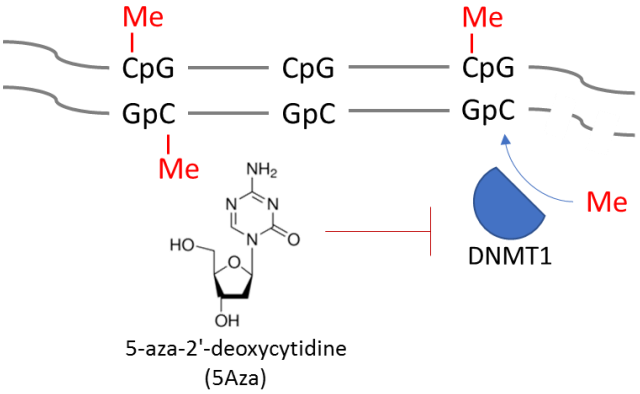


**Figure 1.8.3.1 DNA methylation by DNMT1**

The methylation status of a CpGs is passed on to daughter DNA strands during replication by DNA methyltransferase 1 (DNMT1) which has a high affinity for hemi-methylated DNA. Experimentally we are able to inhibit the action of DNMT1 with 5-aza-2'-deoxycytidine (5Aza) resulting in a loss of methylation in daughter DNA strands.

While the mechanism of methylation of cytosine residues by DNMTs is well characterised, the mechanisms by which cytosine residues are demethylated are less well understood. Demethylation is likely a multistep process mediated by ten-eleven translocation (TET) enzymes producing 5-carboxylcytosine (5caC) which can then undergo thymine-DNA glycosylase (TDG)-mediated base excision repair (BER) to result in unmethylated cytosine (He et al. 2011; Maiti and Drohat 2011). This demethylation process passes through various intermediates including 5-hydroxymethylcytosine (5hmC) and functional roles for these

intermediates in gene regulation are beginning to be elucidated (Spruijt et al. 2013; Iurlaro et al. 2013). Experimentally 5-Aza-2'-deoxycytidine (5Aza), an analogue of cytosine, is used to reduce methylation. 5Aza is incorporated into daughter strands during DNA replication, it then covalently binds to DNMT1 at hemi-methylated sites thereby entrapping the enzyme. 5Aza also leads to the proteolytic degradation of free DNMT1, though the mechanism of this is still unknown (Patel et al. 2010).

### 1.8.4 DNA methylation in PF

Aberrant DNA methylation is characteristic of many cancers with hypomethylation of oncogenes and hypermethylation of tumour suppressors contributing to the disease (Feinberg and Vogelstein 1983; Irizarry et al. 2009). DNA methylation differences in multiple genes have been identified in IPF including hypermethylation of Thy-1 (*THY1*; CD90), an outer membrane glycoprotein important for cell-matrix interaction (Sanders et al. 2008); hypermethylation of prostaglandin E receptor 2 (*PTGER2*) (Steven K. Huang et al. 2010) and epigenetic regulation of cyclooxygenase 2 (*COX2*) (Evans et al. 2016) both involved in the anti-fibrotic signalling of $PGE_2$; and in tenascin XB (*TNXB*) an extracellular matrix glycoprotein (I. M. Garner et al. 2013). Hypermethylation resulting in decreased expression of the collagen repressor Fli-1 proto-oncogene, ETS transcription factor (*FLI1*) has been demonstrated in dermal SSc fibroblasts (Wang, Fan, and Kahaleh 2006).

Methylation array studies in PF have identified numerous genes which may be aberrantly methylated in IPF however most of these studies are either on lung tissue, and therefore include a mixed population of cells (Sanders et al. 2012; I. V. Yang et al. 2014) or lack paired expression data (S. K. Huang et al. 2014). Investigating CpG island methylation Rabinovich et al. (2012) have demonstrated differential methylation in 625 CGIs in IPF tissue when compared to controls. IPF samples had an intermediate methylation profile between that of control and lung cancer, however, the lack of global hypomethylation of LINE-1 retrotransposon which is seen in cancer suggests methylation changes in IPF are specific to certain regions.

A microarray study of lung tissue from IPF and control donors identified 870 genes which were differentially methylated in IPF of which 406 were hypomethylated and 464 hypermethylated (Sanders et al. 2012). When the authors paired this methylation data with mRNA expression arrays in which 373 genes were differentially expressed, only 35 genes had a change in expression with altered methylation, 16 of which had a negative relationship between methylation and expression. A study by I. V. Yang *et al.* (2014) which extended

genome wide methylation analysis beyond CGIs found 2,130 differentially methylated regions (DMRs) mapping to 1,514 genes in IPF lung tissue. 43% of these DMRs were hypomethylated, 60% of DMRs were in the shore regions (1-3,000 bases from CGI) and only 5% were within CGIs. The majority (71%) were within the gene body. 738 of 13,251 genes with differential expression had a DMR within 5kb of the gene. In 69% of genes, hypermethylation of a DMR was associated with decreased expression and vice versa. A study by Huang et al (2014), focused on the methylation in lung fibroblasts specifically, demonstrated 787 CpG loci with altered methylation in IPF fibroblasts compared to those from controls. A caveat to the afore mentioned study it that this data was not paired to genome wide gene expression data. A recently published study by J.-U. Lee et al. (2019) utilised paired methylation and expression array data in IPF (n=8) and control (n=4) lung fibroblasts. The authors identified differential methylation in IPF of 5,850 CpGs relating to 2,282 genes. The methylation level of 80 differentially methylated CpGs correlated with the expression of 34 differentially expressed genes.

## 1.9 Summary, hypothesis and aims

We and others have shown that there is a persistence of phenotype in fibrotic lung fibroblasts explanted from lungs of patients with pulmonary fibrosis and this is at least partly due to epigenetic mechanisms, most notably gene methylation. Pulmonary fibrosis can occur in isolation, such as in IPF, or as the pulmonary manifestation of other diseases, such as SSc. Combining data from these two diseases allows the identification of common dysregulated genes which are more likely to be associated with fibrosis. Through analysis of Illumina expression and methylation array data this thesis will identify fibulin-2 as a gene of interest in pulmonary fibrosis. Fibulin-2, an extracellular matrix (ECM) glycoprotein, interacts with a number of other ECM proteins and growth factors including TGFβ, potentially through competition of matrix binding sites. In this thesis I therefore intend to test the hypothesis:

> **Increased fibulin-2 expression by fibroblasts, induced by mechanisms involving CpG methylation, contributes to the pathogenesis of pulmonary fibrosis and modulating this axis may have therapeutic benefit.**

To test this hypothesis, my aims are:

1. To identify genes of interest in pulmonary fibrosis using bioinformatic filtering of data generated by methylation and expression arrays performed on fibroblasts isolated from fibrotic and control lungs. This will include identification of genes differentially expressed and/or methylated in fibrotic lung fibroblasts compared to controls, and direct correlation of methylation with gene expression to identify genes which may be directly regulated by methylation. Gene Ontology enrichment analysis will then be performed to highlight genes identified in the steps above which may play a role in the pathogenesis of fibrosis.
2. Following identification of fibulin-2 as a gene of interest in aim 1, expression levels of fibulin-2 detected by the array will be confirmed at the mRNA level in lung fibroblasts by real-time PCR. To confirm the potential importance of fibulin-2 in disease pathogenesis, its expression and localization will be assessed by immunohistochemistry in sections of control and fibrotic lung.
3. Identify patterns of fibulin-2 regulation by gene methylation: the methylation status of CpGs across the fibulin-2 gene, quantified by Illumina methylation array, will be related to mRNA expression levels to identify direct relationships between individual CpGs and gene expression both basally and following demethylation treatment.
4. Establish an experimental model in which fibulin-2 levels can be quantified *in vitro* and modulated to elucidate the role it plays in the pathogenesis of the fibrotic fibroblast phenotype.

# 2 Materials and Methods

## 2.1 Cell Culture

### 2.1.1 Cell isolation and routine culture

Primary human lung fibroblasts were isolated from samples of lung obtained during biopsy or post-transplant from histologically confirmed IPF or SSc pulmonary fibrosis, or from distant, histologically normal, regions of lung removed during lung cancer resection as previously described (Keerthisingam et al. 2001). SSc lung fibroblasts were a kind gift from Professor David Abraham (Centre for Rheumatology and Connective Tissue Diseases, UCL). All tissue was obtained with appropriate informed consent and its use approved by the East Midlands – Nottingham 2 NRES Committee, Ref. No. 12/EM/0058.

To isolate primary human lung fibroblasts, multiple ~1mm$^3$ sections of parenchymal tissue were manually attached to petri dishes (Nunc, 150350), and incubated at 37°C, 10% $CO_2$ in a humidified incubator, in 2ml Dulbecco's Modified Eagle Medium (DMEM; Gibco, 41966052), which contains L-glutamine (2mM) and pyruvate (1mM), supplemented with 20% fetal calf serum (FCS, non-heat inactivated; Gibco, 10270106), penicillin (50U/ml) and streptomycin (50µg/ml) (Gibco, 15070063), and amphotericin B (2.5µg/ml; Gibco, 15290018), referred to as explant media. The following day 8ml of explant media was carefully added to each petri dish. Explant media was carefully aspirated and replaced every 2-3 days for 2-4 weeks while cells grew out from biopsies. Upon reaching confluency cells were washed in $Ca^{2+}$ and $Mg^{2+}$ free PBS (Sigma, D8537) and incubated with trypsin-EDTA (0.05%; Gibco, 25300104) at 37°C until visual detachment. Trypsin-EDTA was neutralised with >10ml DMEM containing 10% FCS and cells pelleted by centrifugation at 300g for 5min. Cells were then either frozen in DMEM supplemented with 20% FCS and 10% DMSO (Sigma, D2650) and stored in liquid nitrogen, or plated in tissue culture flasks at 15-30% confluency in DMEM containing 10% FCS (DMEM-10%) and antibiotics only. Cells were subsequently passaged in this manner upon reaching >80% confluency and used between passages 3 and 10. For experimental protocols cells were trypsinised as above and counted with a Cell Scepter 2.0 cell counter (60µm sensor; Millipore, PHCC60050) before seeding at the required density in DMEM (Sigma, D6546) supplemented with fresh L-Glutamine (Gibco, 25030024) containing 10% FCS without antibiotics (DMEM-10%). All routine culture vessels had Nunclon™ Delta surface treatment (Nunc, Thermo Scientific). Cell culture experiments were performed with one control and one IPF cell line (our references 0109 and 0108 respectively). These cells had

FBLN2 expression at approximately the mean of the whole array validation cohort for their respective disease status.

### 2.1.2 Microarray cell culture

Cell culture, 5Aza treatment and RNA/DNA extraction for microarray experiments was performed by Dr Iona Evans.

Prior to extraction of RNA and DNA for expression and methylation array analysis proliferating, human lung fibroblasts were treated with or without the demethylating agent 5-aza-2'-deoxycytidine (5-Aza; Sigma, A3656; 1µM). The patient demographics for the cell lines used are shown in **Table 2.1.2.1**. As DNA replication is required for the actions of 5Aza, cells were seeded at ~5-10% confluency and grown to confluency with daily addition of 5Aza for >7 days to allow >3 population doublings. Routinely cultured fibroblasts were trypsinised as above and 4 flasks of each cell line seeded at 500,000 cells per T175 (Nunc, 159910) in 25ml DMEM-10% and allowed to adhere before addition of 5Aza (2 flasks) or DMSO only control (2 flasks). 5Aza was reconstituted to $1x10^{-2}$M in DMSO, aliquoted and stored at -20°C until used. Daily, a 100x solution of 5Aza or DMSO only control was made fresh (10µl of stock added to 990µl DMEM-10%) and 250µl added to culture flasks. Once cells were visually confluent RNA and DNA was extracted as detailed below.

| Group | Number | Age (mean ±SD) | Sex |
|---|---|---|---|
| Control | **n=6** | **58.3 ±14.6 years** | **2 male** |
| IPF | **n=5** | **66.6 ±8.1 years** | **2 male** |
| SSc | **n=7** | **51.7 ±3.7 years** | **1 male** |

**Table 2.1.2.1 Array sample patient demographics**

### 2.1.3 2D culture time-course

A time-course was performed to assess the kinetics of fibulin-2 expression and accumulation against cell confluency in the proliferating culture conditions required for previous array experiments. Fibroblasts were seeded in 12-well plates at $6.0x10^4$ cells per well (approximately 25% confluency) in 1ml DMEM-10% without antibiotics and incubated overnight at 37°C, 10% $CO_2$. The following day, media was changed to fresh DMEM-10% and samples were collected every 24h. Three biological replicates of each condition were performed for each of RNA extraction (see **section 2.3.3**), protein collection (see **section 2.7.1**) and cell counting. To count cells, culture media was removed by aspiration and the cell layer gently washed twice with PBS followed by incubation with 100µl trypsin/EDTA until cell

detachment. Trypsin was neutralised with 400µl DMEM-10% and diluted with 500µl PBS. Samples were immediately mixed by pipetting before counting as above (**section 2.1.1**).

### 2.1.4 siRNA transfection

Knock down of FBLN2 mRNA expression was utilised to assess the role fibulin-2 may have in the fibrotic phenotype of lung fibroblasts. This was achieved by transfection of cells with a pool of siRNA molecules targeting FBLN2 at a final concentration of 25nM (Dharmacon SMARTpool: ON-TARGETplus, Horizon, L-011655-00-0005). Non-targeting siRNA was used as a negative control (Dharmacon SMARTpool: ON-TARGETplus Non-targeting Pool, D-001810-10-05). siRNA was reconstituted at 10µM and stored at -20°C until used. For all experiments, siRNA transfection complexes were formed by mixing siRNA with Opti-MEM I Reduced Serum Medium (Gibco, 31985062) then vortexing with INTERFERin siRNA transfection reagent (Poly-Plus, 409-50, Lot 08INF0311L1) as per the manufacturers protocol. During complex formation media was removed from the cell layer and replaced with fresh DMEM-10%.

siRNA knockdown of FBLN2 was performed in 2D culture time-course experiments in 12-well plates (**Figure 2.1.4.1A**). Culture was performed as per **section 2.1.3** with the addition of siRNA at 24h post seeding. siRNA complexes were formed at 11x final concentration with 6.0µl of INTERFERin per 100µl and 100µl added to each well containing 1ml fresh DMEM-10% with swirling. Cells were collected at the 120h timepoint for three biological replicates each of RNA and protein.

For collagen deposition (see **section 2.1.5**) and spheroid (see **section 2.2.1**) protocols, siRNA treatment was performed in culture flasks before cells were trypsinised and seeded into experimental conditions (**Figure 2.1.4.1B**). $1x10^6$ fibroblasts were seeded in T75 culture flasks in DMEM-10% and allowed to adhere for 24h. The culture media was replaced with 10ml fresh DMEM-10% and 1ml of 11x siRNA complexes, formed with 30µl INTERFERin, was added. Cells were incubated for 24h before the culture media was replaced with antibiotics-free DMEM containing 0.4% FCS (DMEM-0.4%). For spheroid experiments, TGFβ (40pM) was also added to some flasks 4h after addition of starvation media. After 24h of starvation, cells were then trypsinised as above, counted and used for collagen deposition or spheroid experiments.

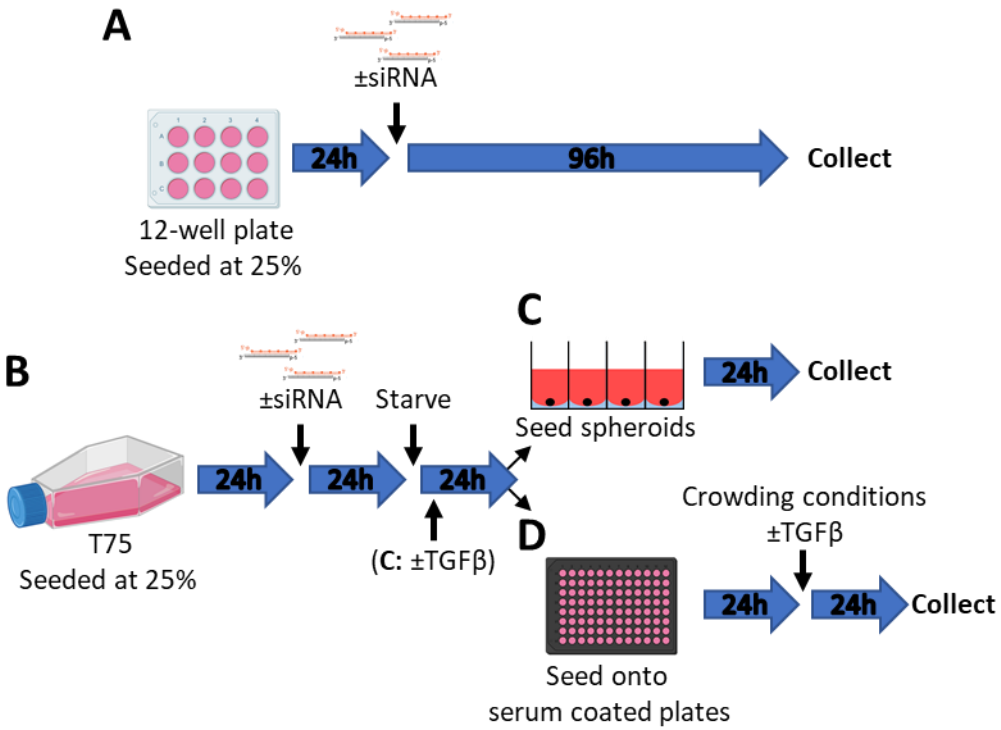


**Figure 2.1.4.1 siRNA treatment schema**

(**A**) For 2D culture, cells were seeded at 25% confluency, allowed to adhere for 24h before siRNA treatment. Samples were collected at 120h post seeding. (**B**) Alternatively, cells were seeded in tissue culture flasks at 25% confluency, treated with siRNA after 24h then serum starved for 24h before use in either: (**C**) Spheroids: FBLN2 deficient cells were seeded on agarose coated plates and spheroids collected after 24h. TGFβ was added to some cells 20h before seeding; or (**D**) Crowded collagen deposition assay: molecular crowding was applied 24h after seeding of FBLN2 deficient cells.

### 2.1.5 ECM Deposition Assay

As a measure of fibroblast fibrotic phenotype, *in vitro* collagen deposition was assayed as previously described by Chen et al. (2009) where crowded media conditions facilitate the rapid deposition of collagen. ECM deposition of collagen I and fibulin-2 were immunofluorescently quantified along with cellular alpha smooth muscle actin (αSMA). Crowding conditions were achieved by supplementing media with the macromolecules Ficoll 70 (37.5mg/ml; Sigma, F2878) and Ficoll 400 (25.0mg/ml; sigma, F4375), along with ascorbic acid (L-Ascorbic acid 2-phosphate sesquimagnesium salt hydrate, 16.6ug/ml; Sigma, A8960).

Non-siRNA experiments

Cells were seeded at $1x10^4$ cells per well in the central 60 wells of black-walled 96-well plates (Corning, 3603) in 100µl of DMEM-10%, with DMEM-10% in surrounding wells, and allowed to adhere overnight. Seeding media was removed by aspiration and replaced with 100µl DMEM-0.4% and incubated overnight. Starvation media was removed and replaced with 150µl DMEM-0.4% containing ascorbic acid with or without Ficolls and/or TGFβ (40pM; Porcine $TGF\beta_1$, R&D Systems, 101-B1-001). For the TGFβ dose response curve a serial dilution was performed to yield a range of $1.26x10^{-14}$ – $1.26x10^{-10}$M. Three biological replicate wells were treated for each condition.

ECM deposition following siRNA treatment

For siRNA experiments cells were first treated with siRNA for 24h then serum starved for a further 24h in culture flasks (see **section 2.1.4**). Cells were then trypsinised and seeded at $1x10^4$ cells per well in DMEM-0.4% containing ascorbic acid. To enable cell adhesion in low serum media, black-walled 96-well plates were coated with 100µl DMEM-10% for 30min prior to cell seeding. After allowing cells to adhere for 24h culture media was replaced with 150µl crowding media, as detailed above, and cells incubated for 24h before fixation.

For collagen and αSMA quantification, incubation media was removed and cells were fixed with 100µl ice-cold methanol for 2min. Following 3 x 100µl PBS (Oxoid, BR0014G) washes cells were stored in PBS at 4°C until staining. For fibulin-2 immunofluorescence, media was removed from the cell layer and wells washed with 100µl Hank's Buffered Salt Solution (HBSS; Gibco, 14025100) which contains calcium. The cell layer was fixed with 100µl 4% PFA in PBS for 30min at room temperature, washed twice with HBSS and stored in HBSS at 4°C until staining. Immunofluorescent staining and quantification is detailed in **section 2.6.4**.

## 2.2 Spheroid 3D culture model

A 3D fibroblast spheroid model was used to better recapitulate the ECM-ECM and cell-ECM interactions which may be lacking in 2D culture on plastic. In the spheroid model, culture plates were coated with agarose which forms a non-adherent surface. When performed in a 96-well plate the resulting meniscus shape encourages seeded cells to accumulate in the centre of the well resulting in the formation of a single spheroid. These spheroids were then collected for analysis by immunohistochemistry, western blotting and RT-qPCR.

### 2.2.1 Spheroid formation

4% low melting point agarose (MP: 65.6°C, SP: <25°C; Invitrogen, 16520-100) was dissolved in milliQ water (Millipore) by microwave heating and autoclaved in a benchtop autoclave (Prestige Medical; 121°C, 15min). Following autoclaving, agarose was cooled to ~50°C in an oven before being mixed with an equal volume of pre-warmed (~50°C) serum free DMEM. 50µl warm 2% agarose / DMEM was added to each of the central 60 wells of flat-bottom 96-well plates (Nunc, 167008) using pre-warmed multi-dispenser tips (Multipette, Eppendorf) and allowed to set at room temperature for 30-60min. 150µl media alone was added to outer wells.

Primary lung fibroblasts were trypsinised as above with neutralisation in DMEM-10%. Following counting, cells were centrifuged at 300g for 5min and resuspended in DMEM supplemented with 0.4% FCS and ascorbic acid to yield $1x10^5$ cells per ml. 100µl cell suspension was added to agarose coated wells ($1x10^4$ cells per well). Plates were incubated for 24h at 37°C, 10% $CO_2$ to allow spontaneous spheroid formation.

In some experiments, before seeding, fibroblasts were treated with siRNA to deplete FBLN2 as per **section 2.1.4**. TGFβ pre-treatment was also performed in some experiments in a similar manner. Fibroblasts were seeded at $1x10^6$ in T75 culture flasks and allowed to adhere for 24h before serum starvation in 10ml DMEM-0.4% for 4h. 1ml of 11x TGFβ in DMEM-0.4% was then added to a final concentration of 40pM and cells incubated for 20h before spheroid formation as above.

### 2.2.2 Spheroid collection

For RNA, Protein or HPLC, eight spheroids were collected by pipetting (P1000) and pooled in microcentrifuge tubes. After pooling, analysis was performed on three biological replicates each containing eight spheroids. Spheroids were pulsed down, media removed and spheroids washed with HBSS. HBSS was removed and spheroids stored at -80°C until further processing. RNA and DNA were isolated from pooled spheroids with Qiagen All-Prep columns as per **section 2.3.3**. Protein was extracted by lysing spheroids in 20µl RIPA buffer supplemented with 4% SDS and western blot was performed with 6µg total protein as detailed in **section 2.7**. Spheroids were processed for hydroxyproline quantification by HPLC as detailed in **section 2.8**.

### 2.2.3 Spheroid histology processing

Four spheroids were pooled by pipetting and allowed to settle in microcentrifuge tubes. Media was carefully removed and spheroids washed with 100µl HBSS. Spheroids were again allowed to settle before HBSS was removed and spheroids fixed with 30µl 4% Paraformaldehyde (PFA; Sigma, 441244) in PBS for 20min at room temperature. After fixation, PFA was removed and spheroids stored in 200µl 70% Ethanol (VWR, 20821.330) at 4°C until processing.

For paraffin embedding, spheroids were first embedded in agarose to allow handling. 4% agarose (MP: 90°C, SP: 37°C; Bioline, BIO-41025) in milliQ water was prepared by microwaving and allowed to cool to 45-50°C. Ethanol was removed from spheroids and the microcentrifuge tube briefly incubated on a 50°C hot block. ~500µl agarose was carefully added as to not disturb spheroid cluster and allowed to set to room temperature. Once set, the agarose plug was gently pulled from the microcentrifuge tube and the spheroid containing tip trimmed. Spheroids in agarose were placed in cassettes (Cell Path, EIA-0109-10A) between biopsy pads (Cell Path, EBA-0101-03A0 and processed in a Leica TP1050 automated processor with the protocol shown in **Table 2.2.3.1**. The processed agarose plug was then carefully embedded in paraffin wax (Raymond Lamb W1, 8415R2010) on a Tissue-Tek TEC5 embedding station. FFPE sections were cut and stained as detailed in **section 2.6.1**.

| Reagent | Time h:min | Temperature | Pressure / vacuum |
|---|---|---|---|
| 70% EtOH | **2:00** | **Ambient** | **P/V** |
| 80% EtOH | **1:30** | **Ambient** | **P/V** |
| 90% EtOH | **1:30** | **Ambient** | **P/V** |
| 100% EtOH | **1:00** | **Ambient** | **P/V** |
| 100% EtOH | **1:15** | **Ambient** | **P/V** |
| 100% EtOH | **1:15** | **Ambient** | **P/V** |
| 100% EtOH | **1:15** | **Ambient** | **P/V** |
| Xylene | **1:00** | **Ambient** | **P/V** |
| Xylene | **1:00** | **Ambient** | **P/V** |
| Xylene | **1:00** | **40°C** | **P/V** |
| Paraffin | **1:00** | **60°C** | **Ambient** |
| Paraffin | **1:00** | **60°C** | **Ambient** |
| Paraffin | **1:00** | **60°C** | **Ambient** |

**Table 2.2.3.1 Tissue Processor protocol for spheroid IHC**

PFA fixed spheroids were embedded in agarose and processed to wax using a Leica TP1050 automated processor.

## 2.3 RNA and DNA Isolation

### 2.3.1 RNA isolation for expression array

For expression array experiments RNA was collected by precipitation from TRI Reagent (Sigma, T9424) as per the manufacturer's protocol. Confluent cells were trypsinised as above, resuspended in 20ml DMEM-10% and cells pelleted by centrifugation at 300g for 5min. Media supernatant was removed, cells resuspended in 1ml TRI Reagent and incubated at room temperature for 5min. Samples were then frozen at -80°C until RNA extraction. To extract RNA 200µl chloroform was added and samples were vortexed. Following incubation at room temperature for 5min and centrifugation at 16,000g, 4°C, for 15min to establish phase separation, the upper aqueous phase (250µl) was collected and transferred to a clean microcentrifuge tube. Addition of 250µl propan-2-ol and incubation at room temperature for 10min was used to precipitate RNA which was then pelleted by centrifugation at 16,000g, 4°C, for 15min. The supernatant was removed and replaced with 1ml nuclease free 70% ethanol and vortexed to wash the pellet. Samples were then centrifuged 16,000g, 4°C, for 10min, the supernatant removed and the RNA pellet allowed to air dry. RNA was then resuspended in 60µl nuclease free water (Ambion, AM9937) and quantified by absorbance at 260nm on a Nanodrop (ND8000, Thermo Scientific) and quality assessed as 260/280nm ratio of 1.8-2.2. RNA was stored at -80°C until used.

Array validation PCR was performed on aliquots of RNA from samples processed for array analysis. RNA was DNase treated with Precision DNase (Primer Design, DNASE-50) in 20µl reactions containing 1µl DNase with incubation at 30°C for 10min followed by inactivation at 55°C for 5min on a peltier thermocycler (MJ Research) and processed directly to cDNA synthesis.

### 2.3.2 DNA isolation for methylation array

For methylation array analysis DNA was precipitated from trypsinised cells with Nucleon blood and cell culture DNA extraction kit (Amersham, BACC2) as per the manufacturer's protocol. Cell pellets were resuspended in 1ml Reagent A and incubated on ice for 5 min. Samples were centrifuged at 1300g for 5min, supernatants discarded and pellets resuspended in 2ml Reagent B. 500µl sodium perchlorate solution was added for deproteinisation and samples were mixed by inversion. 2ml chloroform was added per sample, samples were mixed by inversion and 300µl Nucleon resin was added per sample before samples was centrifuged at 1300g for 3min. The upper phase (2.5ml) was collected

into a new tube and DNA was precipitated by addition of 5ml cold absolute ethanol and mixing by inversion. DNA was pelleted by centrifugation >4000g for 5min and the supernatant was discarded. The pellet was washed by addition of 2ml 70% ethanol and inversion. The DNA pellet was once again centrifuged, the supernatant removed and allowed to air dry. DNA was then dissolved in 500µl nuclease free water and stored at -80°C. Genomic DNA was quantified by fluorescence of Quant-iT Picogreen double stranded DNA dye (Invitrogen, P11496) against a lambda DNA standard curve.

### 2.3.3 DNA / RNA isolation from cell culture experiments

For non-array cell culture experiments, total RNA was extracted with either Qiagen RNeasy (74106) or All-Prep (80204) spin columns. For 2D experiments, cells were lysed with RTL or RLT-Plus buffer (Qiagen, 350µl per well), scraped and collected in microcentrifuge tubes. Lysates were stored at -80°C until further processing as per manufacturers protocol with on column DNAse digestion (RNeasy). In 3D, spheroids were thawed in 600µl RLT-plus buffer (Qiagen) and homogenised by passing 5 times through an insulin needle (BD) before RNA and DNA extraction with Qiagen All-Prep kit as per manufacturer's protocol. In both cases RNA was double eluted in 30µl nuclease free water. RNA quantity and quality was assessed by Nanodrop as above. Eluted RNA was stored at -80°C until cDNA synthesis (section 2.5.1). DNA was eluted from All-Prep columns in 100µl Elution Buffer and stored at -80°C until use. DNA yield was quantified by Qubit dsDNA HS assay (Invitrogen, Q32854).

## 2.4 Expression and methylation microarray

### 2.4.1 Expression microarray

Extracted RNA was processed by Cambridge Genomic Services (CGS, UK) for expression analysis using Illumina Infinium HT-12 v4 BeadChips (Illumina, USA). Following quality control, biotin labelled complementary RNA was generated and hybridised to a bead chip containing 50-base probes to 47,231 transcripts and splice variants from NCBI RefSeq Release 38. Hybridisation of transcripts was visualised with fluorescently labelled streptavidin and analysed with Illumina's GenomeStudio software followed by normalisation with the Lumi R package (Du, Kibbe, and Lin 2008). A basic analysis was performed by CGS using the Limma R package (Smyth 2004) to calculate probe detection above background, the fold change in expression between groups and the associated false-discovery P-value.

### 2.4.2 Methylation microarray

Extracted genomic DNA was analysed for methylation status by Cambridge Genomic Services (CGS, UK) using Illumina Infinium HumanMethylation 450k BeadChips (Illumina, USA). DNA was bisulfite converted (EZ DNA Methylation-Gold, Zymo Research, USA), this first chemically converts unmethylated cytosine residues to uracil which, following PCR amplification, results in thymine in positions of unmethylated cytosine while leaving methylated cytosine residues unaffected. Genomic DNA is then hybridised to 50-nucleotide probes with complementary sequences and first nucleotide extension is fluorescently detected. The Illumina Infinium 450k array contains two types of probe, type I probes operate as a pair, one each for methylated and unmethylated CpGs with extension of both in the same colour; type II are a single probe with extension by a different colour fluorescent nucleotide depending on the methylation status of the CpG. Fluorescent data was analysed using GenomeStudio (Illumina) and data imported into the Lumi R package (Du, Kibbe, and Lin 2008) for normalisation. Probes demonstrating detection p-values > 0.01 were removed and the % methylation beta values were calculated as β = methylated / (methylated + unmethylated) for each CpG.

### 2.4.3 Array data analysis

In this thesis array data generated within our lab was reanalysed using updated annotation to find a gene of interest for further study. Bulk analysis of data to identify genome wide methylation differences and differential gene expression was previously performed by Dr Ian Garner (I. Garner 2016). Analysis in this thesis began with the most unprocessed data available which had undergone normalisation and group-pair analysis by Cambridge Genomic Services as detailed in **sections 2.4.1** and **2.4.2** above. Further analysis and extraction of methylation and expression data was performed using R and python 3 packages within the anaconda environment (anaconda.org).

Expression data was annotated using data from the Re-Annotator program (Arloth et al. 2015) which improves upon the manufacturer's annotation by *in silico* alignment of probe sequences to the hg19 reference genome. Only probes meeting the authors 'reliable' grade for genes on autosomes and those detected in at least one sample were included for analysis. Due to the small sample sizes and heterogeneity within samples, a threshold number of misclassifications (TNoM) of ≤ 1 was used to identify genes in which control and disease formed two populations. The TNoM is the count of samples misclassified by an optimised arbitrary threshold (**Figure 2.4.3.1**). A custom python script was written to calculate the minimum TNoM for each probe on the expression array.

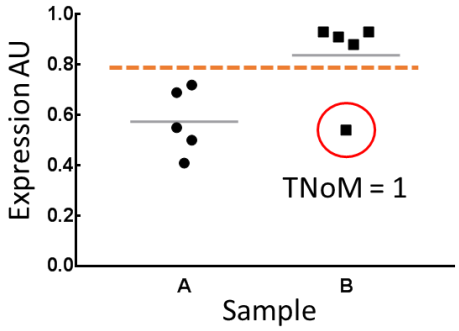


**Figure 2.4.3.1 Threshold Number of Misclassifications (TNoM)**

The TNoM was calculated to determine genes in which expression split samples into two populations (TNoM ≤ 1, $p < 0.05$) as the number of misclassified samples with an optimum arbitrary threshold.

For methylation array analysis the ChAMP R-package was used to annotate and filter probe data. This package utilises annotation from (Nordlund et al. 2013; Zhou, Laird, and Shen 2017) and removes non-specific probes and those mapping to known SNPs near the target CpG. Probes mapping to sex chromosomes were also removed. A difference in mean methylation β-value of 13.6% with a non-corrected p-value < 0.05 was used to identify differentially methylated CpGs as this has been shown previously to be detectable with 95% confidence (Bibikova et al. 2009).

Correlation between $Log_2$ expression and methylation β-value was utilised to identify genes in which methylation may be regulating expression. The Pearson $R^2$ and Spearman Rho correlation coefficients, and associated p-values, were calculated for expression and methylations probes paired by their closest gene annotation for all 18 non-5-Aza treated samples using the scipy.stats python package. The false discovery rate corrected p-value for these correlations was calculated using the Benjamini-Hochberg method (Hochberg, Benjamini, and Hochberg 1995) within the statsmodels.stats.multitest python package.

### 2.4.4 Methylation assessment by bisulfite sequencing

Bisulfite Sanger sequencing was used to validate array methylation data for FBLN2 and quantify gene methylation in cell culture experiments. For array validation, aliquots of DNA samples which had been used for the array were used. For tissue culture experiments whole DNA was isolated from samples as detailed in **section 2.3.3**. DNA (500ng) was bisulfite converted using EZ DNA Methylation-Gold kit (Zymo Research, D5005) as per the manufacturer's protocol. PCR amplification of the region of interest was performed in a 20µl

reaction with the primers detailed in **Table 2.4.4.1** at 500nM. Primers were designed using Methyl Primer Express v1.0.

| CpG | Primer name | Primer sequence | Tm °C | Product Length |
|---|---|---|---|---|
| CpG4 | 4-F1 | TATTTTTAAGGAAATTTTGGGAGTT | 60.22 | 502bp |
| | 4-R1 | CAACCTTAAATTTCAAATCAATTTC | 60.02 | |
| | 4-F2 | TAATGGGTGTAATTTGTTTGTTTTA | 59.56 | 556bp |
| | 4-R2 | ACTAATCTTAAAATTCTCCCCAAAT | 59.55 | |
| CpG42 | 42-F1 | AGTATTTGGAAATTAGTAAGGGTATGT | 58.65 | 433bp |
| | 42-R1 | TTTATCTCCAAACAACTAAACAAAC | 58.73 | |
| | 42-F2 | TTAAAGTAGTTGGGATTTAGGGTAGA | 58.00 | 522bp |
| | 42-R2 | TCTCCAAACAACTAAACAAACCTAC | 57.97 | |

**Table 2.4.4.1 FBLN2 bisulfite sequencing primers**

Primers were designed using Methyl Primer Express v1.0. Successful sequencing was achieved for CpG4 with the PCR product of 4-F2 and 4-R2 sequenced with primer 4-R1.

AmpliTaq Gold DNA Polymerase with Gold buffer (Life Technologies, 4311806) was used with 2mM $MgCl_2$ and 250nM deoxynucleotide mix (Sigma, D7295). Touchdown PCR was performed on a tetrad thermocycler (MJ Research) with the conditions shown in **Table 2.4.4.2**. The PCR product was run on a 2% agarose gel (Bioline, B10-41025) using 0.5x TBE (Invitrogen, 15580-044) and the band of interest (**Figure 3.2.6.1**) cut out on a UV transilluminator. The PCR product was purified with QIAquick Gel Extraction kit (Qiagen, 28704) before Sanger sequencing was performed by Source BioScience (Cambridge). Although PCR products were successfully isolated with all 4 primer pairs, reliable quantification was achieved only for CpG4 with PCR primers 4-F2 and 4-R2 and sequencing performed by primer 4-R1. Sequencing of CpG42 or any adjacent CpGs could not be achieved due to repetitive regions. A bespoke python script was written to align the sequencing data to an *in silico* PCR product using the Biopython Bio.pairwise2 package. The area under the curve for the methylated and unmethylated base of interest was quantified and the ratio of these used to calculate percent methylation.

| | | |
|---|---|---|
| 95°C | 10min | |
| 95°C | 20s | } 10 cycles @ x = 60-50°C (-1°C / cycle) |
| x°C | 20s | } 40 cycles @ x = 50°C |
| 72°C | 30s | } |
| 72°C | 5min | |

**Table 2.4.4.2 Bisulfite sequencing PCR conditions**

PCR amplification of bisulfite converted DNA was performed using a touchdown PCR protocol in 20µl reactions before purification and Sanger sequencing.

## 2.5 RT-qPCR

### 2.5.1 cDNA Synthesis

250-1,000ng of whole RNA, as determined by Nanodrop, was reverse transcribed with qScript master mix (Quanta, 733-1177) in a 20µl final volume reaction in 0.2ml PCR tubes (StarLab, A1402-3700). Thermocycler (MJ Research) conditions were; 5min at 25°C, 30min at 42°C and 5min at 85°C. cDNA was diluted 1:4 by the addition of 60µl nuclease free water and stored at -20°C until used.

### 2.5.2 Housekeeping gene selection

Expression array data was used to determine reliable housekeeping genes for further experiments. Expression array probes including those mapping to typical housekeeping genes (Vandesompele et al. 2002) and those available in the geNORM kit (Primer Design) were ranked by coefficient of variation (CV = standard deviation of Log2 expression / mean Log2 expression) to indicate those most stably expressed across the already-normalised untreated fibroblast data (de Jonge et al. 2007) (**Table 2.5.2.1**). Those with the lowest CV, and available within our lab, were used for subsequent experiments: YWHAZ (tyrosine 3-monooxygenase/tryptophan 5-monooxygenase activation protein zeta), CYC1 (cytochrome c1), EIF4A2 (eukaryotic translation initiation factor 4A2). In 3D spheroid culture experiments, EIF4A2 was excluded from analysis due to high relative variability.

| Rank (CV) | Gene Symbol | probe_id | Mean Log2 Expression | Standard Deviation | Coefficient of Variation |
|---|---|---|---|---|---|
| **3** | **UBC** | **ILMN_2331501** | **14.2** | **0.08** | **0.006** |
| **321** | **UBC** | **ILMN_2038773** | **14.0** | **0.17** | **0.012** |
| **367** | **CYC1** | **ILMN_1815115** | **9.9** | **0.12** | **0.012** |
| **380** | **YWHAZ** | **ILMN_1801928** | **11.4** | **0.14** | **0.013** |
| **398** | **ATP5B** | **ILMN_1772132** | **12.9** | **0.16** | **0.013** |
| **485** | **EIF4A2** | **ILMN_1685722** | **12.3** | **0.16** | **0.013** |
| **1096** | **ACTB** | **ILMN_2038777** | **13.5** | **0.20** | **0.015** |
| **1163** | **ACTB** | **ILMN_2152131** | **13.6** | **0.21** | **0.015** |
| **2709** | **TBP** | **ILMN_1697117** | **7.5** | **0.14** | **0.018** |
| **2867** | **GAPDH** | **ILMN_2038778** | **13.3** | **0.25** | **0.018** |
| **2933** | **RPL13A** | **ILMN_1713369** | **11.9** | **0.22** | **0.019** |
| **3295** | **SDHA** | **ILMN_2051232** | **9.0** | **0.17** | **0.019** |
| **5261** | **ACTB** | **ILMN_1777296** | **13.2** | **0.29** | **0.022** |
| **6430** | **GAPDH** | **ILMN_1802252** | **11.8** | **0.28** | **0.024** |
| **6867** | **HPRT1** | **ILMN_1736940** | **8.4** | **0.21** | **0.024** |
| **6905** | **B2M** | **ILMN_1725427** | **13.1** | **0.32** | **0.025** |
| **7437** | **B2M** | **ILMN_2148459** | **12.1** | **0.31** | **0.025** |
| **7557** | **HPRT1** | **ILMN_2056975** | **9.2** | **0.24** | **0.026** |
| **7594** | **SDHA** | **ILMN_1744210** | **8.6** | **0.22** | **0.026** |
| **7869** | **HMBS** | **ILMN_1726306** | **8.0** | **0.21** | **0.026** |
| **8049** | **GAPDH** | **ILMN_1343295** | **12.7** | **0.34** | **0.027** |
| **9247** | **HMBS** | **ILMN_1685954** | **7.6** | **0.23** | **0.030** |
| **10552** | **TOP1** | **ILMN_2192316** | **7.0** | **0.24** | **0.035** |
| **20039** | **HMBS** | **ILMN_1694476** | **5.6** | **0.12** | **Not Detected** |
| **29757** | **TOP1** | **ILMN_1763419** | **6.0** | **0.11** | **Not Detected** |
| **30236** | **UBC** | **ILMN_2252160** | **6.1** | **0.24** | **Not Detected** |
| **30810** | **YWHAZ** | **ILMN_1669286** | **5.8** | **0.12** | **Not Detected** |

**Table 2.5.2.1 Housekeeping gene selection**

Housekeeping genes were selected based on their coefficient of variation within the normalised expression array

### 2.5.3 Primer Design

Commercially designed housekeeping gene primers were used from Primer Design. Custom PCR primers were created with sequences from the literature, those designed previously within this laboratory by Drs Chris Scotton and Iona Evans, or designed for genes of interest using the Primer-BLAST online tool (ncbi.nlm.nih.gov/tools/primer-blast/; Zhang et al., 2000) with the following preferred search parameters: amplicon length: 70 – 150bp; primer length: 18 – 22bp; primer melting temperature: 57-63°C, optimum 60°C, with a maximum difference of 1°C; preference for exon-exon junction spanning. Custom primers were purchased from

Invitrogen at desalted grade, reconstituted to 100µM with nuclease free water and stored at -20°C. Primer sequences used are in **Table 2.5.3.1**.

| Gene | Forward (5'->3') | Reverse (5'->3') | Product size | Reference |
|---|---|---|---|---|
| **FBLN2** | CTCCTGCTGTGAGGGTGAAG | TGCCTCTGAAACTCTCCGTG | 91bp | designed |
| **COL1A1** | GAGAGCATGACCGATGGATT | ATGTAGGCCACGCTGTTCTT | 149bp | In-house[1] |
| **ACTA2** | ATCCTGACTGAGCGTGGCTATT | GGCCATCTCATTTTCAAAGTCC | 111bp | In-house[1] |
| **YWHAZ** | [Primer Design Ltd] | | | |
| **CYC1** | [Primer Design Ltd] | | | |
| **EIF4A2** | [Primer Design Ltd] | | | |

**Table 2.5.3.1 PCR primer sequences**

PCR primers were designed using NCBI Primer BLAST (FBLN2) or [1]previously designed within our laboratory (COL1A1, ACTA2). Housekeeping primers were supplied by Primer Design Ltd.

### 2.5.4 Real Time PCR

Custom primers were diluted to a working mix containing forward and reverse primers at 8µM each in nuclease free water. Realtime PCR was performed with 2µl of diluted cDNA and 8µl master mix containing primers (housekeeping 300nM final, custom primers 800nM final) and Power SYBR PCR master mix (Applied Bioscience, 4367659) in white 96-well PCR plates (Thermo Scientific, AB0800W) on a Realplex Mastercycler EP[3] (Eppendorf) with the flowing conditions: 10min at 95°C; 40 cycles of: 15sec at 95°C and 60sec at 60°C; with final melting curve analysis. The $2^{-\Delta\Delta Ct}$ method was used to calculate relative gene expression (Livak and Schmittgen 2001; Vandesompele et al. 2002). Briefly, the PCR cycle number at which SYBR fluorescence crossed an arbitrary threshold in the exponential phase (Ct) was exported to Microsoft Excel. The geometric mean Ct of the housekeeping genes was subtracted from the Ct for the gene of interest to give the ΔCt. The mean ΔCt for control samples was then subtracted from the ΔCt of each sample to give the ΔΔCt value. Fold expression relative to the control samples was then calculated as $2^{-\Delta\Delta Ct}$.

## 2.6 Immunohistochemistry

### 2.6.1 Sectioning

3µm sections of formalin-fixed paraffin-embedded (FFPE) 3D culture spheroids in agarose or of lung from donors with IPF (n=5), SSc (n=1) or histologically normal regions removed during lung cancer resection (referred to as 'control'; n=5) were cut on a microtome (Microm HM325) and dried onto polysine coated histology slides (VWR, 631-0107).

### 2.6.2 Immunostaining

Sections were dewaxed and rehydrated with an autostainer (Tissue-Tek DRS-2000, Sakura) using the protocol shown in **Table 2.6.2.1**. Following a 5min wash in tris-buffered saline (TBS; 50mM Tris, 150mM NaCl prepared from a 20x stock, pH7.6) and marking with a hydrophobic pen (Invitrogen, 00-8877), antigen retrieval was performed as detailed in **Table 2.6.2.2**. Saponin antigen retrieval was performed with 0.05% saponin (Sigma, S4521) in distilled water for 30min at room temperature. Slides were washed twice with TBS (2x5min) incubated with 3% hydrogen peroxide (sigma, H1009) in distilled water for 30min to block endogenous peroxidases. Following two washes, sections were blocked with ImmPRESS ready-to-use 2.5% normal horse serum solution (Vector Labs, S-2012) for 20min at room temperature. Blocking solution was removed and slides incubated with primary antibody diluted in TBS with 1% bovine serum albumin (BSA; Millipore, 1.12018) at 4°C overnight. Antibodies and concentrations used are shown in **Table 2.6.2.2**. Negative control staining was performed with a non-immune IgG (isotype) primary antibody at the same concentration. The following day sections were washed twice in TBS and incubated with ImmPRESS secondary-HRP conjugate (Vector Labs) for 30min at room temperature. Following 2 final washes in TBS sections were incubated with Nova Red substrate (Vector Labs, SK-4805) until colour developed (3-5min). Sections were then counterstained with GILL 2 Haematoxylin (Thermo Scientific, 6765008), differentiated in acidic alcohol and dehydrated using the autostainer (protocol shown in **Table 2.6.2.1**) before adding coverslips with an automated coverslipper (Sakura Coveraid. Tape: Cell Path, SAZ-0100-00A). Slides were digitised with a Nanozoomer NDP slide scanner (Hamamatsu) at 40x magnification and images exported with NDP.View2.

| Dewax | |
|---|---|
| **Step** | **Time** |
| Xylene | 3min |
| Xylene | 3min |
| 100% EtOH | 2min |
| 100% EtOH | 2min |
| 70% EtOH | 2min |
| 30% EtOH | 2min |
| $dH_2O$ | - |

| Counterstain | |
|---|---|
| **Step** | **Time** |
| $dH_2O$ | 30sec |
| Haematoxylin | 6sec |
| Tap Water | 20sec |
| 1% HCl, 70% EtOH | 15sec |
| Tap Water | 2min |
| $dH_2O$ | 30sec |
| 70% EtOH | 2min |
| 100% EtOH | 2min |
| 100% EtOH | 2min |
| Xylene | 3min |
| Xylene | 3min |

**Table 2.6.2.1 Autostainer protocols used for immunohistochemistry**

| Application | Antigen | Host | Manufacture | Product Number | Concentration | Antigen retrieval |
|---|---|---|---|---|---|---|
| **IHC- Primary** | Fibulin-2 | Rabbit | Novus Biologivals | NBP1-88115 | 2.0 ug/ml | 0.05% Saponin |
| **IHC- Primary** | Collagen I | Rabbit | Abcam | ab34710 | 2.5 ug/ml | 0.05% Saponin |
| **IHC- Primary** | Isotype control | Rabbit | Abcam | ab27478 | | |
| **IHC- Secondary** | Anti-Rabbit | | Vector Labs ImmPRESS ready to use HRP-conjugate, MP-7401 | | | |
| **IF- Primary** | Fibulin-2 | Rabbit | Novus Biologicals | NBP1-88115 | 0.4 ug/ml | 0.1% Triton-x-100 |
| **IF- Primary** | Collagen I | Mouse | Sigma | C2456 | 1:1000 | 0.1% Triton-x-100 |
| **IF- Primary** | αSMA | Rabbit | Abcam | ab5694 | 1:750 | 0.1% Triton-x-100 |
| **IF- Secondary** | Anti-Mouse: 488 | Goat | Invitrogen | A11001 | 1:1000 | |
| **IF- Secondary** | Anti-Rabbit: 488 | Donkey | Invitrogen | A21206 | 1:1000 | |
| **IF- Secondary** | Anti-Rabbit: 555 | Goat | Invitrogen | A21428 | 1:1000 | |

**Table 2.6.2.2 Antibodies used for immunohistochemistry and immunofluorescence**

αSMA: alpha smooth muscle actin. IHC: FFPE immunohistochemistry, IF: immunofluorescence

### 2.6.3 Histochemistry

Trichrome (a modified Martius Scarlet Blue, MSB) staining was used on sections of FFPE lung to stain collagen/ECM in blue, cellular components such as the bronchial epithelium in red and erythrocytes in yellow. Following dewaxing as above, the autostainer was used to perform the staining protocol outlined in **Table 2.6.3.1**. Celestine Blue (0.5% Celestine Blue, 5% Ferric Ammonium Sulphate, 14% Glycerol in distilled water) and GILL 2 Haematoxylin (an alum haematoxylin) were used to produce an acid resistant nuclear stain. This procedure was followed by a sequence of dyes, generally of increasing size, which act to differentially stain

the tissues. Erythrocytes were stained with 0.2% Orange G in saturated picric alcohol. Cytoplasm was then stained with 'Red mixture' (0.5% Ponceau 2R, 0.5% Acid Fuchsin in 1% Acetic Acid) and collagen with 0.5% Chicago Sky Blue 6BX (Direct Blue) in 1% acetic acid. Sections were then dehydrated and imaged as above.

| Trichrome | |
|---|---|
| **Step** | **Time** |
| Tap Water | 1min |
| Celestine Blue | 10min |
| Tap Water | 1min |
| Distilled Water | 30sec |
| Haematoxylin | 5min |
| Tap Water | 30sec |
| 1% HCl 70% EtOH | 20sec |
| Tap Water | 30sec |
| Tap Water | 2min |
| 100% EtOH | 30sec |
| 0.2% Orange G Picric alcohol | 8min |
| Distilled Water | 5sec |
| Red Mixture | 7min |
| Distilled Water | 20sec |
| 1% phosphotungstic acid | 30sec |
| Distilled Water | 20sec |
| 0.5% Chicago Sky Blue | 5min |
| 1% acetic acid | 20sec |
| Dehydrate to xylene | |

**Table 2.6.3.1 Autostainer protocol used for trichrome stain of FFPE human lung**

### 2.6.4 Immunofluorescence staining

Immunofluorescent staining was performed on cell layers which were fixed as per **section 2.1.5**.

The cell layer was permeabilised with 50µl 0.1% Triton-x-100 in PBS for 90sec, washed with PBS a further 3 times and co-incubated with primary antibodies in 50µl PBS overnight at 4°C (see **Table 2.6.2.2** for antibody details). Wells were washed 3 times with 100µl PBS containing 0.05% tween-20 and incubated with anti-mouse and anti-rabbit fluorescently conjugated secondary antibodies (see **Table 2.6.2.2** for antibody details) and DAPI (1:10,000; Invitrogen, D1306) in 50µl PBS for 1h at room temperature. Finally, cells were washed 3 times with PBS-tween and stored in 200µl PBS at 4°C in the dark until imaging. For fibulin-2 staining HBSS (containing calcium) was substituted for PBS throughout and an additional blocking

step was performed with 5% BSA in HBSS for 1h at room temperature before primary antibody incubation in HBSS containing 1% BSA.

Wells were imaged with an ImageXpress high content plate reader (Molecular Devices) using x20 objective capturing 4 images of 720µm x 720µm fields per well. Cell count (DAPI stained nuclei), stain area and stain intensity (both normalised to cell count) for each colour were exported from MetaXpress software and the mean of each 4 images for each well calculated in Excel. Data is presented as area of each image positive for staining normalised to cell number as the mean of three biological replicate wells.

## 2.7 Western Blotting

### 2.7.1 Protein collection

Optimal ECM lysis for western blotting was determined to be using radioimmunoprecipitation assay buffer (RIPA; Thermo Scientific, 89900) supplemented with 4% Sodium dodecyl sulfate (SDS; Sigma, L3771) and protease and phosphatase inhibitors (HALT, Thermo Scientific, 78441), referred to below as RIPA-SDS, followed by heating at 100°C for 10min. 2D cell cultures in 12-well plates were washed twice with PBS and incubated with 40µl RIPA-SDS on ice for 30min. The cell layer was scraped with a cell scraper (Corning, 3010), pipetted into microcentrifuge tubes and stored at -80°C until use. Frozen spheroids (x8) were directly lysed by resuspending in 30µl RIPA-SDS. All RIPA-SDS samples were heated on a 100°C hot-block for 10min to dissociate the ECM, vortexed and briefly pulsed down in a mini-centrifuge.

### 2.7.2 Protein quantification

Protein quantification was performed by bicinchoninic acid (BCA) assay whereby a purple-coloured complex of $Cu^{+}$ and bicinchoninic acid is produced through the reduction of $Cu^{2+}$ to $Cu^{+}$ by peptide bonds and is therefore proportional to the protein content of the reaction. 2µl neat sample was incubated with 100µl BCA reagent mix in a 96-well plate (Nunc, 167008) for 30min at 37°C and the absorbance read at 562nm. The absorbance of a blank (RIPA-SDS) sample was deducted from all samples before protein content was calculated against a standard curve of Bovine Serum Albumin (Millipore, 1.12018) diluted in milliQ water (0.03 - 2.00 mg/ml).

### 2.7.3 Western blot

6ug protein samples were made up to 13.7µl with variable volumes of milliQ water and mixed with 5µl 10x Bolt sample reducing buffer (final 2x; Novex, B0009) and 6.3µl 4x Bolt LDS sample buffer (Novex, B0007). Samples were reduced by incubating at 100°C for 10min and loaded on Bolt 4-12% Bis-Tris Plus Gels (Invitrogen, NW04125) along with PageRuler plus prestained ladder (Thermo Scientific, 26619). Electrophoresis was performed in Bolt MES SDS running buffer (Novex, B0002) at 150v for 45-90min.

Proteins were transferred to a PVDF membrane (Immobilon-P, Millipore, IPSN07852) which had been activated by brief incubation with 100% ethanol. Transfer was performed in wet transfer buffer (25mM Tris, 190mM Glycine, 20% methanol) at 30v for 16.5h at 4°C. Protein transfer was confirmed by incubating the membrane with Ponceau S solution (Sigma, P7170) for 1min.

### 2.7.4 Protein detection

Luminescent detection of protein of interest was performed using specific primary antibodies followed by HRP-conjugated secondary antibodies and incubation with an enhanced chemiluminescence (ECL) reagent.

Membranes were first washed for 5 min with tris buffered saline containing tween-20 (TBS-T; 50mM Tris, 150mM NaCl prepared from a 20x stock, pH7.6; 0.05% tween-20; Sigma, 70116). Non-specific antibody binding was blocked by incubating the membrane with TBS-T containing 2.5% skimmed milk (Sigma, 70166) and 2.5% BSA for 1-8h at room temperature with rocking. Primary antibody incubations were performed in 5ml TBS-T containing 5% BSA in 50ml falcon tubes on a roller at 4°C for 16h. Membranes were washed in TBS-T (3x5min) before incubation with HRP conjugated antibodies in 5ml TBS-T / 5% BSA on a roller for 90min at room temperature. Membranes were again washed with TBS-T (3x5min). Chemiluminescence was detected by incubating membranes with Luminata Forte HRP substrate (Millipore, WBLUF0500) for 3min and imaging on an ImageQuant system (GE). Membranes were stripped of bound antibodies by incubation with 15ml Restore Plus stripping buffer (Thermo Scientific, 46428) for 15min at room temperature and washed and blocked as above. Stripped membranes were re-probed for α-Tubulin loading control by incubation with HRP conjugated primary antibody in TBS-T / 5% BSA for 90min at room temperature and washed and imaged as before. Antibodies and concentrations used are detailed in **Table 2.7.4.1**.

| Application | Antigen | Host | Manufacture | Product Number | Conc. |
|---|---|---|---|---|---|
| **WB- Primary** | Fibulin-2 | Rabbit | GeneTex | GTX105108 | 1:500 |
| **WB- Primary** | αSMA | Mouse | Dako | M0851 | 1:4,000 |
| **WB- Primary** | α-Tubulin | - | Cell Signalling | 9099S | 1:3,000 |
| **WB- Secondary** | Anti-Rabbit | - | Cell Signalling | 7074P2 | 1:4,000 |
| **WB- Secondary** | Anti-Mouse | - | Cell Signalling | 7076P2 | 1:4,000 |

**Table 2.7.4.1 Antibodies used for western blotting**

### 2.7.5 Western blot quantification

Semi-quantitative densitometry analysis of western blot images was performed on 16-bit Tiff images with the "Gel analyzer" tool in ImageJ software. Data is presented as densitometry of the band of interest normalised to the corresponding α-tubulin band of each lane.

## 2.8 Collagen quantification by HPLC

Collagen accumulation in spheroids was determined by reverse-phase high performance liquid chromatography (HPLC) of hydroxyproline which constitutes approximately 12.2% of collagen but is not found at significant levels in other proteins.

### 2.8.1 Sample preparation

For HPLC analysis, 8 spheroids previously collected as above were thawed, transferred to Pyrex tubes (Corning, 99449-16) in 2ml 6M HCl (VWR, 20252.335) and hydrolysed by boiling at 110°C for 16h. Once cooled, samples were cleared with ~120mg activated charcoal (Sigma, C-5260) and filtered through 0.65µm PVDF membranes (Durapore, Millipore, DVPP02500) into acid resistant tubes (Simport, T334-7SPR). 500µl hydrolysate was evaporated to dryness on a hot block at ~50°C overnight to remove HCl before reconstituting in 100µl milliQ $H_2O$ for 1h at room temperature with frequent vortexing. A standard curve of hydroxyproline (25µM – 0.20µM 1:2 serial dilution) was prepared from a 250µm stock solution (Sigma, H54409 in milliQ water; stored at -20°C) and treated alongside samples throughout.

### 2.8.2 Hydroxyproline derivatisation

Hydroxyproline (Hypro) was derivatised with 4-chloro-7-nitro-2,1,3-benzoxadiazole (NBD-Cl; Acros Organics, 172390050) to yield NBD-Hypro which was detected at 495nm. This reaction happens an order of magnitude faster with hydroxyproline than primary amino acids and to ensure this specificity, the reaction was strictly performed at 37°C for 20min.

100µl 0.4M potassium tetraborate (pH9.5; sigma, P5754) was added to 100µl samples in 1.5ml microcentrifuge tubes followed by 100µl 36mM NBD-Cl in methanol (Fisher Chemical, M/3900/17) and tubes incubated on a hot block at 37°C for 20min. The derivatisation reaction was stopped by acidifying samples with 50µl 1.5M HCl. 150µl 3.33x HPLC buffer A (see **Table 2.8.3.1**) was added to give derivatised samples in 500µl 1x buffer A. Finally, samples were filtered through 0.22µm regenerated cellulose filters (Sartorius, 17821) into vial inserts (JG Finneran, 4025PBS-631). Derivatised samples were kept protected from light before quantification by HPLC.

### 2.8.3 HPLC

HPLC was performed on Agilent series 1100 (Agilent Technologies) with 100µl derivatised sample / standards injected into a LiChrospher reverse-phase column (phase: PR-18, pore size: 100Å, particle size: 5µm, 4 x 250mm; Millipore, 1.50983) at 40°C and eluted in 1.0ml/min flow of mobile phase as detailed in **Table 2.8.3.1**.

| **Mobile Phase (1.0ml/min)**<br>**Buffer A – aqueous acetonitrile (8% v/v), 50mM sodium acetate (pH 6.4)**<br>**Buffer B – aqueous acetonitrile (75% v/v)** | | |
|---|---|---|
| **Elution gradient** | **Time (min)** | **% Buffer B** |
| | **0** | **0** |
| | **5** | **5** |
| | **6** | **80** |
| | **12** | **80** |
| | **12.5** | **0** |
| | **25** | **0** |

**Table 2.8.3.1 HPLC mobile phase conditions**

The hydroxyproline derivative eluted 5min after sample injection (**Figure 2.8.3.1**) and the area under the curve for this peak was exported for quantification of hydroxyproline in derivatisation reactions against the standard curve in Excel. The collagen content of spheroids was calculated assuming 12.2% hydroxyproline content (Laurent et al. 1981; Campa, McAnulty, and Laurent 1990) and normalised to DNA yield of parallel spheroids extracted as per **section 2.3.3** per condition. Data is presented as the mean of three biological replicates, each of eight pooled spheroids, for each condition.

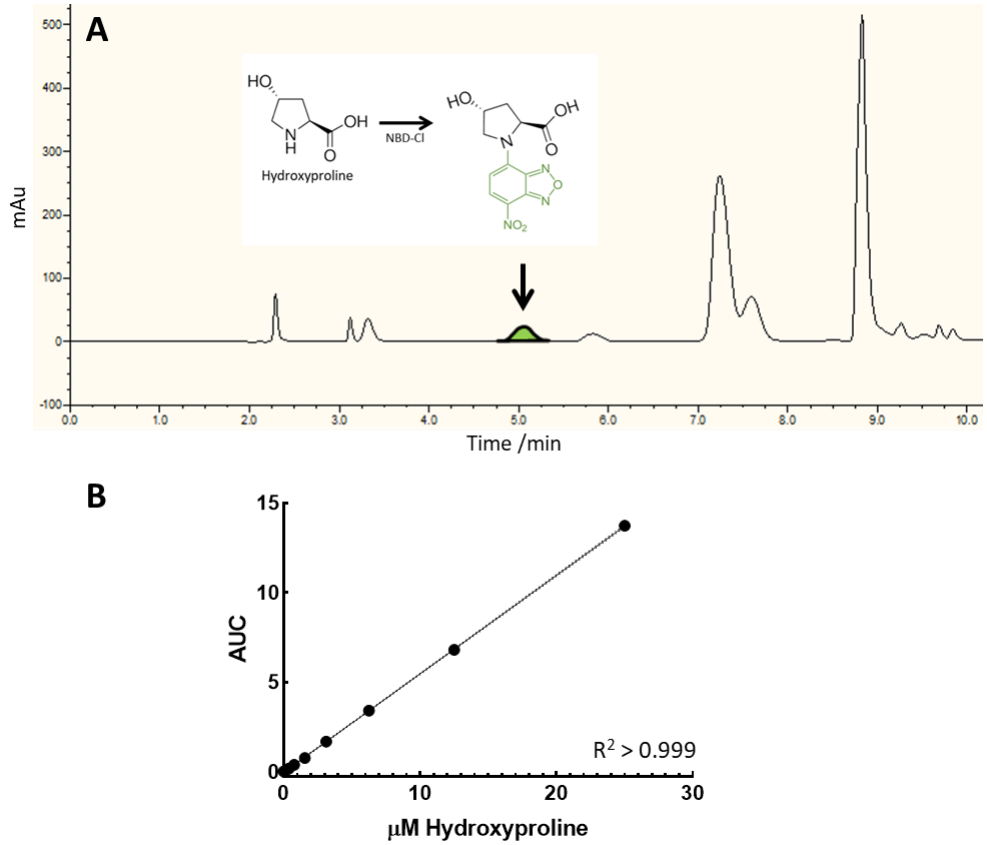


**Figure 2.8.3.1 Typical hydroxyproline HPLC trace and standard curve**

(**A**): A typical 495nm absorption elution trace for a standard showing derivatised hydroxyproline peak at 5min (green). Hydroxyproline content of samples was determined against a standard curve (**B**).

## 2.9 Statistics

All data is presented as mean ± SEM unless otherwise stated. The Limma R package (Smyth 2004) was used to calculate t-test p-values and associated false-discovery p-value for array data. The scipy.stats python package was used to calculate Pearson $R^2$ and Spearman Rho correlation and associated p-values. For experiments containing two experimental groups a Student's T-test was used to determine significance difference between group means. Where experiments contained more than two groups, one-way or two-way ANOVAs with Tukey post-test were performed as appropriate in Graphpad Prism (GraphPad Software, USA). In qPCR experiments, ΔCt values were used to test significance of fold change data presented. A p-value <0.05 was considered to be statistically significant.

# 3 Results

## 3.1 Illumina microarray

There is a persistence of fibrotic phenotype in fibroblasts derived from fibrotic lungs, we and others have shown that this is at least partly due to differences in gene methylation (Keerthisingam et al. 2001; Evans et al. 2016). In order to identify differentially expressed genes which may be regulated by methylation in pulmonary fibrosis expression (Illumina Infinium HT-12 v4) and methylation (Illumina Infinium HumanMethylation 450k) microarrays were performed on human lung fibroblasts from control (n=6), IPF (n=5) and SSc (n=7) donors with and without the demethylating agent 5-aza-2'-deoxycytidine (5Aza). Bulk analysis of data to identify genome wide methylation differences and differential gene expression was performed previously by Dr Ian Garner (I. Garner 2016). In this section, I however began with the most unprocessed data available to us from Cambridge Genomic Services. This data had undergone normalisation and group-pair analysis utilising the Lima R-package. The aim of this section is to apply updated array annotation, filtering and sequential analysis to identify a gene of interest for further study. In order to identify biologically interesting genes, throughout this section the gene lists generated by analysing expression differences were checked for Gene Ontology (GO) enrichment. GO is an ever-expanding database of manually curated gene annotations which includes associating a gene with various biological processes using data from the literature. GO is hierarchical with 'child' terms being more specific than their 'parents'. GO term enrichment was performed using the GOrilla online tool (Eden et al. 2009) against an appropriate background for the gene set being analysed. The most specific 'child' terms for each branch were then selected in order to exclude generic terms with little biological significance.

### 3.1.1 Expression array: Altered gene expression in pulmonary fibrosis

Expression array data for control, IPF and SSc lung fibroblasts was annotated using data from the Re-Annotator program (Arloth et al. 2015). This annotation improves upon the manufacturer's annotation data for a number of probes utilising *in silico* alignment of probe sequences to the hg19 reference genome. Probes are also graded on their specificity to the target transcript and accuracy of sequence alignment. Only probes meeting the authors 'reliable' grade and genes on autosomes were included for analysis. Analysis was performed at the probe level for transcripts which had been detected above background in at least one sample. This resulted in the inclusion of 17,381 detected transcript probes mapping to 12,445 genes.

Because of the small sample size few genes reached statistical significance when correcting for multiple testing. Therefore, a threshold number of misclassifications (TNoM) of ≤ 1 was used to identify genes in which expression levels in fibrotic and control fibroblasts formed two populations. Analysis was performed at the probe level; therefore, a gene may be present with both increased and decreased expression depending on the transcript specificity of each probe. Altered expression (TNoM ≤ 1, $p < 0.05$) was found in 522 genes in IPF (287 increased, 235 decreased) and 678 genes in SSc (335 increased, 341 decreased, 2 with probes both increased and decreased) when compared to control lung fibroblasts (**Figure 3.1.1.1**). Approximately 8.7% of differently expressed genes were shared between IPF and SSc (41 increased, 55 decreased, **Figure 3.1.1.1**), these may represent a population of genes most relevant to the pathogenesis of pulmonary fibrosis. A further two genes had expression which was altered in different directions in IPF and SSc.

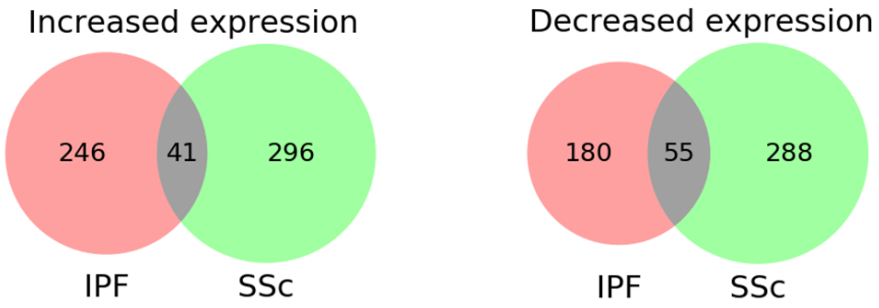


**Figure 3.1.1.1 Number of genes with differential expression in IPF and SSc**

A number of genes were identified as differentially expressed by microarray (TNoM ≤ 1, $p < 0.05$) in isolate IPF (n=5) and SSc (n=7) lung fibroblasts when compared to those from control donors (n=6).

GO analysis of the genes identified as differentially expressed in IPF and/or SSc was performed against a background of all genes detected in the array. No GO terms were enriched above a false discovery rate (FDR) q-value < 0.05 however uncorrected significant enrichment was observed in some GO terms which may be relevant to fibrosis. The GO term GO:0030198 'extracellular matrix organization' was annotated in genes upregulated in both IPF and SSc compared to controls. GO:0051972 'regulation of telomerase activity' was annotated for genes downregulated in both IPF and SSc. The genes contained within these terms may therefore highlight those of greatest interest in the pathogenesis on pulmonary fibrosis.

**Upregulated in IPF and SSc**

| GO Term | Description | P-value | FDR q-value | No. Genes |
|---|---|---|---|---|
| GO:0006663 | platelet activating factor biosynthetic process | 3.52E-05 | 5.03E-01 | 2 |
| GO:0030198 | extracellular matrix organization | 9.06E-04 | 1.00E+00 | 5 |

**Downregulated in IPF and SSc**

| GO Term | Description | P-value | FDR q-value | No. Genes |
|---|---|---|---|---|
| GO:0002253 | activation of immune response | 8.87E-05 | 6.34E-01 | 8 |
| GO:0045088 | regulation of innate immune response | 4.68E-04 | 1.00E+00 | 7 |
| GO:0001906 | cell killing | 4.80E-04 | 1.00E+00 | 3 |
| GO:0010468 | regulation of gene expression | 5.18E-04 | 1.00E+00 | 26 |
| GO:0060100 | positive regulation of phagocytosis, engulfment | 9.47E-04 | 1.00E+00 | 2 |
| GO:0051972 | regulation of telomerase activity | 9.81E-04 | 1.00E+00 | 3 |
| GO:1903506 | regulation of nucleic acid-templated transcription | 9.99E-04 | 1.00E+00 | 21 |

**Table 3.1.1.1 Gene Ontology process enrichment in genes differentially expressed in IPF and SSc compared to controls**

Enriched GO terms in genes with overlapping expression changes in both IPF and SSc compared to control cells. No terms reach a significant FDR q-value against the background of all genes detected in the array.

### 3.1.2 Methylation array: Altered gene methylation in pulmonary fibrosis

CpG methylation levels were assessed across the genome with Illumina Infinium HumanMethylation 450k bead chips. Many probes have been identified as covering a known single nucleotide polymorphism (SNP) or binding more than one region on the genome (Price et al. 2013; Nordlund et al. 2013; Zhou, Laird, and Shen 2017) and may therefore not accurately report methylation levels. The ChAMP R-package (Morris et al. 2014) was used to remove non-specific probes and those mapping to known SNPs near the target CpG. This utilises annotation from Nordlund *et al.* (2013) and Zhou *et al.* (2016). Probes mapping to sex chromosomes were also removed. This left 412,481 CpGs included in analysis.

As in the expression array, due to the small sample size and heterogeneity in IPF only two CpGs were identified as differentially methylated in IPF using FDR $p < 0.05$. Instead, a difference in mean methylation beta value (the fraction of each CpG methylated in the population of cells) of 13.6% (non-corrected $p < 0.05$) was used to identify differentially methylated CpGs. This threshold has been shown to detect differences with 95% confidence (Bibikova et al. 2009). 11,073 CpGs in IPF and 11,161 SSc had altered methylation when compared to control cells, these CpGs corresponded to 4,182 and 4,481 genes respectively. There was a bias towards decreased methylation in IPF, 68% of differentially methylated CpGs, and increased methylation in SSc, 66%, **Figure 3.1.2.1**.

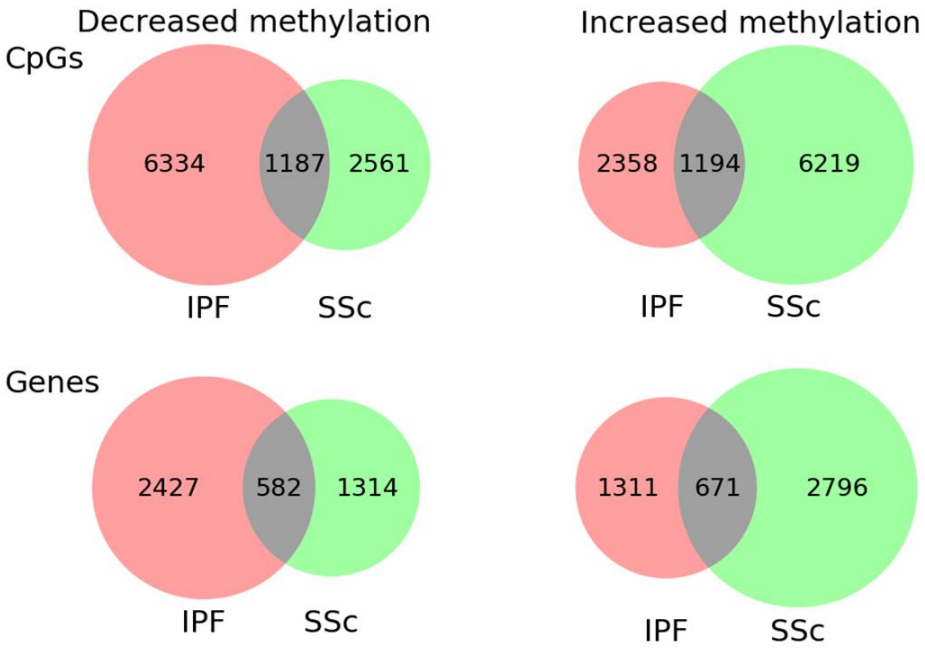


**Figure 3.1.2.1 Number of CpGs and genes differentially methylated in IPF and SSc**

Significant differences in CpG methylation ($\Delta\beta \geq 13.6\%$, $P < 0.05$) were identified in IPF (n=5) and SSc (n=7) lung fibroblasts compared to controls (n=6). The number of genes relating to these probes is shown. Note, many genes are covered by multiple CpG probes and may be represented with simultaneously increased and decreased methylation.

### 3.1.3 Identification of genes potentially regulated by methylation and involved in the pathogenesis of pulmonary fibrosis.

To identify genes in which CpG methylation may be directly regulating expression correlation analysis was conducted between the CpG methylation level and $Log_2$ expression. This was conducted pairwise between methylation and expression probes matched by gene symbol in the annotations used above. In total 308,861 methylation-expression probe pairs relating to 11,435 genes were analysed. Primarily the Pearson correlation coefficient ($R^2$) was calculated within all 18 fibroblast cell lines. Using a FDR of 5%, 146 genes were identified with expression correlating to methylation in at least one probe-pair. This equated to a minimum $R^2$ value of approximately 0.67. In order to maximise the number of genes of interest taken forward a less stringent cut-off of $R^2 \geq 0.50$ with a non-corrected $p < 0.05$ was used. This equates to a FDR of approximately 20%.

932 genes were identified with significant correlation ($R^2 \geq 0.50$, $P < 0.05$) to a total of 1402 CpGs. Of these genes, 410 had a positive correlation to CpG methylation, 445 had negative correlation and 77 contained multiple CpGs with both positive and negative correlation.

| | Correlation | | | Total |
|---|---|---|---|---|
| | Positive | Both | Negative | |
| **Genes** | 410 | 77 | 445 | 932 |
| **CpGs** | 672 | - | 730 | 1402 |

**Table 3.1.3.1 Number of CpGs and genes in which methylation correlated with expression**

Significant Pearson correlation ($R^2 \geq 0.5$, $P < 0.05$), both positive and negative, was identified between methylation β-level of 1402 CpGs and $Log_2$ expression level of 932 associated genes within all 18 untreated isolated fibroblast lines.

Pearson correlation analysis assumes as linear relationship between two variables which may not be true for methylation and expression. In order to include non-linear relationships, the Spearman's ranked correlation coefficient was also calculated for each probe-pair. 67 probe pairs mapping to 56 genes had a significant Spearman correlation with a FDR of 5%. Three of these genes were not identified by Pearson correlation analysis above and were included in the list of genes where methylation correlated with expression going forward (935 genes).

### 3.1.4 Effect of DNMT inhibition on gene expression

Changes in gene expression induced by inhibition of DNA methyltransferase enzymes enable the identification of genes potentially regulated by DNA methylation. Although 5-Aza-2'-deoxycytidine (5Aza) treatment had significant ($p < 0.05$) effects on many CpGs, most did not reach a $\Delta\beta \geq 13.6\%$ cut off.

5Aza treatment altered mean methylation ($\Delta\beta \geq 13.6\%$, $P < 0.05$) in 284 CpGs in control (283 decreased, 1 increased), 670 CpGs in IPF (666 decreased, 5 increased) and only 1 in SSc (increased). Analysis of methylation changes in individual cell lines identified a sub-population of lines that responded to 5Aza treatment more strongly (control n=3, IPF n=3, SSc n=0). The number of CpGs responding to 5Aza treatment ($\Delta\beta \geq 13.6\%$) in each cell line is shown in **Table 3.1.4.1**.

548 genes in control, 2912 genes in IPF and 940 genes in SSc has significant changes in mean expression with 5Aza treatment (TNoM ≤ 1, $p < 0.05$). The number of genes in each cell line

with ≥ 2-fold change in expression with 5Aza treatment identifies the same 6 cell lines as strongly responding to 5Aza (**Table 3.1.4.1**). These 6 cell lines may therefore be of interest in investigating the effects of 5Aza treatment and the role of methylation in individual genes.

| Cell line | Methylation altered by 5Aza. Number of CpGs: | | | Expression altered by 5Aza. Number of Genes: | | |
|---|---|---|---|---|---|---|
| | Control | IPF | SSc | Control | IPF | SSc |
| **1** | **12101** | **8985** | 582 | **250** | **618** | 7 |
| **2** | 781 | **31194** | 2063 | 9 | **632** | 5 |
| **3** | **26608** | 1375 | 1235 | **496** | 111 | 3 |
| **4** | **14848** | 313 | 458 | **656** | 127 | 102 |
| **5** | 321 | **15942** | 620 | 0 | **625** | 117 |
| **6** | 704 | - | 495 | 115 | - | 52 |
| **7** | - | - | 596 | - | - | 151 |

**Table 3.1.4.1 Number of CpGs with altered methylation and genes with altered expression in each cell line following 5Aza treatment**

A change in methylation of individual CpGs (≥ 13.6%) and genes (≥ 2-fold) following 5Aza treatment split the array cell lines into two populations. 3 control, 3 IPF and no SSc cell lines were deemed strong responders to 5Aza (bold).

### 3.1.5 Identification of genes of interest which are potentially involved in the pathogenesis of pulmonary fibrosis.

The aim of this section is to identify a gene of primary interest from the 47,000+ transcripts on the Illumina expression array. As gene regulation by methylation was a key interest in this array experiment, the 935 genes which had at least one methylation probe correlating to expression were chosen as a starting point for a filtering scheme (summarised in **Figure 3.1.5.1**). In the second step, those genes which showed a difference in expression (TNoM ≤ 1, $p < 0.05$; section 3.1.1) in IPF or SSc compared to control lung fibroblasts were then taken forward, yielding 177 genes. Subsequently, a change in mean expression of any magnitude ($p < 0.05$) in any of control, IPF or SSc following 5Aza treatment was used to further reduce the number of genes. Although not a particularly stringent threshold this resulted in a list of 99 genes which should be enriched for those differentially expressed in PF and potentially controlled by methylation.

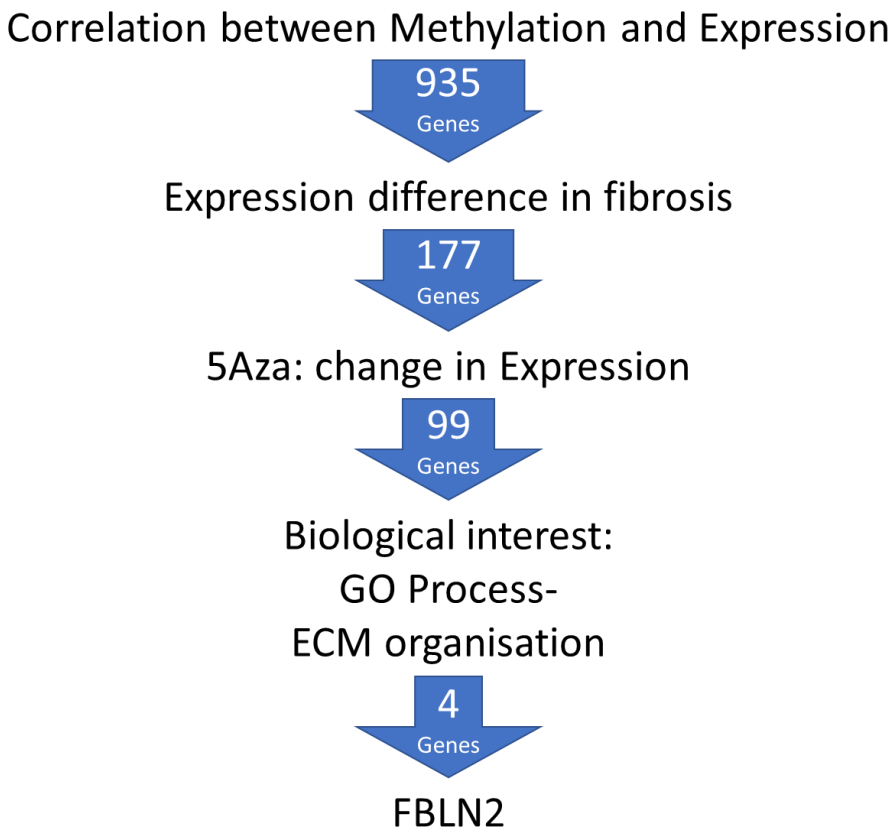


**Figure 3.1.5.1 Filtering scheme used to identify a gene of interest**

Filtering was performed to identify genes of interest from the lists generated by bulk array analysis. Gene Ontology annotation helped to identify fibulin-2 (FBLN2) as a potential gene of interest which may be regulated by CpG methylation.

The next step was identifying a gene of biological interest from this list of 99 genes. For this, Gene Ontology (GO) process enrichment analysis was used. No GO terms were statistically enriched in the lists of 177 and 99 genes detailed above when compared to the full list of genes input into the beginning of correlation analysis (11,435 genes). I therefore used GO to simply annotate the list of 99 candidate genes of interest for manual filtering. Multiple GO terms were included in this gene list, those with the most relevance to pulmonary fibrosis are shown in **Table 3.1.5.1**. In particular 4 genes were annotated for GO:0030198 'extracellular matrix organization' which was identified above in genes upregulated in both IPF and SSc (**Table 3.1.1.1**). These 4 genes are listed in **Table 3.1.5.2** and their $Log_2$ expression levels are shown in **Appendix 1** and **Appendix 2**.

| GO Term | Description | Number of genes |
|---|---|---|
| GO:0030154 | cell differentiation | 27 |
| GO:0007155 | cell adhesion | 10 |
| GO:0008219 | cell death | 8 |
| GO:0007010 | cytoskeleton organization | 8 |
| GO:0030198 | extracellular matrix organization | 4 |
| GO:0008283 | cell population proliferation | 3 |

**Table 3.1.5.1 GO process terms annotated in 99 genes of interest**

Although GO enrichment did not return any significant results, GO annotation of 99 genes of interest included multiple processes of interest in pulmonary fibrosis. These are shown alongside the number of genes with each annotation.

| Gene Symbol | Gene Name |
|---|---|
| ADAM15 | ADAM metallopeptidase domain 15 |
| CD47 | CD47 molecule |
| FBLN2 | Fibulin-2 |
| PTK2 | protein tyrosine kinase 2 |

**Table 3.1.5.2 Genes of interest annotated for GO:0030198 'extracellular matrix organization'**

Four genes of interest have been identified through sequential filtering to identify genes dysregulated in pulmonary fibrosis derived lung fibroblasts. The genes are differentially expressed in IPF and/or SSc compared to controls, have altered gene methylation and are GO annotated for ECM organisation.

Following literature review, fibulin-2 (FBLN2) was selected for further investigation. The currently annotated GO functions and processes for fibulin-2 are shown in **Table 3.1.5.3**. These terms are likely incomplete either through incomplete annotation of the available literature or due to the lack of knowledge relating to fibulin-2. For example, from data in the literature it would be expected that fibulin-2 could be annotated for other processes such as GO:0007155: cell adhesion.

| **Process** | |
|---|---|
| GO:0030198 | extracellular matrix organization |
| GO:0010811 | positive regulation of cell-substrate adhesion |
| **Function** | |
| GO:0005509 | calcium ion binding |
| GO:0050840 | extracellular matrix binding |
| GO:0005201 | extracellular matrix structural constituent |
| GO:0030023 | extracellular matrix constituent conferring elasticity |

**Table 3.1.5.3 Gene Ontology (GO) terms associated with fibulin-2**

Fibulin-2 was identified as a potential gene of interest in pulmonary fibrosis. The above GO terms were associated with fibulin-2. Retrieved from: http://amigo.geneontology.org/

### 3.1.6 Summary

- Expression array analysis of human lung fibroblasts identified numerous dysregulated genes in IPF or SSc compared to control cells. A small proportion of these (96; 8.7%) were shared between IPF and SSc.

- Differential methylation was observed in 19,853 CpGs mapping to 9,101 genes in IPF and/or SSc compared to controls. 13.8% of these genes overlapped between IPF and SSc.

- Correlation analysis identified a potential direct relationship between CpG methylation and gene expression in 935 genes across all 18 cell lines.

- Through sequential filtering fibulin-2 was identified as a gene of interest which is dysregulated in pulmonary fibrosis and potentially regulated by CpG methylation.

## 3.2 Fibulin-2: array data and validation

Fibulin-2 was identified above as a gene of interest which may be differentially expressed in fibrotic lung fibroblasts and the expression of which may be regulated by gene methylation. Fibulin-2 was of biological interest through its GO annotation for 'extracellular matrix organization' and through literature review. Fibulin-2 is upregulated during wound healing (Fässler et al. 1996; Kanan et al. 2014), in decellularized IPF lung (Booth et al. 2012) and in the bleomycin mouse model of fibrosis (Schiller et al. 2015). Fibulin-2 deficiency is protective in a mouse model of cardiac fibrosis (H. Zhang et al. 2014; Khan et al. 2016).

In this section the expression levels of fibulin-2 were further investigated and validated by real-time PCR in cultured cells and investigated in human lung tissue by immunohistochemistry. CpG methylation across the *FBLN2* gene was mapped and related to gene expression.

### 3.2.1 Fibulin-2 expression – mRNA

Three expression array probes were annotated to fibulin-2 (FBLN2), two of which (ILMN_2390919 and ILMN_1774602) were detected above background levels while probe ILMN_1721769 was not ($Log_2$ expression data for each probe is shown in **Appendix 1**). The binding location of each probe was mapped to the transcriptome using NCBI nucleotide BLAST (blast.ncbi.nlm.nih.gov/Blast.cgi, Zhang et al. 2000) and the corresponding FBLN2 exon locations downloaded for Genome assembly: GRCh37.p13.

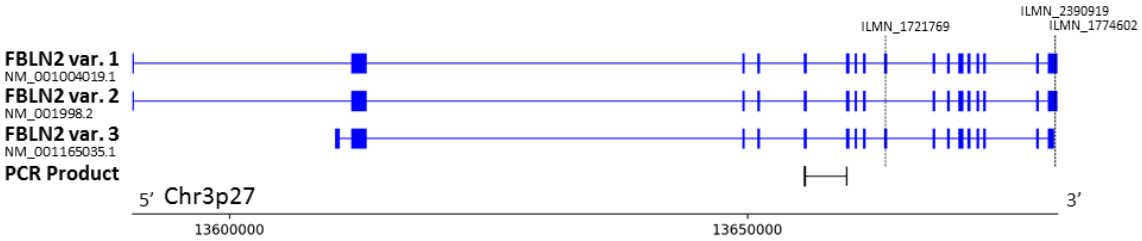


**Figure 3.2.1.1 Alignment of expression array probes and RT-qPCR product on FBLN2 transcript variants**

The binding location of Illumina expression array probes enables identification of the transcript variants expressed in human lung fibroblasts. Expression was detected in probes ILMN_2390919 and ILMN_1774602 but not ILMN_1721769 suggesting that only variant 2, referred to in publications as FBLN2-short, is expressed. **Blue**: Probe binding sites are shown on an exon schematic of the three FBLN2 transcripts (GRCh37.p13 RefSeq assembly, grch37.ensembl.org/Homo_sapiens). **Black**: RT-qPCR product used for expression validation produced using an exon-exon junction spanning reverse primer, product length 91bp.

When mapped to GRCh37.p13, probes ILMN_2390919 and ILMN_1774602 overlapped by 35 bases and mapped to 3' regions on all three FBLN2 transcripts. ILMN_1721769 which was not detected in the array aligned to alternatively spliced exon 9 that is found in transcript variants 1 and 3 only. This suggests that variant 1 and 3 are not expressed by human lung fibroblasts. Detection of only variant 2 is in agreement with literature which shows only 'fibulin-2 short' (lacking the alternatively spliced exon) is detected in nasopharyngeal carcinoma (Law et al. 2012).

The two detected probes had significantly increased expression in IPF (mean of both probes 5.9-fold, $p < 0.01$, TNoM = 1) and SSc (mean 4.4-fold, $p < 0.01$, TNoM = 1) compared to control cells (**Figure 3.2.1.2A**). This was validated by reverse transcription real-time PCR (**Figure 3.2.1.2B**) using custom primers which amplify all three transcript variants (**Figure 3.2.1.1**). There was a strong correlation ($R^2 = 0.827$, $p < 0.001$) between array expression values ($Log_2$ expression, mean of both probes) and PCR dCt value (**Figure 3.2.1.2C**) validating the expression levels detected on the Illumina array.

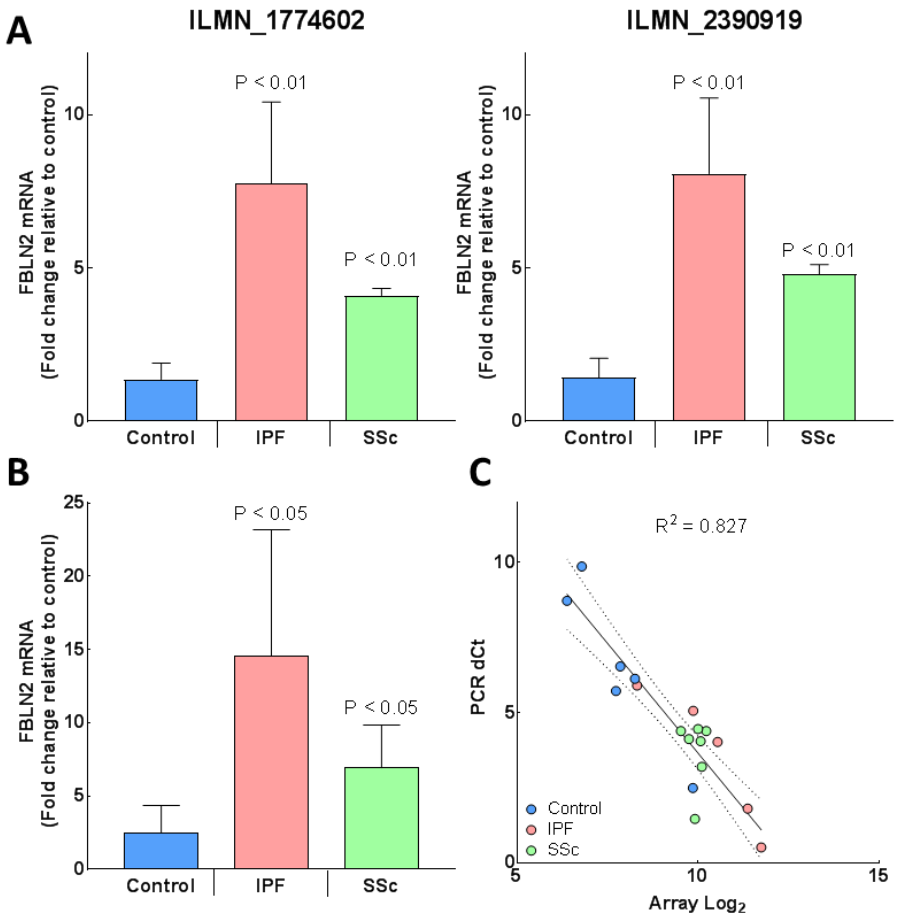


**Figure 3.2.1.2 Expression of FBLN2 mRNA by array and PCR validation**

Expression of FBLN2 was significantly increased in IPF (n=5) and SSc (n=7) isolated lung fibroblasts when compared to those from Control donors (n=6) by (**A**) Illumina Infinium HumanHT-12 v4 array. The specificity of this array result was validated in the same samples by (**B**) RT-qPCR with a strong correlation ($p < 0.001$) (**C**). FBLN2 probes ILMN_1774602 and ILMN_2390919 $p<0.01$, TNoM ≤ 1; probe ILMN_1721769 was not detected above background. Mean ±SEM, p vs control cells. PCR data: one-way ANOVA, Tukey post-test. Correlation: Pearson $R^2$ with 95% confidence region.

A further cohort of control (n=7) and IPF (n=7) derived fibroblasts were grown in identical conditions to those used in the array and FBLN2 expression assessed by RT-qPCR. Mean expression in IPF cells was 5.75 ±2.76 fold higher than that of controls. Due to the large variability of expression in IPF this did not reach significance (Student's t-test $p = 0.22$). Combining the array samples and this validation cohort did yield a significant increase of 10.56 ±5.01 fold in IPF ($n = 12$, $p < 0.05$) compared to controls ($n = 15$).

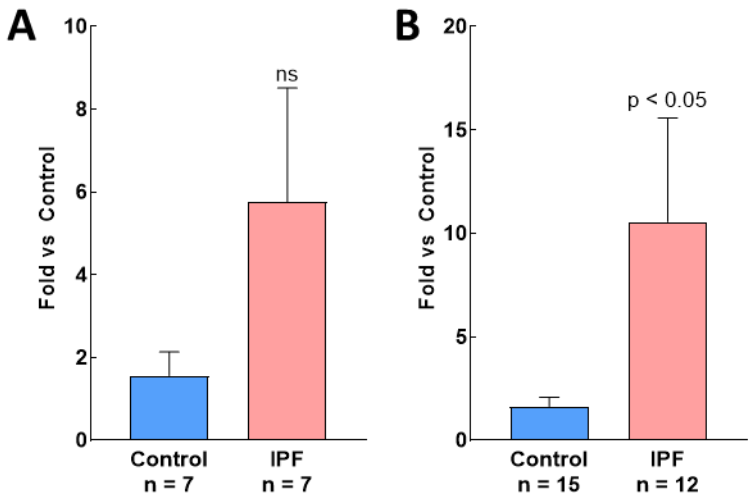


**Figure 3.2.1.3 Expression of FBLN2 mRNA in a validation cohort**

An independent validation cohort of control (n=7) and IPF (n=7) fibroblasts grown in identical conditions to array cells showed a large but non-significant increase in FBLN2 expression in IPF by RT-qPCR (**A**). Combining RT-qPCR samples from both validation and array cohorts, FBLN2 was significantly upregulated in IPF fibroblasts (n=12) compared to controls (n=12) (**B**). Student's t-test.

### 3.2.2 Fibulin-2 expression – immunohistochemistry

Having identified high expression levels of fibulin-2 mRNA in isolated lung fibroblasts immunohistochemistry was used to investigate expression and localisation of fibulin-2 protein in human lung tissue. Formalin-fixed paraffin-embedded lung tissue from control (n=5), IPF (n=5) and SSc (n=1) donors showed strong positive staining with a fibulin-2 specific antibody; there was no staining observed with a non-specific isotype control primary antibody (**Figure 3.2.2.1D**). In agreement with data from the literature staining was localised to vascular and airway walls and in regions associated with elastin fibre localisation. In control lung tissue positive staining of individual fibroblast-like cells could be identified (**Figure 3.2.2.1A**, arrows). Fibrotic lung tissue had more widespread and diffuse staining within the alveolar interstitium associated with areas of extracellular matrix deposition. These results suggest expression in the fibrotic lung is both increased and has more dysregulated localisation.

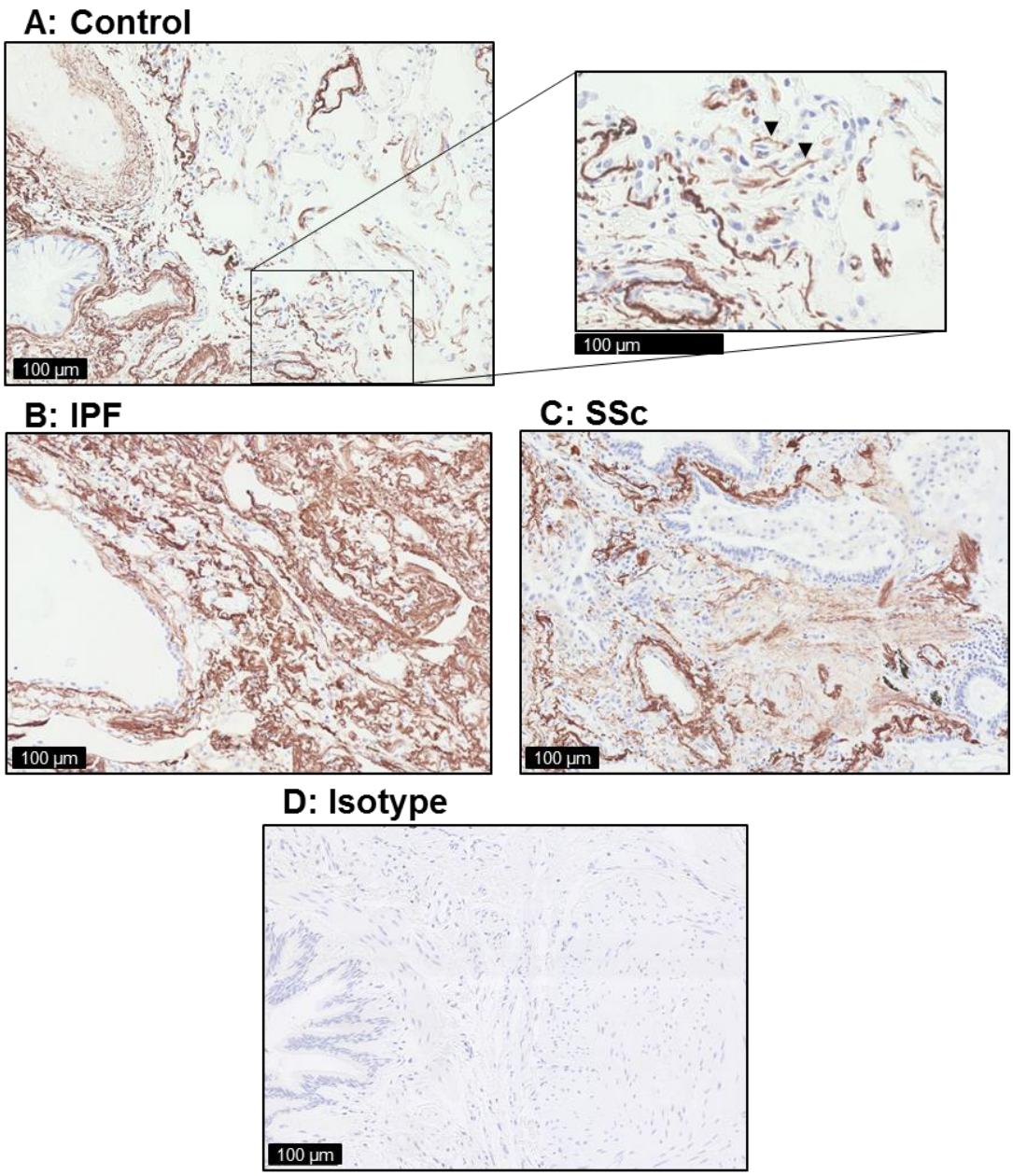


**Figure 3.2.2.1 Fibulin-2 expression in lung tissue by immunohistochemistry**

Representative immunohistochemical staining in Control (**A**, n=5), IPF (**B**, n=5) and SSc (**C**, n=1) donor tissue localised predominantly to the airway and vessel walls, alveolar interstitium and regions associated with elastin fiber localisation. Positive staining of individual fibroblast-like cells could be seen in control tissue (arrows). In addition to regions highlighted for control lung, fibrotic lung tissue showed widespread diffuse staining associated with areas of ECM deposition. There was no staining observed with an isotype control primary antibody (**D**).

### 3.2.3 Fibulin-2 methylation by microarray

One potential mechanism regulating the increased expression of fibulin-2 in fibrotic lung fibroblasts is CpG methylation of the FBLN2 gene. To assess the methylation status of CpGs

across the genome, DNA extracted in parallel to mRNA analyzed above was assessed using Illumina 450k methylation arrays. Methylation data is reported as β-values (% CpG methylation within the sample population). A difference in methylation β-value of 13.6% was used as the threshold for determining differential methylation.

57 CpG probes were annotated to FBLN2 or manually included in the intergenic span upstream, however once those covering SNPs or mapping to more than one region on the genome (Nordlund et al. 2013; Zhou, Laird, and Shen 2017) were removed 53 CpGs remained for analysis.

Altered methylation ($\Delta\beta \geq 13.6\%$, $p < 0.05$) of FBLN2 was detected in fibrotic lung fibroblasts compared to those controls; 1 CpG site had decreased methylation in both IPF and SSc compared to control cells, a further 5 CpG sites had hypermethylation in IPF only. The location and mean methylation level of each array CpG probe by disease group is shown in **Figure 3.2.3.1**.

Regions of increased CpG frequency, CpG islands (CGI) are found in ~70% of gene promoters and their methylation is traditionally thought to repress expression (Price et al. 2013). UCSC genome browser defines a CpG island as CG content >50%, Observed/ Expected (O/E) CpG ratio >0.6 and length >200 bps however annotation from Price et al. (2013) further classified regions of DNA within the categories:

- High-density CpG islands (HCs): CG content >55%, O/E CpG ratio >0.75 and length >500 bps
- Intermediate-density CpG islands (ICs): CG content >50%, O/E ratio >0.48 and length >200 bps
- Non-islands (low-density CpG regions, LCs): non-HC/IC regions

1 HC island was annotated in FBLN2, this was at the transcription start site for variants 1 and 2 and methylation across all untreated cell lines was low within this region (mean ±SEM for all samples 18.2% ±1.2%). A further 8 IC regions were annotated within the gene which had 73.3% ±1.0% mean methylation. Mean methylation of non-island CpGs within the gene was 65.3% ±1.9%.

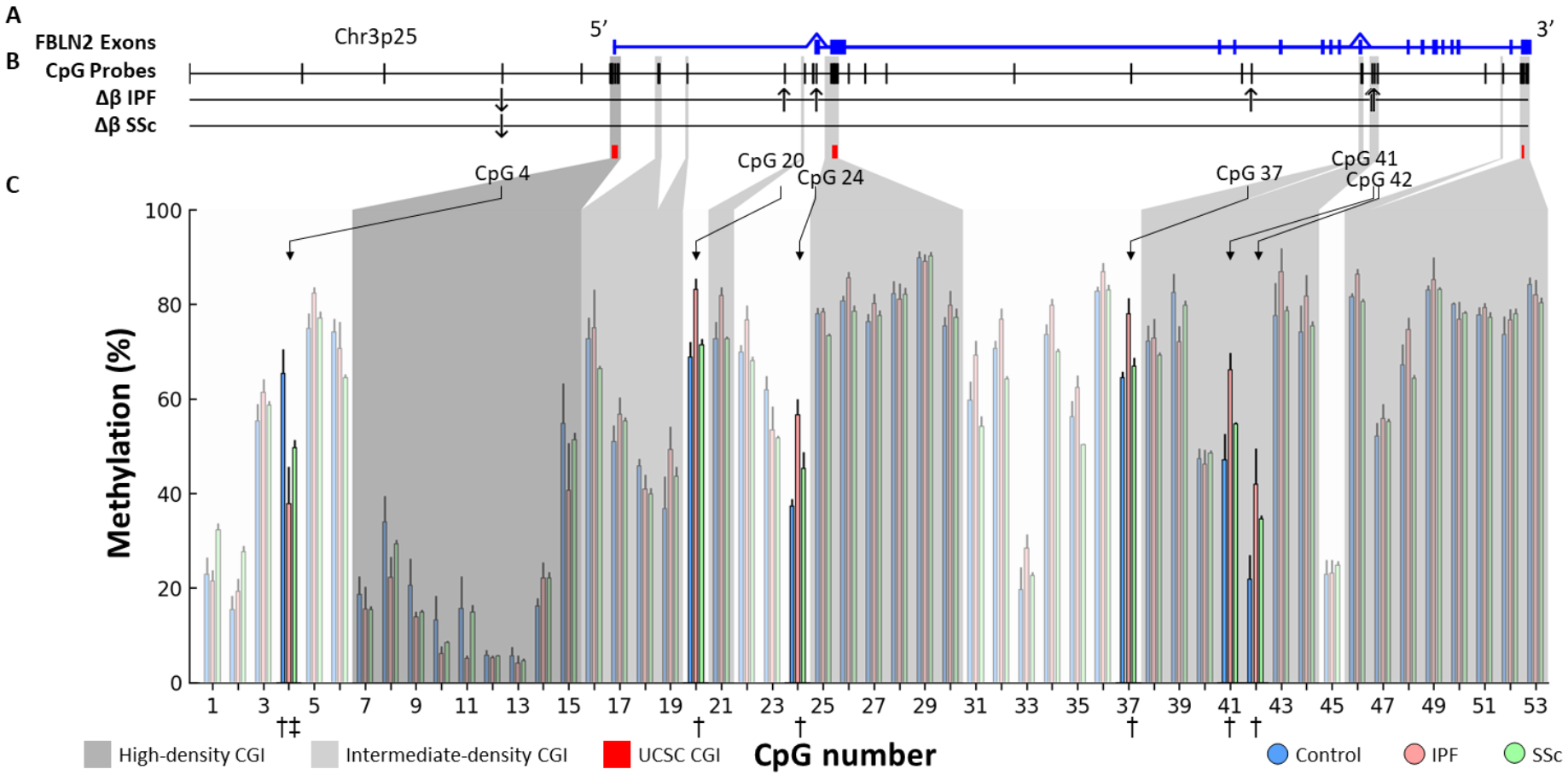


**Figure 3.2.3.1 Methylation of the FBLN2 gene**

(**A**): Schematic of FBLN2 gene showing exons for all transcript variants (blue boxes). (**B**): Of the 53 Illumina probes targeting CpGs within FBLN2 (B-upper) one was differentially methylated (Δβ ≥ 13.6%, $p < 0.05$) in both IPF (B-middle, n=5) and SSc (B-lower, n=7) compared with Control (n=7) and five were differentially methylated in IPF only. CpG islands (CGI), regions increased CpG frequency, are shown from Price et al. 2013 (grey) and UCSC genome browser (red). (**C**): Percentage methylation at each CpG site (Mean ±SEM) is shown with differentially methylated CpGs in IPF (†) and SSc (‡) highlighted.

### 3.2.4 Correlation between fibulin-2 methylation and expression

To identify any direct relationship between methylation of individual CpGs and expression of the fibulin-2 gene the Pearson $R^2$ correlation coefficient was calculated for each CpG. The methylation β value of 2 CpG probes had significant correlation ($R^2 \geq 0.50$, $p \leq 0.05$) with $Log_2$ expression levels. CpG 4 (probe cg12886406) had negative correlation, with increased methylation relating to decreased expression ($R^2 = 0.763$, $p < 0.001$). CpG 42 (probe cg24632944) had the reverse, with increased methylation relating to increased expression ($R^2 = 0.660$, $p < 0.001$). A further two CpGs had moderate negative correlation with expression however methylation differences were small and these CpGs did not have a significant difference in methylation in IPF or SSc compared to control (CpG 18: $R^2 = 0.547$, $p < 0.001$; CpG 39 $R^2 = 0.511$, $p < 0.001$; **Appendix 3**).

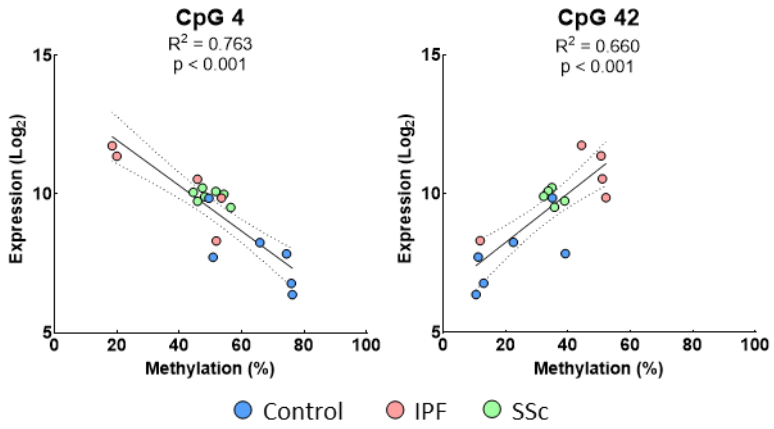


**Figure 3.2.4.1 Correlation between methylation and expression in fibulin-2**

There was a significant correlation between expression (mean of both detected array probes) and methylation in all 18 cell lines of two differentially methylated CpG array probes, CpG 4 ($R^2 = 0.763$, $p < 0.001$) and CpG 42 ($R^2 = 0.660$, $p < 0.001$) suggesting expression may be regulated by the methylation of these CpGs. Pearson $R^2$ with 95% confidence region.

### 3.2.5 Fibulin-2 methylation and expression following demethylation treatment

Treatment with the demethylating agent 5-Aza-2'-deoxycytidine (5Aza, 1µM) was used to elucidate the relationship between gene methylation and expression. It would be expected that demethylation treatment reduced methylation β-values across the genome and this would increase the expression of genes regulated by methylation. We have shown that within this array experiment 5Aza treatment was successful in affecting methylation and expression of other target genes which are known to be regulated by methylation including TCIM (Evans et al. 2016) and TNXB (I. M. Garner et al. 2013).

5Aza treatment did not affect the mean methylation of the fibulin-2 CpGs on the array (**Figure 3.2.5.1A**) in analysis of all 18 cell lines. Expression of fibulin-2 was unchanged in control and IPF cells but there was a small but significant decrease in expression in SSc cells (**Figure 3.2.5.1B**).

There was a significant correlation between the change in methylation and expression in individual cell lines in the sub-population of cells shown to globally respond more strongly to 5Aza (control n=3, IPF n=3, SSc n=0, section **3.1.4**) which was not seen when all 18 cell lines were analysed. Three CpGs had significant correlation between change in methylation and change in expression ($R^2 \geq 0.57$, $p < 0.05$), one of these (CpG 4; $R^2 = 0.753$, $p = 0.025$) was identified as differentially methylated basally in fibrotic lung fibroblasts and therefore methylation of this CpG may be important in regulating fibulin-2 gene expression (**Figure 3.2.5.1C**, data for CpGs 36 and 45 are in **Appendix 4**).

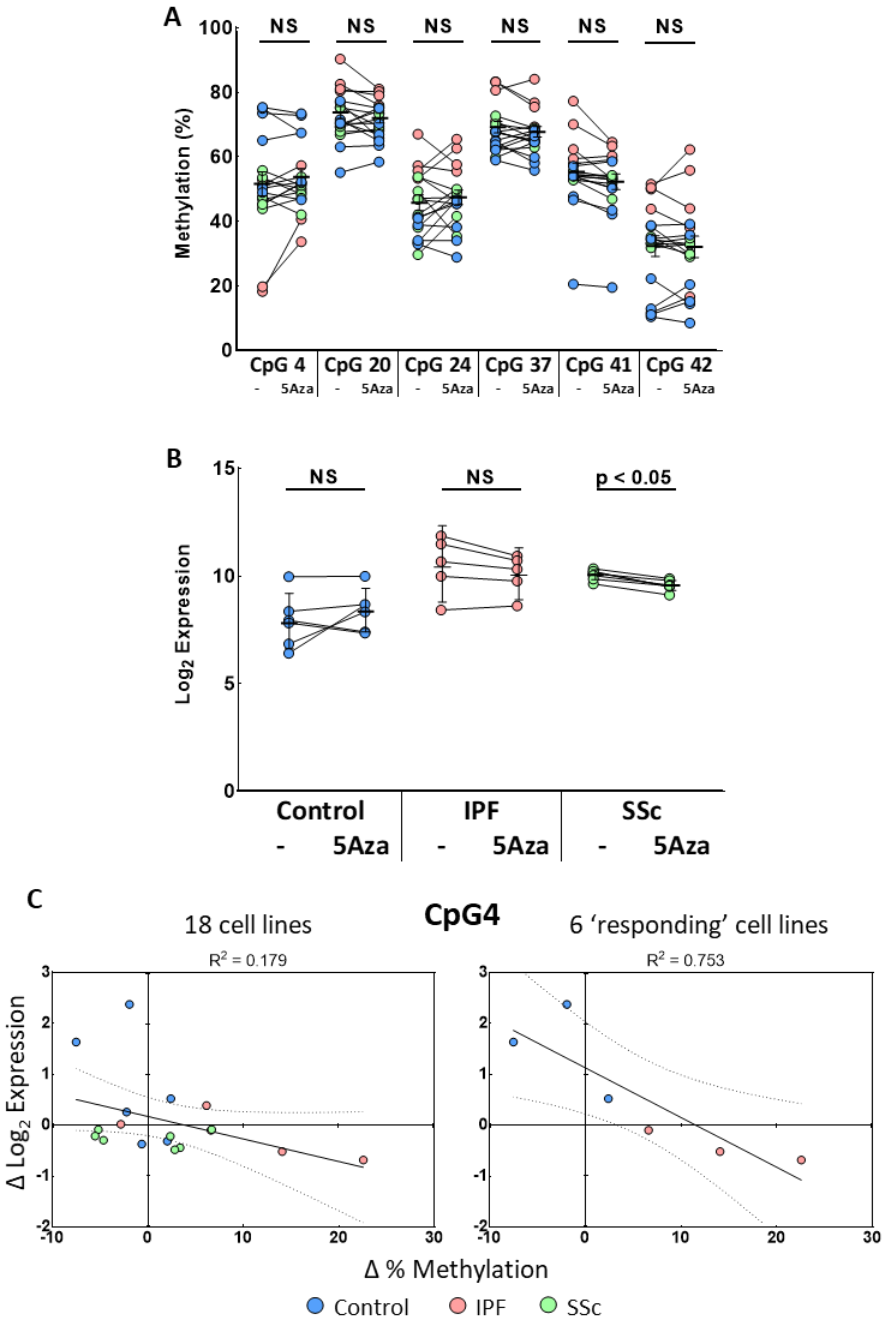


**Figure 3.2.5.1 Effect of demethylation treatment on fibulin-2 methylation and expression**

Treatment of array cells with 5-Aza-2'-deoxycytidine (5Aza, 1µM) did not affect mean CpG methylation of FBLN2 across all 18 cell lines (6 differentially methylated CpGs shown in **A**). (**B**) FBLN2 expression was not affected in control or IPF but there was a slight but significantly down regulation in SSc. (**C**) The change in methylation and expression in individual cell lines did not correlate when all 18 cell lines were analysed. However, analysis of 5Aza 'responding' cell lines identified in section **3.1.4** showed a strong negative correlation supporting the potential role of CpG 4 methylation in regulating FBLN2 expression.

### 3.2.6 Bisulfite sequencing for methylation validation

Experimental assessment of DNA methylation can be achieved using bisulfite chemical treatment. This first chemically converts unmethylated cytosine residues to uracil which, following PCR amplification, results in thymine in positions of unmethylated cytosine while leaving methylated cytosine residues unaffected. This technique is used for the Illumina methylation array and I applied it here before targeted PCR amplification and Sanger sequencing. PCR primers were designed to amplify the regions containing CpG 4 and CpG 42 as these correlated with gene expression. PCR products were generated as expected (**Figure 3.2.6.1A**) and excised before being submitted for Sanger sequencing. A bespoke python script was written to align the sequencing data to an *in silico* PCR product and quantify the methylated-unmethylated base intensity ratio. However due to a lack of sequence complexity in the surrounding region following bisulfite treatment, the sequencing readout degraded rapidly. This is caused by slippage of the sequencing readout or of Taq polymerase in PCR amplification due to a base repeating multiple times. As a consequence, CpG 42 was not quantifiable using two different primer sets tested. CpG 4 was quantifiable in most samples with a strong agreement to array data (**Figure 3.2.6.1B**). It was not possible to quantify other CpGs in the PCR product due to a repetitive region downstream of CpG 4.

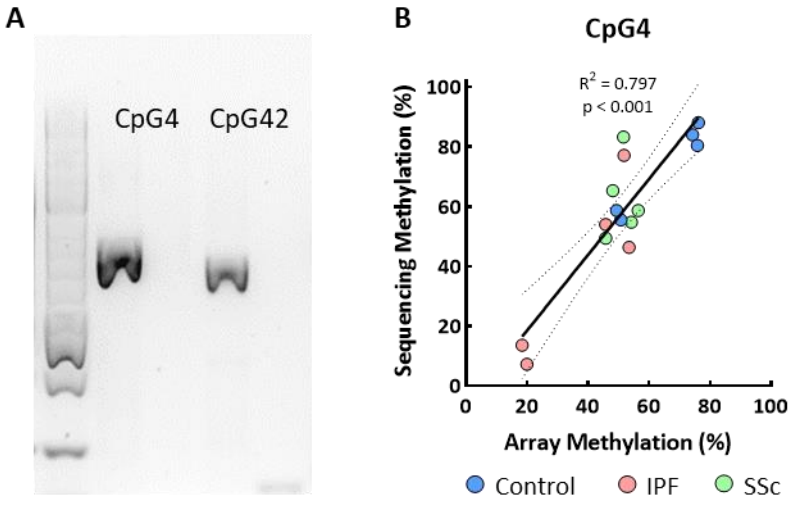


**Figure 3.2.6.1 Bisulfite sequencing of FBLN2**

Bisulfite converted PCR products were generated for CpG 4 and CpG 42 in all array DNA samples for sequencing to validate array results (**A**). Due to technical constraints, only CpG 4 could be reliably sequenced in most cell lines. Sequencing of CpG 4 (n= 15 / 18) strongly validated array methylation data (**B**).

### 3.2.7 Summary

- Fibulin-2 expression is upregulated at the mRNA level in IPF and SSc primary lung fibroblasts compared to controls. Array expression data was validated by RT-qPCR.

- Fibulin-2 protein expression is increased and shows a dysregulated pattern in lung tissue from IPF and SSc donors by immunohistochemistry.

- One CpG had decreased methylation in both IPF and SSc (CpG 4) and 5 had increased methylation in IPF only. Methylation of one CpG correlated negatively with expression and one CpG correlated positively.

- Bisulfite sequencing confirmed the array data for CpG 4 but I could not assess other CpGs.

## 3.3 Fibulin-2 expression in cultured fibroblasts: 2D

I have shown above that expression of fibulin-2 was upregulated in array datasets and in human lung tissue. Subsequent experiments were performed to demonstrate that fibulin-2 protein is deposited by lung fibroblasts and determine if this has a role in fibroblast activation as quantified by collagen I and αSMA expression. *In vitro* investigation of fibulin-2 was conducted with one representative control and one IPF cells line. The cell lines chosen had FBLN2 expression close to the mean of their groups in the full array and validation cohort.

### 3.3.1 Collagen deposition in 2D culture requires crowding conditions

In order to assess the deposition of fibulin-2 in 2D lung fibroblast culture I first demonstrated that the culture conditions are suitable for ECM deposition and quantification by assessing collagen deposition. Collagen deposition in 2D cell culture is thought to be limited by the kinetics of processing soluble procollagen into mature collagen fibrils. This is despite the rapid production and secretion of procollagen by lung fibroblasts in culture (Robin J. McAnulty and Laurent 1987). Rapid collagen deposition can be demonstrated in the accelerated deposition 'scar-in-a-jar' assay whereby fibroblasts in a 2D monolayer are cultured under molecular crowding conditions created by Ficoll containing media. These crowding conditions are thought to increase the bioavailability of procollagen to procollagen C-proteinase (PCP/BMP-1) through the excluded volume effect (Lareu et al. 2007; Z. C. C. Chen et al. 2009). **Figure 3.3.1.1A** demonstrates the extracellular deposition of collagen I, immunofluorescently labelled green, by control fibroblasts grown in 2D culture. These cells were seeded and allowed to adhere in DMEM containing 10% FCS before serum starvation in DMEM containing 0.4% FCS to induce cell cycle arrest. Following 24h starving, media was changed for DMEM-0.4%FCS with or without Ficoll (F+) and / or TGFβ (T+, 40pM) containing ascorbic acid, which is required for the hydroxylation of proline and lysine residues. At the time of collection, cells were fixed with methanol before high-content immunofluorescent quantification of the area of collagen I stain above an arbitrary intensity threshold which is shown normalised to the cell count by DAPI stained nuclei (blue).

Addition of TGFβ alone was sufficient to induce a significant increase in collagen deposition which had an extracellular deposition pattern (**Figure 3.3.1.1A**) though this was minor compared to the effect of crowding conditions which greatly increased the deposition of collagen I into a fibrillar extracellular matrix. Treatment with both TGFβ and Ficoll yielded a robust collagen I rich matrix proportional to the TGFβ dose (**Figure 3.3.1.1B**). The kinetics of this deposition in the presence of TGFβ and crowding conditions was assessed against time

following addition of Ficoll, TGFβ and ascorbic acid (**Figure 3.3.1.1C**). This showed that the majority of collagen was deposited between the 12 and 24-hour timepoints with very little collagen deposited between the seeding of cells and timepoints before 12-hours after crowding conditions. As a result, further experiments were analysed at 24h post crowding.

I subsequently assessed the deposition of fibulin-2 under the conditions required for collagen deposition.

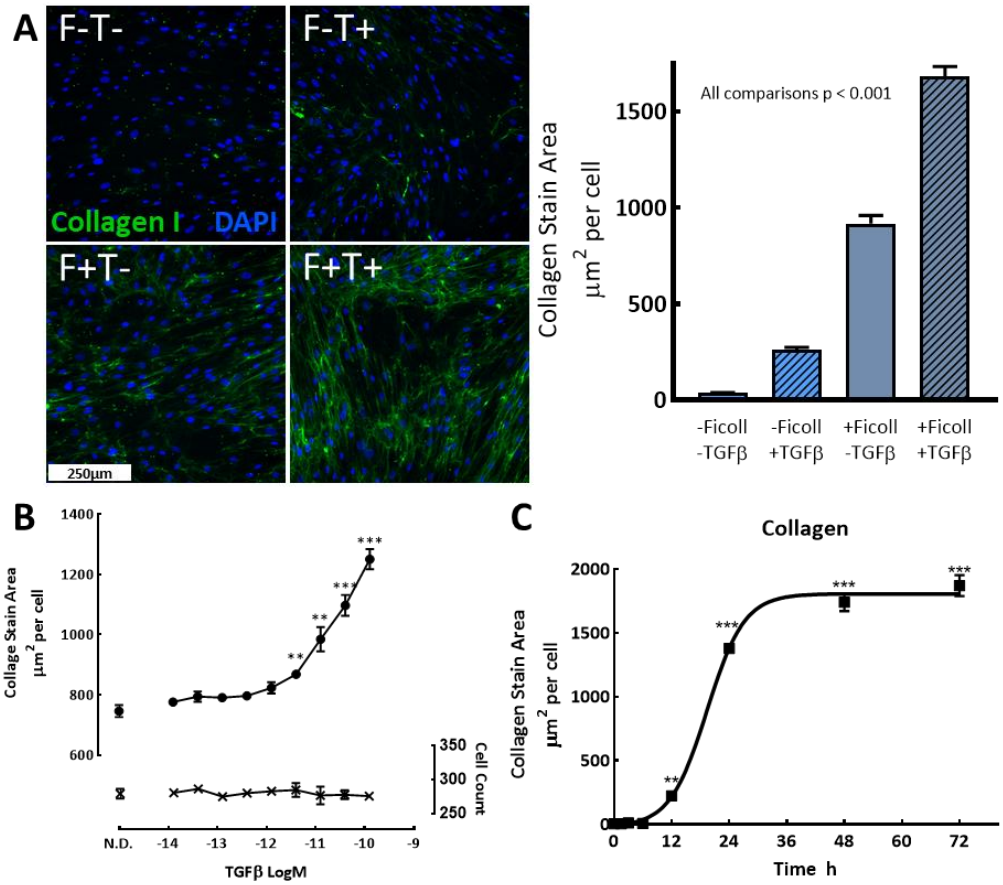


**Figure 3.3.1.1 Collagen deposition in the 'scar-in-a-jar' model**

Conditions for optimal collagen deposition in 2D culture were assessed for comparison with fibulin-2 deposition and for use as a readout of fibroblast phenotype. Data shown here is representative of n > 7 fibroblast cell lines. (**A**) Area of collagen (green) staining above an arbitrary intensity threshold, normalised to cell count by DAPI nuclear stain (blue) is used to quantify collagen deposition. Deposition with and without TGFβ (40pM) and / or crowding conditions (+Ficoll) is shown. All pair comparisons $p < 0.001$. (**B**) Collagen deposition was stimulated in a dose dependant manner in response to TGFβ following 24h incubation under crowded conditions. (**C**) Collagen is rapidly deposited after application of crowding media with TGFβ. n = 3 wells per condition. All panels one-way ANOVA, Tukey's post-test. ** $p < 0.01$, *** $p < 0.001$ vs no-drug (ND) or time 0h.

### 3.3.2 Fibulin-2 deposition does not require crowding conditions

Expression microarray and qPCR validation data demonstrated that both control and IPF primary lung fibroblasts express FBLN2 mRNA in 2D cell culture with expression by IPF cells approximately 10- to 15-fold higher than that of controls (**Figure 3.2.1.2**). To assess if fibulin-2 is deposited by lung fibroblasts in 2D cell culture, and if this requires crowding conditions,

fibulin-2 was immunofluorescently labelled following culture in conditions identical to collagen I staining in **section 3.3.1**. Staining for fibulin-2 could only be achieved by fixation with PFA whereas fixation with methanol was required for collagen I staining; this meant that co-staining to interrogate any co-localisation of fibulin-2 with collagen I was not possible.

Fibulin-2 deposition showed a strong extracellular pattern in IPF derived lung fibroblasts (**Figure 3.3.2.1A**). This was independent of crowding conditions (F+) which were not necessary for fibulin-2 deposition and did not increase the quantified stain area compared to untreated cells (F-) (**Figure 3.3.2.1B**). There was a significant upregulation of fibulin-2 as quantified by stain area when cells were incubated with TGFβ (40pM).

No fibulin-2 staining was detected in non-fibrotic (control) lung fibroblasts under these conditions with or without crowding and / or TGFβ (**Figure 3.3.2.1C**) despite depositing a collagen I rich matrix under identical crowding (**Figure 3.3.1.1A**). These rapid ECM deposition conditions are in contrast to the conditions used for array experiments; in the next sub-section I investigate fibulin-2 expression in conditions similar to those used to collect array samples.

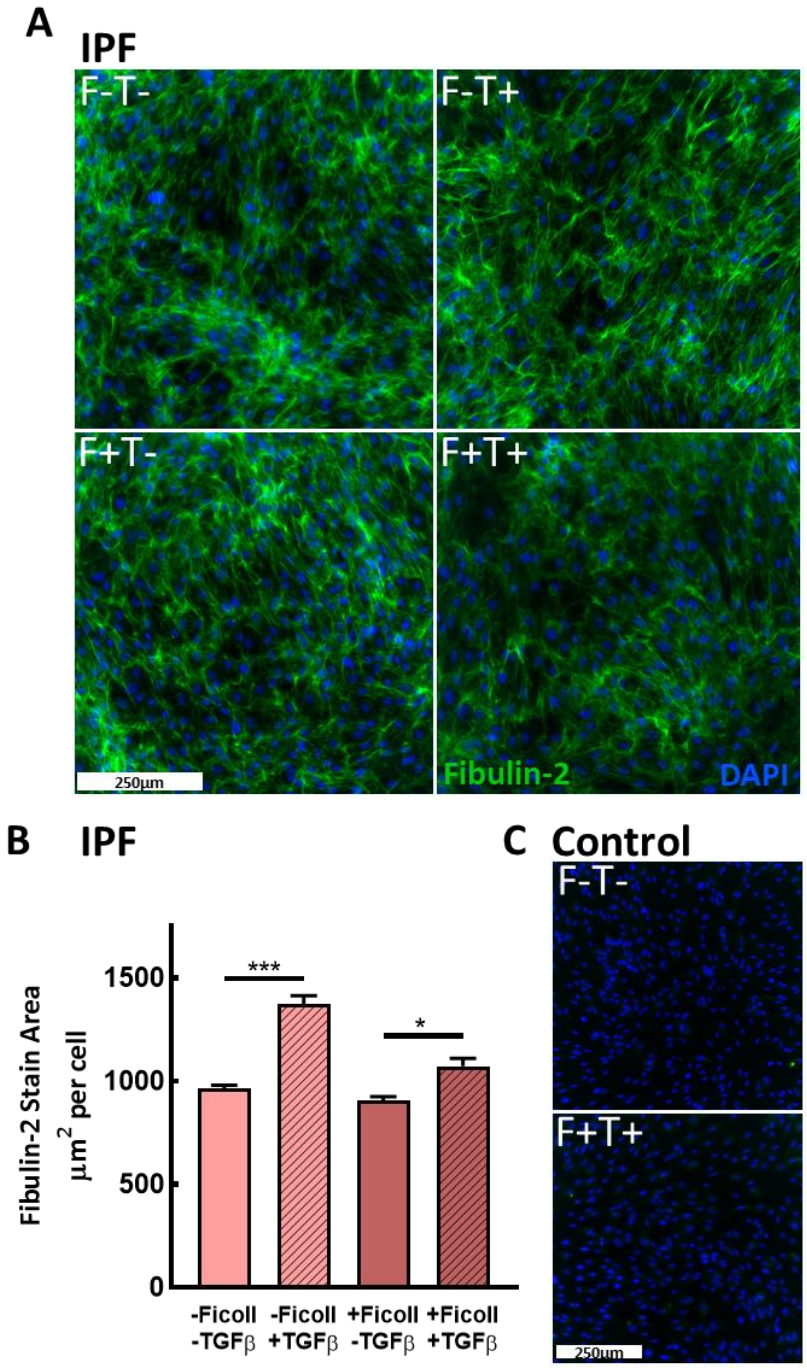


**Figure 3.3.2.1 Fibulin-2 deposition in the 'scar-in-a-jar' model**

Fibulin-2 (**A**, green) deposition (48h post-seeding, 24h post-dosing) by IPF fibroblasts (n=1) did not require crowding conditions (F+) and was enhanced by TGFβ (40pM, T+). (**B**) Quantification of fibulin-2 stain area in IPF fibroblasts normalised to cell count by DAPI (A: blue). n = 3 wells per condition. One-way ANOVA, Tukey's post-test: * $p < 0.05$, *** $p < 0.001$. (**C**) No fibulin-2 staining was seen in control fibroblasts (n=1) under any conditions. Scale bar 250µm. Data is representative of two independent experiments performed with each cell line.

### 3.3.3 RIPA buffer supplemented with SDS is required for fibulin-2 western blot

Initial western blot experiments using RIPA buffer failed to detect a fibulin-2 band at the predicted size of ~180kDa. A literature review suggested supplementation of lysis buffer with sodium dodecyl sulfate (SDS) (P. Singh and Schwarzbauer 2014) or EDTA (T Sasaki et al. 1996) was required to liberate ECM components. Optimal lysis conditions for fibulin-2 solubilisation were determined in fibroblasts which had reached confluency in 12-well plates 48h prior to lysis. No fibulin-2 band was detected in RIPA buffer alone, however lysis in phosphosafe buffer (Novagen) and RIPA buffer supplemented with 4% sodium dodecyl sulfate (SDS), 10mM EDTA or SDS + EDTA yielded robust bands of the expected size (**Figure 3.3.3.1A**). Homogenisation of samples was optimally achieved by heating to 100°C for 10min compared to vortexing alone or homogenisation by multiple passes through an insulin needle which resulted in high sample loss (**Figure 3.3.3.1B**). Following heating, samples were pulsed to the bottom of eppendorfs but no centrifugation to remove debris was necessary. RIPA-SDS followed by heating was selected for all experiments due to its optimal yield of both fibulin-2 and αTubulin loading control.

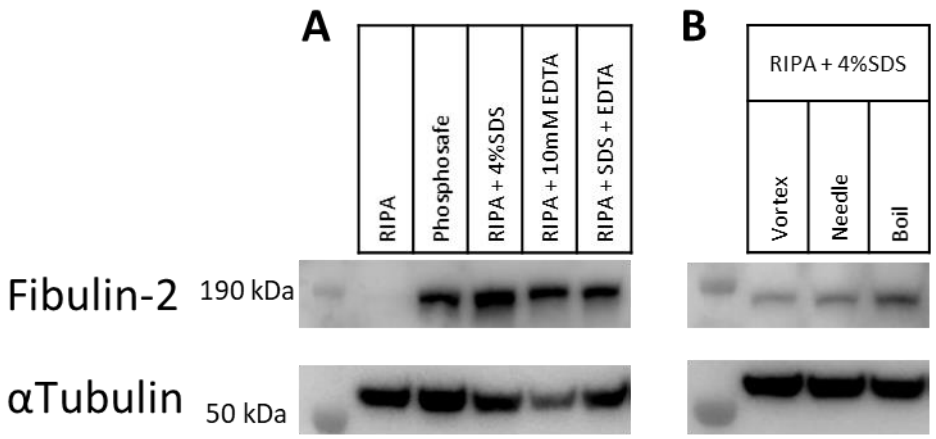


**Figure 3.3.3.1 Efficient solubilisation of fibulin-2 for western blot**

Optimal lysis conditions for fibulin-2 detection by western blot were determined to be (**A**) RIPA buffer supplemented with 4% SDS followed by (**B**) heating to 100°C for 10min. Loading volume, and therefore intensity, in B is lower due to losses during needle homogenisation.

### 3.3.4 Fibulin-2 deposition in 2D culture

In the molecular crowding assays performed above, cells are seeded at approximately the final density and only able to proliferate during the adherence phase before serum starving.

Previous microarray and validation experiments which detected FBLN2 mRNA expression in both control and IPF derived fibroblasts were however performed by growing cells to confluency in DMEM containing 10% FCS following seeding at approximately 5-10% confluency. This was to allow for treatment with the demethylating agent 5Aza which acts primarily during DNA replication. In this section I investigated the kinetics of fibulin-2 expression at the mRNA and protein level in proliferating cells similar to the conditions under which the array was performed. This also allowed optimisation of siRNA treatment conditions for subsequent experiments. Fibroblasts were seeded at the recommended density for siRNA treatment (approximately 25% confluency) in 12-well plates in DMEM supplemented with 10% FCS and ascorbic acid. Cells were allowed to grow to visual confluency plus an additional 48h with collection of cells for counting, and the cell layer for mRNA and protein analysis every 24h.

As is typically seen within our lab, cells from a non-IPF (control) donor grew rapidly with an approximate doubling time of 24h until they reached visual confluency between 48h and 72h. IPF fibroblasts grew at a slower rate, having a larger, flatter morphology with the cell number continuing to rise despite the wells looking visually confluent from 72h to 96h onwards (**Figure 3.3.4.1A**).

FBLN2 mRNA expression (**Figure 3.3.4.1B**) across these timepoints was markedly higher in IPF fibroblasts than in control with expression in IPF derived fibroblasts 58.6-fold higher at the 24h timepoint than that of controls. Expression in both control and IPF fibroblasts rose significantly through the time-course with 10.4- and 2.2-fold increases respectively at 120h compared to 24h (both $p < 0.001$). In control cells the most rapid increase in expression coincided with when the cells reached confluency at approximately 72h. In confluent cells, at 96h and 120h timepoints FBLN2 expression was 11.8- and 12.3-fold higher, respectively, in IPF cells compared to controls. This is in accordance with expression levels seen in the array experiments which were performed on confluent cells (**Figure 3.2.1.2**).

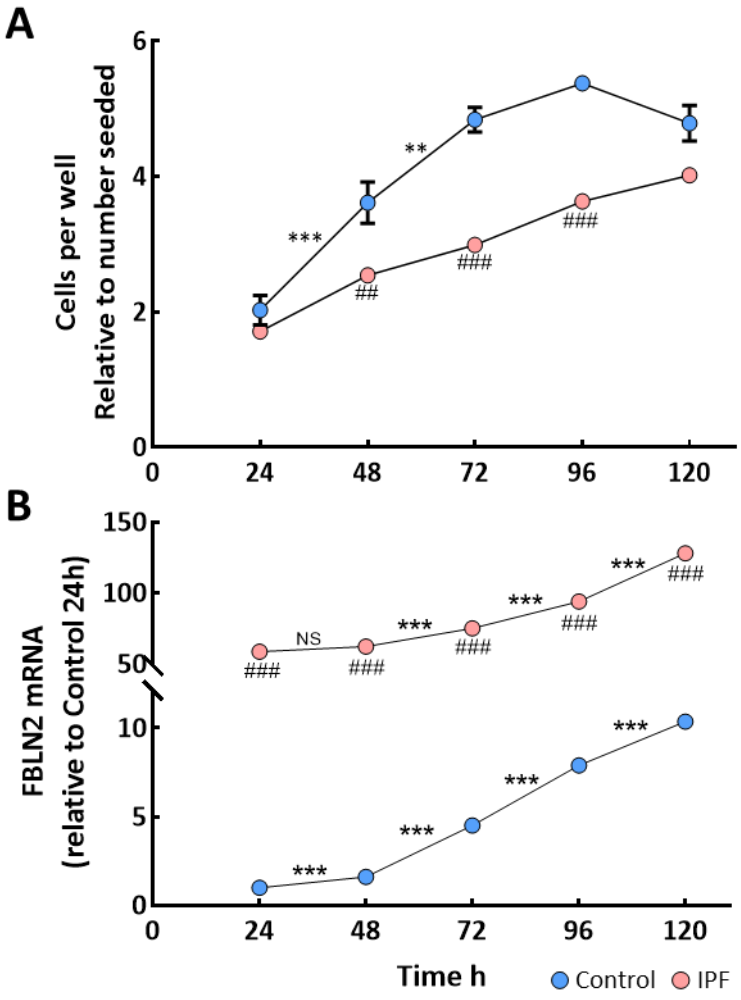


**Figure 3.3.4.1 FBLN2 expression against time in culture**

The kinetics of fibulin-2 mRNA expression (**B**) in 2D proliferating culture in a representative control and IPF cell line were assessed. (**A**) Cell count of proliferating fibroblasts seeded at ~25% at 0h. n = 3 replicates per condition, data is representative of two independent experiments for each cell line. Two-way ANOVA, Tukey's post-tests. ** $p < 0.01$, *** $p < 0.001$ within 24h period. ## $p < 0.01$, ### $p < 0.001$ IPF compared to control at each timepoint.

At each timepoint, in parallel wells, the cell layer was scraped into lysis buffer for the assessment of fibulin-2 deposition into the extracellular matrix by Western blotting. Fibulin-2 protein expression, shown in **Figure 3.3.4.2**, was barely detected in proliferating control lung fibroblasts at the 24h timepoint but rose over time with a significant increase seen from 96-120h which follows the increase seen in mRNA levels once cells are confluent. Across the time course, there was a 9.5-fold increase in fibulin-2 deposited by control cells. Fibulin-2 was readily detected in IPF derived fibroblasts from 24h and increased 3.2-fold by 120h yielding a strong band.

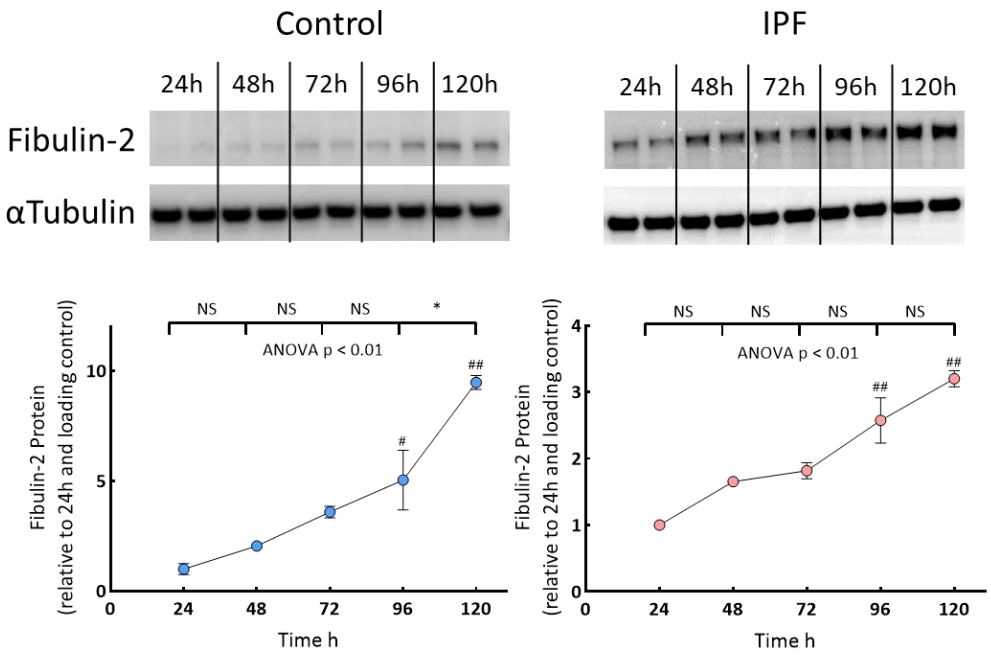


**Figure 3.3.4.2 Fibulin-2 protein expression against time in 2D culture**

Fibulin-2 protein deposition in control and IPF fibroblast proliferating cell layers from **Figure 3.3.4.1** was assessed by western blot, with densitometry normalised to α-tubulin and 24h timepoint. 10µg total protein was loaded for all wells. One-way ANOVA with Tukey's post-test. * $p < 0.05$ between adjacent timepoints. # $p < 0.05$, ## $p < 0.01$ compared to 24h. Data is representative of two independent experiments for each cell line.

### 3.3.5 Fibulin-2 expression is depleted by siRNA treatment

To begin to elucidate a functional role for fibulin-2 in the pathogenesis of IPF, expression of fibulin-2 was knocked-down in primary lung fibroblasts from a non-IPF (control) and an IPF donor by treatment with a commercially available pool of four siRNA molecules targeting FBLN2 transcripts. Negative control transfections were performed using a non-targeting (NT) siRNA pool recommended by the manufacturer under equal conditions.

Fibroblasts were seeded in 12-well plates at approximately 25% confluency and allowed to adhere for 24h before treatment with siRNA (25nM). Proliferating cells were collected at the 120h timepoint as above to assess if treatment was effective through to the point where expression was reliably detected in control cells. siRNA treatment almost completely abolished the expression of FBLN2 mRNA in control cells and markedly reduced expression in IPF fibroblasts towards the level seen in untreated non-IPF cells (**Figure 3.3.5.1A**). Fibulin-2 protein content of the cell layer, as assessed by western blot, was barely detectable in

siRNA treated control or IPF fibroblasts (**Figure 3.3.5.1B**) indicating that siRNA knockdown of FBLN2 was successful in both IPF and control fibroblasts in 2D culture.

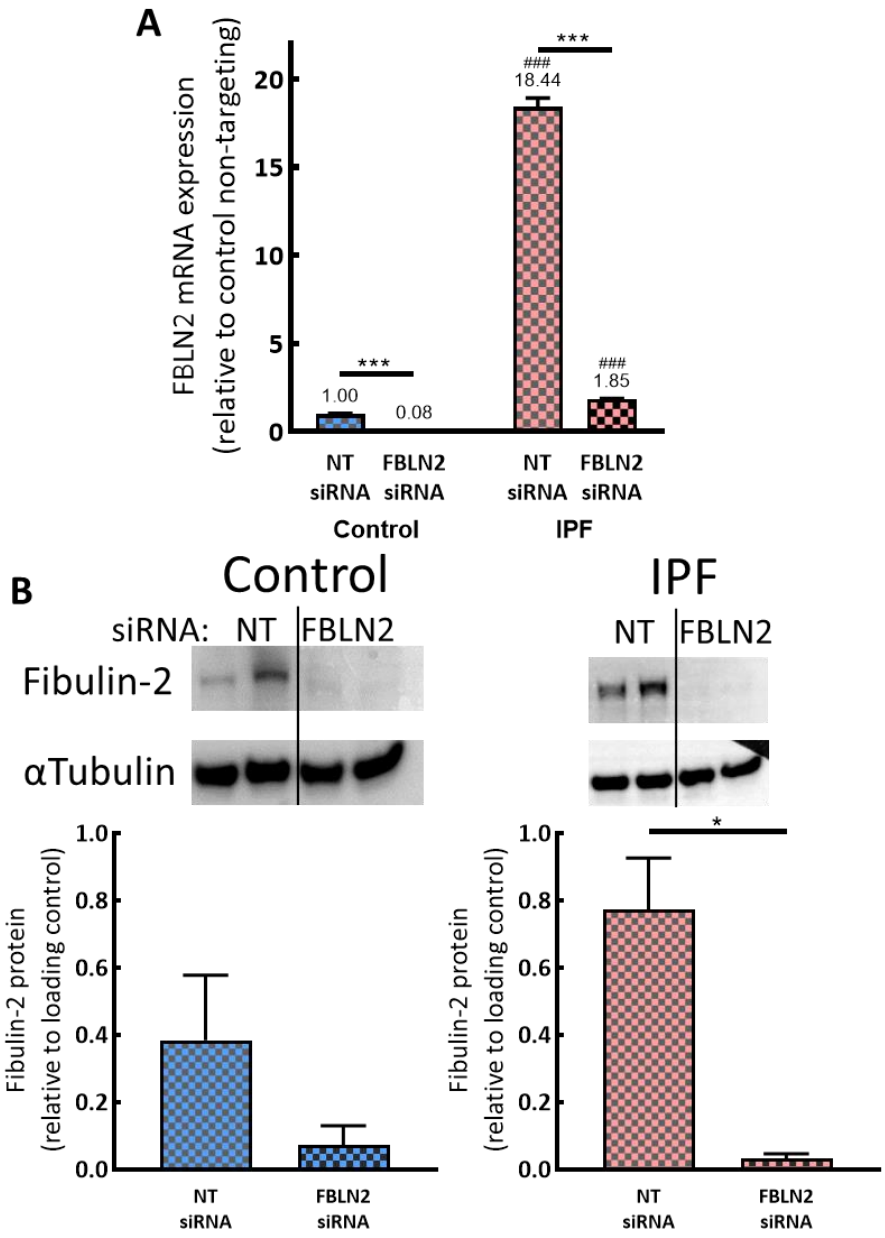


**Figure 3.3.5.1 siRNA depletes fibulin-2 expression in control and IPF fibroblasts**

(**A**) Treatment of proliferating lung fibroblasts with siRNA targeting FBLN2 significantly reduces FBLN2 mRNA expression at the 120h timepoint compared to non-targeting (NT) treated cells. Two-way ANOVA, Tukey's post-test. *** $p < 0.001$ compared to NT; ### $p < 0.001$ compared to control NT. (**B**) This translated into a marked reduction in fibulin-2 protein in the cell layer. Student's T-test, * $p < 0.05$. Data is representative of two independent experiments for each of the cell lines used in **Figure 3.3.4.1**.

In **section 3.3.2** above I have shown that a significant amount of fibulin-2 is deposited in the first 48h of cell culture by IPF fibroblasts seeded at a moderate hight density but this is independent of the crowding conditions (**Figure 3.3.2.1**). This would mean that siRNA treatment at 24h after the cells have been allowed to adhere, as in **Figure 3.3.5.1**, may be too late to deplete fibulin-2 protein levels in the cell layer and therefore would not be suitable for the assessment in the rapid collagen deposition model. In order to utilise siRNA mediated FBLN2 knockdown in molecular crowding assays I therefore established a protocol where fibroblasts were treated with siRNA in 2D culture for 24h then serum starved for another 24h before being trypsinised and seeded in serum starve media into 96-well plates. This timeframe would allow the rapid use of siRNA treated cells in the molecular crowing assays while ensuring there is no initial fibulin-2 deposition in the assay plates. A schematic of siRNA treatment regimens is shown in methods section (**Figure 2.1.4.1**).

To validate the siRNA treatment regime and ensure fibulin-2 remained depleted in these conditions IPF cells were seeded into 96-well assay plates following siRNA treatment and PFA fixed 48h post-seeding. 24h after seeding, some wells were treated with TGFβ (40pM) to ensure that knockdown was not overcome by exogenous TGFβ treatment. Immunofluorescent quantification of fibulin-2 protein showed a significant reduction in stain area by anti-FBLN2 siRNA treatment compared to NT siRNA treated cells (**Figure 3.3.5.2**). FBLN2 siRNA and NT siRNA had no significant difference in the number of cells which attached following seeding at identical cell densities with 285 ±7.4 and 295 ±3.4 cells per image respectively (Student's T-test $p = 0.35$).

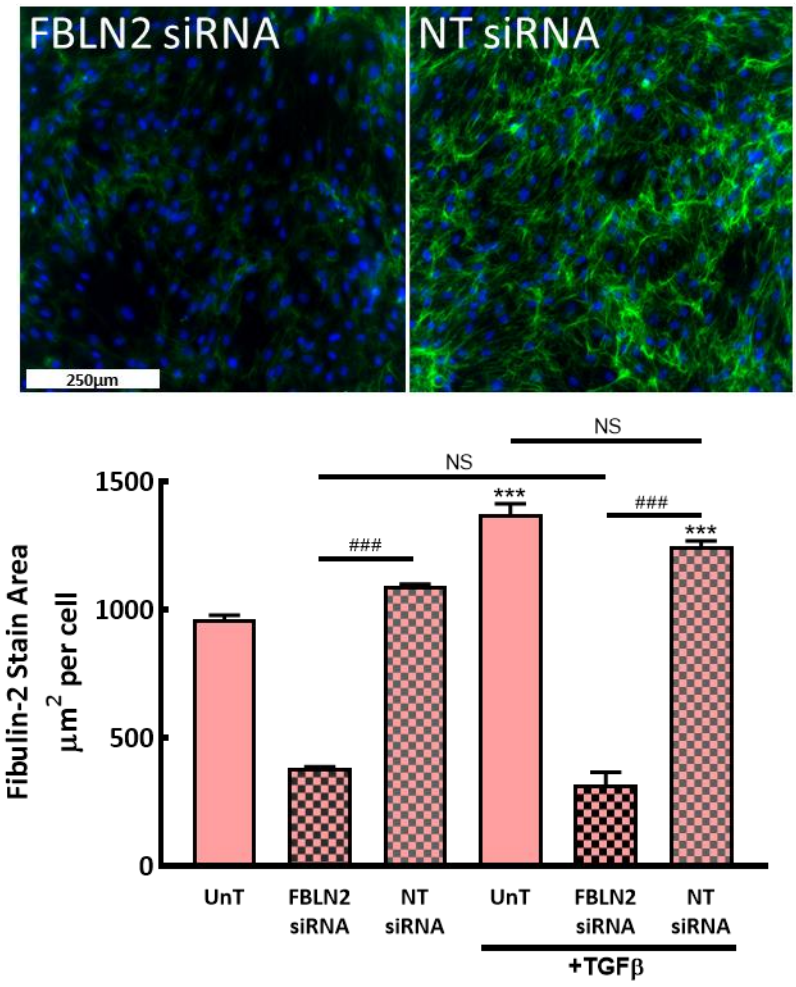


**Figure 3.3.5.2 Fibulin-2 can be depleted in the rapid deposition assay**

A protocol was established where treatment of IPF fibroblasts with siRNA prior to seeding in the rapid deposition assay resulted in a significant reduction in fibulin-2 protein deposition (compared to non-targeting, NT, siRNA) allowing functional readouts in fibulin-2 deficient cultures. Stain area positive for fibulin-2 (green) was normalised to DAPI (blue) cell count. n = 3 wells per condition. One-way ANOVA, Turkey's post-test. *** $p < 0.001$ vs untreated, ### $p < 0.001$.

### 3.3.6 Effect of FBLN2 siRNA knockdown on collagen I

The effect of FBLN2 deficiency on collagen I expression and deposition was assessed in both proliferating 2D cell culture and the accelerated deposition assay.

COL1A1 mRNA expression was quantified against time in proliferating lung fibroblasts from control and IPF donors from the samples shown in **Figure 3.3.4.1**. COL1A1 expression in control fibroblasts fluctuated a minor amount however at no timepoint was the expression significantly changed from 24h (two-way ANOVA, Tukey's post-test). Expression in IPF fibroblasts was significantly higher than in control cells at every timepoint ($p < 0.001$) with

3.08-fold higher expression at 24h rising to 4.78-fold higher at 120h post seeding (**Figure 3.3.6.1A**). COL1A1 expression increased 1.58-fold in IPF fibroblasts by 120h compared to 24h ($p < 0.05$). This change in COL1A1 expression correlated with FBLN2 expression shown in **Figure 3.3.4.1** in IPF fibroblasts (Pearson $R^2 = 0.844$, $p < 0.05$) but not in controls ($R^2 = 0.397$). The correlation between deltaCt values is shown in **Appendix 5.**

Treatment of fibroblasts with siRNA targeting FBLN2 significantly reduced COL1A1 mRNA at 120h in IPF fibroblasts compared to non-targeting (NT) siRNA treatment ($p < 0.01$). There was however no effect of FBLN2 deficiency on COL1A1 expression in control fibroblasts (**Figure 3.3.6.1B**).

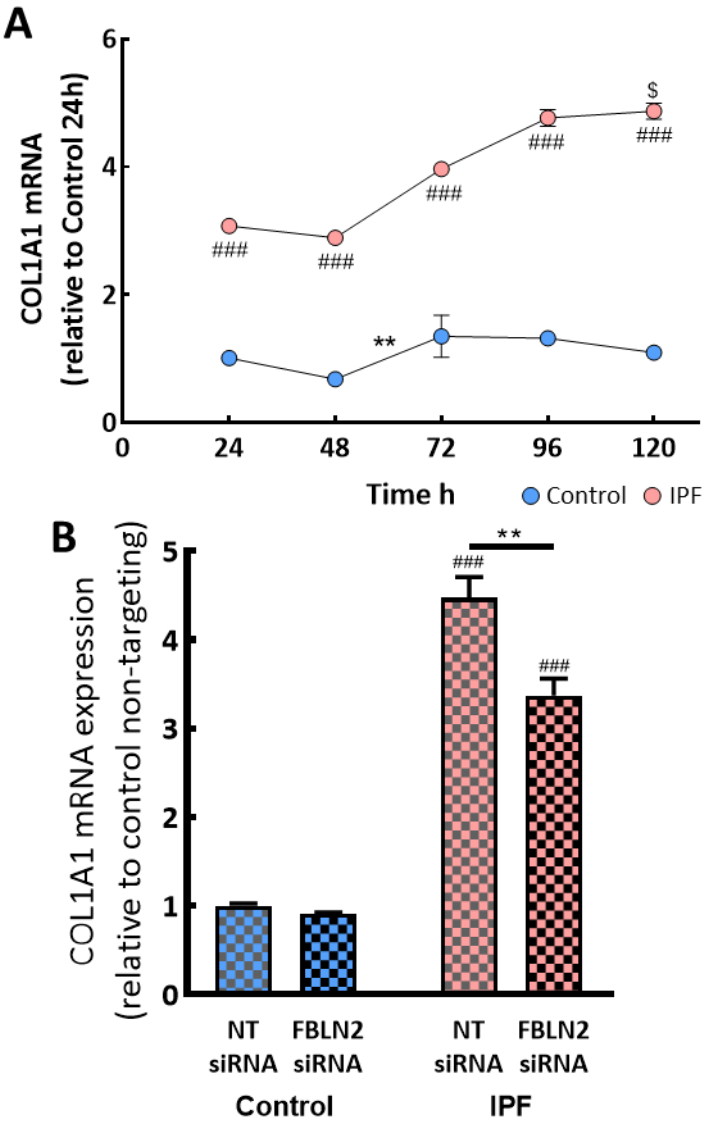


**Figure 3.3.6.1 The effect of FBLN2 siRNA on collagen I mRNA expression**

(**A**) COL1A1 mRNA expression is higher in proliferating IPF fibroblasts than controls (see **Figure 3.3.4.1** for cell count information). n = 3 replicates per timepoint. Two-way ANOVA, Tukey's post-test. ** $p < 0.01$ during 24h interval, ### $p < 0.001$ vs control, $ $p < 0.05$ vs 24h. (**B**) FBLN2 deficiency significantly reduces COL1A1 mRNA in IPF fibroblast, but not controls, grown in 2D conditions (120h). n = 3 per condition. ** $p < 0.01$, ### $p < 0.001$ vs control. Data is representative of two independent experiments for one control and one IPF line.

In order to assess collagen deposition in FBLN2 deficient cells under the rapid deposition assay, IPF fibroblasts, which I have shown above deposit fibulin-2 under these conditions were used. The cells were siRNA treated in culture flasks before seeding directly into serum coated 96-well plates in serum starvation media. Cells were allowed to adhere for 24h before

application of crowding conditions with or without TGFβ (40pM). After 24h under crowding conditions the cell layer was fixed with methanol and collagen immunofluorescently quantified (**Figure 3.3.6.2**). TGFβ treatment significantly increased collagen I deposition in all siRNA conditions, $p < 0.001$ by two-way ANOVA, all Tukey's post-tests $p < 0.05$. siRNA treatment depleting FBLN2 expression however had no effect on collagen I deposition, two-way ANOVA not significant.

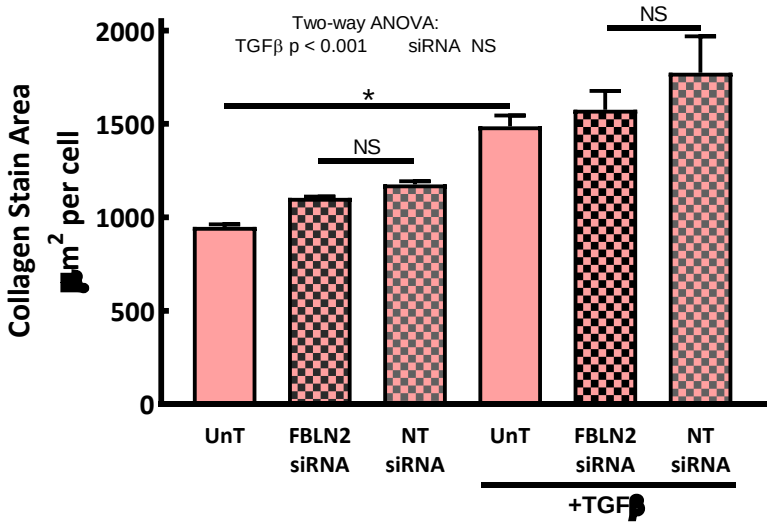


**Figure 3.3.6.2 The effect of FBLN2 siRNA on collagen I deposition**

Despite a significant reduction of COL1A1 expression in longer term 2D culture, collagen I deposition by fibroblasts treated with FBLN2 or non-targeting (NT) siRNA before seeding in the rapid deposition assay was not affected by FBLN2 deficiency. n ≥ 3 per condition. Two-way ANOVA: TGFβ $p < 0.001$, siRNA NS. Tukey's post-test: * $p < 0.05$. Data is representative of three experiments performed with one IPF cell line.

### 3.3.7 Effect of FBLN2 siRNA knockdown on α smooth muscle actin

I have demonstrated above that over time when proliferating to confluency, primary lung fibroblasts from both control and IPF donors develop a more synthetic phenotype with upregulated expression of fibulin-2 and collagen I. To further characterise the phenotype of these fibroblasts through time I quantified the expression of α smooth muscle actin (αSMA) which is the prototypic marker of contractile activated myofibroblasts (Hinz et al. 2001).

In proliferating control and IPF fibroblasts from **Figure 3.3.4.1**, ACTA2 mRNA expression was initially highest in control compared to IPF fibroblasts at the 24h timepoint ($p < 0.01$, two-way ANOVA, Tukey's post-tests) but rapidly decreased to below that of IPF fibroblasts from

48h onwards (**Figure 3.3.7.1A**). This rapid decrease in ACTA2 mRNA in control cells translated to a steady decline in αSMA protein as assessed in cell layer lysates by western blot and normalised to αTubulin (**Figure 3.3.7.1B**). mRNA expression in IPF fibroblasts remained stable throughout the time-course with no significant change between timepoints, this however translated to a significant accumulation in αSMA protein in each 24h period and a total 2.0-fold higher αSMA protein content at 120h than 24h (**Figure 3.3.7.1B**). There was no correlation between the changes in FBLN2 expression and ACTA2 across these timepoints in either control or IPF fibroblasts (see **Appendix 6**).

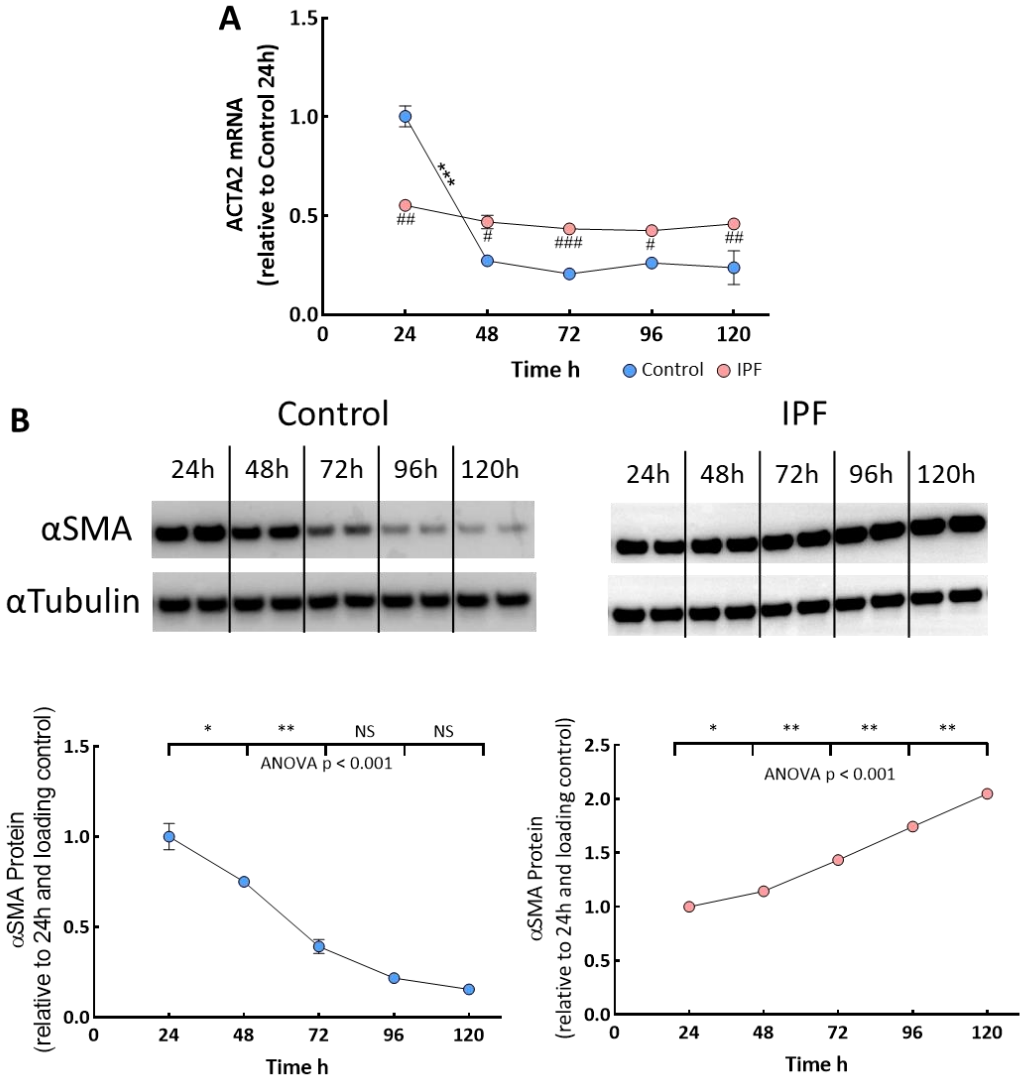


**Figure 3.3.7.1 αSMA expression against time**

ACTA2 mRNA (**A**) and αSMA protein (**B**) were assessed in proliferating lung fibroblasts from **Figure 3.3.4.1**. A: n = 3 per timepoint. Two-way ANOVA, Tukey's post-tests: *** $p < 0.001$ between timepoints. # $p < 0.05$, ## $p < 0.01$, ### $p < 0.001$ IPF compared to control. B: Densitometric quantification normalised to αTubulin loading control and 24h expression. One-way ANOVA, Tukey's post-test: * $p < 0.05$, ** $p < 0.01$ between timepoints. Data is representative of two independent experiments with one control and one IPF cell line.

FBLN2 siRNA treatment of proliferating fibroblasts resulted in a significant decrease in ACTA2 mRNA expression at the 120h timepoint in both control ($p < 0.05$) and IPF ($p < 0.001$) fibroblasts compared to non-targeting siRNA with IPF levels returning towards those of controls (**Figure 3.3.7.2A**). At the protein level in cell layer lysates at 120h, there was a marked decrease in αSMA protein in IPF fibroblasts but this not reach significance ($p = 0.07$).

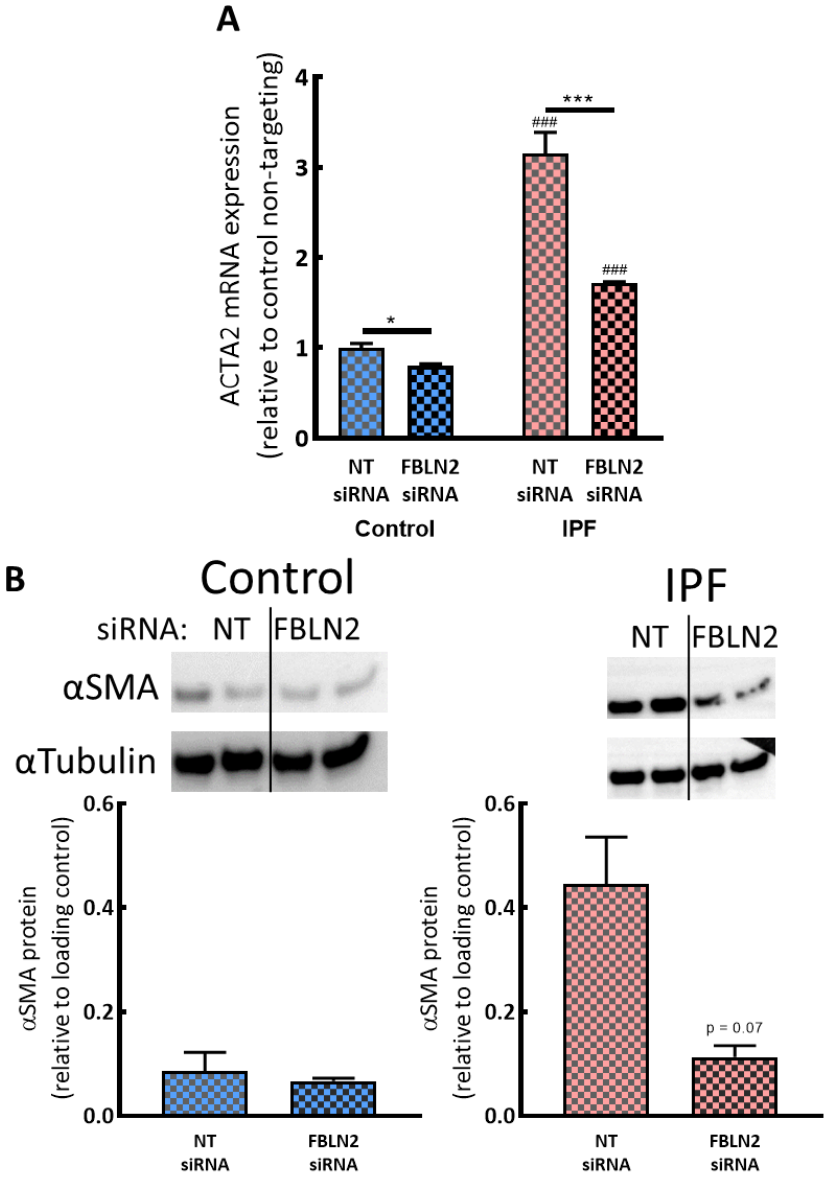


**Figure 3.3.7.2 The effect of FBLN2 siRNA on αSMA expression**

ACTA2 mRNA (**A**) and αSMA protein (**B**) in fibroblasts treated with FBLN2 or non-targeting (NT) siRNA were quantified at the 120h timepoint. A: n = 3 per condition. Two-way ANOVA, Tukey's post-test, * $p < 0.05$, ** $p < 0.001$ between siRNA treatments. ### $p < 0.001$ vs Control NT. B: Student's T-test. Data is representative of two independent experiments for one control and one IPF line.

### 3.3.8 Summary: Fibulin-2 in 2D cell culture

- Fibulin-2 deposition into an extracellular matrix, unlike collagen I, does not require molecular crowding conditions. Deposition occurs rapidly by IPF derived primary lung fibroblasts but not by those from a control donor and is upregulated by TGFβ treatment.

- In proliferating 2D culture conditions, as required for siRNA treatment and used in array experiments, FBLN2 expression increases over time in both control and IPF fibroblasts. Expression was significantly higher in IPF than control fibroblasts with expression in confluent cells 12-fold higher, in agreement with array experiments. These increases translate into increasing fibulin-2 content of the cell-matrix layer.

- COL1A1 is upregulated by IPF fibroblasts over time in 2D culture but doesn't change in control cells. COL1A1 mRNA expression is reduced by FBLN2 siRNA treatment in IPF cells following 120h in culture but collagen I protein is unchanged in the rapid deposition model.

- ACTA2 mRNA is greatly and rapidly downregulated by control fibroblasts within the first 48h of culture which corresponds to a significant reduction in αSMA protein. mRNA levels do not change significantly in IPF cells resulting in an accumulation of αSMA protein over time. FBLN2 deficiency reduces ACTA2 mRNA in both control and IPF cells. Subsequently, there is a trend towards reduced αSMA protein in fibulin-2 deficient cells.

## 3.4 Fibulin-2 expression in 3D cultured fibroblasts

The primary hypothesis of this thesis is that elevated fibulin-2 expression in the fibrotic lung plays a role in a feed-forward system involving ECM-ECM and ECM-cell interactions. These interactions are likely not well recapitulated in 2D cell culture where cell-plastic interactions are likely to dominate. In order to elucidate any role that fibulin-2 may play within the pathogenesis of pulmonary fibrosis through these interactions, studies were performed utilising a 3D spheroid culture model.

In the spheroid model, fibroblasts are seeded into agarose coated tissue culture plates. The agarose coating forms a non-adherent surface and when performed in a 96-well plate the resulting meniscus shape encourages seeded cells to accumulate in the centre of the well resulting in the formation of a single spheroid. Previous data from our lab (Kanda 2015) has shown that these accumulated human lung fibroblasts from normal and IPF donors form spheroid aggregates within ~4h when seeded in to non-adherent agarose coated wells and that these spheroids mature within the first 24h. Further, it was shown that within spheroids, fibroblasts, particularly those from non-IPF donors, underwent $PGE_2$ driven apoptosis during culture beyond 48-72h (Kanda 2015).

I therefore performed a series of experiments where spheroids were formed by human lung fibroblasts from control and IPF donors. Unless otherwise stated, spheroids were collected for analysis 24h post seeding. The effect of FBLN2 deficiency was assessed using fibroblasts which had undergone siRNA treatment in 2D before spheroid seeding.

### 3.4.1 Human lung fibroblasts form ECM rich spheroids

The initial step in re-establishing the spheroid model within our lab was to confirm that human lung fibroblasts form spheroids rich in ECM in the conditions used. Collagen content was quantified, as with 2D experiments this was to form the primary output from subsequent experiments in the spheroid model and serves as a good positive control for immunohistochemical processing of spheroids.

Spheroids were formed with fibroblasts from a control and an IPF donor on agarose coated plates in DMEM containing 0.4% FCS and ascorbic acid. As spheroid formation occurs rapidly and treatment with TGFβ at the time of seeding has been previously shown to not induce an upregulation of collagen deposition (Kanda 2015) spheroids were formed from fibroblasts with or without pre-treatment with TGFβ (40pM) for 24h in 2D prior to trypsinisation to induce a myofibroblast-like phenotype prior to seeding.

Collagen I deposition was immunohistochemically (IHC) stained in PFA fixed, double embedded sections. Strong staining was observed in spheroids from both control and IPF fibroblasts with increased staining in IPF and with TGFβ pre-treatment (**Figure 3.3.1.1A**). Staining was predominantly of an extracellular pattern as can be seen at higher magnification. No staining was present using a non-targeting isotype control primary antibody (inset). Collagen content was quantified by measuring the hydroxyproline present in whole spheroids hydrolysed in 6M HCl. Hydroxyproline, which constitutes 12.2% of collagen by mass but is found in few other proteins and at a lower abundance than in collagens (Laurent et al. 1981; Campa, McAnulty, and Laurent 1990), was measured by HPLC and used to calculate the collagen mass per spheroid. Data is presented as mass of collagen normalised to DNA content of spheroids processed in parallel. Collagen content was approximately 5.8-fold higher in IPF spheroids than those from a control donor ($p < 0.001$, two-way ANOVA with Tukey's post-test). Pre-treatment significantly upregulated collagen content in IPF spheroids compared to those formed without TGFβ stimulation (1.76-fold, $p < 0.001$). Although a similar increase of 1.51-fold was seen in control spheroids the effect of TGFβ pre-treatment did not reach significance (**Figure 3.3.1.1B**).

In agreement with HPLC data, COL1A1 mRNA expression, as quantified by RT-qPCR, was 5.75-fold higher in IPF fibroblasts than controls ($p < 0.001$, two-way ANOVA with Tukey's post-test) and increased 2.50 and 1.43-fold by TGFβ treatment in control and IPF respectively ($p < 0.001$; **Figure 3.3.1.1C**). Although histology sections are from variable planes through the spheroids, macroscopically there was no observable difference in the size of spheroids formed under various conditions.

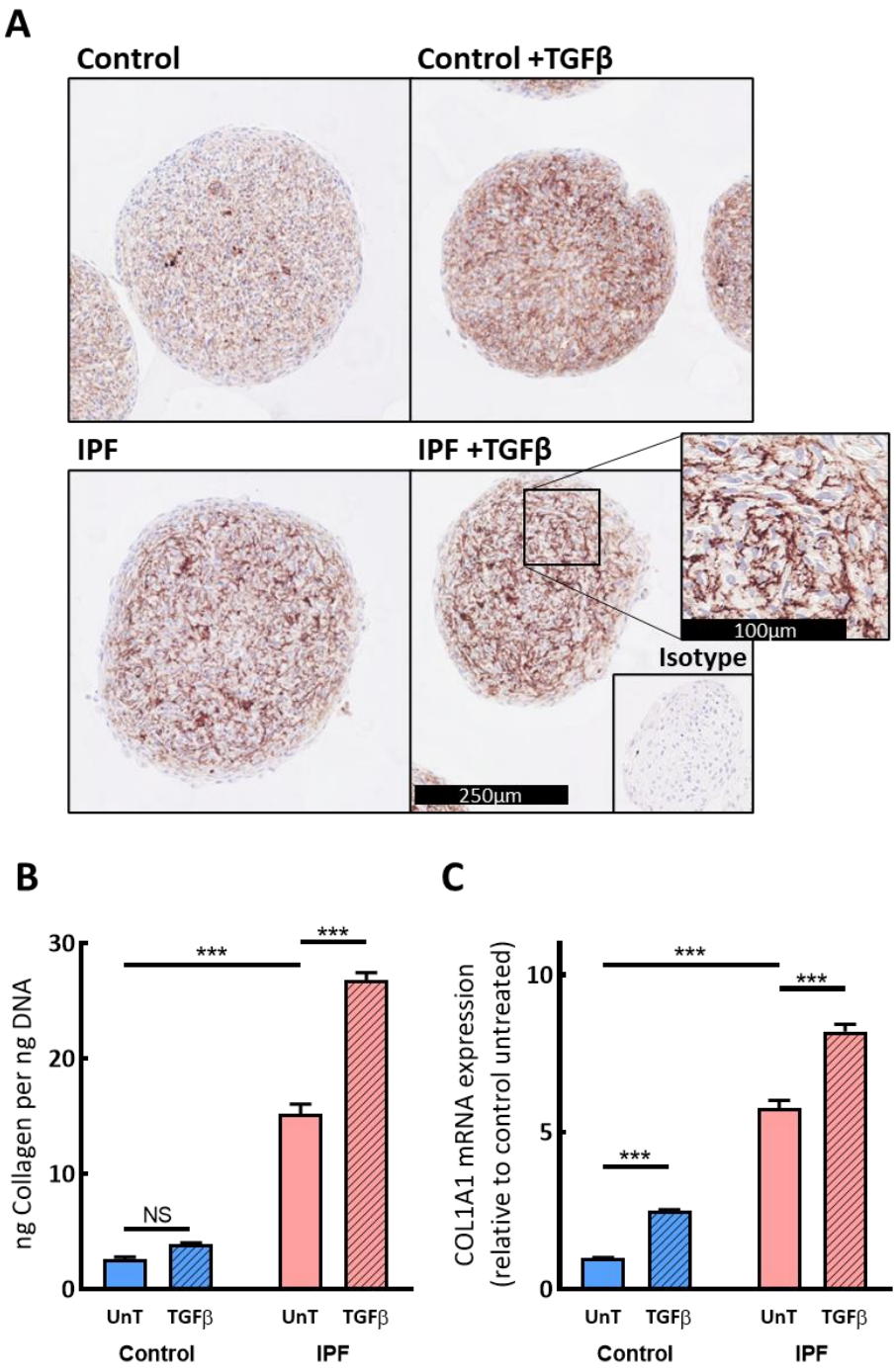


**Figure 3.4.1.1 Collagen deposition in the spheroid model**

(**A**) Collagen staining (red) in sections from control and IPF derived fibroblast spheroids, with / without treatment with TGFβ (40pM) for 24h before spheroid formation. Inset: negative staining with an isotype antibody. (**B**) Quantification of collagen content by measurement of hydroxyproline in whole spheroid hydrolysate, collagen mass shown normalised to DNA content of parallel spheroids. (**C**) mRNA levels for COL1A1 in whole spheroid lysates. All panels 24h post seeding. Two-way ANOVA, Tukey's post-test. *** $p < 0.001$. Each bar represents three pools of eight spheroids for one IPF and one control cell line.

### 3.4.2 Fibrotic human lung fibroblast spheroids contain fibulin-2

Following re-validation of the lung fibroblast spheroid model and demonstration of collagen deposition by both control and IPF lung fibroblasts I investigated the deposition of fibulin-2 within these spheroids. Sections of 24h spheroids were IHC stained for fibulin-2 which, consistent with 2D cultures (**Figure 3.3.2.1**), demonstrated a strong extracellular deposition in spheroids formed by IPF lung fibroblasts whereas staining was absent in spheroids formed by control fibroblasts (**Figure 3.4.2.1**). This markedly increased expression in IPF spheroids was further demonstrated in western blots of whole spheroids homogenised in RIPA buffer containing 4% SDS, where expression in control spheroids was barely detectable (**Figure 3.4.2.2A**). Quantitative RT-qPCR of FBLN2 mRNA was performed in whole spheroid homogenates 24h post seeding showing an approximately 37-fold higher expression in IPF spheroid fibroblasts than in controls ($p < 0.001$, two-way ANOVA with Tukey's post-test; **Figure 3.4.2.2B**).

Earlier data in 2D cell culture showed a significant upregulation of fibulin-2 by the profibrotic cytokine TGFβ (**Figure 3.3.2.1**). Pre-treatment of fibroblasts with TGFβ (40pM) for 24h in 2D culture before trypsinisation and spheroid formation did not increase FBLN2 mRNA in either control or IPF spheroids at the 24h timepoint post seeding (**Figure 3.4.2.1**). At the protein level, TGFβ treatment was not sufficient to induce fibulin-2 expression and staining in control fibroblast spheroids by either IHC (**Figure 3.4.2.2B**) or western blot (**Figure 3.4.2.2C**); it did however significantly increase the fibulin-2 content of IPF spheroids compared to untreated fibroblasts seeded in parallel (UnT) by densitometry of western blot (Student's t-test, $p < 0.01$; **Figure 3.4.2.2C**).

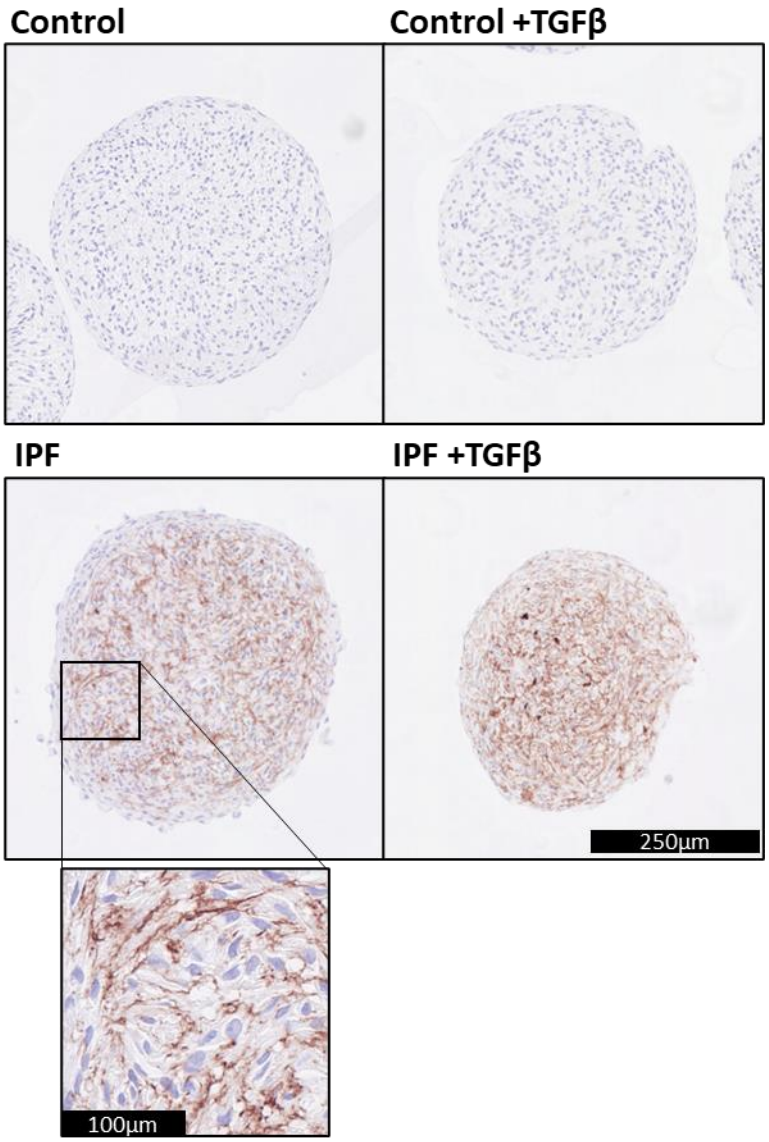


**Figure 3.4.2.1 Fibulin-2 expression in spheroids - immunohistochemistry**

Fibulin-2 staining (red) was seen in IPF derived spheroids but not control fibroblasts at 24h post-seeding, with or without 24h pre-treatment with TGFβ (40pM). Scale bar 250µm. Inset: Higher magnification of IPF untreated spheroid section showing extracellular staining pattern. Scale bar 100µm. Images are representative of four experiments using one control and one IPF cell line.

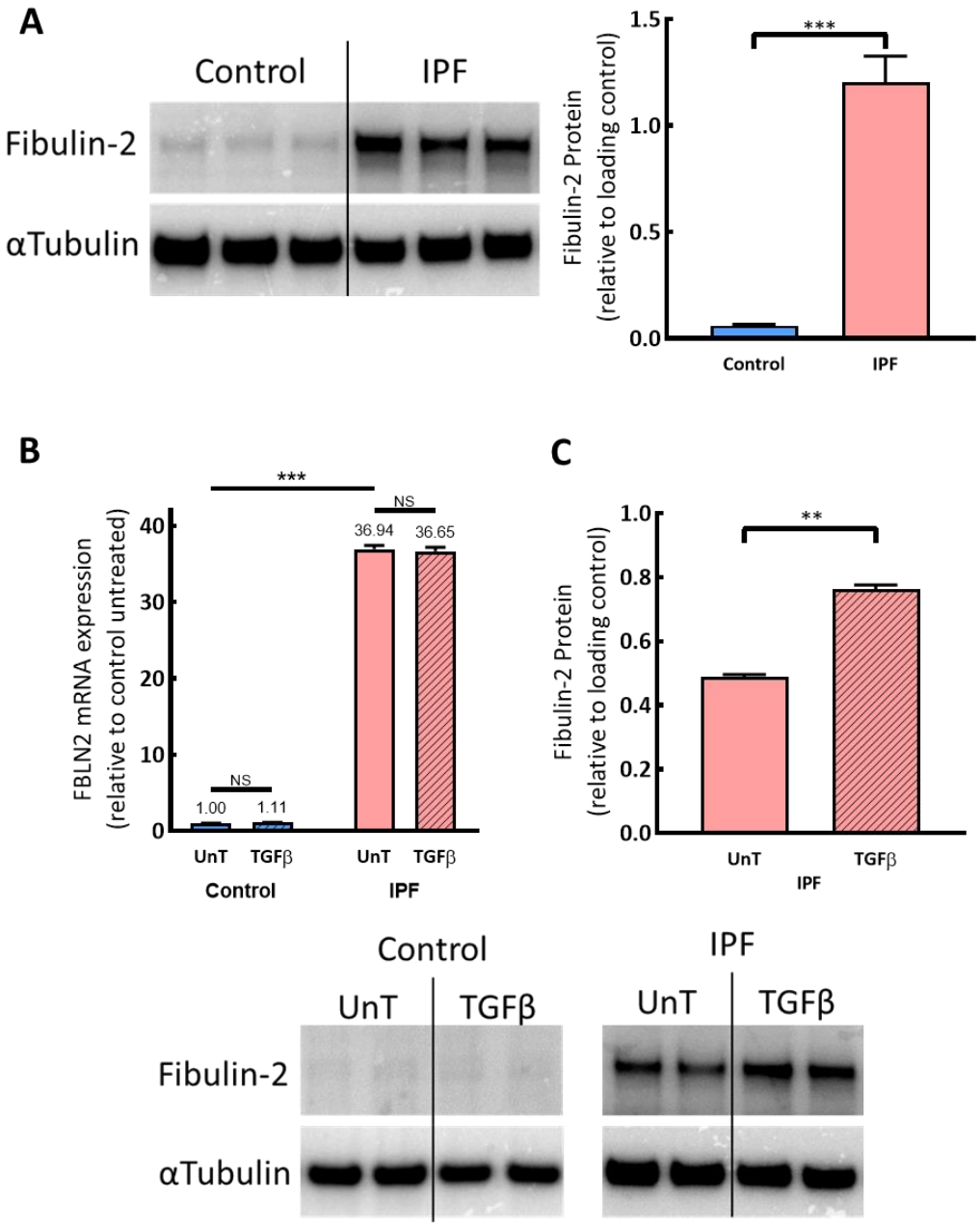


**Figure 3.4.2.2 Fibulin-2 expression in spheroids - quantification**

(**A**) Western blot of fibulin-2 protein in whole spheroid lysates with densitometry quantification relative to loading control. Student's t-test, *** $p < 0.001$. (**B**) RT-qPCR quantification of FBLN2 mRNA in spheroids from a control and IPF donor without (UnT) and with TGFβ pre-treatment (40pM). Two-way ANOVA, Tukey's post-test *** $p < 0.001$. (**C**) Quantification of fibulin-2 protein upregulation by TGFβ in IPF spheroids by densitometry of western blot. Control samples could not be quantified. Student's t-test, ** $p < 0.01$. All data at 24h post-seeding. Each sample is a pool of eight spheroids. RT-qPCR was performed in triplicate. Representative of two independent experiments.

### 3.4.3 siRNA knockdown of fibulin-2 persists in the spheroid model

To elucidate a pro-fibrotic role that fibulin-2 might be playing during spheroid formation expression of FBLN2 was knocked down using siRNA in IPF derived fibroblasts. Formation of spheroids in media containing liposomes based on the transfection reagent INTERFERin resulted in significant amounts of cellular debris, poor spheroid formation and a poor knockdown (**Appendix 7**). 2D experiments had shown a good knockdown by 24h post siRNA treatment which had persisted to 120h. I therefore devised an alternative strategy, as utilised in crowding 2D conditions above, whereby fibroblasts were pre-treated with siRNA in 2D culture. Fibroblasts in 2D culture were treated with siRNA for 24h, serum starved for a further 24h then trypsinised and seeded into spheroid culture conditions for 24h before collection.

Treatment with siRNA specifically targeting FBLN2 achieved an approximately 80% reduction in FBLN2 mRNA compared to untreated (UnT) cells or cells treated with a non-targeting (NT) siRNA (**Figure 3.4.3.1A**). The reduction in mRNA translated to an almost complete abolition of staining for fibulin-2 by IHC (**Figure 3.4.3.1B**), however spheroids formed were otherwise indistinguishable by gross morphology. Western blot quantification showed a greater than 60% reduction in fibulin-2 protein content of spheroids treated with FBLN2 siRNA compared to untreated (UnT) or non-targeting (NT) treatment (one-way ANOVA, Tukey's post-test $p < 0.01$. **Figure 3.4.3.1C**).

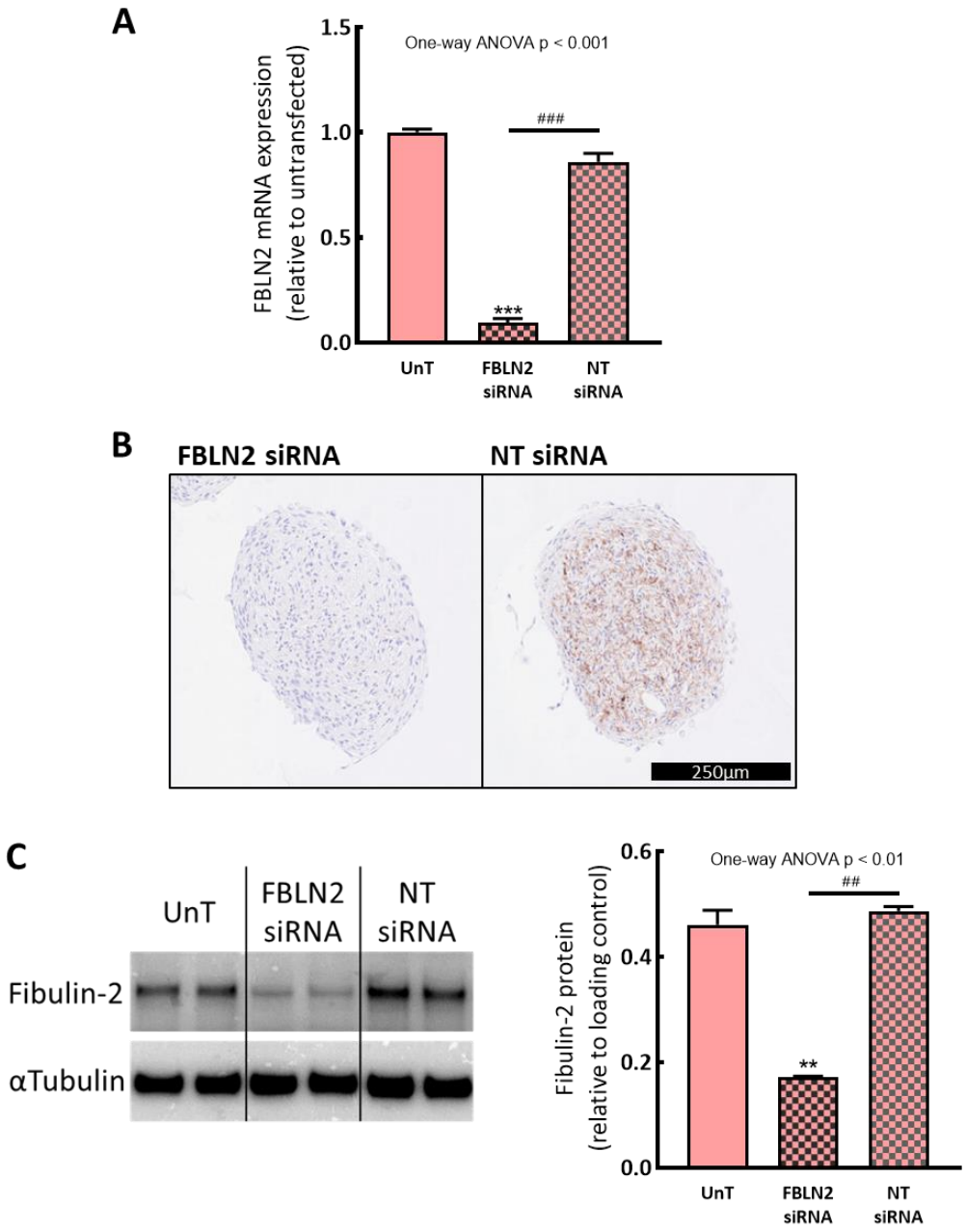


**Figure 3.4.3.1 Fibulin-2 knockdown in spheroids by siRNA**

(**A**) Successful knockdown of FBLN2 mRNA was achieved in IPF spheroids by FBLN2 siRNA treatment 24h before seeding compared to untreated (UnT) or transfection with non-targeting (NT) siRNA. Three pools of eight spheroids were analysed. (**B**) IHC staining for fibulin-2 (red) in IPF spheroids following FBLN2 siRNA pre-treatment. Scale bar 250µm. (**C**) Densitometric quantification of fibulin-2 protein content in IPF spheroids by western blot following FBLN2 siRNA pre-treatment. One-way ANOVAs, Tukey's post-tests, ** $p < 0.01$, *** $p < 0.001$. Data representative of three independent experiments.

### 3.4.4 The effect of FBLN2 knockdown in IPF spheroids

The primary functional readout from spheroid experiments was spheroid collagen content. This was assessed in spheroids formed by fibroblasts following knockdown of FBLN2 by siRNA treatment for 24h in 2D culture prior to spheroid formation. COL1A1 mRNA levels were modestly reduced by FBLN2 deficiency however this did not reach significance against either untreated or non-targeting siRNA transfected fibroblasts (one-way ANOVA; **Figure 3.4.4.1A**). Collagen protein content was measured by quantifying hydroxyproline in whole spheroid hydrolysates at 24h post-seeding and is presented as collagen mass normalised to DNA content of spheroids collected in parallel. There was again a modest reduction in collagen content of spheroids formed by FBLN2 deficient cells which was significant compared to non-targeting (NT) siRNA transfection ($p < 0.01$) but not against untreated (UnT) spheroids (one-way ANOVA, Tukey's post-test; **Figure 3.4.4.1B**).

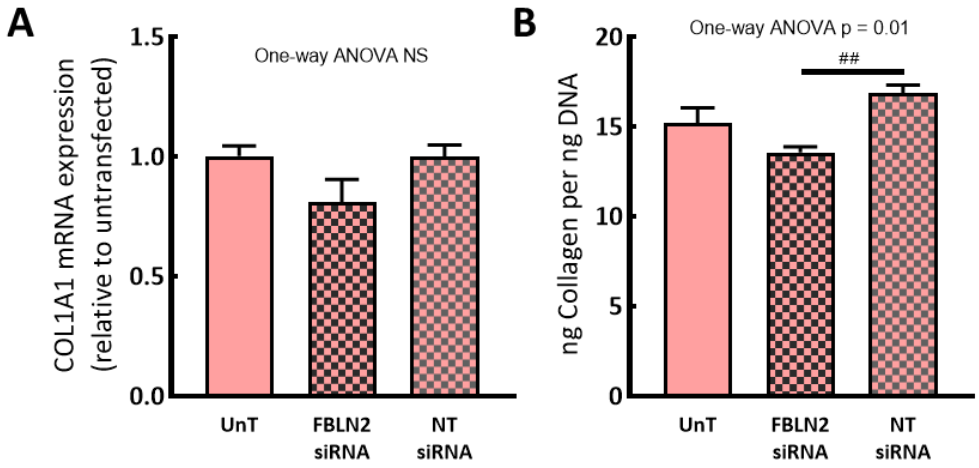


**Figure 3.4.4.1 Collagen expression in FBLN2 deficient IPF spheroids**

(**A**) COL1A1 mRNA in IPF spheroids formed following FBLN2 siRNA treatment or treatment with a non-targeting (NT) siRNA relative to untreated (UnT) spheroids. (**B**) Collagen content was quantified by HPLC of hydroxyproline, calculated collagen mass shown normalised to spheroid DNA content. One-way ANOVA, Tukey's post-test, ## $p < 0.01$. Each bar represents three pools of eight spheroids. Representative of two independent experiments.

A significant decrease in ACTA2 mRNA expression was seen in spheroids formed by IPF fibroblasts following FBLN2 siRNA transfection compared to untreated ($p < 0.01$) or fibroblasts transfected with non-targeting siRNA ($p < 0.05$) (**Figure 3.4.4.2A**). Western blot for αSMA however did not show any significant difference with FBLN2 deficiency (**Figure 3.4.4.2B**).

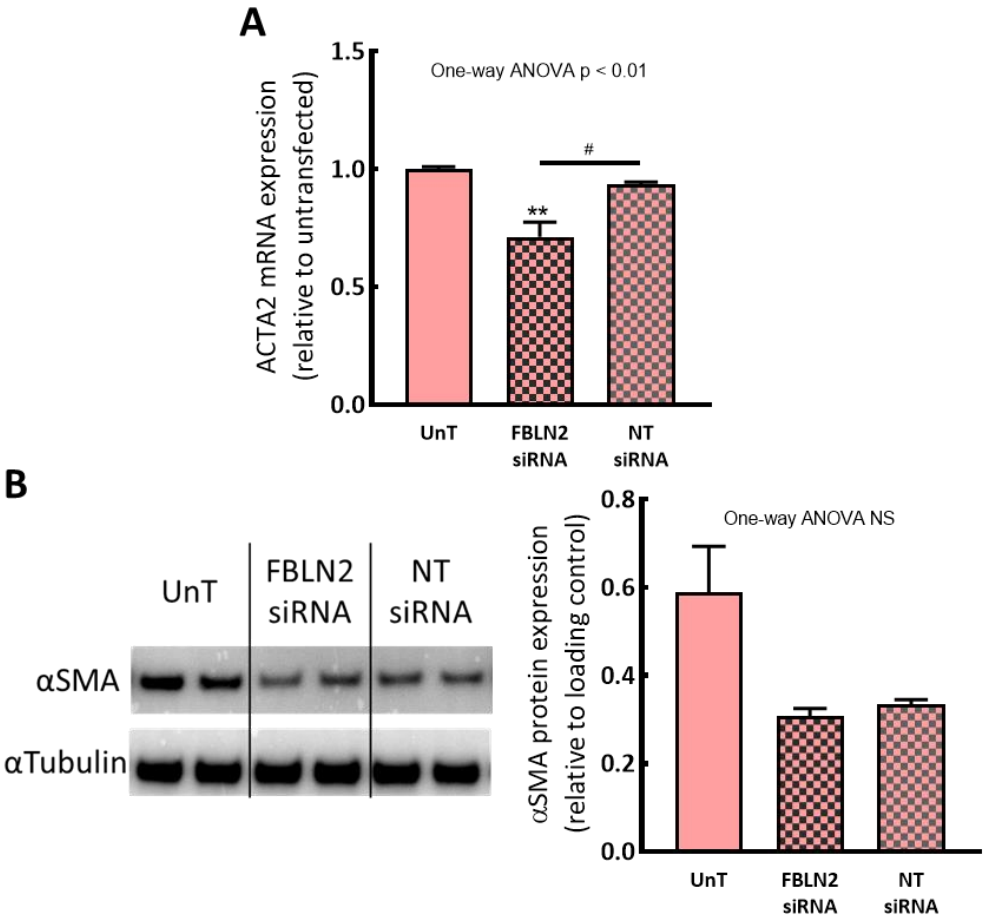


**Figure 3.4.4.2 αSMA expression in FBLN2 deficient IPF spheroids**

(**A**) ACTA2 mRNA in IPF spheroids transfected with FBLN2 siRNA or non-targeting (NT) siRNA or those untreated (UnT). One-way ANOVA, Tukey's post-test * $p < 0.05$, ** $p < 0.01$. Each bar represents three pools of eight spheroids. (**B**) Western blot for αSMA protein with densitometry quantification. One-way ANOVA not significant. All panels at 24h post-seeding. Representative of two independent experiments.

### 3.4.5 FBLN2 expression and methylation in tissue culture conditions

Above, I have shown that fibulin-2 is produced and deposited by fibrotic lung fibroblasts in both 2D monolayer culture and in 3D spheroids. These culture conditions vary greatly with enhanced cell-cell and cell-ECM interaction in 3D and a greatly reduced stiffness compared to 2D culture plastic (Stewart et al. 2019). mRNA expression of FBLN2 was compared in 2D culture (24h and 120h timepoints) and 3D spheroid culture (24h) (**Figure 3.4.5.1A**). While expression was significantly higher in IPF compared to control in all conditions (two-way ANOVA $p < 0.001$) the expression pattern within each cell line was different. In control cells, expression was highest in 2D culture at 120h (14.5 ±0.3-fold of 2D 24h control) and

expression was at an intermediate level in 3D (6.5 ±0.2-fold). In IPF 3D culture demonstrated the highest expression (4.2 ±0.1-fold of 2D 24h IPF) with 2D culture at 120h at a level between 2D and 3D 24h (2.7 ±0.1-fold).

To investigate if these expression changes were due to altered methylation the methylation status of CpG 4 in FBLN2 was assessed by bisulfite sequencing in the corresponding timepoints. In the array data this CpG is significantly hypomethylated in IPF and its methylation correlates to expression (**Figure 3.2.4.1**). This is also the only CpG for which I achieved a reliable sequencing readout. Methylation was significantly lower in the IPF fibroblast line than in controls (overall means 11.7% ±3.0 and 82.3% ±3.0 respectively, two-way ANOVA $p < 0.001$). There was however no difference in methylation within each cell line for the varying culture conditions despite the changes in expression (**Figure 3.4.5.1B**).

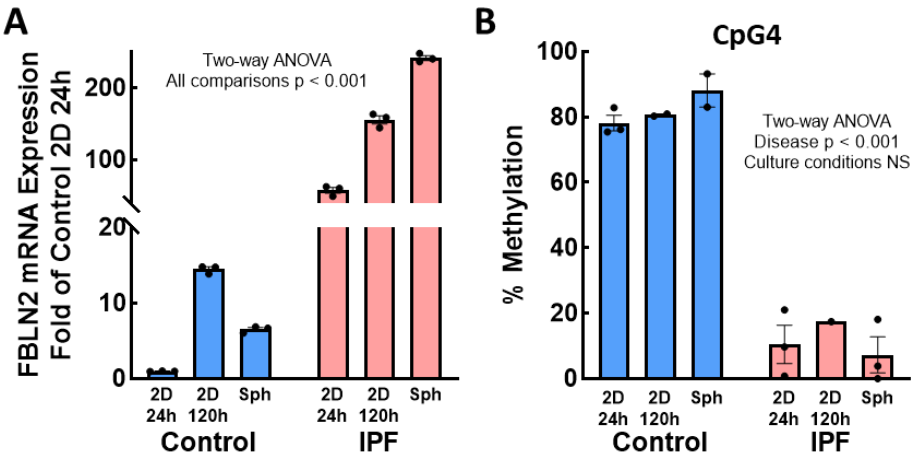


**Figure 3.4.5.1 FBLN2 expression and methylation level of CpG4 in 2D and 3D culture**

(**A**) FBLN2 mRNA expression varied by culture condition. Expression is normalised to the expression in control cells at 24h of 2D culture. Two-way ANOVA, Tukey's post-test: all comparisons $p < 0.001$. 2D data is of a single well, 3D data is each a pool of eight spheroids. (**B**) There was no change in methylation of CpG 4 in different culture conditions within each cell line by bisulfite sequencing. Two-way ANOVA, Tukey's post-test: disease $p < 0.001$, conditions not significant (NS).

### 3.4.6 Summary

- While human lung fibroblasts from IPF and controls form spheroids rich in collagen I, fibulin-2 is much more highly expressed in IPF derived spheroids.

- A method of fibulin-2 depletion by siRNA preceding spheroid formation was successfully devised.

- Spheroids deficient in FBLN2 were grossly unchanged but had lower αSMA mRNA expression and reduced collagen content compared to non-targeting siRNA controls.

- FBLN2 expression varies with cell culture conditions with 3D culture having increased expression in both control and IPF fibroblasts compared to an equivalent timepoint on 2D plastic.

- Methylation of FBLN2 CpG 4 is significantly lower in IPF than control but is not changed by cell culture conditions despite significant differences in gene expression.

# 4 Discussion

## 4.1 Overview

The pathomechanisms leading to the development and progression of pulmonary fibrosis remain poorly understood. We and others have shown that there is a persistence of fibrotic phenotype in fibroblasts isolated from patients with pulmonary fibrosis when compared to those from histologically normal lung and that this is at least partly due to gene methylation (Keerthisingam et al. 2001; Evans et al. 2016). Previous studies in IPF and SSc have identified multiple genes which are dysregulated by aberrant methylation.

The first section of this thesis is based upon data from methylation and expression microarrays performed within our lab by Dr Iona Evans using control, IPF and SSc human lung fibroblasts. This thesis built upon analysis previously performed within our lab by Dr Ian Garner (I. Garner 2016) which assessed global methylation differences in PF including the location of differentially methylated CpGs in relation to CGIs. In this thesis updated annotation was applied to the primary methylation and expression array data and differential analysis utilised to identify a gene of interest for further study.

Differential expression (TNoM ≤ 1, $p < 0.05$) was identified in 522 and 678 genes in IPF and SSc respectively compared to non-diseased controls. There was an overlap of 96 genes between IPF and SSc which may represent a population of genes likely to be related to pulmonary fibrosis. Genome wide methylation analysis identified altered methylation ($\Delta\beta \geq 13.6\%$, $p < 0.05$) of CpGs relating to 4,182 genes in IPF and 4,481 in SSc when compared to controls. Direct correlation between methylation beta level and $Log_2$ expression was used to identify a subset of 935 genes in which methylation was potentially regulating expression. Treatment with the demethylating agent 5Aza was further used in array experiments to identify genes in which expression may be controlled by CpG methylation.

Array data was subjected to sequential filtering at the gene list level to identify a gene for further study. The criteria used to filter the array gene list were chosen to identify a gene which is regulated by gene methylation and aberrantly expressed in pulmonary fibrosis and included genes with:

- A correlation between methylation and expression
- Differential expression in fibrotic fibroblasts compared to controls
- A change in expression following 5Aza treatment

Filtering identified a list of 99 genes which was subsequently refined by gene ontology (GO) annotation to yield 4 genes of interest annotated for 'ECM organisation' including fibulin-2. Fibulin-2 is an ECM structural protein which binds multiple ECM components. Its expression is low in most adult tissues however it has been found to be upregulated in decellularized IPF lung (Booth et al. 2012) and recently in human lung fibroblasts (Hadjicharalambous et al. 2019). It is also upregulated in skin wound healing (Fässler et al. 1996), and both up- and down-regulated in various cancers. The role of fibulin-2 in TGFβ based autocrine-loop driven cardiac fibrosis (H. Zhang et al. 2014) makes it an exciting candidate for study in pulmonary fibrosis.

This thesis therefore investigated the hypothesis:

> **Increased fibulin-2 expression by fibroblasts, induced by mechanisms involving CpG methylation, contributes to the pathogenesis of pulmonary fibrosis and modulating this axis may have therapeutic benefit.**

In agreement with literature above and array data, fibulin-2 expression was upregulated in isolated lung fibroblasts and lung tissue from IPF and SSc donors compared to controls. FBLN2 was significantly differentially methylated in fibrotic lung fibroblasts and there was a strong correlation between methylation and expression of FBLN2.

In both 2D and 3D culture, fibulin-2 expression results in its protein deposition into the ECM with significantly higher deposition seen in IPF derived fibroblasts compared to controls. Fibulin-2 expression increased with time in 2D culture, this however was not accompanied by a change in methylation of a CpG of interest. As with fibroblasts isolated from FBLN2 deficient mice (H. Zhang et al. 2014), siRNA mediated depletion of FBLN2 in 2D and 3D culture demonstrated anti-fibrotic effects on IPF lung fibroblasts resulting in downregulation of collagen I and αSMA.

These data suggest that increased expression of fibulin-2, potentially as a result of enhancer hypomethylation, may play a role in maintaining the fibrotic lung fibroblast phenotype. Further studies are required to fully elucidate the role of gene methylation in fibulin-2 expression and the mechanisms through which fibulin-2 protein affects fibroblast activation.

## 4.2 Expression array

Expression array data was obtained using the Illumina HumanHT-12 expression microarray to quantify mRNA expression in isolated lung fibroblasts. This array contains probes targeting 47,230 sequences. Updated annotation of array data was performed for analysis in this thesis using data from the Re-Annotator program (Arloth et al. 2015). The program authors claim

that *in silico* alignment of the array probes to a reference cDNA library and the hg19 reference genome improves annotation of 25% of expression probes compared to the original Illumina annotation. Only probes which Arloth *et al.* graded 'reliable' (34,936 transcripts) were included in subsequent analysis. Probes were also only included in analysis where they were detected above background in at least one sample. This resulted in a dataset containing 17,381 probes mapping to 12,445 genes.

Differential expression analysis was performed at the single probe level with no averaging of expression where a gene has multiple probes. This ensured that any differences resulting from alternative transcript expression were not lost. Few genes were identified as differentially expressed in either IPF or SSc compared to controls using a FDR < 0.05 so the non-parametric threshold number of misclassifications (TNoM) of ≤ 1 was used with a non-stringent $p < 0.05$ to avoid excluding potential genes of interest. TNoM is a measure of the separation of two populations which doesn't require the use of an arbitrary threshold for the difference meaning that potentially meaningful small differences in expression can be identified. Previous studies using expression microarrays in fibrotic lung or lung fibroblasts have used a minimum absolute fold change in expression ≥ 2 (Sanders et al. 2012) or a fold-change ≥ 2 with a TNoM = 0 (J.-U. Lee et al. 2017). Using TNoM ≤ 1 ($p < 0.05$) I identified 522 genes in IPF cell and 678 in SSc that were differentially expressed compared to controls. This is in contrast to 373 genes identified in lung tissue by Sanders *et al.* and 178 genes identified in fibroblasts by Lee *et al.* using their more stringent criteria. 96 genes were shared between IPF and SSc which may represent a population of genes most relevant to the pathogenesis of PF in isolated lung fibroblasts. Although these overlapping genes may be of particular interest, subsequent analysis was not restricted to this small group in order that as many genes of interest were included when combined with methylation data.

GO: Gene ontology enrichment was performed on the lists of dysregulated genes generated through analysis of the expression array. While others use a background of all genes covered by the array for GO enrichment analysis (J.-U. Lee et al. 2017), a background of only those genes with probes included in analysis and detected above background was used in this thesis. While this approach reduces the statistical power of the comparison it does not make the assumption that genes below the array background threshold are not differentially expressed. While no GO terms were enriched with a FDR < 0.05 a number of terms relevant to PF were enriched with a non-stringent $p < 0.05$. In particular, the term 'extracellular matrix organisation' was enriched in genes upregulated in both IPF and SSc while 'regulation of telomerase activity' was enriched in downregulated genes. Although telomerase activity has

been associated with the progression of pulmonary fibrosis (Fingerlin et al. 2013; Noth et al. 2013; T. Liu et al. 2019) the downregulated genes associated with this GO term include both MAP2K7, a positive regulator of telomerase activity (Cerone et al. 2011) and PPARG, a negative regulator (Toaldo et al. 2010) demonstrating the limitations of GO. GO is discussed further in **section 4.6** below.

## 4.3 Methylation array

This thesis utilised data from the Illumina Infinium Human Methylation 450k microarray which contains probes covering 482,421 CpGs. CpG targets were chosen by a consortium of researchers with priority given to providing comprehensive coverage of genes and CpG island regions but also those regions deemed most biologically relevant by members of the consortium. Although 98.9% of RefSeq genes were covered at the time of designing and each with an average of 17.2 probes, coverage is biased towards CpG islands, their shores (0-2kb from CGI) and shelves (2-4kb from CGI) (Bibikova et al. 2011). Subsequent *in silico* characterisation of the probe sequences by a number of groups has identified probes which may be influenced by common SNPs and probes which map to more than one genomic location (Price et al. 2013; Nordlund et al. 2013; Zhou, Laird, and Shen 2017). Although annotation from Price *et al.* (2013) has previously been used within our lab (I. Garner 2016), it removes probes which contain a SNP anywhere within the probe sequence whereas more recently Zhou *et al.* (2016) have demonstrated that SNPs greater than 5 bases of the 3'-end of the probe have negligible effect on array hybridisation. Probe exclusion was therefore limited to those identified by Nordlund *et al.* (2013) and Zhou *et al.* (2016) as potentially influenced by a SNP or mapping to more than one genomic location. Probes which map to sex chromosomes were also removed as these would be confounded by hemimethylation regulated X-chromosome inactivation (Klebaner et al. 2016). 412,481 probes were included for subsequent analysis.

Data normalisation and group-pair statistical analysis of array data had been performed by Cambridge Genomic Services using the Lima R-package. Utilising a FDR $p < 0.05$ only two probes were differentially methylated between control and IPF groups. Instead, an absolute difference methylation β-value with a non-stringent p-value was used to identify deferentially methylated CpGs. The β-value is easily interpretable as the fraction of each CpG methylated within the population of cells sampled. An absolute change of 13.6% methylation with a non-corrected $p < 0.05$ was used as this has previously been shown to detect differences with 95% confidence (Bibikova et al. 2009) and was previously used within our lab (I. Garner 2016). The selection of an absolute difference threshold is a balance between

cutting off meaningful small changes in methylation and excluding false positive differences. While small changes in methylation have been shown to regulate gene expression the underlying array technology is not sensitive enough to identify these differences (Dedeurwaerder et al. 2013), especially given the heterogenous nature of IPF and the relatively small sample numbers available. Previous studies utilising methylation microarrays in IPF have defined differential methylation in a number of ways including by FDR < 0.05 (Rabinovich et al. 2012; I. V. Yang et al. 2014) or by initially utilising a non-stringent p-value < 0.05 followed by FDR correction in later analysis (Sanders et al. 2012). Most recently, and in a study directly comparable to this array experiment, Lee *et al.* (2019) did not identify any CpGs which passed a FDR < 0.05 between IPF (n=8) and control (n=4) lung fibroblasts and subsequently used an absolute $\Delta\beta > 10.21$ with $p < 0.05$.

In IPF 11,073 CpGs had altered methylation compared to controls with a bias towards hypomethylation (68%). This is significantly more than the 5,850 loci which Lee *et al.* identified with the less stringent threshold though they did also show a bias towards hypomethylation (72% of loci) in IPF fibroblasts, possibly due to the authors having fewer control samples (J.-U. Lee et al. 2019). SSc fibroblasts had 11,161 CpGs with altered methylation compared to controls with a bias towards hypermethylation (66%). Although I am not aware of any other studies showing global methylation patterns in SSc lung fibroblasts this is in contrast to global hypomethylation which has been reported in dermal SSc fibroblasts using the same microarray (Altorok et al. 2015). A difference which likely reflects a site-specific epigenotype of SSc fibroblasts.

## 4.4 Correlation between expression and methylation

As the primary aim of the first part of this thesis was to identify a gene which was differentially expressed in PF and potentially regulated by gene methylation, the direct correlation of individual CpG methylation to expression at the probe level was calculated covering all 18 cell lines. Although a causal relationship between methylation and expression cannot be assumed from correlation alone it remains a powerful tool for identifying the statistical relationship between the two. Correlation was calculated in a location—independent manner utilising the methylation array annotation for CpG-gene pairing. As a consequence, intergenic CpGs lacking annotation were not paired with expression and therefore were excluded from correlation analysis. This is discussed further with regard to CpG 4 in **section 4.13.1** below.

Correlation is routinely used to pair methylation and expression data however there is no consensus as to if the Pearson or Spearman correlation coefficient is most appropriate. For example, Pearson's correlation has been used to analyse large datasets investigating location of methylation within a gene (Varley et al. 2013; Spainhour et al. 2019) while Spearman correlation has been used in publications linking methylation and expression in PF (J.-U. Lee et al. 2019) and other diseases (Wagner et al. 2014; Bell et al. 2016). Because the relationship between methylation and expression is not necessarily linear data from both the Pearson and Spearman correlation was used to define the list of 935 genes in this thesis where methylation correlated with expression. These genes were linked to a total of 1469 CpGs with 77 genes containing at least one CpG with positive correlation and one with negative correlation to expression.

While the prototypic relationship between methylation and expression is of negative regulation whereby addition of the methyl group results in reduced gene transcription it has been shown that both negative and positive relationships occur and that this relationship varies by genetic location of the CpG (Varley et al. 2013; Spainhour et al. 2019). It has also been shown that methylation may regulate alternate exon inclusion and therefore the expression of only one transcript variant (Maunakea et al. 2013). Therefore, a significant correlation in either direction between any individual CpG – gene probe pair was included for further analysis.

## 4.5 5Aza & 'responders'

The demethylating agent 5Aza was used in the array experiments detailed in this thesis to study how changes in DNA methylation related to gene expression. 5Aza is an analogue of cytosine which, when incorporated during DNA replication, covalently binds to DNMT1 entrapping the enzyme. 5Aza also acts through unknown mechanisms to lead to the proteolytic degradation of free DNMT1 (Patel et al. 2010).

While we have previously shown that in this array experiment genes known to be regulated by methylation were affected by 5Aza (Evans et al. 2016; I. M. Garner et al. 2013), analysis of all 18 samples showed no difference in methylation of CpGs mapped to fibulin-2 with 5Aza treatment. There was no change in mean expression of fibulin-2 mRNA following 5Aza treatment in control or IPF however there was a small but significant reduction in expression in SSc fibroblasts. Global analysis of the methylation and expression array data identified that while group mean methylation of a small number of CpGs was altered by 5Aza ($\Delta\beta \geq 13.6\%$, $P < 0.05$), analysis of individual cell lines highlighted a sub-population of control and IPF

donors in which methylation (Δβ ≥ 13.6%) and expression (≥ 2-fold change) were more strongly affected by 5Aza treatment (**Table 3.1.4.1**). Resistance to 5Aza has been shown in cancer cells through deficiency in deoxycytidine kinase which is required to convert 5Aza into the active form which can be incorporated into DNA (Qin et al. 2009).

In the 'responding' cell lines, although most changes were less than the 13.6% threshold there was a correlation between the change in methylation and change in expression with 5Aza treatment in three CpG sites including CpG 4. This CpG had a negative correlation between the change in methylation and expression which supports the relationship found in analysis of all 18 untreated cell lines above. Methylation of CpG 4 was increased in 4 of these 6 'responding' cell lines with 5Aza treatment. This unexpected result was also seen in the group mean methylation of a small number of CpGs on the array. Hypermethylation of a limited number of CpGs upon treatment with a demethylation agent has been recently documented in a number of cancer cell lines and showed variation in hypermethylation by tissue of origin (Giri and Aittokallio 2019). However, the mechanism by which this hypermethylation occurs is yet to be elucidated and may include activation of the *de novo* methylation machinery including DNMT3a and DNMT3b and histone modifications which could lead to the maintenance or increase of CpG methylation in the presence of a demethylation agent.

## 4.6 Filtering to a gene of interest

The aim of this thesis was to identify a gene of interest for further study from expression and methylation microarray data of primary lung fibroblasts from disease and controls. Differential array data analysis yielded a number of gene lists which contained genes differentially expressed in pulmonary fibrosis and potentially regulated by gene methylation. To filter these gene lists to a gene of interest, sequential analysis was performed.

Genes with a significant correlation between methylation and expression, in either direction, were taken as the starting point of array filtering as these genes are the most likely to be regulated by gene methylation. Genes in which there was no difference in expression in fibrosis were then excluded. The genes of highest interest were likely those in which there was significant differential expression in both IPF and SSc compared to controls. However, as pulmonary fibrosis is a heterogenous disease and the array group sizes are small, in order to not exclude genes which may not have reached this threshold in both diseases, genes in which there was a difference in either IPF or SSc were taken forward. Similarly, due to the likely small, heterogenous, effects of 5Aza treatment on gene expression genes were

included for further analysis where 5Aza caused a change in expression in any of control, IPF or SSc groups. This filtering yielded 99 genes of interest for which there is a difference in expression in pulmonary fibrosis and which are likely to be regulated by gene expression. Manual filtering utilising GO annotation was then used to identify a gene for further study.

**GO annotation**

GO is an ever-expanding database of manually curated annotations based on published functional data. As such it is limited by the quality and quantity of published data for each gene and the limits of manual curation. The database is therefore incomplete and has heterogenous, biased, coverage which favours highly studied genes (Haynes, Tomczak, and Khatri 2018). GO based omics research also leads to a self-perpetuating cycle where genes with no annotation are excluded from studies and therefore stand a lower chance of gaining GO annotation. The literature for the annotated genes identified then expands, further perpetuating the cycle. However, all 99 genes which had passed the unbiased filtering stages in this thesis to be included in GO analysis had at least one GO annotation.

Despite its limitations, GO is a useful tool for adding context to otherwise one-dimensional lists of genes. Numerous tools are available to annotate gene lists and perform enrichment analysis. In this thesis, the GOrilla online tool (Eden et al. 2009) was used, primarily as it was based on the most up to date GO database of the tools compared. GO enrichment analysis was performed against a background of those genes which were included at the start of filtering, for which correlation data was available. This means that only genes which were detected on the expression microarray were included in the background as the differential expression status of genes which were not expressed above array detection levels remains unknown and their inclusion as 'non-differentially expressed' would bias enrichment analysis. Using this limited background however comes at the cost of decreasing the enrichment p-value.

GO enrichment of the 99 genes which were differentially expressed and potentially regulated by gene methylation did not yield any significantly enriched GO processes so GO was used purely to annotated the gene list for manual review. The GO term GO:0030198 'extracellular matrix organization' was previously enriched in genes significantly upregulated in both IPF and SSc compared to controls, although this did not pass false discovery testing (**Table 3.1.1.1**). This term therefore was likely of high relevance to the pathogenesis of pulmonary fibrosis. Four genes out of the 99 genes which passed filtering were annotated for this GO term and were taken forward for literature review.

## 4.7 Other genes of interest

In addition to FBLN2, final filtering of array data identified three other genes which were differentially expressed in IPF or SSc, potentially regulated by gene methylation and annotated for the GO term ECM organisation. These genes were ADAM15, CD47 and PTK2.

**ADAM15**

ADAM15 is a type-I transmembrane molecule which contains a metalloproteinase and a disintegrin domain. It has been shown to bind to integrin (Nath et al. 1999), to interact with FAK (PTK2) resulting in enhanced apoptosis resistance in chondrocytes (Böhm, Schirner, and Burkhardt 2009; Fried et al. 2012), and to promote endothelial cell survival (Babendreyer et al. 2019). ADAM15 is also pro-metastatic in non-small cell lung cancer through direct activation of MMP9 (Dong, Zhou, and Li 2015). In our array data, ADAM15 was down regulated in IPF but not SSc compared to controls in one of three array probes (**Appendix 2**). This probe had the lowest Log2 expression of the three but no difference in expression was seen in either of the two more highly expressed probes. This suggests that overall ADAM15 mRNA and protein levels are unlikely to be differentially expressed by fibrotic lung fibroblasts.

**CD47**

Cluster of differentiation 47 (CD47) is a transmembrane glycoprotein which has antiphagocytic activity mediating a so called “Don’t-Eat-Me” signal inhibiting macrophage phagocytosis. As such CD47 is upregulated in many cancers including in the lung (Zhao et al. 2016) and CD47 expression prevents elimination of diseased fibroblasts in dermal fibrosis (Lerbs et al. 2020). CD47 is upregulated by fibroblasts in digested fibrotic lung (Wernig et al. 2017; Cui et al. 2020) and anti-CD47 antibody treatment is antifibrotic in c-Jun-mediated murine fibrosis (Wernig et al. 2017). I am however not aware of any studies which demonstrate that the difference in expression is preserved in isolated fibroblasts grown on culture plastic.

Expression array data contained two probes which targeted CD47. One probe had Log2 expression levels which were at the lower limit of detection above background but showed significantly reduced expression in SSc fibroblasts compared to controls but not in IPF. The second probe had much higher Log2 expression of CD47 but no difference in expression between the three groups (**Appendix 2**). It is therefore possible to conclude that CD47

expression is unlikely to be altered at the protein level in isolated fibrotic lung fibroblasts compared to controls.

**PTK2**

Protein tyrosine kinase 2 (PTK2), also known as focal adhesion kinase (FAK), is a non-receptor tyrosine kinase which signals through a number of downstream pathways and regulates cell adhesion, migration, activation and survival. FAK is autoinhibited within the cytoplasm and is activated through interaction with integrins within the focal adhesion complex enabling transduction of mechanosensing (Dugina et al. 2001; Lietha et al. 2007). FAK expression and activity is increased in myofibroblasts in lung tissue of IPF and SSc donors (Lagares et al. 2012) and it's inhibition is antifibrotic in isolated fibroblasts and in the bleomycin model of fibrosis (Lagares et al. 2012; Kinoshita et al. 2013; Giménez et al. 2017).

Expression array data detected PTK2 expression in two probes; one had low expression and no difference between the three experimental groups, while the other detected high Log2 expression and had upregulated expression in both IPF and SSc compared to control (**Appendix 2**). The upregulation seen is in keeping with published literature.

ADAM15 and CD47 were discounted for further study as, although they had passed filtering with some probes, their most highly expressed array probes were not differentially expressed and they are therefore unlikely to have altered protein expression controlled by direct gene methylation. PTK2 expression and activation has already been extensively studied in pulmonary fibrosis whereas, beyond being identified as upregulated in proteomic studies, FBLN2 was a potentially novel gene of study.

## 4.8 Fibulin-2 expression

Filtering of array data identified FBLN2 as a gene which was differentially expressed in fibrotic lung fibroblasts compared to controls (TNoM = 1, $p<0.05$). FBLN2 expression was upregulated in both IPF and SSc derived lung fibroblasts compared to control cells by 5.9-fold and 4.4-fold respectively in array data (**Section 3.2.1**). Expression data was validated by RT-qPCR of the original RNA samples using custom primers specific for FBLN2. There was a strong correlation between array and RT-qPCR data which acts to validate the array probes. FBLN2 expression was further assessed by RT-qPCR in a validation cohort of fibroblasts from control and IPF donors. When all RT-qPCR data was combined this demonstrated a 10.56-fold higher FBLN2 expression in IPF fibroblasts compared to controls. This result was supported by recently published data showing a 5.38-fold higher expression of FBLN2 in

isolated IPF derived lung fibroblasts than in controls and a 4.26-fold higher mRNA expression in IPF lung tissue than controls (Hadjicharalambous et al. 2019). FBLN2 was not identified as differentially expressed by Lee *et al.* (2017) utilising the Illumina HumanHT-12 expression microarray on isolated IPF fibroblasts. Lee *et al.* however utilised the stricter threshold of TNoM = 0 with an absolute expression fold-change >2 which would not have identified FBLN2 in our data.

Strong immunohistochemical staining for fibulin-2 was achieved in sections of human lung from control, IPF and SSc donors. In control tissue, this staining was localised to regions surrounding blood vessels and airways, areas associated with elastin fibres. This is consistent with the predicted expression of fibulin-2 as an extracellular structural protein which binds to numerous ECM components including tropoelastin. The staining pattern in control lung is identical to the published staining of normal lung tissue by Baird et al. (2013). Staining in fibrotic lung from IPF and SSc donors was stronger with a more diffuse staining pattern in regions of increased ECM deposition. This is in agreement with mass spectroscopy data of decellularized lung in which Booth et al. (2012) showed a 2.60-fold higher content of fibulin-2 in IPF lung than that of normal controls. I have therefore demonstrated an upregulation of fibulin-2 at the mRNA level in cultured fibrotic lung fibroblasts and that this *in vitro* data is representative of *in vivo* protein expression in fibrotic human lung tissue.

Proteomic data in the bleomycin mouse model of lung fibrosis has demonstrated an upregulation of fibulin-2 protein in the fibrotic phase of the model (days 14 and 28) (Schiller et al. 2015). Unfortunately, due to the immunoreactivity of commercially available antibodies it was not possible to stain for fibulin-2 protein in sections of mouse lung. Publications assessing fibulin-2 protein in mice appear to exclusively use an antibody generated by Dr Takako Sasaki (T Sasaki et al. 1996) and this could potentially be valuable for the future assessment of the fibulin-2 expression pattern in bleomycin treated mouse lungs.

## 4.9 Fibulin-2 splice variants

Expression of FBLN2 was detected by two of three probes on the Illumina Infinium HT12v4 expression array: ILMN_1774602 and ILMN_2390919. The sequences of these two probes overlap, as such there was a strong correlation of $Log_2$ expression levels detected between these probes. These two probes map to all three transcript variants of fibulin-2 taken from GRCh37.p13 reference assembly (**Figure 3.2.1.1**). A third probe, ILMN_1721769, was not detected above background in any fibroblast cell lines either before or after 5Aza treatment. This probe maps to transcript variants 1 and 3 but not variant 2. The mapping and detection

of these probes therefore suggests that only variant 2 is expressed in lung fibroblasts. Transcript variant 2 lacks alternatively spliced exon 9 which codes an EGF-like domain. This transcript variant is referred to as fibulin-2 short (FBLN2S) by Law et al. (2012). In their paper investigating fibulin-2 expression in nasopharyngeal carcinoma Law et al. demonstrate that the short isoform is predominantly expressed in both tumour and normal cells with the long isoform barely detectable. In contrast, Danan-Gotthold et al. (2015) demonstrate equal or higher expression of FBLN2 mRNA containing the alternatively spliced exon in 5 normal tissues including lung, and a switch to exon exclusion in the respective cancers. In lung adenocarcinoma, despite a strong switch to exon exclusion there was no change in overall FBLN2 expression suggesting the regulation of expression and splicing are independent. There was a significant link between a stronger switch to exon exclusion and poor patient survival in this disease. While this data may be confounded by the cell type composition of the samples differing between tumour and normal tissue it does demonstrate that 'fibulin-2 long' is expressed in the human lung. The roles of these different variants however have not been investigated in comparative functional studies and there is no data on the mechanisms regulating the exclusion of exon 9 of fibulin-2. Data in this thesis has shown that fibroblasts grown *in vitro* from both normal and fibrotic lungs do not express alternatively spliced exon 9 at a level detectable by microarray. It remains unknown however if this is representative of fibroblasts within the normal or fibrotic lung architecture.

## 4.10 Fibulin-2 deposition in cell culture

For in vitro experiments investigating fibulin-2 expression and deposition in culture, representative cell lines from a control and an IPF donor were chosen. Cell lines were chosen which had FBLN2 mRNA expression close to the mean of their respective groups within the whole RT-qPCR cohort. Initial experiments utilised immunofluorescent staining within a molecular crowding assay used routinely within our lab. While molecular crowding conditions are required for the timely conversion of soluble procollagen into the fibrillar matrix *in vitro*, the deposition of fibulin-2 proceeded rapidly under normal, non-crowded, culture conditions in IPF fibroblasts and was not further enhanced by crowding (**Section 3.3.2**). The lack of requirement for molecular crowding is in agreement with images from Sicot et al. (2008) which demonstrate deposition of fibulin-2 into the ECM under non-crowded conditions by isolated murine embryonic fibroblasts which were grown to 7 days post confluency.

In the initial experiments in this thesis, there was however no fibulin-2 deposition by control fibroblasts seen within the rapid assay with or without crowding and TGFβ stimulation. This

is in contrast to array data which shows that although FBLN2 expression is lower in control cells, it is still detected at a robust normalised Log2 expression level. This discrepancy is likely due to the differing culture conditions for the deposition assay and array experiments. The rapid deposition assay was assessed 48h post-seeding, in serum-starvation conditions and sub-confluent cells, whereas array experiments were performed on cells in 10% FCS once they had proliferated to confluency (approximately 7 days). mRNA and protein were therefore collected over time from control and IPF fibroblasts which were seeded at ~25% confluency in media containing 10% FCS as these conditions recreated those of the array experiment. These were also the conditions required for subsequent siRNA-based knock-down of FBLN2. Western blotting for fibulin-2 required establishment of optimal dissociation conditions to liberate fibulin-2 from the initially insoluble fraction. The binding between fibulin-2 and many ECM partners is $Ca^{2+}$ dependant, therefore EDTA was required by Sasaki *et al.* (1996) to solubilise fibulin-2. Fibulin-2 yield was however higher in RIPA buffer supplemented with an increased concentration of the detergent SDS as utilised by Singh and Schwarzbauer (2014), this was therefore used for assessment of fibulin-2 deposition.

FBLN2 expression in 2D culture was, as expected, significantly higher in IPF fibroblasts than controls at all timepoints, however there was an increase in expression in both cell lines over time. This increase between 24h and 120h was greatest in control cells which had a 10.4-fold increase in expression compared to 2.2-fold in IPF. As a consequence of these differing increases, the difference in expression between the two cell lines varied from 59-fold at 24h to approximately 12-fold at later timepoints. Interestingly, the mRNA expression of FBLN2 remained low in control fibroblasts until they reached visual confluency at approximately 72h. These increases in mRNA expression resulted in an accumulation of fibulin-2 protein in the cell layer of both control and IPF cells over time as determined by western blot (**Figure 3.3.4.2**).

Fibroblasts grown as a monolayer on culture plastic experience supraphysiological stiffness while likely lacking normal cell-cell and cell-ECM interactions experienced *in vivo*. These can be partially recreated utilising 3D spheroid culture which, although a monoculture, recreates some of the features of a fibrotic focus (Kanda 2015; Jorgenson et al. 2017). Under these conditions with rapid spheroid formation, fibulin-2 was deposited in an extracellular pattern by IPF fibroblasts but not controls. Pre-treatment with TGFβ before spheroid formation was not sufficient to induce extracellular deposition of fibulin-2 by control cells. In IPF spheroids there was significantly more fibulin-2 following TGFβ pre-treatment however there was no difference in FBLN2 mRNA expression (**Figure 3.4.2.2**). Further investigation is required to

determine if this is a result of changing mRNA levels not yet being represented at the protein level or if it is due to reduced fibulin-2 degradation in TGFβ treated cells. Although spheroid culture is likely more representative of the fibrotic focus, it is a rapid monoculture formed within hours of seeding with longer term culture being non-viable (Kanda 2015; Jorgenson et al. 2017). Data from our lab has shown that fibroblasts within spheroids become apoptotic from 48h of culture (Kanda 2015), therefore spheroids in this thesis were collected 24h post seeding. However, it is unclear if this allows sufficient time for the establishment of a representative ECM or if the fibroblast phenotype which is being sampled is mainly associated with spheroid formation.

The deposition of fibulin-2 over time in 2D culture and the depletion of fibulin-2 by siRNA were subsequently used to identify any role it may play in the activation of fibrotic lung fibroblasts.

## 4.11 Fibulin-2 depletion by siRNA

Results in this thesis identify and validate an upregulation of fibulin-2 in fibrotic lung fibroblasts compared to those of controls. To determine if this overexpression plays a role in the fibrotic phenotype, it was necessary to exogenously reduce fibulin-2 expression. As I have demonstrated that fibulin-2 is rapidly deposited into the ECM in vitro, the experimental protocol for siRNA treatment and subsequent experiments required consideration to ensure that downstream rapid culture, such as crowding and spheroid experiments, was deficient in fibulin-2 protein. Knockdown of FBLN2 by siRNA was shown to persist to the 120h timepoint in 2D culture (**Figure 3.3.5.1**), therefore siRNA treatment was performed in proliferating cultures before seeding directly into the relevant experimental conditions.

Fibulin-2 deficient fibrotic fibroblasts, along with control fibroblasts which do not express significant amounts of fibulin-2 at early timepoints, were not impaired in their ability to adhere to serum coated culture plastic, as assessed by DAPI stained nuclear count (**Section 3.3.5**). Similarly, fibulin-2 deficient fibrotic fibroblasts, along with control fibroblasts, formed spheroids which were macroscopically indistinguishable from non-targeting transfected cells. This is in contrast to the impaired spheroid formation by dermal fibroblasts deficient in fibronectin (Salmenperä et al. 2008). Fibulin-2 depletion by siRNA was therefore used to begin to elucidate the role of fibulin-2 in fibroblast activation.

## 4.12 Effect of fibulin-2 expression on collagen I and αSMA

Fibulin-2 has multiple binding partners including competing with LTBP sequestering into the matrix and fibulin-2 deficiency has been shown to be protective in murine models of cardiac

fibrosis through reduced TGFβ activation (H. Zhang et al. 2014; Khan et al. 2016). Therefore, to investigate if increased expression of fibulin-2 contributes to the phenotype of fibrotic lung fibroblasts, collagen I and αSMA expression were assessed in conditions in which fibulin-2 expression varied and following fibulin-2 depletion by siRNA transfection.

In 2D culture of IPF fibroblasts COL1A1 expression increased over time in culture in a manner which correlated with increasing FBLN2 expression (**Appendix 5**). This however did not occur in control cells where COL1A1 expression remained unchanged despite an increase in FBLN2 expression. ACTA2 expression was unchanged in IPF cells with rising FBLN2 expression although this resulted in an accumulation of αSMA protein. In contrast, ACTA2 was rapidly downregulated by control cells after 24h leading to a progressive decrease in αSMA protein. These data suggest that while high fibulin-2 expression may feed forward into the fibrotic phenotype of IPF cells the same is not true in control cells highlighting that fibulin-2, collagen I and αSMA are not co-regulated. The potential mechanisms regulating fibulin-2, collagen I and αSMA expression under these conditions is discussed further in **section 4.13.5** below.

Collagen I expression in IPF cells following siRNA depletion of fibulin-2 was assessed in three culture conditions: 2D proliferating culture, 2D rapid deposition assay and 3D spheroid culture. In 2D culture of IPF cells, the results in this thesis demonstrate that depletion of FBLN2 by siRNA resulted in reduced COL1A1 mRNA however this was not seen at the protein level in the rapid deposition assay. This may represent a limitation of the molecular crowding assay which does not allow for the co-evolution of the ECM and the cell phenotype which is possible in longer 2D cultures. It is also possible that the potentially supraphysiological crowding alters the dynamics of ECM-ECM interactions and disrupts the mechanisms being investigated. Validation of these results by quantifying paired mRNA and protein for both conditions is required. 3D cell culture of spontaneously formed spheroids was therefore used to better recreate the cell-cell and cell-ECM interactions in a more physiologically relevant structure. Under these conditions, spheroids from control and IPF cells deposited collagen I into an extracellular matrix pattern which was quantified by HPLC of hydroxyproline. Fibulin-2 deficient IPF spheroids, while showing a non-significant reduction in COL1A1 expression, had reduced collagen content compared to non-targeting siRNA transfected cells.

ACTA2 expression was also downregulated in FBLN2 deficient IPF fibroblasts in both 2D and 3D culture with a significant decrease in αSMA content of 2D cultured cells. These results suggest that fibulin-2 may contribute to an increase in fibrotic fibroblast activation as measured by collagen and αSMA expression. This data requires verification in further cell

lines along with testing if this effect is sensitive to TGFβ inhibition such as a neutralising antibody in the same way seen in murine cardiac fibroblasts (H. Zhang et al. 2014). To validate these findings, exogenous fibulin-2 or its over-expression would be expected to have pro-fibrotic effects in control cells.

## 4.13 Fibulin-2 regulation by methylation

### 4.13.1 Fibulin-2 methylation by microarray

Fibulin-2 was identified as a gene of interest in this thesis due to its upregulation in pulmonary fibrosis and its potential regulation by gene methylation. Suppression of fibulin-2 expression by promoter hypermethylation has been previously reported in numerous cancers (Dunwell et al. 2009; Hill et al. 2010; Law et al. 2012) however, the role of methylation changes in fibulin-2 upregulation has not been characterised. In our isolated lung fibroblasts, significantly altered methylation ($\Delta\beta \geq 13.6\%$, $p < 0.05$) compared to control was observed in 6 CpG sites (**Section 3.2.3**). One site had decreased methylation in both IPF and SSc whereas a further 5 were increased in IPF only. There was a correlation between methylation and expression levels in 2 CpG sites in analysis including all 18 untreated cell lines; a negative correlation at CpG 4 which is upstream of the transcription start site and a positive correlation at CpG 42 which is within an intragenic CpG island. The negative correlation of CpG 4 with expression and its location near the transcription start site fits the classical model of methylation directly or indirectly blocking the binding of transcription factors. The positive relationship between methylation of CpG 42 and expression of the gene however does not fit this traditional relationship. Methylation of intragenic CpGs has been shown to both positively and negatively correlate to gene expression depending on whether it is within a CpG island (Varley et al. 2013), and to support exon inclusion (Maunakea et al. 2013). Varley et al., correlating methylation to expression across the genome, demonstrated a bias towards negative correlation with CpGs near the transcription start site (whether within a CpG island or not), a bias of positive correlation with intragenic CpGs which are not within CpG islands and a bimodal distribution of both positive and negative correlation with CpGs in intragenic CpG islands. Therefore, due to their locations both the negative and positive correlations with CpGs 4 and 42 respectively could demonstrate a potential regulation of fibulin-2 expression by CpG methylation.

Interestingly, CpG 4 was not annotated to FBLN2 in the resources used for bulk array analysis due to its distance from FBLN2 classifying it as intergenic. CpGs 1-4 were added manually during FBLN2 specific workup and would therefore not be included in most genome wide

analysis studies where methylation was simply linked to a specific gene by annotation, or where intergenic CpGs were explicitly excluded from analysis (such as in Lee et al. 2019). Further annotation of intergenic CpGs to link them to nearby genes would be achievable using their genomic location data and would extend CpG-gene pairs to include local intergenic regions. Alternatively, annotation independent correlation of individual CpG methylation to the expression of all genes on a chromosome or the integration of chromatin structure and binding profiles may identify long range interactions which are missed by simple annotation pairing. This would however be computationally intensive and require a large dataset for any interactions to pass a false discovery correction. Such long-range interactions have been published between the methylation of enhancer and promoter sites of cancer genes in a large panel of tumour cells where distal expression-related methylation sites were more predictive of gene expression than promoter methylation (Aran, Sabato, and Hellman 2013). CpG 4 is within a GeneHancer annotated high-confidence enhancer region containing binding sequences for 76 transcription factors (GH03J013532; Fishilevich et al. 2017), and both CpG 4 and 42 are within regions annotated for histone H3K27Ac marks from the ENCODE project (as displayed on the UCSC genome browser) increasing the confidence for these being regulatory sites where CpG methylation may be contributing to expression regulation.

### 4.13.2 The effect of 5Aza on fibulin-2

To further elucidate the role of CpG methylation in regulating fibulin-2 expression fibroblasts methylation was assessed following treatment with the demethylating agent 5Aza. In cancer cells, 5Aza treatment is sufficient to induce re-expression of fibulin-2 which was suppressed by promoter hypermethylation (Dunwell et al. 2009; Law et al. 2012). We have shown that methylation and expression of other genes known to be regulated by methylation were affected by 5Aza in this array experiment (Evans et al. 2016; I. M. Garner et al. 2013) but there was no difference in expression of fibulin-2 with 5Aza treatment in control or IPF cells and only a small decrease in expression seen in SSc fibroblasts. Across all 18 cell lines no CpGs within FBLN2 demonstrated a change in methylation with 5Aza treatment. However, analysis of those cells previously determined to be stronger responders to 5Aza identified negative correlation at two CpG sites, including CpG 4, where an increase in methylation was associated with a decrease in expression. 4 of these 6 responding cell lines had an increase in methylation with 5Aza treatment. This unexpected change following 5Aza treatment could be through a demethylation related increase in another factor which is in turn increasing

methylation of FBLN2 through mechanisms not susceptible to 5Aza, for example initiating *de novo* methylation. Although increased methylation in response to DMNT inhibition has been characterised in a number of cell lines (Giri and Aittokallio 2019) I have been unable to find any studies detailing the mechanism through which this occurs. Further work will be required to identify which factors are influencing fibulin-2 methylation.

### 4.13.3 Validation of fibulin-2 methylation

53 CpG probes are annotated to FBLN2 after exclusion of those covering SNPs and which are not specific (**Figure 3.2.3.1**), there are however >2,000 CpG dinucleotides in the fibulin-2 gene and the upstream intergenic region. In nasopharyngeal carcinoma, Law et al. (2012) have identified a downregulation of fibulin-2 expression by methylation within the high-content CpG island (HC CGI) at the transcription start site which was susceptible to demethylation by 5Aza. In their study methylation was assessed by bisulfite sequencing of a region within the HC CGI which covered 91 CpGs, including 7 Illumina 450k array probes (CpGs 7-13). These probes in our data did not have significantly altered methylation in fibrotic fibroblasts compared to controls.

Validation of array methylation data and the additional analysis of neighbouring CpG dinucleotides was attempted using bisulfite sanger sequencing (**Section 3.2.6**). Due to the lack of template complexity caused by the conversion of all unmethylated cytosine residues to thymine, sequencing reads degraded rapidly with significant slippage through regions of a repeating base. This could be occurring at the sequencing stage or during PCR amplification. Custom PCR primers were designed and combinations of two forward primers and two reverse primers were trialled for each region. As a result of the poor-quality reads, it was not possible to quantify methylation of CpG 42 in array samples or samples from tissue culture despite amplification of a single band by PCR. Quantification of CpG 4 was possible in most samples and had a strong correlation to array data but further CpGs within the PCR product could not be read.

### 4.13.4 Fibulin-2 methylation in cell culture conditions

Two cell lines were chosen for cell culture experiments which had FBLN2 expression that was representative of expression for control and IPF groups respectively. Methylation of CpG 4 was markedly different in these cell lines with approximately 82% methylation in control cells and 12% in IPF cells (**Figure 3.4.5.1**). Significant differences in FBLN2 expression were seen within each cell line across time in 2D culture, and in 3D culture conditions compared to 2D.

However, these changes in expression were not accompanied by changes in CpG 4 methylation within either cell line. While this suggests that CpG 4 methylation is not directly regulating FBLN2 expression, it supports a model where methylation of this enhancer region influences FBLN2 expression and altered methylation here results in expression differences in fibroblasts from different donors under identical culture conditions, such as those used for the microarray experiment. Further factors must therefore be regulating the relative expression levels of FBLN2 in identical cells under different culture conditions.

### 4.13.5 Other factors which may be regulating FBLN2 expression

In tissue culture experiments, expression of FBLN2 and methylation of CpG 4 were evaluated in three culture conditions: non-confluent, proliferating, 2D cultures on plastic; confluent cell monolayer after 120h growth on culture plastic; and 3D culture of fibroblast spheroids spontaneously formed in non-adherent culture. Fibulin-2 was greatly upregulated in IPF fibroblasts compared to controls but within each cell line expression varied between culture conditions by up to 14.5-fold (**Figure 3.4.5.1**).

While hypomethylation of the enhancer region in which CpG 4 is located may give rise to the increased expression potential of FBLN2 in fibrotic lung fibroblasts compared to controls, the variation in expression of fibulin-2 within the same cells in different cell culture conditions was not accompanied by a change in CpG 4 methylation (**Figure 3.4.5.1**). Expression of fibulin-2 must therefore also be regulated through other mechanisms in differing microenvironmental conditions.

The accumulation and maturation of the extracellular matrix and the increase in cell number over time in 2D culture, along with the compact 3D nature of the spheroid model may enhance the bioavailability of endogenously produced cytokines which have been shown to upregulate fibulin-2, such as TGFβ and angiotensin II (H. Zhang et al. 2014). The loss of αSMA expression in control cells over time in culture, which is the opposite to fibulin-2 expression, however suggests that there is not an increase in TGFβ signalling.

Fibulin-2 has been further demonstrated to be upregulated by simvastatin treatment in human coronary artery smooth muscle cells through inhibition of the RhoA/ROCK pathway (Serra et al. 2015). The authors showed that direct ROCK inhibition increased fibulin-2 expression while its direct activation reduced expression. The importance of the ROCK pathway in mechanosensing has been characterised with ROCK dependant upregulation of αSMA on stiff substrates (Oh et al. 2018). It would therefore be expected that ROCK activity

could be regulating fibulin-2 expression in varied culture conditions. In 2D culture, sub-confluent cells sense the stiffness of the substrate, and would therefore be expected to have high ROCK activation, but this activation may be lost when confluentency results in decreased mechanosensing (Yeung et al. 2005). 3D culture is markedly less stiff than culture plastic (~400Pa and ~3GPa respectively; Stewart et al. 2019) and would be associated with lowest ROCK activation. The expression of αSMA within control cells in 2D follows the expected pattern with lower expression once conditions reach the 'less stiff' confluent stage (**Figure 3.3.7.1**). Fibulin-2 is upregulated in later 2D culture and 3D culture, conditions that are associated with decreased stiffness and therefore lower ROCK activity; this is in keeping with the findings of Serra et al. (2015). The RhoA/ROCK axis may therefore have a role in the varied fibulin-2 expression seen in within each cell line in different culture condition and should be investigated further.

Fibulin-2 has also recently been identified as a potential NOTCH signalling effector gene, although the intermediates of this axis remain to be elucidated (Torregrosa-Carrión et al. 2019). The NOTCH ligands JAG1 and DLL1 were detected in array data, though not differentially expressed, suggesting they are expressed by fibroblasts from both diseased and control lung. Signalling of these ligands via the NOTCH pathway is dependent on cell-cell contact and the activity of NOTCH signalling therefore increases with cell density (Matsuno et al. 2018). It could be hypothesised that NOTCH signalling would be upregulated in confluent fibroblast monolayers and in 3D culture, compared to low density 2D culture, and that this could upregulate fibulin-2 mRNA expression in these conditions. This is particularly supported by the rapid upregulation of fibulin-2 mRNA seen in control cells from the point at which they become confluent (72h post seeding, **Figure 3.3.4.1**). αSMA however has also been shown to be upregulated by NOTCH signalling in lung fibroblasts (T. Liu et al. 2009) and is lost in control fibroblasts in these conditions.

The contributions of these pathways to fibulin-2 expression and the often-contradictory expression of αSMA I have demonstrated in primary lung fibroblasts could be elucidated utilising small molecule inhibitors and activators in the culture systems established in this thesis.

## 4.14 Summary and future directions

In this thesis expression and methylation array data for cultured human lung fibroblasts from donors with IPF and SSc related PF were compared to that of controls to identify a gene of further study which has altered expression in PF and may be regulated by gene methylation.

Data from the Illumina 450K methylation array has been extensively reported in the literature and although it is a significant improvement on its predecessor, the 27k array, which has been previously utilised in the study of pulmonary fibrosis it still only covers approximately 2% of the methylome with a bias towards CpGs located near gene promoters. Data in this thesis has shown that the methylation of a CpG (CpG 4) within an intergenic enhancer region correlates with the expression of fibulin-2. Expansion of methylation data to include more CpG sites would be valuable and could be achieved using whole genome or reduced representation bisulfite sequencing. Alternatively, the 450k array has been succeeded by the Illumina MethylationEPIC array which contains 853,307 CpGs. This array includes 91% of 450K probes with the additional CpGs predominantly located in otherwise previously unexplored regions outside of CGIs and their shores and shelves, increasing the coverage of intergenic enhancer regions (Moran, Arribas, and Esteller 2016). While assaying the methylation status of more of the genome is itself worthwhile, it would be of particular interest to combine methylation data with annotation of long-range chromosome interaction data such as that collated within the ENCODE project (Dunham et al. 2012) to further extend methylation-gene pairing beyond the relatively simple genetic location annotation used in this and many other studies. This is particularly noteworthy as CpG 4 was only identified by manual inclusion with fibulin-2 data.

This thesis has demonstrated a correlation between methylation of CpG 4 and the expression of fibulin-2 in cells under identical conditions. However, fibulin-2 expression varies through cell culture conditions with no change in CpG 4 methylation. The role that methylation of the region containing CpG 4 may be playing in regulating fibulin-2 expression therefore requires further study. Initially, this would require complete bisulfite sequencing of this region to determine its full methylation status and potentially its targeted methylation (McDonald et al. 2016; Vojta et al. 2016). Subsequently, the effect that methylation is having with the binding of transcription factors and methyl-binding complexes should be determined.

The variability in fibulin-2 expression in cell culture conditions was not accompanied by a change in CpG 4 methylation, while supporting the enhancer role of this region, other mechanisms must be regulating fibulin-2 expression. These could include TGFβ, RhoA/ROCK (Serra et al. 2015) and NOTCH (Torregrosa-Carrión et al. 2019) mediated pathways which should be interrogated through small molecule agonist and antagonist studies in the culture systems utilised within this thesis.

The enhancer region containing CpG 4 is annotated to influence the expression of other genes including HDAC11, which although detected in most samples was not differentially expressed in IPF or SSc derived fibroblasts compared to controls. It was also annotated to influence WNT7A, which was not detected in any samples on the array, and LINC00620, which is not covered by a probe on the expression array. Quantification of these genes by RT-qPCR could further elucidate the role that methylation of this enhancer region is playing in the fibrotic lung fibroblast phenotype.

Fibulin-2, an ECM scaffold glycoprotein, was identified as upregulated in fibrotic lung fibroblasts by microarray and subsequently shown to be upregulated at the protein level in fibrotic human lung tissue and in cultured IPF fibroblasts in both 2D and 3D culture. In IPF derived fibroblasts, COL1A1 expression correlated with FBLN2 expression changes over time and FBLN2 deficiency through siRNA transfection resulted in reduced COL1A1 expression in 2D culture and reduced collagen content of 3D spheroids. Although αSMA expression did not vary with fiblin-2 expression in different culture conditions it was also reduced in FBLN2 deficient IPF cells in both 2D and 3D culture. Published data suggest that FBLN2 deficiency protects against cardiac fibrosis through TGFβ mediated mechanisms. The bioavailability of TGFβ in FBLN2 deficient cells should therefore be assessed. Liberating TGFβ from spheroids will however result in its activation so this would be best assessed indirectly though the quantification of downstream signalling such as SMAD phosphorylation.

Primarily, these results should be reproduced in cells from a wider cohort of donors and extended to include other measures of fibroblast biology such as migration as fibulin-2 deficiency has been shown to impair the migratory capacity of lung tumour cells (Baird et al. 2013). The contribution of fibulin-2 to TGFβ activation may also be affected by the stiffness of the growth substrate or ECM, this should be assessed by culture in other systems including matrices of varying stiffness. Lentiviral based over expression of fibulin-2 in control cells would also demonstrate if fibulin-2 overexpression is sufficient to induce a more fibrotic phenotype in otherwise normal cells.

Mice deficient in fibulin-2 have been characterised in the literature and are protected from cardiac fibrosis (H. Zhang et al. 2014; Khan et al. 2016). Fibulin-2 has also been shown to be upregulated in the bleomycin mouse model of lung fibrosis (Schiller et al. 2015). I am not however aware of any studies of PF in fibulin-2 deficient animals. I believe preliminary data in this thesis showing antifibrotic effects of fibuln-2 knockdown, once validated in further

cells lines, support performing the bleomycin model in *Fbln2*$^{-/-}$ animals to investigate if they are protected from PF.

In conclusion, fibulin-2 was identified as a gene which is overexpressed in fibroblasts and tissue from IPF and SSc lungs. This overexpression may be due to enhancer hypomethylation though other mechanisms regulating fibulin-2 expression under varying culture conditions remain to be elucidated. Depletion of fibulin-2 by siRNA resulted in downregulation of collagen I and αSMA in IPF fibroblasts suggesting it may play a role in sustaining the fibrotic phenotype. Further research into the mechanisms of fibulin-2 regulation and its role in profibrotic signalling is required. This may yield targets of therapeutic potential in the treatment of pulmonary fibrosis.

# 5 References


Alcendor, Donald J., Susan Knobel, Prashant Desai, Wen Qui Zhu, and Gary S. Hayward. 2011. "KSHV Regulation of Fibulin-2 in Kaposi's Sarcoma: Implications for Tumorigenesis." *The American Journal of Pathology* 179 (3): 1443–54. https://doi.org/10.1016/j.ajpath.2011.05.024.

Allen, Richard J., Joanne Porte, Rebecca Braybrooke, Carlos Flores, Tasha E. Fingerlin, Justin M. Oldham, Beatriz Guillen-Guio, et al. 2017. "Genetic Variants Associated with Susceptibility to Idiopathic Pulmonary Fibrosis in People of European Ancestry: A Genome-Wide Association Study." *The Lancet. Respiratory Medicine* 5 (11): 869–80. https://doi.org/10.1016/S2213-2600(17)30387-9.

Altorok, Nezam, Pei Suen Tsou, Patrick Coit, Dinesh Khanna, and Amr H. Sawalha. 2015. "Genome-Wide DNA Methylation Analysis in Dermal Fibroblasts from Patients with Diffuse and Limited Systemic Sclerosis Reveals Common and Subset-Specific DNA Methylation Aberrancies." *Annals of the Rheumatic Diseases* 74 (8): 1612–20. https://doi.org/10.1136/annrheumdis-2014-205303.

Aluwihare, Poshala, Zhenyu Mu, Zhicheng Zhao, Dawen Yu, Paul H. Weinreb, Gerald S. Horan, Shelia M. Violette, and John S. Munger. 2009. "Mice That Lack Activity of Alphavbeta6- and Alphavbeta8-Integrins Reproduce the Abnormalities of Tgfb1- and Tgfb3-Null Mice." *Journal of Cell Science* 122 (Pt 2): 227–32. https://doi.org/10.1242/jcs.035246.

Angiolilli, Chiara, Wioleta Marut, Maarten van der Kroef, Eleni Chouri, Kris A. Reedquist, and Timothy R D J Radstake. 2018. "New Insights into the Genetics and Epigenetics of Systemic Sclerosis." *Nature Reviews. Rheumatology* 14 (11): 657–73. https://doi.org/10.1038/s41584-018-0099-0.

Aran, Dvir, Sivan Sabato, and Asaf Hellman. 2013. "DNA Methylation of Distal Regulatory Sites Characterizes Dysregulation of Cancer Genes." *Genome Biology* 14 (3): R21. https://doi.org/10.1186/gb-2013-14-3-r21.

Arloth, Janine, Daniel M. Bader, Simone Röh, and Andre Altmann. 2015. "Re-Annotator: Annotation Pipeline for Microarray Probe Sequences." *PLoS ONE* 10 (10): 1–13. https://doi.org/10.1371/journal.pone.0139516.

Assoian, R. K., and M. B. Sporn. 1986. "Type β Transforming Growth Factor in Human Platelets: Release during Platelet Degranulation and Action on Vascular Smooth Muscle Cells." *Journal of Cell Biology* 102 (4): 1217–23. https://doi.org/10.1083/jcb.102.4.1217.

Aumiller, Verena, Benjamin Strobel, Merrit Romeike, Michael Schuler, Birgit E. Stierstorfer, and Sebastian Kreuz. 2017. "Comparative Analysis of Lysyl Oxidase (like) Family Members in Pulmonary Fibrosis." *Scientific Reports* 7 (1): 1–13. https://doi.org/10.1038/s41598-017-00270-0.

Avsar, Mukaddes, Makbule Tambas, Zubeyde Yalniz, Demet Akdeniz, Seref Bugra Tuncer, Seda Kilic, Ozge Sukruoglu Erdogan, et al. 2019. "The Expression Level of Fibulin-2 in the Circulating RNA (CtRNA) of Epithelial Tumor Cells of Peripheral Blood and Tumor Tissue of Patients with Metastatic Lung Cancer." *Molecular Biology Reports* 46 (4): 4001–8. https://doi.org/10.1007/s11033-019-04846-z.

Babendreyer, A., Lisa Molls, Indra M. Simons, Daniela Dreymueller, Kristina Biller, Holger Jahr, B. Denecke, et al. 2019. "The Metalloproteinase ADAM15 Is Upregulated by Shear Stress and Promotes Survival of Endothelial Cells." *Journal of Molecular and Cellular Cardiology* 134 (July): 51–61. https://doi.org/10.1016/j.yjmcc.2019.06.017.

Baird, Brandi N., Mark J. Schliekelman, Young-Ho Ahn, Yulong Chen, Jonathon D. Roybal, Bartley J. Gill, Dhruva K. Mishra, et al. 2013. "Fibulin-2 Is a Driver of Malignant Progression in Lung Adenocarcinoma." Edited by Alan P. Fields. *PLoS ONE* 8 (6): e67054. https://doi.org/10.1371/journal.pone.0067054.

Barry-Hamilton, Vivian, Rhyannon Spangler, Derek Marshall, Scott McCauley, Hector M. Rodriguez, Miho Oyasu, Amanda Mikels, et al. 2010. "Allosteric Inhibition of Lysyl Oxidase-like-2 Impedes the Development of a Pathologic Microenvironment." *Nature Medicine* 16 (9): 1009–17.

https://doi.org/10.1038/nm.2208.

Bartis, Domokos, Nikica Mise, Rahul Y Mahida, Oliver Eickelberg, and David R Thickett. 2014. "Epithelial–Mesenchymal Transition in Lung Development and Disease: Does It Exist and Is It Important?" *Thorax* 69 (8): 760–65. https://doi.org/10.1136/thoraxjnl-2013-204608.

Bateman, E. D., M. Turner-Warwick, and B. C. Adelmann-Grill. 1981. "Immunohistochemical Study of Collagen Types in Human Foetal Lung and Fibrotic Lung Disease." *Thorax* 36 (9): 645–53. https://doi.org/10.1136/thx.36.9.645.

Baumgartner, Kathy B, Jonathan M Samet, David B Coultas, Christine A Stidley, William C Hunt, Thomas V Colby, and James A Waldron. 2000. "Occupational and Environmental Risk Factors for IPF Baumgartner et Al Occupational and Environmental Risk Factors for Idiopathic Pulmonary Fibrosis: A Multicenter Case-Control Study." *American Journal of Epidemiology* 152 (4): 307–15. http://aje.oxfordjournals.org/.

Bell, Rachel E., Tamar Golan, Danna Sheinboim, Hagar Malcov, David Amar, Avi Salamon, Tamar Liron, et al. 2016. "Enhancer Methylation Dynamics Contribute to Cancer Plasticity and Patient Mortality." *Genome Research* 26 (5): 601–11. https://doi.org/10.1101/gr.197194.115.

Bibikova, Marina, Bret Barnes, Chan Tsan, Vincent Ho, Brandy Klotzle, Jennie M. Le, David Delano, et al. 2011. "High Density DNA Methylation Array with Single CpG Site Resolution." *Genomics* 98 (4): 288–95. https://doi.org/10.1016/j.ygeno.2011.07.007.

Bibikova, Marina, Jennie Le, Bret Barnes, Shadi Saedinia-Melnyk, Lixin Zhou, Richard Shen, and Kevin L Gunderson. 2009. "Genome-Wide DNA Methylation Profiling Using Infinium ® Assay." *Epigenomics* 1 (1): 177–200. https://doi.org/10.2217/epi.09.14.

Blakytny, Robert, Anna Ludlow, Gail E M Martin, Grenham Ireland, Leif R Lund, Mark W J Ferguson, and Georg Brunner. 2004. "Latent TGF- b 1 Activation by Platelets" 76 (September 2003): 67–76. https://doi.org/10.1002/jcp.10454.

Blanchette, F., R. Day, W. Dong, M. H. Laprise, and C. M. Dubois. 1997. "TGFβ1 Regulates Gene Expression of Its Own Converting Enzyme Furin." *Journal of Clinical Investigation* 99 (8): 1974–83. https://doi.org/10.1172/JCI119365.

Böhm, Beate B., Andrea Schirner, and Harald Burkhardt. 2009. "ADAM15 Modulates Outside-in Signalling in Chondrocyte-Matrix Interactions." *Journal of Cellular and Molecular Medicine* 13 (8 B): 2634–44. https://doi.org/10.1111/j.1582-4934.2008.00490.x.

Bonnans, Caroline, Jonathan Chou, and Zena Werb. 2014. "Remodelling the Extracellular Matrix in Development and Disease." *Nature Reviews Molecular Cell Biology* 15 (12): 786–801. https://doi.org/10.1038/nrm3904.

Booth, Adam J., Ryan Hadley, Ashley M. Cornett, Alyssa A. Dreffs, Stephanie A. Matthes, Jessica L. Tsui, Kevin Weiss, et al. 2012. "Acellular Normal and Fibrotic Human Lung Matrices as a Culture System for In Vitro Investigation." *American Journal of Respiratory and Critical Care Medicine* 186 (9): 866–76. https://doi.org/10.1164/rccm.201204-0754OC.

Brazel, D, I Oberbäumer, H Dieringer, W Babel, R W Glanville, R Deutzmann, and K Kühn. 1987. "Completion of the Amino Acid Sequence of the Alpha 1 Chain of Human Basement Membrane Collagen (Type IV) Reveals 21 Non-Triplet Interruptions Located within the Collagenous Domain." *European Journal of Biochemistry* 168 (3): 529–36. https://doi.org/10.1111/j.1432-1033.1987.tb13450.x.

Burgstaller, Gerald, Bettina Oehrle, Michael Gerckens, Eric S. White, Herbert B. Schiller, and Oliver Eickelberg. 2017. "The Instructive Extracellular Matrix of the Lung: Basic Composition and Alterations in Chronic Lung Disease." *The European Respiratory Journal* 50 (1): 1601805. https://doi.org/10.1183/13993003.01805-2016.

Callahan, Catherine L., Matthew R. Bonner, Jing Nie, Daikwon Han, Youjin Wang, Meng Hua Tao, Peter G. Shields, et al. 2018. "Lifetime Exposure to Ambient Air Pollution and Methylation of Tumor Suppressor Genes in Breast Tumors." *Environmental Research* 161 (November 2017): 418–24. https://doi.org/10.1016/j.envres.2017.11.040.

Campa, Juan S., Robin J. McAnulty, and Geoffrey J. Laurent. 1990. "Application of High-Pressure Liquid

Chromatography to Studies of Collagen Production by Isolated Cells in Culture." *Analytical Biochemistry* 186 (2): 257–63. https://doi.org/10.1016/0003-2697(90)90076-L.

Cangemi, Claudia, Maria Lyck Hansen, William Scott Argraves, and Lars Melholt Rasmussen. 2014. *Fibulins and Their Role in Cardiovascular Biology and Disease*. *Advances in Clinical Chemistry*. 1st ed. Vol. 67. Elsevier Inc. https://doi.org/10.1016/bs.acc.2014.09.008.

Canty, Elizabeth G., and Karl E. Kadler. 2005. "Procollagen Trafficking, Processing and Fibrillogenesis." *Journal of Cell Science* 118 (Pt 7): 1341–53. https://doi.org/10.1242/jcs.01731.

Cerone, Maria Antonietta, Darren J. Burgess, Cristina Naceur-Lombardelli, Christopher J. Lord, and Alan Ashworth. 2011. "High-Throughput RNAi Screening Reveals Novel Regulators of Telomerase." *Cancer Research* 71 (9): 3328–40. https://doi.org/10.1158/0008-5472.CAN-10-2734.

Cesana, Marcella, Davide Cacchiarelli, Ivano Legnini, Tiziana Santini, Olga Sthandier, Mauro Chinappi, Anna Tramontano, and Irene Bozzoni. 2011. "A Long Noncoding RNA Controls Muscle Differentiation by Functioning as a Competing Endogenous RNA." *Cell* 147 (2): 358–69. https://doi.org/10.1016/j.cell.2011.09.028.

Chen, Qiuyun, Teng Zhang, Joseph F. Roshetsky, Zhufeng Ouyang, Jeroen Essers, Chun Fan, Qing Wang, Aleksander Hinek, Edward F. Plow, and Paul E. Dıcorleto. 2009. "Fibulin-4 Regulates Expression of the Tropoelastin Gene and Consequent Elastic-Fibre Formation by Human Fibroblasts." *Biochemical Journal* 423 (1): 79–89. https://doi.org/10.1042/BJ20090993.

Chen, Z. C C, Y. YX Peng, M. Raghunath, CZC Z C Chen, Y. YX Peng, ZB Wang, PV Fish, et al. 2009. "The Scar-in-a-Jar: Studying Potential Antifibrotic Compounds from the Epigenetic to Extracellular Level in a Single Well." *British Journal of Pharmacology* 158 (5): 1196–1209. https://doi.org/10.1111/j.1476-5381.2009.00387.x.

Chifflot, Hélène, Bruno Fautrel, Christelle Sordet, Emmanuel Chatelus, and Jean Sibilia. 2008. "Incidence and Prevalence of Systemic Sclerosis: A Systematic Literature Review." *Seminars in Arthritis and Rheumatism* 37 (4): 223–35. https://doi.org/10.1016/j.semarthrit.2007.05.003.

Chowdhury, Arpita, Lisa Hasselbach, Frank Echtermeyer, Nidhi Jyotsana, Gregor Theilmeier, and Christine Herzog. 2017. "Fibulin-6 Regulates pro-Fibrotic TGF-β Responses in Neonatal Mouse Ventricular Cardiac Fibroblasts." *Scientific Reports* 7: 1–13. https://doi.org/10.1038/srep42725.

Costanza, Brunella, Ijeoma Adaku Umelo, Justine Bellier, Vincent Castronovo, and Andrei Turtoi. 2017. "Stromal Modulators of TGF-β in Cancer." *Journal of Clinical Medicine* 6 (1): 7. https://doi.org/10.3390/jcm6010007.

Coward, William R., Carol A. Feghali-Bostwick, Gisli Jenkins, Alan J. Knox, and Linhua Pang. 2014. "A Central Role for G9a and EZH2 in the Epigenetic Silencing of Cyclooxygenase-2 in Idiopathic Pulmonary Fibrosis." *FASEB Journal : Official Publication of the Federation of American Societies for Experimental Biology* 28 (7): 3183–96. https://doi.org/10.1096/fj.13-241760.

Coward, William R., Keiria Watts, Carol A. Feghali-Bostwick, Alan Knox, and Linhua Pang. 2009. "Defective Histone Acetylation Is Responsible for the Diminished Expression of Cyclooxygenase 2 in Idiopathic Pulmonary Fibrosis." *Molecular and Cellular Biology* 29 (15): 4325–39. https://doi.org/10.1128/MCB.01776-08.

Crawford, Susan E, Veronica Stellmach, Joanne E Murphy-ullrich, Solange M F Ribeiro, Jack Lawler, Richard O Hynes, and Gregory P Boivin. 1998. "Thrombospondin-1 Is a Major Activator of TGF- 1 In Vivo" 93: 1159–70.

Crestani, Bruno, Sylvain Marchand-Adam, Christophe Quesnel, Laurent Plantier, Keren Borensztajn, Joelle Marchal, Arnaud Mailleux, Paul Soler, and Monique Dehoux. 2012. "Hepatocyte Growth Factor and Lung Fibrosis." *Proceedings of the American Thoracic Society* 9 (3): 158–63. https://doi.org/10.1513/pats.201202-018AW.

Crowe, Maria J., Thomas Doetschman, and David G. Greenhalgh. 2000. "Delayed Wound Healing in Immunodeficient TGF-B1 Knockout Mice." *Journal of Investigative Dermatology* 115 (1): 3–11. https://doi.org/10.1046/j.1523-1747.2000.00010.x.

Cui, Lu, Shih Yu Chen, Tristan Lerbs, Jin Wook Lee, Pablo Domizi, Sydney Gordon, Yong hun Kim, Garry

Nolan, Paola Betancur, and Gerlinde Wernig. 2020. “Activation of JUN in Fibroblasts Promotes Pro-Fibrotic Programme and Modulates Protective Immunity.” *Nature Communications* 11 (1). https://doi.org/10.1038/s41467-020-16466-4.

Dabovic, Branka, Ian B. Robertson, Lior Zilberberg, Melinda Vassallo, Elaine C. Davis, and Daniel B. Rifkin. 2015. “Function of Latent TGFβ Binding Protein 4 and Fibulin 5 in Elastogenesis and Lung Development.” *Journal of Cellular Physiology* 230 (1): 226–36. https://doi.org/10.1002/jcp.24704.

Dakhlallah, Duaa, Kara Batte, Yijie Wang, Carmen Z. Cantemir-Stone, Pearlly Yan, Gerard Nuovo, Adel Mikhail, et al. 2013. “Epigenetic Regulation of MiR-17~92 Contributes to the Pathogenesis of Pulmonary Fibrosis.” *American Journal of Respiratory and Critical Care Medicine* 187 (4): 397–405. https://doi.org/10.1164/rccm.201205-0888OC.

Danan-Gotthold, Miri, Regina Golan-Gerstl, Eli Eisenberg, Keren Meir, Rotem Karni, and Erez Y. Levanon. 2015. “Identification of Recurrent Regulated Alternative Splicing Events across Human Solid Tumors.” *Nucleic Acids Research* 43 (10): 5130–44. https://doi.org/10.1093/nar/gkv210.

Dayer, Cynthia, and Ivan Stamenkovic. 2015. “Recruitment of Matrix Metalloproteinase-9 (MMP-9) to the Fibroblast Cell Surface by Lysyl Hydroxylase 3 (LH3) Triggers Transforming Growth Factor-β (TGF-β) Activation and Fibroblast Differentiation.” *Journal of Biological Chemistry* 290 (22): 13763–78. https://doi.org/10.1074/jbc.M114.622274.

Dedeurwaerder, Sarah, Matthieu Defrance, Martin Bizet, Emilie Calonne, Gianluca Bontempi, and François Fuks. 2013. “A Comprehensive Overview of Infinium Human Methylation450 Data Processing.” *Briefings in Bioinformatics* 15 (6): 929–41. https://doi.org/10.1093/bib/bbt054.

Dodi, Amos E., Iyabode O. Ajayi, Christine Chang, Meghan Beard, Shanna L. Ashley, Steven K. Huang, Victor J. Thannickal, Daniel J. Tschumperlin, Thomas H. Sisson, and Jeffrey C. Horowitz. 2018. “Regulation of Fibroblast Fas Expression by Soluble and Mechanical Pro-Fibrotic Stimuli.” *Respiratory Research* 19 (1): 1–12. https://doi.org/10.1186/s12931-018-0801-4.

Domene, Carmen, Christian Jorgensen, and Sumra Wajid Abbasi. 2016. “A Perspective on Structural and Computational Work on Collagen.” *Physical Chemistry Chemical Physics : PCCP* 18 (36): 24802–11. https://doi.org/10.1039/c6cp03403a.

Dong, Dan Dan, Hui Zhou, and Gao Li. 2015. “ADAM15 Targets MMP9 Activity to Promote Lung Cancer Cell Invasion.” *Oncology Reports* 34 (5): 2451–60. https://doi.org/10.3892/or.2015.4203.

Doyle, Jefferson J., Elizabeth E. Gerber, and Harry C. Dietz. 2012. “Matrix-Dependent Perturbation of TGFβ Signaling and Disease.” *FEBS Letters* 586 (14): 2003–15. https://doi.org/10.1016/j.febslet.2012.05.027.

Du, Pan, Warren A. Kibbe, and Simon M. Lin. 2008. “Lumi: A Pipeline for Processing Illumina Microarray.” *Bioinformatics* 24 (13): 1547–48. https://doi.org/10.1093/bioinformatics/btn224.

Dugina, V., L. Fontao, C. Chaponnier, J. Vasiliev, and G. Gabbiani. 2001. “Focal Adhesion Features during Myofibroblastic Differentiation Are Controlled by Intracellular and Extracellular Factors.” *Journal of Cell Science* 114 (18): 3285–96.

Dunham, Ian, Anshul Kundaje, Shelley F. Aldred, Patrick J. Collins, Carrie A. Davis, Francis Doyle, Charles B. Epstein, et al. 2012. “An Integrated Encyclopedia of DNA Elements in the Human Genome.” *Nature* 489 (7414): 57–74. https://doi.org/10.1038/nature11247.

Dunwell, Thomas L., Luke B. Hesson, Tatiana Pavlova, Veronika Zabarovska, Vladimir Kashuba, Daniel Catchpoole, Raffaella Chiaramonte, et al. 2009. “Epigenetic Analysis of Childhood Acute Lymphoblastic Leukemia.” *Epigenetics* 4 (3): 185–93. https://doi.org/10.4161/epi.4.3.8752.

Eden, Eran, Roy Navon, Israel Steinfeld, Doron Lipson, and Zohar Yakhini. 2009. “GOrilla: A Tool for Discovery and Visualization of Enriched GO Terms in Ranked Gene Lists.” *BMC Bioinformatics* 10: 1–7. https://doi.org/10.1186/1471-2105-10-48.

El-Hallous, Ehab, Takako Sasaki, Dirk Hubmacher, Melkamu Getie, Kerstin Tiedemann, Jürgen Brinckmann, Boris Bätge, Elaine C. Davis, and Dieter P. Reinhardt. 2007. “Fibrillin-1 Interactions with Fibulins Depend on the First Hybrid Domain and Provide an Adaptor Function to Tropoelastin.” *The Journal of Biological Chemistry* 282 (12): 8935–46.

https://doi.org/10.1074/jbc.M608204200.

Evans, Iona C, Josephine L Barnes, Ian M Garner, David R Pearce, Toby M Maher, Xu Shiwen, Elisabetta A Renzoni, et al. 2016. “Epigenetic Regulation of Cyclooxygenase-2 by Methylation of C8orf4 in Pulmonary Fibrosis.” *Clinical Science (London, England : 1979)* 130 (8): 575–86. https://doi.org/10.1042/CS20150697.

Falke, Lucas L., Shima Gholizadeh, Roel Goldschmeding, Robbert J. Kok, and Tri Q. Nguyen. 2015. “Diverse Origins of the Myofibroblast-Implications for Kidney Fibrosis.” *Nature Reviews Nephrology* 11 (4): 233–44. https://doi.org/10.1038/nrneph.2014.246.

Farina, Antonella, Mara Cirone, Michael York, Stefania Lenna, Cristina Padilla, Sarah McLaughlin, Alberto Faggioni, Robert Lafyatis, Maria Trojanowska, and Giuseppina a Farina. 2014. “Epstein-Barr Virus Infection Induces Aberrant TLR Activation Pathway and Fibroblast-Myofibroblast Conversion in Scleroderma.” *The Journal of Investigative Dermatology* 134 (4): 954–64. https://doi.org/10.1038/jid.2013.423.

Fässler, R, T Sasaki, R Timpl, M L Chu, and S Werner. 1996. “Differential Regulation of Fibulin, Tenascin-C, and Nidogen Expression during Wound Healing of Normal and Glucocorticoid-Treated Mice.” *Exp Cell Res* 222 (1): 111–16. https://doi.org/10.1006/excr.1996.0014.

Feghali-Bostwick, Carol, Thomas A Medsger, and Timothy M Wright. 2003. “Analysis of Systemic Sclerosis in Twins Reveals Low Concordance for Disease and High Concordance for the Presence of Antinuclear Antibodies.” *Arthritis and Rheumatism* 48 (7): 1956–63. https://doi.org/10.1002/art.11173.

Feinberg, Andrew P., and Bert Vogelstein. 1983. “Hypomethylation Distinguishes Genes of Some Human Cancers from Their Normal Counterparts.” *Nature* 301 (5895): 89–92. https://doi.org/10.1038/301089a0.

Feitosa, Natália Martins, Jinli Zhang, Thomas J. Carney, Manuel Metzger, Vladimir Korzh, Wilhelm Bloch, and Matthias Hammerschmidt. 2012. “Hemicentin 2 and Fibulin 1 Are Required for Epidermal-Dermal Junction Formation and Fin Mesenchymal Cell Migration during Zebrafish Development.” *Developmental Biology* 369 (2): 235–48. https://doi.org/10.1016/j.ydbio.2012.06.023.

Fernández Pérez, Evans R., Craig E. Daniels, Darrell R. Schroeder, Jennifer St. Sauver, Thomas E. Hartman, Brian J. Bartholmai, Eunhee S. Yi, and Jay H. Ryu. 2010. “Incidence, Prevalence, and Clinical Course of Idiopathic Pulmonary Fibrosis a Population-Based Study.” *Chest* 137 (1): 129–37. https://doi.org/10.1378/chest.09-1002.

Fingerlin, Tasha E., Elissa Murphy, Weiming Zhang, Anna L. Peljto, Kevin K. Brown, Mark P. Steele, James E. Loyd, et al. 2013. “Genome-Wide Association Study Identifies Multiple Susceptibility Loci for Pulmonary Fibrosis.” *Nature Genetics* 45 (6): 613–20. https://doi.org/10.1038/ng.2609.

Fiore, Vincent F, Simon S Wong, Coleen Tran, Chunting Tan, Wenwei Xu, Todd Sulchek, Eric S White, James S Hagood, and Thomas H Barker. 2018. “Avβ3 Integrin Drives Fibroblast Contraction and Strain Stiffening of Soft Provisional Matrix during Progressive Fibrosis.” *JCI Insight* 3 (20). https://doi.org/10.1172/jci.insight.97597.

Fishilevich, Simon, Ron Nudel, Noa Rappaport, Rotem Hadar, Inbar Plaschkes, Tsippi Iny Stein, Naomi Rosen, et al. 2017. “GeneHancer: Genome-Wide Integration of Enhancers and Target Genes in GeneCards.” *Database : The Journal of Biological Databases and Curation* 2017 (January): 1–17. https://doi.org/10.1093/database/bax028.

Flynt, Alex S., and Eric C. Lai. 2008. “Biological Principles of MicroRNA-Mediated Regulation: Shared Themes amid Diversity.” *Nature Reviews Genetics* 9 (11): 831–42. https://doi.org/10.1038/nrg2455.

Fontanil, Tania, Saúl Álvarez-Teijeiro, M. Ángeles Villaronga, Yamina Mohamedi, Laura Solares, Angela Moncada-Pazos, José A. Vega, et al. 2017. “Cleavage of Fibulin-2 by the Aggrecanases ADAMTS-4 and ADAMTS-5 Contributes to the Tumorigenic Potential of Breast Cancer Cells.” *Oncotarget* 8 (8): 13716–29. https://doi.org/10.18632/oncotarget.14627.

Fontanil, Tania, Susana Rúa, María Llamazares, Angela Moncada-Pazos, Pedro M Quirós, Olivia García-

Suárez, Jose A. Vega, et al. 2014. “Interaction between the ADAMTS-12 Metalloprotease and Fibulin-2 Induces Tumor-Suppressive Effects in Breast Cancer Cells.” *Oncotarget* 5 (5): 1253–64. https://doi.org/10.18632/oncotarget.1690.

Frantz, Christian, Kathleen M Stewart, and Valerie M Weaver. 2010. “The Extracellular Matrix at a Glance.” *Journal of Cell Science* 123: 4195–4200. https://doi.org/10.1242/jcs.023820.

Fried, Dorothee, Beate B. Böhm, Kristin Krause, and Harald Burkhardt. 2012. “ADAM15 Protein Amplifies Focal Adhesion Kinase Phosphorylation under Genotoxic Stress Conditions.” *Journal of Biological Chemistry* 287 (25): 21214–23. https://doi.org/10.1074/jbc.M112.347120.

Furukawa, Hiroshi, Shomi Oka, Aya Kawasaki, Kota Shimada, Shoji Sugii, Takashi Matsushita, Atsushi Hashimoto, et al. 2016. “Human Leukocyte Antigen and Systemic Sclerosis in Japanese: The Sign of the Four Independent Protective Alleles, DRB1 13:02, DRB1 14:06, DQB1 03:01, and DPB1 02:01.” *PLoS ONE* 11 (4): 1–13. https://doi.org/10.1371/journal.pone.0154255.

Gabrielli, Armando, Enrico V Avvedimento, and Thomas Krieg. 2009. “Scleroderma.” *New England Journal of Medicine* 360 (19): 1989–2003. https://doi.org/10.1056/NEJMra0806188.

Garner, I. M., I. C. Evans, J. L. Barnes, T. M. Maher, E. A. Renzoni, C. P. Denton, C. J. Scotton, D. J. Abraham, and R. J. McAnulty. 2013. “Hypomethylation of the TNXB Gene Contributes to Increased Expression and Deposition of Tenascin X in Idiopathic Pulmonary Fibrosis.” *British Society for Matrix Biology – Spring 2013, International Journal of Experimental Pathology* 94 (5): A1–19. https://doi.org/10.1111/iep.12047.

Garner, Ian. 2016. “DNA Methylation in Lung Fibroblasts and Its Role in Pulmonary Fibrosis.” UCL.

Ge, Qi, Ling Chen, Jade Jaffar, William Scott Argraves, Waleed O. Twal, Phil Hansbro, Judith L. Black, Janette K. Burgess, and Brian Oliver. 2015. “Fibulin1C Peptide Induces Cell Attachment and Extracellular Matrix Deposition in Lung Fibroblasts.” *Scientific Reports* 5 (1): 9496. https://doi.org/10.1038/srep09496.

Gehr, P, M Bachofen, and E R Weibel. 1978. “The Normal Human Lung: Ultrastructure and Morphometric Estimation of Diffusion Capacity.” *Respiration Physiology* 32 (2): 121–40. https://doi.org/10.1016/0034-5687(78)90104-4.

Gill, Sean E., Isham Huizar, Eli M. Bench, Samuel W. Sussman, Ying Wang, Rama Khokha, and William C. Parks. 2010. “Tissue Inhibitor of Metalloproteinases 3 Regulates Resolution of Inflammation Following Acute Lung Injury.” *American Journal of Pathology* 176 (1): 64–73. https://doi.org/10.2353/ajpath.2010.090158.

Giltay, Richard, Rupert Timpl, and Günter Kostka. 1999. “Sequence, Recombinant Expression and Tissue Localization of Two Novel Extracellular Matrix Proteins, Fibulin-3 and Fibulin-4.” *Matrix Biology : Journal of the International Society for Matrix Biology* 18 (5): 469–80. https://doi.org/10.1016/S0945-053X(99)00038-4.

Giménez, Alícia, Paula Duch, Marta Puig, Marta Gabasa, Antoni Xaubet, and Jordi Alcaraz. 2017. “Dysregulated Collagen Homeostasis by Matrix Stiffening and TGF-B1 in Fibroblasts from Idiopathic Pulmonary Fibrosis Patients: Role of FAK/Akt.” *International Journal of Molecular Sciences* 18 (11). https://doi.org/10.3390/ijms18112431.

Giri, Anil K., and Tero Aittokallio. 2019. “DNMT Inhibitors Increase Methylation in the Cancer Genome.” *Frontiers in Pharmacology* 10 (APR): 1–11. https://doi.org/10.3389/fphar.2019.00385.

Groppe, Jay, Cynthia S. Hinck, Payman Samavarchi-Tehrani, Chloe Zubieta, Jonathan P. Schuermann, Alexander B. Taylor, Patricia M. Schwarz, Jeffrey L. Wrana, and Andrew P. Hinck. 2008. “Cooperative Assembly of TGF-β Superfamily Signaling Complexes Is Mediated by Two Disparate Mechanisms and Distinct Modes of Receptor Binding.” *Molecular Cell* 29 (2): 157–68. https://doi.org/10.1016/j.molcel.2007.11.039.

Grotendorst, Gary R., Georgeann Smale, and Dobromir Pencev. 1989. “Production of Transforming Growth Factor Beta by Human Peripheral Blood Monocytes and Neutrophils.” *Journal of Cellular Physiology* 140 (2): 396–402. https://doi.org/10.1002/jcp.1041400226.

Guida, Florence, Torkjel M. Sandanger, Raphaële Castagné, Gianluca Campanella, Silvia Polidoro,

Domenico Palli, Vittorio Krogh, et al. 2015. “Dynamics of Smoking-Induced Genome-Wide Methylation Changes with Time since Smoking Cessation.” *Human Molecular Genetics* 24 (8): 2349–59. https://doi.org/10.1093/hmg/ddu751.

Hadjicharalambous, Marina R., Benoit T. Roux, Eszter Csomor, Carol A. Feghali-Bostwick, Lynne A. Murray, Deborah L. Clarke, and Mark A. Lindsay. 2019. “Long Intergenic Non-Coding RNAs Regulate Human Lung Fibroblast Function: Implications for Idiopathic Pulmonary Fibrosis.” *Scientific Reports* 9 (1): 6020. https://doi.org/10.1038/s41598-019-42292-w.

Hadjicharalambous, Marina R., Benoit T. Roux, Carol A. Feghali-Bostwick, Lynne A. Murray, Deborah L. Clarke, and Mark A. Lindsay. 2018. “Long Non-Coding RNAs Are Central Regulators of the IL-1β-Induced Inflammatory Response in Normal and Idiopathic Pulmonary Lung Fibroblasts.” *Frontiers in Immunology* 9 (December): 2906. https://doi.org/10.3389/fimmu.2018.02906.

Hahn, Oliver, Sebastian Grönke, Thomas M. Stubbs, Gabriella Ficz, Oliver Hendrich, Felix Krueger, Simon Andrews, et al. 2017. “Dietary Restriction Protects from Age-Associated DNA Methylation and Induces Epigenetic Reprogramming of Lipid Metabolism.” *Genome Biology* 18 (1): 1–18. https://doi.org/10.1186/s13059-017-1187-1.

Hashimoto, Naozumi, Sem H. Phan, Kazuyoshi Imaizumi, Masaki Matsuo, Harunori Nakashima, Tsutomu Kawabe, Kaoru Shimokata, and Yoshinori Hasegawa. 2010. “Endothelial-Mesenchymal Transition in Bleomycin-Induced Pulmonary Fibrosis.” *American Journal of Respiratory Cell and Molecular Biology* 43 (2): 161–72. https://doi.org/10.1165/rcmb.2009-0031OC.

Haynes, Winston A., Aurelie Tomczak, and Purvesh Khatri. 2018. “Gene Annotation Bias Impedes Biomedical Research.” *Scientific Reports* 8 (1): 1–7. https://doi.org/10.1038/s41598-018-19333-x.

He, Yu-Fei, Bin-Zhong Li, Zheng Li, Peng Liu, Yang Wang, Qingyu Tang, Jianping Ding, et al. 2011. “Tet-Mediated Formation of 5-Carboxylcytosine and Its Excision by TDG in Mammalian DNA.” *Science (New York, N.Y.)* 333 (6047): 1303–7. https://doi.org/10.1126/science.1210944.

Helling, Britney A., Anthony N. Gerber, Vineela Kadiyala, Sarah K. Sasse, Brent S. Pedersen, Lenore Sparks, Yasushi Nakano, et al. 2017. “Regulation of MUC5B Expression in Idiopathic Pulmonary Fibrosis.” *American Journal of Respiratory Cell and Molecular Biology* 57 (1): 91–99. https://doi.org/10.1165/rcmb.2017-0046OC.

Henderson, Neil C, Thomas D Arnold, Yoshio Katamura, Marilyn M Giacomini, Juan D Rodriguez, Joseph H. McCarty, Antonella Pellicoro, et al. 2013. “Targeting of Av Integrin Identifies a Core Molecular Pathway That Regulates Fibrosis in Several Organs.” *Nature Medicine* 19 (12): 1617–24. https://doi.org/10.1038/nm.3282.

Hergeth, Sonja P., Wilhelm K. Aicher, Mike Essl, Thomas D. Schreiber, Takako Sasaki, and Gerd Klein. 2008. “Characterization and Functional Analysis of Osteoblast-Derived Fibulins in the Human Hematopoietic Stem Cell Niche.” *Experimental Hematology* 36 (8): 1022–34. https://doi.org/10.1016/j.exphem.2008.03.013.

Herrera, Jeremy, Colleen Forster, Thomas Pengo, Angeles Montero, Joe Swift, Martin A. Schwartz, Craig A. Henke, and Peter B. Bitterman. 2019. “Registration of the Extracellular Matrix Components Constituting the Fibroblastic Focus in Idiopathic Pulmonary Fibrosis.” *JCI Insight* 4 (1). https://doi.org/10.1172/jci.insight.125185.

Herrera, Jeremy, Craig A. Henke, and Peter B. Bitterman. 2018. “Extracellular Matrix as a Driver of Progressive Fibrosis.” *Journal of Clinical Investigation* 128 (1): 45–53. https://doi.org/10.1172/JCI93557.

Hill, Victoria K., Luke B. Hesson, Temuujin Dansranjavin, Ashraf Dallol, Ivan Bieche, Sophie Vacher, Stella Tommasi, et al. 2010. “Identification of 5 Novel Genes Methylated in Breast and Other Epithelial Cancers.” *Molecular Cancer* 9 (May 2014): 51. https://doi.org/10.1186/1476-4598-9-51.

Hinz, B., G. Celetta, J. J. Tomasek, G. Gabbiani, and C. Chaponnier. 2001. “Alpha-Smooth Muscle Actin Expression Upregulates Fibroblast Contractile Activity.” *Molecular Biology of the Cell* 12 (9): 2730–41. https://doi.org/10.1091/mbc.12.9.2730.

Hochberg, Yosef, Yoav Benjamini, and Yosef Hochberg. 1995. “Controlling the False Discovery Rate: A Practical and Powerful Approach to Multiple Testing.” *J. R. Statist. Soc. B* 57 (1): 289–300. http://www.jstor.org/stable/2346101.

Horejs, Christine-maria. 2016. “Basement Membrane Fragments in the Context of the Epithelial-to-Mesenchymal Transition.” *European Journal of Cell Biology* 95 (11): 427–40. https://doi.org/10.1016/j.ejcb.2016.06.002.

Horowitz, Jeffrey C., David S. Rogers, Vishal Sharma, Ragini Vittal, Eric S. White, Zongbin Cui, and Victor J. Thannickal. 2007. “Combinatorial Activation of FAK and AKT by Transforming Growth Factor-B1 Confers an Anoikis-Resistant Phenotype to Myofibroblasts.” *Cellular Signalling* 19 (4): 761–71. https://doi.org/10.1016/j.cellsig.2006.10.001.

Horowitz, Jeffrey C, and Victor J Thannickal. 2019. “Mechanisms for the Resolution of Organ Fibrosis.” *Physiology* 34 (1): 43–55. https://doi.org/10.1152/physiol.00033.2018.

Hotchkiss, R D. 1948. “The Quantitative Separation of Purines, Pyrimidines, and Nucleosides by Paper Chromatography.” *The Journal of Biological Chemistry* 175 (1): 315–32. http://www.ncbi.nlm.nih.gov/pubmed/18873306.

Huang, S. K., A. M. Scruggs, J. Donaghy, J. C. Horowitz, Z. Zaslona, S. Przybranowski, E. S. White, and M. Peters-Golden. 2013. “Histone Modifications Are Responsible for Decreased Fas Expression and Apoptosis Resistance in Fibrotic Lung Fibroblasts.” *Cell Death & Disease* 4 (5): e621. https://doi.org/10.1038/cddis.2013.146.

Huang, S. K., A. M. Scruggs, Ri. C. McEachin, E. S. White, and M. Peters-Golden. 2014. “Lung Fibroblasts from Patients with Idiopathic Pulmonary Fibrosis Exhibit Genome-Wide Differences in DNA Methylation Compared to Fibroblasts from Nonfibrotic Lung.” Edited by Daniel J. Tschumperlin. *PLoS ONE* 9 (9): e107055. https://doi.org/10.1371/journal.pone.0107055.

Huang, Steven K., Aaron S Fisher, Anne M Scruggs, Eric S White, Cory M Hogaboam, Bruce C Richardson, and Marc Peters-Golden. 2010. “Hypermethylation of PTGER2 Confers Prostaglandin E2 Resistance in Fibrotic Fibroblasts from Humans and Mice.” *The American Journal of Pathology* 177 (5): 2245–55. https://doi.org/10.2353/ajpath.2010.100446.

Huang, Tao, Seth L. Schor, and Andrew P. Hinck. 2014. “Biological Activity Differences between TGF-B1 and TGF-B3 Correlate with Differences in the Rigidity and Arrangement of Their Component Monomers.” *Biochemistry* 53 (36): 5737–49. https://doi.org/10.1021/bi500647d.

Hung, Chi, Geoffrey Linn, Yu Hua Chow, Akio Kobayashi, Kristen Mittelsteadt, William A. Altemeier, Sina A. Gharib, Lynn M. Schnapp, and Jeremy S. Duffield. 2013. “Role of Lung Pericytes and Resident Fibroblasts in the Pathogenesis of Pulmonary Fibrosis.” *American Journal of Respiratory and Critical Care Medicine* 188 (7): 820–30. https://doi.org/10.1164/rccm.201212-2297OC.

Ibrahim, Ayman M., Salwa Sabet, Akmal A. El-Ghor, Nora Kamel, Shady E. Anis, Joanna S. Morris, and Torsten Stein. 2018. “Fibulin-2 Is Required for Basement Membrane Integrity of Mammary Epithelium.” *Scientific Reports* 8 (1): 14139. https://doi.org/10.1038/s41598-018-32507-x.

Idiopathic Pulmonary Fibrosis Clinical Research Network, Ganesh Raghu, Kevin J Anstrom, Talmadge E King, Joseph A Lasky, and Fernando J Martinez. 2012. “Prednisone, Azathioprine, and N-Acetylcysteine for Pulmonary Fibrosis.” *The New England Journal of Medicine* 366 (21): 1968–77. https://doi.org/10.1056/NEJMoa1113354.

Im, Jintaek, Kyutae Kim, Polla Hergert, and Richard Seonghun Nho. 2016. “Idiopathic Pulmonary Fibrosis Fibroblasts Become Resistant to Fas Ligand-Dependent Apoptosis via the Alteration of Decoy Receptor 3.” *Journal of Pathology* 240 (1): 25–37. https://doi.org/10.1002/path.4749.

Irizarry, Rafael A., Christine Ladd-Acosta, Bo Wen, Zhijin Wu, Carolina Montano, Patrick Onyango, Hengmi Cui, et al. 2009. “The Human Colon Cancer Methylome Shows Similar Hypo- and Hypermethylation at Conserved Tissue-Specific CpG Island Shores.” *Nature Genetics* 41 (2): 178–86. https://doi.org/10.1038/ng.298.

Iurlaro, Mario, Gabriella Ficz, David Oxley, Eun-Ang Raiber, Martin Bachman, Michael J. Booth, Simon Andrews, Shankar Balasubramanian, and Wolf Reik. 2013. “A Screen for Hydroxymethylcytosine

and Formylcytosine Binding Proteins Suggests Functions in Transcription and Chromatin Regulation." *Genome Biology* 14 (10): R119. https://doi.org/10.1186/gb-2013-14-10-r119.

Jaffar, Jade, Sofia Unger, Tamera J. Corte, Michael Keller, Paul J. Wolters, Luca Richeldi, Stefania Cerri, et al. 2014. "Fibulin-1 Predicts Disease Progression in Patients with Idiopathic Pulmonary Fibrosis." *Chest* 146 (4): 1055–63. https://doi.org/10.1378/chest.13-2688.

Jonge, Hendrik J M de, Rudolf S N Fehrmann, Eveline S J M de Bont, Robert M W Hofstra, Frans Gerbens, Willem A. Kamps, Elisabeth G E de Vries, Ate G J van der Zee, Gerard J. te Meerman, and Arja ter Elst. 2007. "Evidence Based Selection of Housekeeping Genes." Edited by Michael Lichten. *PLoS ONE* 2 (9): e898. https://doi.org/10.1371/journal.pone.0000898.

Jorgenson, Amy J., Kyoung Moo Choi, Delphine Sicard, Karry M.J. Smith, Samantha E. Hiemer, Xaralabos Varelas, and Daniel J. Tschumperlin. 2017. "TAZ Activation Drives Fibroblast Spheroid Growth, Expression of Profibrotic Paracrine Signals, and Context-Dependent ECM Gene Expression." *American Journal of Physiology - Cell Physiology* 312 (3): C277–85. https://doi.org/10.1152/ajpcell.00205.2016.

Kaartinen, Vesa, Jan Willem Voncken, Charles Shuler, David Warburton, Ding Bu, Nora Heisterkamp, and John Groffen. 1995. "Abnormal Lung Development and Cleft Palate in Mice Lacking TGF-Beta 3 Indicates Defects of Epithelial-Mesenchymal Interaction." *Nature Genetics* 11 (4): 415–21. https://doi.org/10.1038/ng1295-415.

Kanan, Yogita, Daniel Brobst, Zongchao Han, Muna I. Naash, and Muayyad R. Al-Ubaidi. 2014. "Fibulin 2, a Tyrosine O- Sulfated Protein, Is Up-Regulated Following Retinal Detachment." *Journal of Biological Chemistry* 289 (19): 13419–33. https://doi.org/10.1074/jbc.M114.562157.

Kanda, Nisha. 2015. "Fibroblast Spheroids : A Useful Assay for Drug Screening in Idiopathic Pulmonary Fibrosis?" UCL. http://discovery.ucl.ac.uk/1463756/.

Kapranov, Philipp, and Georges St. Laurent. 2012. "Dark Matter RNA: Existence, Function, and Controversy." *Frontiers in Genetics* 3 (APR): 1–9. https://doi.org/10.3389/fgene.2012.00060.

Karakikes, Ioannis, Antoine H. Chaanine, Soojeong Kang, Bertrand N. Mukete, Dongtak Jeong, Shihong Zhang, Roger J. Hajjar, and Djamel Lebeche. 2013. "Therapeutic Cardiac-Targeted Delivery of MiR-1 Reverses Pressure Overload-Induced Cardiac Hypertrophy and Attenuates Pathological Remodeling." *Journal of the American Heart Association* 2 (2): e000078. https://doi.org/10.1161/JAHA.113.000078.

Kassiri, Zamaneh, Gavin Y. Oudit, Vijay Kandalam, Ahmed Awad, Xiuhua Wang, Xiuhua Ziou, Nobuyo Maeda, Andrew M. Herzenberg, and James W. Scholey. 2009. "Loss of TIMP3 Enhances Interstitial Nephritis and Fibrosis." *Journal of the American Society of Nephrology* 20 (6): 1223–35. https://doi.org/10.1681/ASN.2008050492.

Keerthisingam, Carmel B., R. Gisli Jenkins, Nicholas K. Harrison, Norma A. Hernandez-Rodriguez, Helen Booth, Geoffrey J. Laurent, Stephen L. Hart, Martyn L. Foster, and Robin J. McAnulty. 2001. "Cyclooxygenase-2 Deficiency Results in a Loss of the Anti-Proliferative Response to Transforming Growth Factor-β in Human Fibrotic Lung Fibroblasts and Promotes Bleomycin-Induced Pulmonary Fibrosis in Mice." *The American Journal of Pathology* 158 (4): 1411–22. https://doi.org/10.1016/S0002-9440(10)64092-8.

Kelley, J., J. P. Fabisiak, K. Hawes, and M. Absher. 1991. "Cytokine Signaling in Lung: Transforming Growth Factor-Beta Secretion by Lung Fibroblasts." *The American Journal of Physiology* 260 (2 Pt 1): L123-8. https://doi.org/10.1152/ajplung.1991.260.2.L123.

Kettunen, Eeva, Hector Hernandez-Vargas, Marie-Pierre Cros, Geoffroy Durand, Florence Le Calvez-Kelm, Kristina Stuopelyte, Sonata Jarmalaite, et al. 2017. "Asbestos-Associated Genome-Wide DNA Methylation Changes in Lung Cancer." *International Journal of Cancer* 141 (10): 2014–29. https://doi.org/10.1002/ijc.30897.

Khan, Shaukat A, Hailong Dong, Jennifer Joyce, Takako Sasaki, Mon-Li Chu, and Takeshi Tsuda. 2016. "Fibulin-2 Is Essential for Angiotensin II-Induced Myocardial Fibrosis Mediated by Transforming Growth Factor (TGF)-β." *Laboratory Investigation; a Journal of Technical Methods and Pathology* 96 (7): 773–83. https://doi.org/10.1038/labinvest.2016.52.

Kielty, Cay M. 2006. “Elastic Fibres in Health and Disease.” *Expert Reviews in Molecular Medicine* 8 (19): 1–23. https://doi.org/10.1017/S146239940600007X.

Kim, K. K., M. C. Kugler, P. J. Wolters, L. Robillard, M. G. Galvez, A. N. Brumwell, D. Sheppard, and H. A. Chapman. 2006. “Alveolar Epithelial Cell Mesenchymal Transition Develops in Vivo during Pulmonary Fibrosis and Is Regulated by the Extracellular Matrix.” *Proceedings of the National Academy of Sciences* 103 (35): 13180–85. https://doi.org/10.1073/pnas.0605669103.

Kim, Tae Hyung, Sang-Heon Kim, Ji-Young Seo, Hana Chung, Hyun Jung Kwak, Sang-Kyung Lee, Ho Joo Yoon, Dong Ho Shin, Sung Soo Park, and Jang Won Sohn. 2011. “Blockade of the Wnt/β-Catenin Pathway Attenuates Bleomycin-Induced Pulmonary Fibrosis.” *The Tohoku Journal of Experimental Medicine* 223 (1): 45–54. https://doi.org/10.1620/tjem.223.45.

Kinoshita, Katsuhiro, Yoshinori Aono, Momoyo Azuma, Jun Kishi, Akio Takezaki, Masami Kishi, Hideki Makino, et al. 2013. “Antifibrotic Effects of Focal Adhesion Kinase Inhibitor in Bleomycin-Induced Pulmonary Fibrosis in Mice.” *American Journal of Respiratory Cell and Molecular Biology* 49 (4): 536–43. https://doi.org/10.1165/rcmb.2012-0277OC.

Kleaveland, Kathryn R., Miranda Velikoff, Jibing Yang, Manisha Agarwal, Richard A. Rippe, Bethany B. Moore, and Kevin K. Kim. 2014. “Fibrocytes Are Not an Essential Source of Type I Collagen during Lung Fibrosis.” *The Journal of Immunology* 193 (10): 5229–39. https://doi.org/10.4049/jimmunol.1400753.

Klebaner, Daniella, Yunfeng Huang, Qin Hui, Jacquelyn Y. Taylor, Jack Goldberg, Viola Vaccarino, and Yan V. Sun. 2016. “X Chromosome-Wide Analysis Identifies DNA Methylation Sites Influenced by Cigarette Smoking.” *Clinical Epigenetics* 8 (1). https://doi.org/10.1186/s13148-016-0189-2.

Kleifeld, Oded, Alain Doucet, Ulrich auf dem Keller, Anna Prudova, Oliver Schilling, Rajesh K. Kainthan, Amanda E. Starr, Leonard J. Foster, Jayachandran N. Kizhakkedathu, and Christopher M. Overall. 2010. “Isotopic Labeling of Terminal Amines in Complex Samples Identifies Protein N-Termini and Protease Cleavage Products.” *Nature Biotechnology* 28 (3): 281–88. https://doi.org/10.1038/nbt.1611.

Knight, Darryl A., and Stephen T. Holgate. 2003. “The Airway Epithelium: Structural and Functional Properties in Health and Disease.” *Respirology (Carlton, Vic.)* 8 (4): 432–46. https://doi.org/10.1046/j.1440-1843.2003.00493.x.

Kobayashi, Naoyuki, Günter Kostka, Jörg H O Garbe, Douglas R. Keene, Hans Peter Bächinger, Franz-Georg Hanisch, Dessislava Markova, et al. 2007. “A Comparative Analysis of the Fibulin Protein Family. Biochemical Characterization, Binding Interactions, and Tissue Localization.” *The Journal of Biological Chemistry* 282 (16): 11805–16. https://doi.org/10.1074/jbc.M611029200.

Kohan, Martin, Andres F. Muro, Eric S. White, and Neville Berkman. 2010. “ EDA-containing Cellular Fibronectin Induces Fibroblast Differentiation through Binding to α 4 β 7 Integrin Receptor and MAPK/Erk 1/2-dependent Signaling .” *The FASEB Journal* 24 (11): 4503–12. https://doi.org/10.1096/fj.10-154435.

Kolb, Martin, Peter J Margetts, Patricia J Sime, and Jack Gauldie. 2001. “Proteoglycans Decorin and Biglycan Differentially Modulate TGF-β-Mediated Fibrotic Responses in the Lung.” *American Journal of Physiology - Lung Cellular and Molecular Physiology* 280 (6 24-6): 1327–34. https://doi.org/10.1152/ajplung.2001.280.6.l1327.

Kostka, G., R. Giltay, W. Bloch, K. Addicks, R. Timpl, R Fässler, and M L Chu. 2001. “Perinatal Lethality and Endothelial Cell Abnormalities in Several Vessel Compartments of Fibulin-1-Deficient Mice.” *Molecular and Cellular Biology* 21 (20): 7025–34. https://doi.org/10.1128/MCB.21.20.7025-7034.2001.

Krstic, Jelena, and Juan F. Santibanez. 2014. “Transforming Growth Factor-Beta and Matrix Metalloproteinases: Functional Interactions in Tumor Stroma-Infiltrating Myeloid Cells.” *The Scientific World Journal* 2014. https://doi.org/10.1155/2014/521754.

Kulasekaran, Priya, Casey A. Scavone, David S. Rogers, Douglas A. Arenberg, Victor J. Thannickal, and Jeffrey C. Horowitz. 2009. “Endothelin-1 and Transforming Growth Factor-B1 Independently Induce Fibroblast Resistance to Apoptosis via AKT Activation.” *American Journal of Respiratory*

*Cell and Molecular Biology* 41 (4): 484–93. https://doi.org/10.1165/rcmb.2008-0447OC.

Kulkarni, A. B., C. G. Huh, D. Becker, A. Geiser, M. Lyght, K. C. Flanders, A. B. Roberts, M. B. Sporn, J. M. Ward, and S. Karlsson. 1993. "Transforming Growth Factor B1 Null Mutation in Mice Causes Excessive Inflammatory Response and Early Death." *Proceedings of the National Academy of Sciences of the United States of America* 90 (2): 770–74. https://doi.org/10.1073/pnas.90.2.770.

Kumra, Heena, Valentin Nelea, Hana Hakami, Amelie Pagliuzza, Jelena Djokic, Jiongci Xu, Hiromi Yanagisawa, and Dieter P. Reinhardt. 2019. "Fibulin-4 Exerts a Dual Role in LTBP-4L-Mediated Matrix Assembly and Function." *Proceedings of the National Academy of Sciences of the United States of America* 116 (41): 20428–37. https://doi.org/10.1073/pnas.1901048116.

Lagares, David, Oscar Busnadiego, Rosa Ana García-Fernández, Mohit Kapoor, Shangxi Liu, David E. Carter, David Abraham, et al. 2012. "Inhibition of Focal Adhesion Kinase Prevents Experimental Lung Fibrosis and Myofibroblast Formation." *Arthritis and Rheumatism* 64 (5): 1653–64. https://doi.org/10.1002/art.33482.

Lareu, Ricky R, Karthik Harve Subramhanya, Yanxian Peng, Paula Benny, Clarice Chen, Zhibo Wang, Raj Rajagopalan, and Michael Raghunath. 2007. "Collagen Matrix Deposition Is Dramatically Enhanced in Vitro When Crowded with Charged Macromolecules: The Biological Relevance of the Excluded Volume Effect." *FEBS Letters* 581 (14): 2709–14. https://doi.org/10.1016/j.febslet.2007.05.020.

Laurent, Geoffrey J., Peter Cockerill, Robin J. McAnulty, and Jeremy R.B. Hastings. 1981. "A Simplified Method for Quantitation of the Relative Amounts of Type I and Type III Collagen in Small Tissue Samples." *Analytical Biochemistry* 113 (2): 301–12. https://doi.org/10.1016/0003-2697(81)90081-6.

Law, E W L, A K L Cheung, V I Kashuba, T V Pavlova, E R Zabarovsky, H L Lung, Y Cheng, et al. 2012. "Anti-Angiogenic and Tumor-Suppressive Roles of Candidate Tumor-Suppressor Gene, Fibulin-2, in Nasopharyngeal Carcinoma." *Oncogene* 31 (6): 728–38. https://doi.org/10.1038/onc.2011.272.

Lawson, William E., Peter F. Crossno, Vasiliy V. Polosukhin, Juan Roldan, Dong Sheng Cheng, Kirk B. Lane, Thomas R. Blackwell, et al. 2008. "Endoplasmic Reticulum Stress in Alveolar Epithelial Cells Is Prominent in IPF: Association with Altered Surfactant Protein Processing and Herpesvirus Infection." *American Journal of Physiology - Lung Cellular and Molecular Physiology* 294 (6): 1119–26. https://doi.org/10.1152/ajplung.00382.2007.

LeBleu, V S, B Macdonald, and R Kalluri. 2007. "Structure and Function of Basement Membranes." *Exp Biol Med* 232 (9): 1121–29. https://doi.org/10.3181/0703-mr-72.

Lecka-Czernik, B, C K Lumpkin, and S Goldstein. 1995. "An Overexpressed Gene Transcript in Senescent and Quiescent Human Fibroblasts Encoding a Novel Protein in the Epidermal Growth Factor-like Repeat Family Stimulates DNA Synthesis." *Molecular and Cellular Biology* 15 (1): 120–28. https://doi.org/10.1128/mcb.15.1.120.

Lee, Jong-Uk, Hyun Sub Cheong, Eun-Young Shim, Da-Jeong Bae, Hun Soo Chang, Soo-Taek Uh, Young Hoon Kim, et al. 2017. "Gene Profile of Fibroblasts Identify Relation of CCL8 with Idiopathic Pulmonary Fibrosis." *Respiratory Research* 18 (1): 3. https://doi.org/10.1186/s12931-016-0493-6.

Lee, Jong-Uk, Ji-Hye Son, Eun-Young Shim, Hyun Sub Cheong, Seung-Woo Shin, Hyoung Doo Shin, Ae Rin Baek, et al. 2019. "Global DNA Methylation Pattern of Fibroblasts in Idiopathic Pulmonary Fibrosis." *DNA and Cell Biology* 38 (9): 905–14. https://doi.org/10.1089/dna.2018.4557.

Lee, Joyce S., Jay H. Ryu, Brett M. Elicker, Carmen P. Lydell, Kirk D. Jones, Paul J. Wolters, Talmadge E. King, and Harold R. Collard. 2011. "Gastroesophageal Reflux Therapy Is Associated with Longer Survival in Patients with Idiopathic Pulmonary Fibrosis." *American Journal of Respiratory and Critical Care Medicine* 184 (12): 1390–94. https://doi.org/10.1164/rccm.201101-0138OC.

Lee, Nathan V., Juan Carlos Rodriguez-Manzaneque, Shelley N.M. Thai, Waleed O. Twal, Alfonso Luque, Karen M. Lyons, W. Scott Argraves, and M. Luisa Iruela-Arispe. 2005. "Fibulin-1 Acts as a Cofactor for the Matrix Metalloprotease ADAMTS-1." *Journal of Biological Chemistry* 280 (41):

34796–804. https://doi.org/10.1074/jbc.M506980200.

Lehmann, Mareike, Lara Buhl, Hani N Alsafadi, Stephan Klee, Sarah Hermann, Kathrin Mutze, Chiharu Ota, et al. 2018. “Differential Effects of Nintedanib and Pirfenidone on Lung Alveolar Epithelial Cell Function in Ex Vivo Murine and Human Lung Tissue Cultures of Pulmonary Fibrosis.” *Respiratory Research* 19 (1): 175. https://doi.org/10.1186/s12931-018-0876-y.

Lerbs, Tristan, Lu Cui, Megan E. King, Tim Chai, Claire Muscat, Lorinda Chung, Ryanne Brown, Kerri Rieger, Tyler Shibata, and Gerlinde Wernig. 2020. “CD47 Prevents the Elimination of Diseased Fibroblasts in Scleroderma.” *JCI Insight* 5 (16). https://doi.org/10.1172/jci.insight.140458.

Lietha, Daniel, Xinming Cai, Derek F.J. Ceccarelli, Yiqun Li, Michael D Schaller, and Michael J Eck. 2007. “Structural Basis for the Autoinhibition of Focal Adhesion Kinase.” *Cell* 129 (6): 1177–87. https://doi.org/10.1016/j.cell.2007.05.041.

Ligresti, Giovanni, Nunzia Caporarello, Jeffrey A. Meridew, Dakota L. Jones, Qi Tan, Kyoung Moo Choi, Andrew J. Haak, et al. 2019. “CBX5/G9a/H3K9me-Mediated Gene Repression Is Essential to Fibroblast Activation during Lung Fibrosis.” *JCI Insight* 5 (May). https://doi.org/10.1172/jci.insight.127111.

Liu, Fei, David Lagares, Kyoung Moo Choi, Lauren Stopfer, Aleksandar Marinković, Vladimir Vrbanac, Clemens K. Probst, et al. 2015. “Mechanosignaling through YAP and TAZ Drives Fibroblast Activation and Fibrosis.” *American Journal of Physiology - Lung Cellular and Molecular Physiology* 308 (4): L344–57. https://doi.org/10.1152/ajplung.00300.2014.

Liu, Fei, Justin D. Mih, Barry S. Shea, Alvin T. Kho, Asma S. Sharif, Andrew M. Tager, and Daniel J. Tschumperlin. 2010. “Feedback Amplification of Fibrosis through Matrix Stiffening and COX-2 Suppression.” *The Journal of Cell Biology* 190 (4): 693–706. https://doi.org/10.1083/jcb.201004082.

Liu, Gang, Marion A. Cooley, Andrew G. Jarnicki, Alan C-Y. Hsu, Prema M. Nair, Tatt Jhong Haw, Michael Fricker, et al. 2016. “Fibulin-1 Regulates the Pathogenesis of Tissue Remodeling in Respiratory Diseases.” *JCI Insight* 1 (9). https://doi.org/10.1172/jci.insight.86380.

Liu, Gang, Marion A Cooley, Andrew G Jarnicki, Theo Borghuis, Prema M Nair, Gavin Tjin, Alan C Hsu, et al. 2019. “Fibulin-1c Regulates Transforming Growth Factor–β Activation in Pulmonary Tissue Fibrosis.” *JCI Insight* 4 (16). https://doi.org/10.1172/jci.insight.124529.

Liu, Shangxi, Xu Shi-Wen, David J Abraham, and Andrew Leask. 2011. “CCN2 Is Required for Bleomycin-Induced Skin Fibrosis in Mice.” *Arthritis and Rheumatism* 63 (1): 239–46. https://doi.org/10.1002/art.30074.

Liu, Tianju, Biao Hu, Young Choi Yoon, Myoung Ja Chung, Matthew Ullenbruch, Hongfeng Yu, John B. Lowe, and Sem H. Phan. 2009. “Notch1 Signaling in FIZZ1 Induction of Myofibroblast Differentiation.” *American Journal of Pathology* 174 (5): 1745–55. https://doi.org/10.2353/ajpath.2009.080618.

Liu, Tianju, Francina Gonzalez De Los Santos, Yuyue Zhao, Zhe Wu, Andrew E. Rinke, Kevin K. Kim, and Sem H. Phan. 2019. “Telomerase Reverse Transcriptase Ameliorates Lung Fibrosis by Protecting Alveolar Epithelial Cells against Senescence.” *Journal of Biological Chemistry* 294 (22): 8861–71. https://doi.org/10.1074/jbc.RA118.006615.

Liu, Xiaoqiu, Simon S Wong, Carmen A Taype, Jeeyeon Kim, Tzu-pin Shentu, Celia R Espinoza, J Cameron Finley, et al. 2017. “Thy-1 Interaction with Fas in Lipid Rafts Regulates Fibroblast Apoptosis and Lung Injury Resolution.” *Nature Publishing Group* 97 (September 2015): 256–67. https://doi.org/10.1038/labinvest.2016.145.

Livak, Kenneth J., and Thomas D. Schmittgen. 2001. “Analysis of Relative Gene Expression Data Using Real-Time Quantitative PCR and the 2−ΔΔCT Method.” *Methods* 25 (4): 402–8. https://doi.org/10.1006/meth.2001.1262.

Löffek, S., O. Schilling, and C. W. Franzke. 2011. “Biological Role of Matrix Metalloproteinases: A Critical Balance.” *European Respiratory Journal* 38 (1): 191–208. https://doi.org/10.1183/09031936.00146510.

Longmate, Whitney M, Ruby Monichan, Mon-Li Chu, Takeshi Tsuda, My G Mahoney, and C.Michael

Michael DiPersio. 2014. “Reduced Fibulin-2 Contributes to Loss of Basement Membrane Integrity and Skin Blistering in Mice Lacking Integrin A3β1 in the Epidermis.” *Journal of Investigative Dermatology* 134 (6): 1609–17. https://doi.org/10.1038/jid.2014.10.

López-Casillas, Fernando, Jeffrey L. Wrana, and Joan Massagué. 1993. “Betaglycan Presents Ligand to the TGFβ Signaling Receptor.” *Cell* 73 (7): 1435–44. https://doi.org/10.1016/0092-8674(93)90368-Z.

Lu, Pengfei, Ken Takai, Valerie M Weaver, and Zena Werb. 2011. “Extracellular Matrix Degradation and Remodeling in Development and Disease.” *Cold Spring Harbor Perspectives in Biology* 3 (12). https://doi.org/10.1101/cshperspect.a005058.

Lu, Qingchun, Zhongliang Guo, Wang Xie, Wenjing Jin, Dongyi Zhu, Song Chen, and Tao Ren. 2018. “The LncRNA H19 Mediates Pulmonary Fibrosis by Regulating the MiR-196a/COL1A1 Axis.” *Inflammation* 41 (3): 896–903. https://doi.org/10.1007/s10753-018-0744-4.

Lyons, R. M., J. Keski-Oja, and H. L. Moses. 1988. “Proteolytic Activation of Latent Transforming Growth Factor-β from Fibroblast-Conditioned Medium.” *Journal of Cell Biology* 106 (5): 1659–65. https://doi.org/10.1083/jcb.106.5.1659.

Ma, Hongping, Changhong Lian, and Yingming Song. 2019. “Fibulin-2 Inhibits Development of Gastric Cancer by Downregulating β-Catenin.” *Oncology Letters* 18 (3): 2799–2804. https://doi.org/10.3892/ol.2019.10599.

Maher, Toby M., Iona C. Evans, Stephen E. Bottoms, Paul F. Mercer, Andrew J. Thorley, Andrew G. Nicholson, Geoffrey J. Laurent, Teresa D. Tetley, Rachel C. Chambers, and Robin J. McAnulty. 2010. “Diminished Prostaglandin E2 Contributes to the Apoptosis Paradox in Idiopathic Pulmonary Fibrosis.” *American Journal of Respiratory and Critical Care Medicine* 182 (1): 73–82. https://doi.org/10.1164/rccm.200905-0674OC.

Maiti, Atanu, and Alexander C. Drohat. 2011. “Thymine DNA Glycosylase Can Rapidly Excise 5-Formylcytosine and 5-Carboxylcytosine.” *Journal of Biological Chemistry* 286 (41): 35334–38. https://doi.org/10.1074/jbc.C111.284620.

Mak, Angel C.Y., Paul L.F. Tang, Clare Cleveland, Melanie H Smith, M. Kari Connolly, Tamiko R Katsumoto, Paul J Wolters, Pui Yan Kwok, and Lindsey A Criswell. 2016. “Whole-Exome Sequencing for Identification of Potential Causal Variants for Diffuse Cutaneous Systemic Sclerosis.” *Arthritis and Rheumatology* 68 (9): 2257–62. https://doi.org/10.1002/art.39721.

Martinis, Massimo De, Fedra Ciccarelli, Maria Maddalena Sirufo, Lia Ginaldi, Massimo De Martinis, Fedra Ciccarelli, Maria Maddalena Sirufo, and Lia Ginaldi. 2016. “Expert Review of Clinical Immunology An Overview of Environmental Risk Factors in Systemic Sclerosis.” *Expert Review of Clinical Immunology* 12 (4): 465–78. https://doi.org/10.1586/1744666X.2016.1125782.

Mathai, Susan K., Brent S. Pedersen, Keith Smith, Pamela Russell, Marvin I. Schwarz, Kevin K. Brown, Mark P. Steele, et al. 2016. “Desmoplakin Variants Are Associated with Idiopathic Pulmonary Fibrosis.” *American Journal of Respiratory and Critical Care Medicine* 193 (10): 1151–60. https://doi.org/10.1164/rccm.201509-1863OC.

Matsuno, Yosuke, Takumi Kiwamoto, Yuko Morishima, Yukio Ishii, Nobuyuki Hizawa, and Cory M. Hogaboam. 2018. “Notch Signaling Regulates Cell Density-Dependent Apoptosis of NIH 3T3 through an IL-6/STAT3 Dependent Mechanism.” *European Journal of Cell Biology* 97 (7): 512–22. https://doi.org/10.1016/j.ejcb.2018.09.001.

Matsushima, Shingo, and Junichi Ishiyama. 2016. “MicroRNA-29c Regulates Apoptosis Sensitivity via Modulation of the Cell-Surface Death Receptor, Fas, in Lung Fibroblasts.” *American Journal of Physiology - Lung Cellular and Molecular Physiology* 311 (6): L1050–61. https://doi.org/10.1152/ajplung.00252.2016.

Maunakea, Alika K., Iouri Chepelev, Kairong Cui, and Keji Zhao. 2013. “Intragenic DNA Methylation Modulates Alternative Splicing by Recruiting MeCP2 to Promote Exon Recognition.” *Cell Research* 23 (11): 1256–69. https://doi.org/10.1038/cr.2013.110.

McAnulty, R. J. 2007. “Fibroblasts and Myofibroblasts: Their Source, Function and Role in Disease.” *International Journal of Biochemistry and Cell Biology* 39 (4): 666–71.

https://doi.org/10.1016/j.biocel.2006.11.005.

McAnulty, R J, J S Campa, a D Cambrey, and G J Laurent. 1991. “The Effect of Transforming Growth Factor Beta on Rates of Procollagen Synthesis and Degradation in Vitro.” *Biochimica et Biophysica Acta* 1091 (2): 231–35. https://doi.org/10.1016/0167-4889(91)90066-7.

McAnulty, Robin J., and Geoffrey J. Laurent. 1987. “Collagen Synthesis and Degradation in Vivo. Evidence for Rapid Rates of Collagen Turnover with Extensive Degradation of Newly Synthesized Collagen in Tissues of the Adult Rat.” *Collagen and Related Research* 7 (2): 93–104. https://doi.org/10.1016/s0174-173x(87)80001-8.

McDonald, James I., Hamza Celik, Lisa E. Rois, Gregory Fishberger, Tolison Fowler, Ryan Rees, Ashley Kramer, Andrew Martens, John R. Edwardsand, and Grant A. Challen. 2016. “Reprogrammable CRISPR/Cas9-Based System for Inducing Sitespecific DNA Methylation.” *Biology Open* 5 (6): 866–74. https://doi.org/10.1242/bio.019067.

McLaughlin, Precious J., Benjamin Bakall, Jiwon Choi, Zhonglin Liu, Takako Sasaki, Elaine C. Davis, Alan D Marmorstein, and Lihua Y. Marmorstein. 2007. “Lack of Fibulin-3 Causes Early Aging and Herniation, but Not Macular Degeneration in Mice.” *Human Molecular Genetics* 16 (24): 3059–70. https://doi.org/10.1093/hmg/ddm264.

McLaughlin, Precious J., Qiuyun Chen, Masahito Horiguchi, Barry C. Starcher, J. Brett Stanton, Thomas J. Broekelmann, Alan D Marmorstein, et al. 2006. “Targeted Disruption of Fibulin-4 Abolishes Elastogenesis and Causes Perinatal Lethality in Mice.” *Molecular and Cellular Biology* 26 (5): 1700–1709. https://doi.org/10.1128/MCB.26.5.1700-1709.2006.

Mecham, Robert P. 2018. “Elastin in Lung Development and Disease Pathogenesis.” *Matrix Biology : Journal of the International Society for Matrix Biology* 73 (c): 6–20. https://doi.org/10.1016/j.matbio.2018.01.005.

Meiners, Silke, Oliver Eickelberg, and Melanie Königshoff. 2015. “Hallmarks of the Ageing Lung.” *European Respiratory Journal* 45 (3): 807–27. https://doi.org/10.1183/09031936.00186914.

Miao, Chenggui, Youyi Xiong, Guoxue Zhang, and Jun Chang. 2018. “MicroRNAs in Idiopathic Pulmonary Fibrosis, New Research Progress and Their Pathophysiological Implication.” *Experimental Lung Research* 44 (3): 178–90. https://doi.org/10.1080/01902148.2018.1455927.

Milam, Jami E., Venkateshwar G. Keshamouni, Sem H. Phan, Biao Hu, Srinivasa R. Gangireddy, Cory M. Hogaboam, Theodore J. Standiford, Victor J. Thannickal, and Raju C. Reddy. 2008. “PPAR-γ Agonists Inhibit Profibrotic Phenotypes in Human Lung Fibroblasts and Bleomycin-Induced Pulmonary Fibrosis.” *American Journal of Physiology - Lung Cellular and Molecular Physiology* 294 (5): 891–901. https://doi.org/10.1152/ajplung.00333.2007.

Missan, Dara S., Sridar V. Chittur, and C. Michael DiPersio. 2014. “Regulation of Fibulin-2 Gene Expression by Integrin A3β1 Contributes to the Invasive Phenotype of Transformed Keratinocytes.” *The Journal of Investigative Dermatology* 134 (9): 2418–27. https://doi.org/10.1038/jid.2014.166.

Moeller, Antje, Sarah E. Gilpin, Kjetil Ask, Gerard Cox, Deborah Cook, Jack Gauldie, Peter J. Margetts, et al. 2009. “Circulating Fibrocytes Are an Indicator of Poor Prognosis in Idiopathic Pulmonary Fibrosis.” *American Journal of Respiratory and Critical Care Medicine* 179 (7): 588–94. https://doi.org/10.1164/rccm.200810-1534OC.

Moore, Ashleigh E, Lisa E Young, and Dan A Dixon. 2011. “MicroRNA and AU-Rich Element Regulation of Prostaglandin Synthesis.” *Cancer Metastasis Reviews* 30 (3–4): 419–35. https://doi.org/10.1007/s10555-011-9300-5.

Moore, Bethany B., and Thomas A. Moore. 2015. “Viruses in Idiopathic Pulmonary Fibrosis Etiology and Exacerbation.” *Annals of the American Thoracic Society* 12 (November): S186–92. https://doi.org/10.1513/AnnalsATS.201502-088AW.

Moran, Sebastian, Carles Arribas, and Manel Esteller. 2016. “Validation of a DNA Methylation Microarray for 850,000 CpG Sites of the Human Genome Enriched in Enhancer Sequences.” *Epigenomics* 8 (3): 389–99. https://doi.org/10.2217/epi.15.114.

Morris, Tiffany J., Lee M. Butcher, Andrew Feber, Andrew E. Teschendorff, Ankur R. Chakravarthy,

Tomasz K. Wojdacz, and Stephan Beck. 2014. “ChAMP: 450k Chip Analysis Methylation Pipeline.” *Bioinformatics* 30 (3): 428–30. https://doi.org/10.1093/bioinformatics/btt684.

Mu, Dezhi, Stephanie Cambier, Lars Fjellbirkeland, Jody L. Baron, John S. Munger, Hisaaki Kawakatsu, Dean Sheppard, V. Courtney Broaddus, and Stephen L. Nishimura. 2002. “The Integrin Avβ8 Mediates Epithelial Homeostasis through MT1-MMP-Dependent Activation of TGF-B1.” *Journal of Cell Biology* 157 (3): 493–507. https://doi.org/10.1083/jcb.200109100.

Muriel, Joaquin M., Chun Dong, Harald Hutter, and Bruce E. Vogel. 2005. “Fibulin-1C and Fibulin-1D Splice Variants Have Distinct Functions and Assemble in a Hemicentin-Dependent Manner.” *Development (Cambridge, England)* 132 (19): 4223–34. https://doi.org/10.1242/dev.02007.

Naba, Alexandra, Karl R. Clauser, Huiming Ding, Charles A. Whittaker, Steven A. Carr, and Richard O. Hynes. 2016. “The Extracellular Matrix: Tools and Insights for the ‘Omics’ Era.” *Matrix Biology* 49 (January): 10–24. https://doi.org/10.1016/j.matbio.2015.06.003.

Nakamura, Tomoyuki. 2018. “Roles of Short Fibulins, a Family of Matricellular Proteins, in Lung Matrix Assembly and Disease.” *Matrix Biology : Journal of the International Society for Matrix Biology* 73 (2017): 21–33. https://doi.org/10.1016/j.matbio.2018.02.003.

Nakamura, Tomoyuki, Pilar Ruiz Lozano, Yasuhiro Ikeda, Yoshitaka Iwanaga, Aleksander Hinek, Susumu Minamisawa, Ching Feng Cheng, et al. 2002. “Fibulin-5/DANCE Is Essential for Elastogenesis in Vivo.” *Nature* 415 (6868): 171–75. https://doi.org/10.1038/415171a.

Nakasaki, Manando, Yongsung Hwang, Yun Xie, Sunny Kataria, Rupali Gund, Edries Y. Hajam, Rekha Samuel, et al. 2015. “The Matrix Protein Fibulin-5 Is at the Interface of Tissue Stiffness and Inflammation in Fibrosis.” *Nature Communications* 6: 1–11. https://doi.org/10.1038/ncomms9574.

Nath, Deepa, Patrick M. Slocombe, Paul E. Stephens, Alba Warn, Gillian R. Hutchinson, Kenneth M. Yamada, Andrew J.P. Docherty, and Gillian Murphy. 1999. “Interaction of Metargidin (ADAM-15) with α(v)B3 and A5β1 Integrins on Different Haemopoietic Cells.” *Journal of Cell Science* 112 (4): 579–87.

Navaratnam, Vidya, K. M. Fleming, J. West, C. J.P. Smith, R. G. Jenkins, A. Fogarty, and R. B. Hubbard. 2011. “The Rising Incidence of Idiopathic Pulmonary Fibrosis in the UK.” *Thorax* 66 (6): 462–67. https://doi.org/10.1136/thx.2010.148031.

Nishikawa, Ken, and Akira R. Kinjo. 2017. “Essential Role of Long Non-Coding RNAs in de Novo Chromatin Modifications: The Genomic Address Code Hypothesis.” *Biophysical Reviews* 9 (2): 73–77. https://doi.org/10.1007/s12551-017-0259-5.

Noble, Paul W., Carlo Albera, Williamson Z. Bradford, Ulrich Costabel, Marilyn K. Glassberg, David Kardatzke, Talmadge E. King, et al. 2011. “Pirfenidone in Patients with Idiopathic Pulmonary Fibrosis (CAPACITY): Two Randomised Trials.” *Lancet (London, England)* 377 (9779): 1760–69. https://doi.org/10.1016/S0140-6736(11)60405-4.

Nordlund, Jessica, Christofer L Bäcklin, Per Wahlberg, Stephan Busche, Eva C Berglund, Maija-Leena Eloranta, Trond Flaegstad, et al. 2013. “Genome-Wide Signatures of Differential DNA Methylation in Pediatric Acute Lymphoblastic Leukemia.” *Genome Biology* 14 (9): r105. https://doi.org/10.1186/gb-2013-14-9-r105.

Noth, Imre, Yingze Zhang, Shwu-Fan Ma, Carlos Flores, Mathew Barber, Yong Huang, Steven M Broderick, et al. 2013. “Genetic Variants Associated with Idiopathic Pulmonary Fibrosis Susceptibility and Mortality: A Genome-Wide Association Study.” *The Lancet. Respiratory Medicine* 1 (4): 309–17. https://doi.org/10.1016/S2213-2600(13)70045-6.

Nüchel, Julian, Sushmita Ghatak, Alexandra V. Zuk, Anja Illerhaus, Matthias Mörgelin, Katrin Schönborn, Katrin Blumbach, et al. 2018. “TGFB1 Is Secreted through an Unconventional Pathway Dependent on the Autophagic Machinery and Cytoskeletal Regulators.” *Autophagy* 14 (3): 465–86. https://doi.org/10.1080/15548627.2017.1422850.

O’Donoghue, Robert J J, Darryl A. Knight, Carl D. Richards, Cecilia M. Prêle, Hui Ling Lau, Andrew G. Jarnicki, Jessica Jones, et al. 2012. “Genetic Partitioning of Interleukin-6 Signalling in Mice Dissociates Stat3 from Smad3-Mediated Lung Fibrosis.” *EMBO Molecular Medicine* 4 (9): 939–

51. https://doi.org/10.1002/emmm.201100604.

Ochs, Matthias, Jens R Nyengaard, Anja Jung, Lars Knudsen, Marion Voigt, Thorsten Wahlers, Joachim Richter, and Hans Jørgen G Gundersen. 2004. "The Number of Alveoli in the Human Lung." *American Journal of Respiratory and Critical Care Medicine* 169 (1): 120–24. https://doi.org/10.1164/rccm.200308-1107OC.

Oh, Raymond S., Andrew J. Haak, Karry M. J. Smith, Giovanni Ligresti, Kyoung Moo Choi, Tiao Xie, Shaohua Wang, et al. 2018. "RNAi Screening Identifies a Mechanosensitive ROCK-JAK2-STAT3 Network Central to Myofibroblast Activation." *Journal of Cell Science* 131 (10): jcs209932. https://doi.org/10.1242/jcs.209932.

Ohno, Minoru, John P. Cooke, Victor J. Dzau, and Gary H. Gibbons. 1995. "Fluid Shear Stress Induces Endothelial Transforming Growth Factor Beta-1 Transcription and Production: Modulation by Potassium Channel Blockade." *Journal of Clinical Investigation* 95 (3): 1363–69. https://doi.org/10.1172/JCI117787.

Oldham, Justin M., Shwu Fan Ma, Fernando J. Martinez, Kevin J. Anstrom, Ganesh Raghu, David A. Schwartz, Eleanor Valenzi, et al. 2015. "TOLLIP, MUC5B, and the Response to N-Acetylcysteine among Individuals with Idiopathic Pulmonary Fibrosis." *American Journal of Respiratory and Critical Care Medicine* 192 (12): 1475–82. https://doi.org/10.1164/rccm.201505-1010OC.

Olijnyk, D., A. M. Ibrahim, R. K. Ferrier, T. Tsuda, M. L. Chu, B. A. Gusterson, T. Stein, and J. S. Morris. 2014. "Fibulin-2 Is Involved in Early Extracellular Matrix Development of the Outgrowing Mouse Mammary Epithelium." *Cellular and Molecular Life Sciences : CMLS* 71 (19): 3811–28. https://doi.org/10.1007/s00018-014-1577-4.

Olin, Anders I., Matthias Mörgelin, Takako Sasaki, Rupert Timpl, Dick Heinegård, and Anders Aspberg. 2001. "The Proteoglycans Aggrecan and Versican Form Networks with Fibulin-2 through Their Lectin Domain Binding." *Journal of Biological Chemistry* 276 (2): 1253–61. https://doi.org/10.1074/jbc.M006783200.

Ono, Robert N., Gerhard Sengle, Noel L. Charbonneau, Valerie Carlberg, Hans Peter Bächinger, Takako Sasaki, Sui Lee-Arteaga, et al. 2009. "Latent Transforming Growth Factor Beta-Binding Proteins and Fibulins Compete for Fibrillin-1 and Exhibit Exquisite Specificities in Binding Sites." *The Journal of Biological Chemistry* 284 (25): 16872–81. https://doi.org/10.1074/jbc.M809348200.

Ooi, Steen K T, Chen Qiu, Emily Bernstein, Keqin Li, Da Jia, Zhe Yang, Hediye Erdjument-Bromage, et al. 2007. "DNMT3L Connects Unmethylated Lysine 4 of Histone H3 to de Novo Methylation of DNA." *Nature* 448 (7154): 714–17. https://doi.org/10.1038/nature05987.

Pacaud, Romain, Quentin Sery, Lisa Oliver, François M. Vallette, Jörg Tost, and Pierre-François Cartron. 2014. "DNMT3L Interacts with Transcription Factors to Target DNMT3L/DNMT3B to Specific DNA Sequences: Role of the DNMT3L/DNMT3B/P65-NFκB Complex in the (de-)Methylation of TRAF1." *Biochimie* 104 (1): 36–49. https://doi.org/10.1016/j.biochi.2014.05.005.

Pan, Te Cheng, Takako Sasaki, Rui Zhu Zhang, Reinhard Fässler, Rupert Timpl, and Mon Li Chu. 1993. "Structure and Expression of Fibulin-2, a Novel Extracellular Matrix Protein with Multiple EGF-like Repeats and Consensus Motifs for Calcium Binding." *Journal of Cell Biology* 123 (5): 1269–77. https://doi.org/10.1083/jcb.123.5.1269.

Pandit, Kusum V, David Corcoran, Hanadie Yousef, Manohar Yarlagadda, Argyris Tzouvelekis, Kevin F Gibson, Kazuhisa Konishi, et al. 2010. "Inhibition and Role of Let-7d in Idiopathic Pulmonary Fibrosis." *American Journal of Respiratory and Critical Care Medicine* 182 (2): 220–29. https://doi.org/10.1164/rccm.200911-1698OC.

Papaioannou, Ioannis, Shiwen Xu, Christopher P. Denton, David J. Abraham, and Markella Ponticos. 2018. "STAT3 Controls COL1A2 Enhancer Activation Cooperatively with JunB, Regulates Type I Collagen Synthesis Posttranscriptionally, and Is Essential for Lung Myofibroblast Differentiation." *Molecular Biology of the Cell* 29 (2): 84–95. https://doi.org/10.1091/mbc.E17-06-0342.

Pardo, Annie, Sandra Cabrera, Mariel Maldonado, and Moisés Selman. 2016. "Role of Matrix Metalloproteinases in the Pathogenesis of Idiopathic Pulmonary Fibrosis." *Respiratory Research*

17 (1). https://doi.org/10.1186/s12931-016-0343-6.

Parimon, Tanyalak, Changfu Yao, David M Habiel, Lingyin Ge, Stephanie A Bora, Rena Brauer, Christopher M Evans, et al. 2019. "Syndecan-1 Promotes Lung Fibrosis by Regulating Epithelial Reprogramming through Extracellular Vesicles." *JCI Insight* 5 (August). https://doi.org/10.1172/jci.insight.129359.

Parker, Matthew W, Daniel Rossi, Mark Peterson, Karen Smith, Kristina Sikström, Eric S White, John E Connett, Craig A Henke, Ola Larsson, and Peter B Bitterman. 2014. "Fibrotic Extracellular Matrix Activates a Profibrotic Positive Feedback Loop." *The Journal of Clinical Investigation* 124 (4): 1622–35. https://doi.org/10.1172/JCI71386.

Patel, Katan, Jacqueline Dickson, Shahida Din, Kenneth Macleod, Duncan Jodrell, and Bernard Ramsahoye. 2010. "Targeting of 5-Aza-2'-Deoxycytidine Residues by Chromatin-Associated DNMT1 Induces Proteasomal Degradation of the Free Enzyme." *Nucleic Acids Research* 38 (13): 4313–24. https://doi.org/10.1093/nar/gkq187.

Pechkovsky, Dmitri V., Cecilia M. Prêle, John Wong, Cory M. Hogaboam, Robin J. McAnulty, Geoffrey J. Laurent, Samuel S M Zhang, Moisés Selman, Steven E. Mutsaers, and Darryl A. Knight. 2012. "STAT3-Mediated Signaling Dysregulates Lung Fibroblast-Myofibroblast Activation and Differentiation in UIP/IPF." *American Journal of Pathology* 180 (4): 1398–1412. https://doi.org/10.1016/j.ajpath.2011.12.022.

Peix, Lizzy, Iona C. Evans, David R. Pearce, Juliet K. Simpson, Toby M. Maher, and Robin J. McAnulty. 2018. "Diverse Functions of Clusterin Promote and Protect against the Development of Pulmonary Fibrosis." *Scientific Reports* 8 (1): 1906. https://doi.org/10.1038/s41598-018-20316-1.

Pfaff, Martin, Takako Sasaki, Kirsten Tangemann, Mon-Li Chu, and Rupert Timpl. 1995. "Integrin-Binding and Cell-Adhesion Studies of Fibulins Reveal a Particular Affinity for AIIbβ3." *Experimental Cell Research* 219 (1): 87–92. https://doi.org/10.1006/excr.1995.1208.

Ponticos, Markella, Ioannis Papaioannou, Shiwen Xu, Alan M. Holmes, Korsa Khan, Christopher P. Denton, George Bou-Gharios, and David J. Abraham. 2015. "Failed Degradation of JunB Contributes to Overproduction of Type i Collagen and Development of Dermal Fibrosis in Patients with Systemic Sclerosis." *Arthritis and Rheumatology* 67 (1): 243–53. https://doi.org/10.1002/art.38897.

Price, Magda E, Allison M Cotton, Lucia L Lam, Pau Farré, Eldon Emberly, Carolyn J Brown, Wendy P Robinson, and Michael S Kobor. 2013. "Additional Annotation Enhances Potential for Biologically-Relevant Analysis of the Illumina Infinium HumanMethylation450 BeadChip Array." *Epigenetics & Chromatin* 6 (1): 4. https://doi.org/10.1186/1756-8935-6-4.

Proetzel, Gabriele, Sharon A. Pawlowski, Michael V. Wiles, Moying Yin, Gregory P. Boivin, Philip N. Howles, Jixang Ding, Mark W.J. Ferguson, and Thomas Doetschman. 1995. "Transforming Growth Factor–B3 Is Required for Secondary Palate Fusion." *Nature Genetics* 11 (4): 409–14. https://doi.org/10.1038/ng1295-409.

Qi, Jian Hua, Quteba Ebrahem, Nina Moore, Gillian Murphy, Lena Claesson-Welsh, Mark Bond, Andrew Baker, and Bela Anand-Apte. 2003. "A Novel Function for Tissue Inhibitor of Metalloproteinases-3 (TIMP3): Inhibition of Angiogenesis by Blockage of VEGF Binding to VEGF Receptor-2." *Nature Medicine* 9 (4): 407–15. https://doi.org/10.1038/nm846.

Qin, Taichun, Jaroslav Jelinek, Jiali Si, Jingmin Shu, and Jean Pierre J. Issa. 2009. "Mechanisms of Resistance to 5-Aza-2'-Deoxycytidine in Human Cancer Cell Lines." *Blood* 113 (3): 659–67. https://doi.org/10.1182/blood-2008-02-140038.

Rabinovich, Einat I, Maria G Kapetanaki, Israel Steinfeld, Kevin F Gibson, Kusum V Pandit, Guoying Yu, Zohar Yakhini, and Naftali Kaminski. 2012. "Global Methylation Patterns in Idiopathic Pulmonary Fibrosis." Edited by Oliver Eickelberg. *PLoS ONE* 7 (4): e33770. https://doi.org/10.1371/journal.pone.0033770.

Raghu, Ganesh, Harold R. Collard, Jim J. Egan, Fernando J. Martinez, Juergen Behr, Kevin K. Brown, Thomas V. Colby, et al. 2011. "An Official ATS/ERS/JRS/ALAT Statement: Idiopathic Pulmonary

Fibrosis: Evidence-Based Guidelines for Diagnosis and Management." *American Journal of Respiratory and Critical Care Medicine* 183 (6): 788–824. https://doi.org/10.1164/rccm.2009-040GL.

Raghu, Ganesh, Martine Remy-Jardin, Jeffrey L Myers, Luca Richeldi, Christopher J Ryerson, David J Lederer, Juergen Behr, et al. 2018. "Diagnosis of Idiopathic Pulmonary Fibrosis. An Official ATS/ERS/JRS/ALAT Clinical Practice Guideline." *American Journal of Respiratory and Critical Care Medicine* 198 (5): e44–68. https://doi.org/10.1164/rccm.201807-1255ST.

Raghu, Ganesh, Bram Rochwerg, Yuan Zhang, Carlos A. Cuello Garcia, Arata Azuma, Juergen Behr, Jan L. Brozek, et al. 2015. "An Official ATS/ERS/JRS/ALAT Clinical Practice Guideline: Treatment of Idiopathic Pulmonary Fibrosis. An Update of the 2011 Clinical Practice Guideline." *American Journal of Respiratory and Critical Care Medicine* 192 (2): e3-19. https://doi.org/10.1164/rccm.201506-1063ST.

Ramaswamy, Sridhar, Ken N. Ross, Eric S. Lander, and Todd R. Golub. 2003. "A Molecular Signature of Metastasis in Primary Solid Tumors." *Nature Genetics* 33 (1): 49–54. https://doi.org/10.1038/ng1060.

Ramshaw, John A.M., Naina K. Shah, and Barbara Brodsky. 1998. "Gly-X-Y Tripeptide Frequencies in Collagen: A Context for Host-Guest Triple-Helical Peptides." *Journal of Structural Biology* 122 (1–2): 86–91. https://doi.org/10.1006/jsbi.1998.3977.

Richeldi, Luca, Roland M. du Bois, Ganesh Raghu, Arata Azuma, Kevin K. Brown, Ulrich Costabel, Vincent Cottin, et al. 2014. "Efficacy and Safety of Nintedanib in Idiopathic Pulmonary Fibrosis." *New England Journal of Medicine* 370 (22): 2071–82. https://doi.org/10.1056/NEJMoa1402584.

Roark, E. F., D. R. Keene, C. C. Haudenschild, S. Godyna, C. D. Little, and W. S. Argraves. 1995. "The Association of Human Fibulin-1 with Elastic Fibers: An Immunohistological, Ultrastructural, and RNA Study." *The Journal of Histochemistry and Cytochemistry : Official Journal of the Histochemistry Society* 43 (4): 401–11. https://doi.org/10.1177/43.4.7534784.

Robertson, Ian B., Masahito Horiguchi, Lior Zilberberg, Branka Dabovic, Krassimira Hadjiolova, and Daniel B. Rifkin. 2015. "Latent TGF-β-Binding Proteins." *Matrix Biology* 47 (1): 44–53. https://doi.org/10.1016/j.matbio.2015.05.005.

Rock, Jason R., Christina E. Barkauskas, Michael J. Cronce, Yan Xue, Jeffrey R. Harris, Jiurong Liang, Paul W. Noble, and Brigid L.M. Hogan. 2011. "Multiple Stromal Populations Contribute to Pulmonary Fibrosis without Evidence for Epithelial to Mesenchymal Transition." *Proceedings of the National Academy of Sciences of the United States of America* 108 (52). https://doi.org/10.1073/pnas.1117988108.

Rockey, Don C, P. Darwin Bell, and Joseph A Hill. 2015. "Fibrosis-a Common Pathway to Organ Injury and Failure." Edited by Dan L. Longo. *New England Journal of Medicine*. https://doi.org/10.1056/NEJMra1300575.

Rubio, Karla, Indrabahadur Singh, Stephanie Dobersch, Pouya Sarvari, Stefan Günther, Julio Cordero, Aditi Mehta, et al. 2019. "Inactivation of Nuclear Histone Deacetylases by EP300 Disrupts the MiCEE Complex in Idiopathic Pulmonary Fibrosis." *Nature Communications* 10 (1): 2229. https://doi.org/10.1038/s41467-019-10066-7.

Sacco, Oliviero, Debra Romberger, Angie Rizzino, Joe D. Beckmann, Stephen I. Rennard, and John R. Spurzem. 1992. "Spontaneous Production of Transforming Growth Factor-B2 by Primary Cultures of Bronchial Epithelial Cells: Effects on Cell Behavior in Vitro." *Journal of Clinical Investigation* 90 (4): 1379–85. https://doi.org/10.1172/JCI116004.

Salmenperä, Pertteli, Esko Kankuri, Jozef Bizik, Vappu Sirén, Ismo Virtanen, Seiichiro Takahashi, Michael Leiss, Reinhard Fässler, and Antti Vaheri. 2008. "Formation and Activation of Fibroblast Spheroids Depend on Fibronectin – Integrin Interaction." *Experimental Cell Research* 314 (19): 3444–52. https://doi.org/10.1016/j.yexcr.2008.09.004.

Sanders, Yan Y., Namasivayam Ambalavanan, Brian Halloran, Xiangyu Zhang, Hui Liu, David K. Crossman, Molly Bray, Kui Zhang, Victor J. Thannickal, and James S. Hagood. 2012. "Altered DNA Methylation Profile in Idiopathic Pulmonary Fibrosis." *American Journal of Respiratory and*

*Critical Care Medicine* 186 (6): 525–35. https://doi.org/10.1164/rccm.201201-0077OC.

Sanders, Yan Y., Annie Pardo, Moisés Selman, Gerard J. Nuovo, Trygve O. Tollefsbol, Gene P. Siegal, and James S. Hagood. 2008. "Thy-1 Promoter Hypermethylation: A Novel Epigenetic Pathogenic Mechanism in Pulmonary Fibrosis." *American Journal of Respiratory Cell and Molecular Biology* 39 (5): 610–18. https://doi.org/10.1165/rcmb.2007-0322OC.

Sanford, L. Philip, Ilona Ormsby, Adriana C. Gittenberger-de Groot, Hannu Sariola, Rick Friedman, Gregory P. Boivin, Emma Lou Cardell, and Thomas Doetschman. 1997. "TGFβ2 Knockout Mice Have Multiple Developmental Defects That Are Non-Overlapping with Other TGFβ Knockout Phenotypes." *Development* 124 (13): 2659–70.

Sasaki, T, H Wiedemann, M Matzner, M L Chu, and R Timpl. 1996. "Expression of Fibulin-2 by Fibroblasts and Deposition with Fibronectin into a Fibrillar Matrix." *Journal of Cell Science* 109 ( Pt 1: 2895–2904. http://www.ncbi.nlm.nih.gov/pubmed/9013337.

Sasaki, Takako, Walter Göhring, Nicolai Miosge, William R. Abrams, Joel Rosenbloom, and Rupert Timpl. 1999. "Tropoelastin Binding to Fibulins, Nidogen-2 and Other Extracellular Matrix Proteins." *FEBS Letters* 460 (2): 280–84. https://doi.org/10.1016/S0014-5793(99)01362-9.

Sasaki, Takako, Walter Göhring, T C Pan, M L Chu, and Rupert Timpl. 1995. "Binding of Mouse and Human Fibulin-2 to Extracellular Matrix Ligands." *Journal of Molecular Biology* 254 (5): 892–99. https://doi.org/10.1006/jmbi.1995.0664.

Sasaki, Takako, Karlheinz Mann, Gillian Murphy, Mon-Li Chu, and Rupert Timpl. 1996. "Different Susceptibilities of Fibulin-1 and Fibulin-2 to Cleavage by Matrix Metalloproteinases and Other Tissue Proteases." *European Journal of Biochemistry* 240 (2): 427–34. https://doi.org/10.1111/j.1432-1033.1996.0427h.x.

Sasaki, Takako, Karlheinz Mann, Hanna Wiedemann, Walter Göhring, Ariel Lustig, Jürgen Engel, Mon Li Chu, and Rupert Timpl. 1997. "Dimer Model for the Microfibrillar Protein Fibulin-2 and Identification of the Connecting Disulfide Bridge." *The EMBO Journal* 16 (11): 3035–43. https://doi.org/10.1093/emboj/16.11.3035.

Sato, Noriko, Mitsumasa Kondo, and Ken-ichi Arai. 2006. "The Orphan Nuclear Receptor GCNF Recruits DNA Methyltransferase for Oct-3/4 Silencing." *Biochemical and Biophysical Research Communications* 344 (3): 845–51. https://doi.org/10.1016/j.bbrc.2006.04.007.

Savary, Grégoire, Edmone Dewaeles, Serena Diazzi, Matthieu Buscot, Nicolas Nottet, Julien Fassy, Elisabeth Courcot, et al. 2019. "The Long Non-Coding RNA DNM3OS Is a Reservoir of FibromiRs with Major Functions in Lung Fibroblast Response to TGF-β and Pulmonary Fibrosis." *American Journal of Respiratory and Critical Care Medicine*, April. https://doi.org/10.1164/rccm.201807-1237OC.

Schaeffer, Julia, David Tannahill, Jean-Michel Cioni, Dáire Rowlands, and Roger Keynes. 2018. "Identification of the Extracellular Matrix Protein Fibulin-2 as a Regulator of Spinal Nerve Organization." *Developmental Biology* 442 (1): 101–14. https://doi.org/10.1016/j.ydbio.2018.06.014.

Schiller, Herbert B., Isis E. Fernandez, Gerald Burgstaller, Christoph Schaab, Richard A. Scheltema, Thomas Schwarzmayr, Tim M. Strom, Oliver Eickelberg, and Matthias Mann. 2015. "Time- and Compartment-Resolved Proteome Profiling of the Extracellular Niche in Lung Injury and Repair." *Molecular Systems Biology* 11 (7): 819–819. https://doi.org/10.15252/msb.20156123.

Scotton, Chris J., and Rachel C. Chambers. 2007. "Molecular Targets in Pulmonary Fibrosis: The Myofibroblast in Focus." *Chest* 132 (4): 1311–21. https://doi.org/10.1378/chest.06-2568.

Seibold, Max A, Anastasia L Wise, Marcy C Speer, Mark P Steele, Kevin K Brown, James E Loyd, Tasha E Fingerlin, et al. 2011. "A Common MUC5B Promoter Polymorphism and Pulmonary Fibrosis." *New England Journal of Medicine* 364 (16): 1503–12. https://doi.org/10.1056/NEJMoa1013660.

Selman, Moises, Victor Ruiz, Sandra Cabrera, Lourdes Segura, Roberto Barrios, Annie Pardo, Remedios Ramírez, Roberto Barrios, and Annie Pardo. 2000. "TIMP-1, -2, -3, and -4 in Idiopathic Pulmonary Fibrosis. A Prevailing Nondegradative Lung Microenvironment?" *Am J Physiol Lung Cell Mol Physiol* 279 (3): 562–74.

http://ajplung.physiology.org/content/279/3/L562.abstract%5Cnpapers2://publication/uuid/A4F95D87-F132-4A94-A50F-C39318C6418D.

Selvarajah, Brintha, Ilan Azuelos, Manuela Platé, Delphine Guillotin, Ellen J. Forty, Greg Contento, Hannah V. Woodcock, et al. 2019. "MTORC1 Amplifies the ATF4-Dependent de Novo Serine-Glycine Pathway to Supply Glycine during TGF-1-Induced Collagen Biosynthesis." *Science Signaling* 12 (582). https://doi.org/10.1126/scisignal.aav3048.

Senapati, S., V. S. Gnanapragassam, N. Moniaux, N. Momi, and S. K. Batra. 2012. "Role of MUC4-NIDO Domain in the MUC4-Mediated Metastasis of Pancreatic Cancer Cells." *Oncogene* 31 (28): 3346–56. https://doi.org/10.1038/onc.2011.505.

Serini, Guido, M L Bochaton-Piallat, Patricia Ropraz, Antoine Geinoz, Laura Borsi, Luciano Zardi, and Giulio Gabbiani. 1998. "The Fibronectin Domain ED-A Is Crucial for Myofibroblastic Phenotype Induction by Transforming Growth Factor-Beta1." *The Journal of Cell Biology* 142 (3): 873–81. https://doi.org/10.1083/jcb.142.3.873.

Serra, Noemí, Roser Rosales, Lluís Masana, and Joan-Carles Vallvé. 2015. "Simvastatin Increases Fibulin-2 Expression in Human Coronary Artery Smooth Muscle Cells via RhoA/Rho-Kinase Signaling Pathway Inhibition." Edited by Pablo Garcia de Frutos. *PLOS ONE* 10 (7): e0133875. https://doi.org/10.1371/journal.pone.0133875.

Shalginskikh, Natalia, Andrey Poleshko, Anna Marie Skalka, and Richard A Katz. 2013. "Retroviral DNA Methylation and Epigenetic Repression Are Mediated by the Antiviral Host Protein Daxx." *Journal of Virology* 87 (4): 2137–50. https://doi.org/10.1128/JVI.02026-12.

Shapiro, S. D., S. K. Endicott, M. A. Province, J. A. Pierce, and E. J. Campbell. 1991. "Marked Longevity of Human Lung Parenchymal Elastic Fibers Deduced from Prevalence of D-Aspartate and Nuclear Weapons-Related Radiocarbon." *The Journal of Clinical Investigation* 87 (5): 1828–34. https://doi.org/10.1172/JCI115204.

Sharp, Andrew J, Elisavet Stathaki, Eugenia Migliavacca, Manisha Brahmachary, Stephen B Montgomery, Yann Dupre, and Stylianos E Antonarakis. 2011. "DNA Methylation Profiles of Human Active and Inactive X Chromosomes." *Genome Research* 21 (10): 1592–1600. https://doi.org/10.1101/gr.112680.110.

Shi, Minlong, Jianghai Zhu, Rui Wang, Xing Chen, Lizhi Mi, Thomas Walz, and Timothy A. Springer. 2011. "Latent TGF-β Structure and Activation." *Nature* 474 (7351): 343–49. https://doi.org/10.1038/nature10152.

Shull, Marcia M., Ilona Ormsby, Ann B. Kier, Sharon Pawlowski, Ronald J. Diebold, Moying Yin, Ruth Allen, et al. 1992. "Targeted Disruption of the Mouse Transforming Growth Factor-B1 Gene Results in Multifocal Inflammatory Disease [14]." *Nature* 359 (6397): 693–99. https://doi.org/10.1038/359693a0.

Sicot, F.-X., Takeshi Tsuda, Dessislava Markova, John F Klement, Machiko Arita, R.-Z. Zhang, T.-C. Pan, Robert P Mecham, David E Birk, and M.-L. Chu. 2008. "Fibulin-2 Is Dispensable for Mouse Development and Elastic Fiber Formation." *Molecular and Cellular Biology* 28 (3): 1061–67. https://doi.org/10.1128/MCB.01876-07.

Singh, Indrabahadur, Adriana Contreras, Julio Cordero, Karla Rubio, Stephanie Dobersch, Stefan Günther, Sylvia Jeratsch, et al. 2018. "MiCEE Is a NcRNA-Protein Complex That Mediates Epigenetic Silencing and Nucleolar Organization." *Nature Genetics* 50 (7): 990–1001. https://doi.org/10.1038/s41588-018-0139-3.

Singh, Purva, and Jean E. Schwarzbauer. 2014. "Fibronectin Matrix Assembly Is Essential for Cell Condensation during Chondrogenesis." *Journal of Cell Science* 127 (20): 4420–28. https://doi.org/10.1242/jcs.150276.

Skrypek, Nicolas, Steven Goossens, Eva De Smedt, Niels Vandamme, and Geert Berx. 2017. "Epithelial-to-Mesenchymal Transition: Epigenetic Reprogramming Driving Cellular Plasticity." *Trends in Genetics : TIG* 33 (12): 943–59. https://doi.org/10.1016/j.tig.2017.08.004.

Smyth, Gordon K. 2004. "Linear Models and Empirical Bayes Methods for Assessing Differential Expression in Microarray Experiments Linear Models and Empirical Bayes Methods for Assessing

Differential Expression in Microarray Experiments." *Statistical Applications in Genetics and Molecular Biology* 3 (1): 1–26. https://doi.org/10.2202/1544-6115.1027.

Spainhour, John C.G., Hong Seo Lim, Soojin V. Yi, and Peng Qiu. 2019. "Correlation Patterns Between DNA Methylation and Gene Expression in The Cancer Genome Atlas." *Cancer Informatics* 18. https://doi.org/10.1177/1176935119828776.

Spruijt, Cornelia G., Felix Gnerlich, Arne H. Smits, Toni Pfaffeneder, Pascal W.T.C. Jansen, Christina Bauer, Martin Münzel, et al. 2013. "Dynamic Readers for 5-(Hydroxy)Methylcytosine and Its Oxidized Derivatives." *Cell* 152 (5): 1146–59. https://doi.org/10.1016/j.cell.2013.02.004.

Steen, Virginia D., and Thomas A. Medsger. 2007. "Changes in Causes of Death in Systemic Sclerosis, 1972-2002." *Annals of the Rheumatic Diseases* 66 (7): 940–44. https://doi.org/10.1136/ard.2006.066068.

Stewart, A, T Harris, F Jativa, J Jaffar, P V S Lee, G Westall, M Wilson, and A Berhan. 2019. "Stiffness: A 'Master Regulator' of Human Lung Fibroblast Phenotypic Plasticity?" In *A19. LESS IDIOPATHIC: STRUCTURAL AND FUNCTIONAL ABNORMALITIES IN IPF*, A1043–A1043. American Thoracic Society International Conference Abstracts. American Thoracic Society. https://doi.org/doi:10.1164/ajrccm-conference.2019.199.1_MeetingAbstracts.A1043.

Stratton, Richard, Xu Shiwen, Giorgia Martini, Alan Holmes, Andrew Leask, Thomas Haberberger, George R. Martin, Carol M. Black, and David Abraham. 2001. "Iloprost Suppresses Connective Tissue Growth Factor Production in Fibroblasts and in the Skin of Scleroderma Patients." *Journal of Clinical Investigation* 108 (2): 241–50. https://doi.org/10.1172/JCI12020.

Ström, Åsa, Anders I. Olin, Anders Aspberg, and Anna Hultgårdh-Nilsson. 2006. "Fibulin-2 Is Present in Murine Vascular Lesions and Is Important for Smooth Muscle Cell Migration." *Cardiovascular Research* 69 (3): 755–63. https://doi.org/10.1016/j.cardiores.2005.12.001.

Tang, Chao-Zhi, Jun-Tang Yang, Qing-Hui Liu, Ya-Ru Wang, and Wen-Sheng Wang. 2019. "Up-regulated MiR-192-5p Expression Rescues Cognitive Impairment and Restores Neural Function in Mice with Depression via the Fbln2 -mediated TGF-β1 Signaling Pathway." *The FASEB Journal* 33 (1): 606–18. https://doi.org/10.1096/fj.201800210RR.

Taniguchi, H., M. Ebina, Y. Kondoh, T. Ogura, A. Azuma, M. Suga, Y. Taguchie, et al. 2010. "Pirfenidone in Idiopathic Pulmonary Fibrosis." *European Respiratory Journal* 35 (4): 821–29. https://doi.org/10.1183/09031936.00005209.

Tatler, Amanda L., and Gisli Jenkins. 2012. "TGF-β Activation and Lung Fibrosis." *Proceedings of the American Thoracic Society* 9 (3): 130–36. https://doi.org/10.1513/pats.201201-003AW.

Tian, H., J. Liu, J. Chen, M. L. Gatza, and G. C. Blobe. 2015. "Fibulin-3 Is a Novel TGF-β Pathway Inhibitor in the Breast Cancer Microenvironment." *Oncogene* 34 (45): 5635–47. https://doi.org/10.1038/onc.2015.13.

Timpl, Rupert, Takako Sasaki, Günter Kostka, and Mon-Li Chu. 2003. "Fibulins: A Versatile Family of Extracellular Matrix Proteins." *Nature Reviews Molecular Cell Biology* 4 (6): 479–89. https://doi.org/10.1038/nrm1130.

Toaldo, Cristina, Stefania Pizzimenti, Angelo Cerbone, Piergiorgio Pettazzoni, Elisa Menegatti, Berardi Daniela, Rosalba Minelli, et al. 2010. "PPARγ Ligands Inhibit Telomerase Activity and HTERT Expression through Modulation of the Myc/Mad/Max Network in Colon Cancer Cells." *Journal of Cellular and Molecular Medicine* 14 (6 A): 1347–57. https://doi.org/10.1111/j.1582-4934.2009.00966.x.

Tobin, Richard W., Charles E. Pope, Carlos A. Pellegrini, Mary J. Emond, Jim Sillery, and Ganesh Raghu. 1998. "Increased Prevalence of Gastroesophageal Reflux in Patients with Idiopathic Pulmonary Fibrosis." *American Journal of Respiratory and Critical Care Medicine* 158 (6): 1804–8. https://doi.org/10.1164/ajrccm.158.6.9804105.

Torregrosa-Carrión, Rebeca, Luis Luna-Zurita, Fernando García-Marqués, Gaetano D'Amato, Rebeca Piñeiro-Sabarís, Elena Bonzón-Kulichenko, Jesús Vázquez, and José Luis de la Pompa. 2019. "NOTCH Activation Promotes Valve Formation by Regulating the Endocardial Secretome." *Molecular & Cellular Proteomics* 18 (9): 1782–95. https://doi.org/10.1074/mcp.RA119.001492.

Tsuda, Takeshi, Hui Wang, Rupert Timpl, and Mon Li Chu. 2001. “Fibulin-2 Expression Marks Transformed Mesenchymal Cells in Developing Cardiac Valves, Aortic Arch Vessels, and Coronary Vessels.” *Developmental Dynamics* 222 (1): 89–100. https://doi.org/10.1002/dvdy.1172.

Tsuda, Takeshi, Jing Wu, Erhe Gao, Jennifer Joyce, Dessislava Markova, Hailong Dong, Ying Liu, et al. 2012. “Loss of Fibulin-2 Protects against Progressive Ventricular Dysfunction after Myocardial Infarction.” *Journal of Molecular and Cellular Cardiology* 52 (1): 273–82. https://doi.org/10.1016/j.yjmcc.2011.11.001.

Utani, Atsushi, Motoyoshi Nomizu, and Yoshihiko Yamada. 1997. “Fibulin-2 Binds to the Short Arms of Laminin-5 and Laminin-1 via Conserved Amino Acid Sequences.” *The Journal of Biological Chemistry* 272 (5): 2814–20. https://doi.org/10.1074/jbc.272.5.2814.

Vandesompele, Jo, Katleen De Preter, Filip Pattyn, Bruce Poppe, Nadine Van Roy, Anne De Paepe, and Frank Speleman. 2002. “Accurate Normalization of Real-Time Quantitative RT-PCR Data by Geometric Averaging of Multiple Internal Control Genes.” *Genome Biology* 3 (7): RESEARCH0034. https://doi.org/10.1186/gb-2002-3-7-research0034.

Vangeel, E. B., B. Izzi, T. Hompes, K. Vansteelandt, D. Lambrechts, K. Freson, and S. Claes. 2015. “DNA Methylation in Imprinted Genes IGF2 and GNASXL Is Associated with Prenatal Maternal Stress.” *Genes, Brain, and Behavior* 14 (8): 573–82. https://doi.org/10.1111/gbb.12249.

Varga, John, and David Abraham. 2007. “Systemic Sclerosis: A Prototypic Multisystem Fibrotic Disorder.” *The Journal of Clinical Investigation* 117 (3): 557–67. https://doi.org/10.1172/JCI31139.

Varley, Katherine E., Jason Gertz, Kevin M. Bowling, Stephanie L. Parker, Timothy E. Reddy, Florencia Pauli-Behn, Marie K. Cross, et al. 2013. “Dynamic DNA Methylation across Diverse Human Cell Lines and Tissues.” *Genome Research* 23 (3): 555–67. https://doi.org/10.1101/gr.147942.112.

Vega, S. De, T. Iwamoto, and Y. Yamada. 2009. “Fibulins: Multiple Roles in Matrix Structures and Tissue Functions.” *Cellular and Molecular Life Sciences* 66 (11–12): 1890–1902. https://doi.org/10.1007/s00018-009-8632-6.

Vega, Susana De, Tsutomu Iwamoto, Takashi Nakamura, Kentaro Hozumi, Dianalee A. McKnight, Larry W. Fisher, Satoshi Fukumoto, and Yoshihiko Yamada. 2007. “TM14 Is a New Member of the Fibulin Family (Fibulin-7) That Interacts with Extracellular Matrix Molecules and Is Active for Cell Binding.” *Journal of Biological Chemistry* 282 (42): 30878–88. https://doi.org/10.1074/jbc.M705847200.

Vogél, B. E., and E. M. Hedgecock. 2001. “Hemicentin, a Conserved Extracellular Member of the Immunoglobulin Superfamily, Organizes Epithelial and Other Cell Attachments into Oriented Line-Shaped Junctions.” *Development* 128 (6): 883–94.

Vojta, Aleksandar, Paula Dobrinic, Vanja Tadic, Luka Bockor, Petra Korac, Boris Julg, Marija Klasic, and Vlatka Zoldos. 2016. “Repurposing the CRISPR-Cas9 System for Targeted DNA Methylation.” *Nucleic Acids Research* 44 (12): 5615–28. https://doi.org/10.1093/nar/gkw159.

Wagner, James R, Stephan Busche, Bing Ge, Tony Kwan, Tomi Pastinen, and Mathieu Blanchette. 2014. “The Relationship between DNA Methylation, Genetic and Expression Inter-Individual Variation in Untransformed Human Fibroblasts.” *Genome Biology* 15 (2): R37. https://doi.org/10.1186/gb-2014-15-2-r37.

Wahl, Sharon M. 1992. “Transforming Growth Factor Beta (TGF-β) in Inflammation: A Cause and a Cure.” *Journal of Clinical Immunology* 12 (2): 61–74. https://doi.org/10.1007/BF00918135.

Wang, Youngqing, Pan-Sheng Fan, and Bashar Kahaleh. 2006. “Association between Enhanced Type I Collagen Expression and Epigenetic Repression of the FLI1 Gene in Scleroderma Fibroblasts.” *Arthritis and Rheumatism* 54 (7): 2271–79. https://doi.org/10.1002/art.21948.

Weiss, Alexander, and Liliana Attisano. 2013. “The TGFbeta Superfamily Signaling Pathway.” *Wiley Interdisciplinary Reviews: Developmental Biology* 2 (1): 47–63. https://doi.org/10.1002/wdev.86.

Wernig, Gerlinde, Shih Yu Chen, Lu Cui, Camille Van Neste, Jonathan M. Tsai, Neeraja Kambham,

Hannes Vogel, et al. 2017. “Unifying Mechanism for Different Fibrotic Diseases.” *Proceedings of the National Academy of Sciences of the United States of America* 114 (18): 4757–62. https://doi.org/10.1073/pnas.1621375114.

Winters, Nichelle I., Ankita Burman, Jonathan A. Kropski, and Timothy S. Blackwell. 2019. “Epithelial Injury and Dysfunction in the Pathogenesis of Idiopathic PulmonaryFibrosis.” *The American Journal of the Medical Sciences* 357 (5): 374–78. https://doi.org/10.1016/j.amjms.2019.01.010.

Wipff, Pierre Jean, Daniel B. Rifkin, Jean Jacques Meister, and Boris Hinz. 2007. “Myofibroblast Contraction Activates Latent TGF-B1 from the Extracellular Matrix.” *Journal of Cell Biology* 179 (6): 1311–23. https://doi.org/10.1083/jcb.200704042.

Wollin, Lutz, Isabelle Maillet, Valérie Quesniaux, Alexander Holweg, and Bernhard Ryffel. 2014. “Antifibrotic and Anti-Inflammatory Activity of the Tyrosine Kinase Inhibitor Nintedanib in Experimental Models of Lung Fibrosis.” *The Journal of Pharmacology and Experimental Therapeutics* 349 (2): 209–20. https://doi.org/10.1124/jpet.113.208223.

Xu, Ying Dong, Jiesong Hua, Alice Mui, Robert O’Connor, Gary Grotendorst, and Nasreen Khalil. 2003. “Release of Biologically Active TGF-B1 by Alveolar Epithelial Cells Results in Pulmonary Fibrosis.” *American Journal of Physiology - Lung Cellular and Molecular Physiology* 285 (3 29-3): 527–39. https://doi.org/10.1152/ajplung.00298.2002.

Yamauchi, Yoshinori, Eichi Tsuruga, Kazuki Nakashima, Yoshihiko Sawa, and Hiroyuki Ishikawa. 2010. “Fibulin-4 and -5, but Not Fibulin-2, Are Associated with Tropoelastin Deposition in Elastin-Producing Cell Culture.” *Acta Histochemica et Cytochemica* 43 (6): 131–38. https://doi.org/10.1267/ahc.10026.

Yanagisawa, Hiromi, and Elaine C. Davis. 2010. “Unraveling the Mechanism of Elastic Fiber Assembly: The Roles of Short Fibulins.” *The International Journal of Biochemistry & Cell Biology* 42 (7): 1084–93. https://doi.org/10.1016/j.biocel.2010.03.009.

Yang, Ivana V., Brent S. Pedersen, Einat Rabinovich, Corinne E. Hennessy, Elizabeth J. Davidson, Elissa Murphy, Brenda Juan Guardela, et al. 2014. “Relationship of DNA Methylation and Gene Expression in Idiopathic Pulmonary Fibrosis.” *American Journal of Respiratory and Critical Care Medicine* 190 (11): 1263–72. https://doi.org/10.1164/rccm.201408-1452OC.

Yang, Zhiwei, Zhenyu Mu, Branka Dabovic, Vladimir Jurukovski, Dawen Yu, Joanne Sung, Xiaozhong Xiong, and John S. Munger. 2007. “Absence of Integrin-Mediated TGFβ1 Activation in Vivo Recapitulates the Phenotype of TGFβ1-Null Mice.” *Journal of Cell Biology* 176 (6): 787–93. https://doi.org/10.1083/jcb.200611044.

Yeung, Tony, Penelope C. Georges, Lisa A. Flanagan, Beatrice Marg, Miguelina Ortiz, Makoto Funaki, Nastaran Zahir, Wenyu Ming, Valerie Weaver, and Paul A. Janmey. 2005. “Effects of Substrate Stiffness on Cell Morphology, Cytoskeletal Structure, and Adhesion.” *Cell Motility and the Cytoskeleton* 60 (1): 24–34. https://doi.org/10.1002/cm.20041.

Yi, Chun-Hui, David J Smith, William W West, and Michael a Hollingsworth. 2007. “Loss of Fibulin-2 Expression Is Associated with Breast Cancer Progression.” *The American Journal of Pathology* 170 (5): 1535–45. https://doi.org/10.2353/ajpath.2007.060478.

Yoon, Ahram, Stephanie A. Tammen, Soyoung Park, Sung Nim Han, and Sang-Woon Choi. 2017. “Genome-Wide Hepatic DNA Methylation Changes in High-Fat Diet-Induced Obese Mice.” *Nutrition Research and Practice* 11 (2): 105–13. https://doi.org/10.4162/nrp.2017.11.2.105.

Yu, Qin, and Ivan Stamenkovic. 2000. “Cell Surface-Localized Matrix Metalloproteinase-9 Proteolytically Activates TGF-β and Promotes Tumor Invasion and Angiogenesis.” *Genes and Development* 14 (2): 163–76. https://doi.org/10.1101/gad.14.2.163.

Zhang, Hangxiang, Jing Wu, Hailong Dong, Shaukat A. Khan, Mon-Li Chu, and Takeshi Tsuda. 2014. “Fibulin-2 Deficiency Attenuates Angiotensin II-Induced Cardiac Hypertrophy by Reducing Transforming Growth Factor-β Signalling.” *Clinical Science* 126 (4): 275–88. https://doi.org/10.1042/CS20120636.

Zhang, Hong-Yan, Mon-Li Chu, Te-Cheng Pan, Takako Sasaki, Rupert Timpl, and Peter Ekblom. 1995. “Extracellular Matrix Protein Fibulin-2 Is Expressed in the Embryonic Endocardial Cushion Tissue

and Is a Prominent Component of Valves in Adult Heart." *Developmental Biology* 167 (1): 18–26. https://doi.org/10.1006/dbio.1995.1003.

Zhang, Hong-Yan, Rupert Timpl, Takako Sasaki, Mon-Li Chu, and Peter Ekblom. 1996. "Fibulin-1 and Fibulin-2 Expression during Organogenesis in the Developing Mouse Embryo." *Developmental Dynamics* 205 (3): 348–64. https://doi.org/10.1002/(SICI)1097-0177(199603)205:3<348::AID-AJA13>3.0.CO;2-0.

Zhang, Na, Keliang Liu, Kai Wang, Ci Zhou, Hejing Wang, Shuangshuang Che, Zhihong Liu, and Huifang Yang. 2019. "Dust Induces Lung Fibrosis through Dysregulated DNA Methylation." *Environmental Toxicology*, no. February: 728–41. https://doi.org/10.1002/tox.22739.

Zhang, R Z, T C Pan, Z Y Zhang, M G Mattei, Rupert Timpl, and M L Chu. 1994. "Fibulin-2 (FBLN2): Human CDNA Sequence, MRNA Expression, and Mapping of the Gene on Human and Mouse Chromosomes." *Genomics* 22 (2): 425–30. https://doi.org/10.1006/geno.1994.1404.

Zhang, Zheng, Scott Schwartz, Lukas Wagner, and Webb Miller. 2000. "A Greedy Algorithm for Aligning DNA Sequences." *Journal of Computational Biology* 7 (1–2): 203–14. https://doi.org/10.1089/10665270050081478.

Zhao, Hui, Jianxin Wang, Xiaodan Kong, Encheng Li, Yuanbin Liu, Xiaohui Du, Zhijie Kang, et al. 2016. "CD47 Promotes Tumor Invasion and Metastasis in Non-Small Cell Lung Cancer." *Scientific Reports* 6 (July): 1–11. https://doi.org/10.1038/srep29719.

Zhou, Wanding, Peter W Laird, and Hui Shen. 2017. "Comprehensive Characterization, Annotation and Innovative Use of Infinium DNA Methylation BeadChip Probes." *Nucleic Acids Research* 45 (4): e22. https://doi.org/10.1093/nar/gkw967.

Zhu, Heng, Guohua Wang, and Jiang Qian. 2016. "Transcription Factors as Readers and Effectors of DNA Methylation." *Nature Reviews Genetics* 17 (9): 551–65. https://doi.org/10.1038/nrg.2016.83.

Zhu, Yuanjue, Yong Liu, Weixun Zhou, Ruolan Xiang, Lei Jiang, Kewu Huang, Yu Xiao, Zijian Guo, and Jinming Gao. 2010. "A Prostacyclin Analogue, Iloprost, Protects from Bleomycin-Induced Pulmonary Fibrosis in Mice." *Respiratory Research* 11: 1–12. https://doi.org/10.1186/1465-9921-11-34.

Zuo, Fengrong, Naftali Kaminski, Elsie Eugui, John Allard, Zohar Yakhini, Amir Ben-Dor, Lance Lollini, et al. 2002. "Gene Expression Analysis Reveals Matrilysin as a Key Regulator of Pulmonary Fibrosis in Mice and Humans." *Proceedings of the National Academy of Sciences of the United States of America* 99 (9): 6292–97. https://doi.org/10.1073/pnas.092134099.

# 6 Appendix

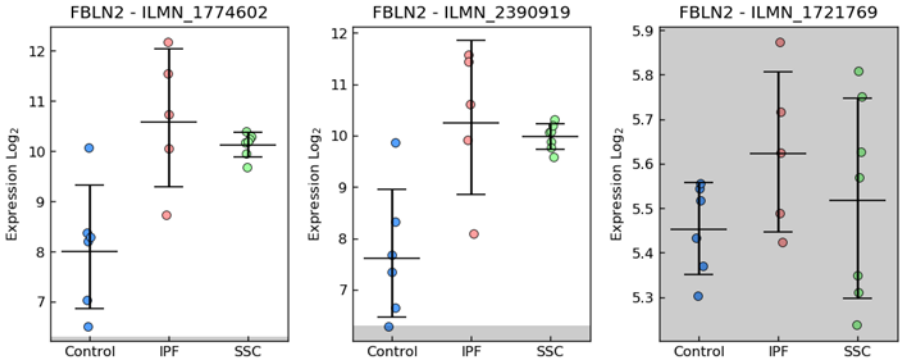


**Appendix 1: Fibulin-2 expression probes $Log_2$ values**

Expression of FBLN2 was significantly increased in IPF (n=5) and SSc (n=7) lung fibroblasts when compared to those from Control donors (n=6) in the Illumina Infinium HumanHT-12 v4 array (probes ILMN_1774602 and ILMN_2390919 $p<0.01$, TNoM ≤ 1; probe ILMN_1721769 was not detected above background). Geometric mean with geometric standard deviation shown. Detection below approximate background level (~6.3) is shaded in grey.

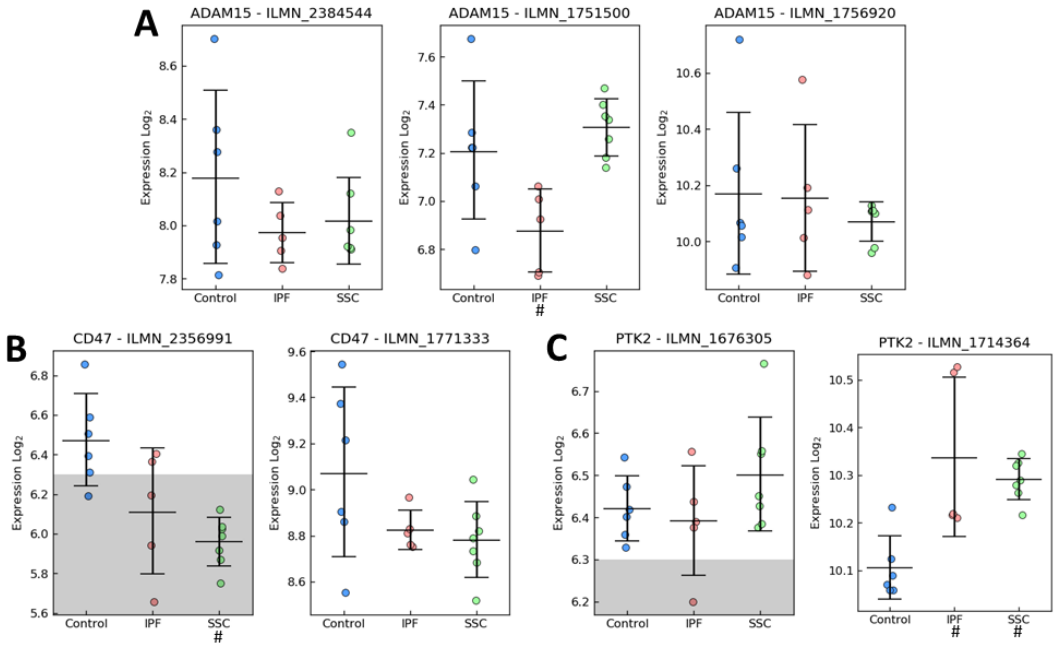


**Appendix 2: Expression probes $Log_2$ values for 3 further genes of interest**

Filtering identified three further genes of interest (**A**) ADAM15, (**B**) CD47 and (**C**) PTK2. Array expression $Log_2$ values with geometric mean and geometric standard deviation are shown for their detected probes. Detection below approximate background level (~6.3) is shaded in grey. # TNoM ≤ 1 vs control.

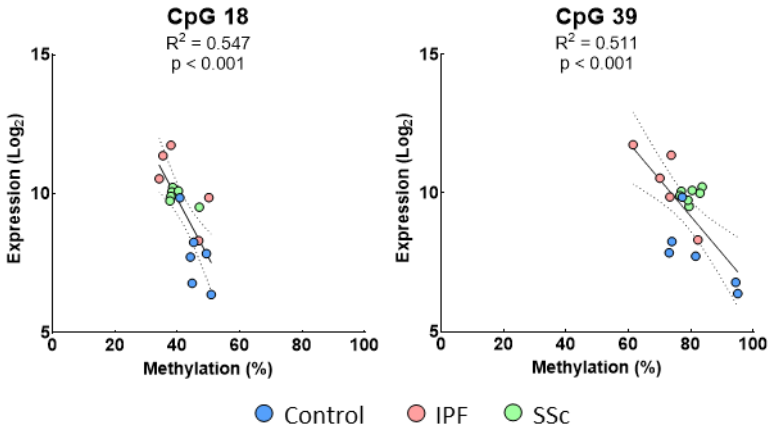


**Appendix 3: Correlation between methylation and expression in FBLN2**

A further two CpGs had moderate negative correlation with expression however methylation differences were small and these CpGs did not have a significant difference in methylation in IPF or SSc compared to control.

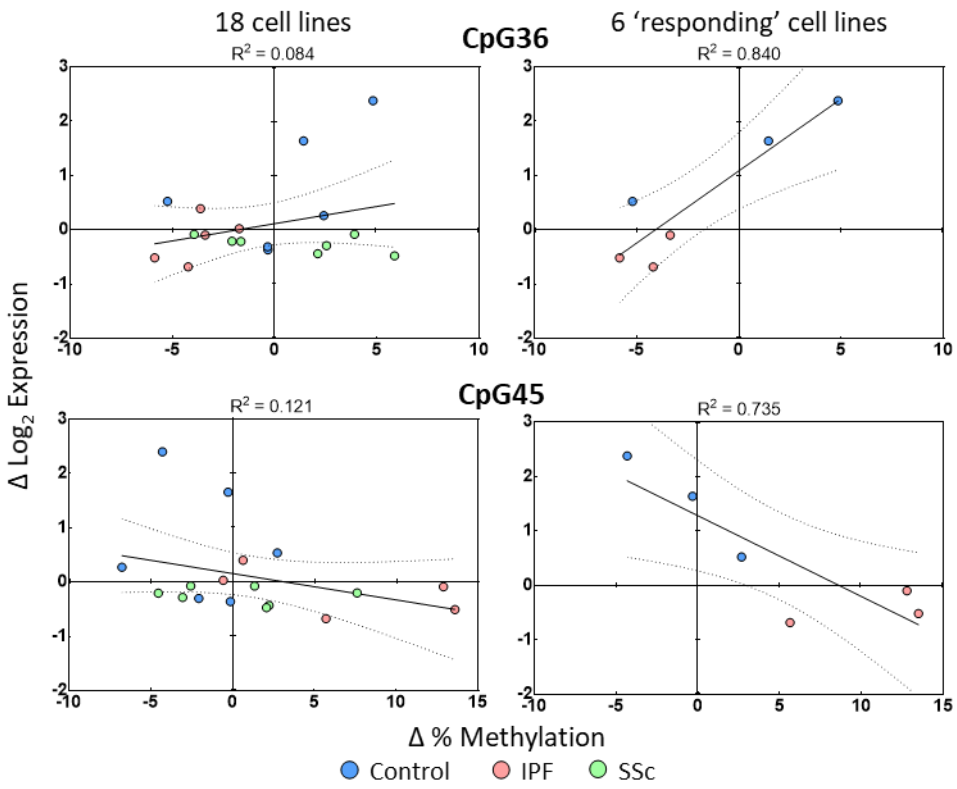


**Appendix 4: Correlation between Δβ and $\Delta Log_2$ with demethylation treatment in CpGs 21 and 28**

There was no correlation between change in methylation and change in expression in analysis of all 18 cell lines however a subset of cells, which were determined to be 5Aza responders by methylation change across the genome (Control n=3, IPF n=3, SSc n=0) had correlation in three CpGs. CpGs 36 and 45 did not have differential methylation basally and are therefore unlikely to be regulating fibulin-2 expression.

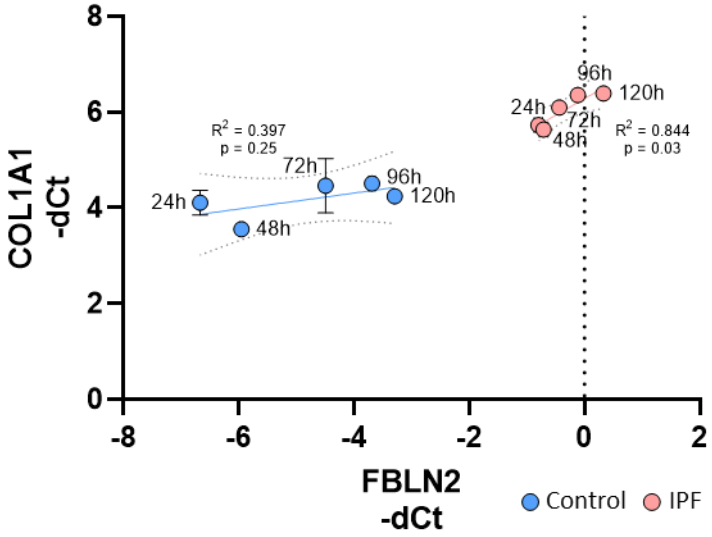


**Appendix 5: Correlation between FBLN2 and COL1A1 mRNA in 2D culture**

Expression of FBLN2 and COL1A1 correlated strongly in IPF fibroblasts against time. Pearson $R^2 = 0.844$, $p < 0.05$. There was no correlation seen in control fibroblasts where COL1A1 expression did not change over time. Data for FBLN2 is shown in **Figure 3.3.4.1**. Data for COL1A1 is shown in **Figure 3.3.6.1**.

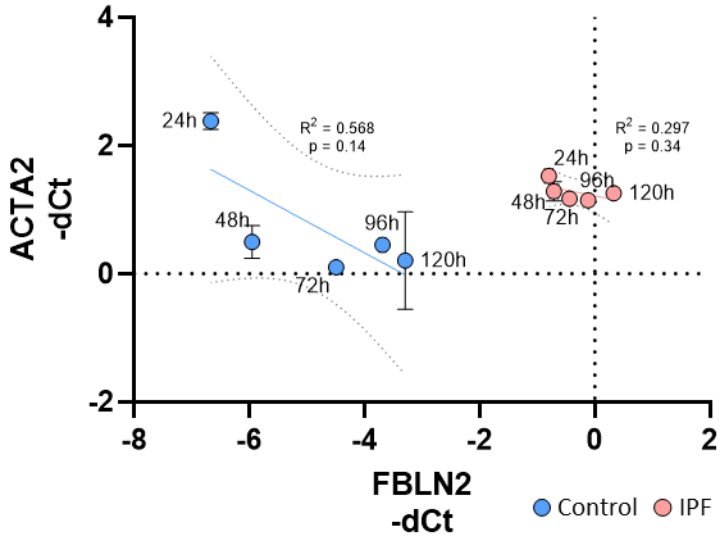


**Appendix 6: Correlation between FBLN2 and ACTA2 mRNA in 2D culture**

Expression of FBLN2 and ACTA2 did not correlate by Pearson $R^2$ in either control or IPF fibroblasts against time in culture. Data for FBLN2 is shown in **Figure 3.3.4.1**. Data for ACTA2 is shown in **Figure 3.3.7.1**.

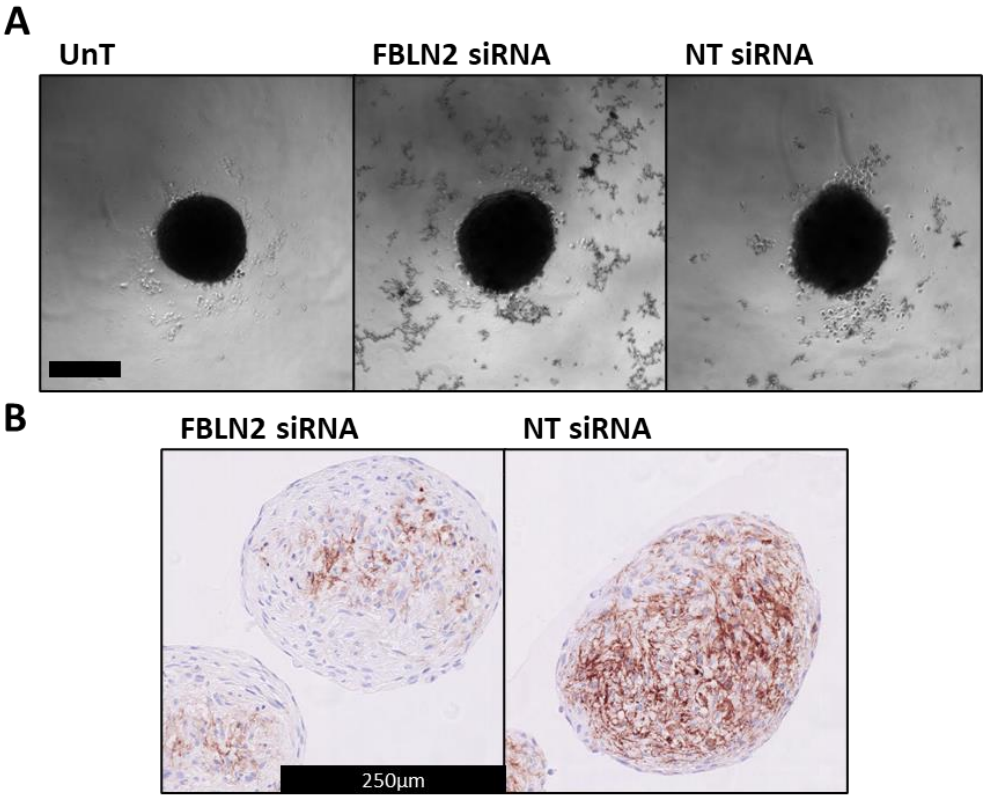


**Appendix 7: siRNA transfection during spheroid formation**

Spheroid formation was interrupted by the presence of transfection reagents in a one-step protocol (**A**). FBLN2 was not successfully depleted in the spheroids formed (**B**: 24h fibrotic spheroids). Scale bars 250µm.